Silica-supported ligands and organometallics : preparation, advanced characterization and catalytic applications

Tom Vancompernolle

Numéro d'ordre : 42478

Université de Lille 1 Sciences et Technologies

UFR CHIMIE

Ecole doctorale : Sciences de la Matière, du Rayonnement et de l'Environnement

Unité de Catalyse et de Chimie du Solide, UMR CNRS 8181

THÈSE

présentée par

Tom VANCOMPERNOLLE

pour l'obtention du grade de

DOCTEUR DE L'UNIVERSITE DE LILLE

Mention Molécules et Matière Condensée

SILICA-SUPPORTED LIGANDS AND ORGANOMETALLICS: PREPARATION, ADVANCED CHARACTERIZATION AND CATALYTIC APPLICATIONS

Rapporteur	M. Christophe THOMAS, Professeur, IRCP, Chimie ParisTech
Rapporteur	M. Abderrahmane AMGOUNE, Professeur, ICBMS, Lyon 1
Examinatrice	Mme Frédérique POURPOINT, Maître de conférences, UCCS, Lille 1
Membre invité	Mr Mostafa Taoufik, Ingénieur de recherche, C2P2, Lyon 1
Directeur de thèse	M. Régis GAUVIN, Chargé de Recherche CNRS, UCCS, Lille 1

Université de Lille 1 SCIENCES ET TECHNOLOGIES

UCCS UNITÉ DE CATALYSE ET CHIMIE DU SOLIDE

Acknowledgments

Mes premiers remerciements vont à mon directeur de thèse, Régis Gauvin, qui m'a fait confiance à la suite de mon stage de master en me proposant cette thèse. Merci pour toutes les connaissances scientifiques qu'il m'a transmises, tous les conseils qu'il m'a donnés afin que je devienne autonome au labo. Je lui suis reconnaissant de m'avoir fait progresser tout au long de ces presque 4 ans autant sur le plan scientifique que dans l'organisation de mon travail. Je souhaite aussi le remercier pour ses bons jeux de mots toujours bien sentis qui ont instauré dans l'équipe une ambiance inégalée.

Mes remerciements vont aussi aux rapporteurs de ce manuscrit, Christophe Thomas et Abderrahmane Amgoune qui ont pris sur leur temps pour lire et juger ce manuscrit. Au même titre, l'autre membre du jury, Frédérique Pourpoint, est chaleureusement remerciée pour sa participation à ma soutenance mais également pour son aide lors de nos collaborations. Merci également à Mostafa Taoufik pour sa présence en tant que membre du jury invité.

Je souhaite aussi remercier Yohann Morin pour m'avoir formé au sein du laboratoire en tant qu'ainé mais aussi en tant qu'ami. Il m'a accordé de son précieux temps afin de m'expliquer les rudiments des manipulations sous atmosphère contrôlées mais aussi à éviter correctement les seaux d'azote liquide. Les karaokés en créole resteront parmi les grands moments de ma thèse, à égalité avec notre tour d'ambulance pour éviter un McDo.

Au sein du laboratoire, j'ai eu le plaisir de côtoyer de nombreuses personnes parmi les thésards, les post docs et les permanents. N'omettre personne relevant de l'impossible, toutes mes excuses en avance aux oubliés. Je commence par mes collègues du labo 911. Duc-Han Nguyen pour son expertise, sa tolérance face à mes blagues vaseuses et sa volonté à m'aider à organiser le laboratoire par la technique du contre-exemple. Sirine Pereira pour tous ses casse-croûtes, ses coups de pied et sa bonne humeur. Les métalleux : Alexis Mifleur et Guillaume Raffa pour avoir partagé leur savoir scientifique mais aussi d'autres savoirs moins enviés (Petit poney, kaamelott, Steel Panthers et j'en passe pour des soucis de décence). J'inclus également Laurent Delevoye comme un membre à part entière du labo 911. Merci à lui pour avoir eu la patience de m'expliquer les techniques RMN, pour sa répartie cinglante et pour ses saluts très amicaux de la main.

Je n'oublie pas mes collègues qui ont partagés mon bureau et qui ont été assez gentils pour être des cibles sans résistance face à mes nerfs. Je commencerai par Adrien et Corentin. Le dynamique duo composé d'un portugais et de Captain Ifmas. Bonne chance à vous pour votre soutenance et merci pour toutes ces références à OSS117. Merci aussi à tous les stagiaires de l'équipe que j'ai dû encadrer sans jamais profiter de leur main d'œuvre pour ma thèse : Julien, Jordan, Romain, Maxime et surtout Mohammed. Je tiens à remercier Mathieu Sauthier pour son extraordinaire bonne humeur communicative et ses conseils toujours utiles. Son équipe a également joué un rôle lors de ma thèse et je vais commencer la liste que j'espère exhaustive dès à présent. Mathieu Drelon pour Nos échAnges geek, nos séaNces de sport et son amItié sans faille. Clément Dumont, une épaule sur laquelle on peut à la fois se saluer, frapper et se confier autour d'une bière ou d'un vélo. Vincent Rysak beaucoup trop sérieux et alcoolique pour son âge. Yann Bernhard, dernier arrivé mais inclus içi car il est fin bien et c'est ça c'est pas faux.

Viens le tour des polymèristes avec qui j'ai partagé à la fois le labo mais aussi de très bons moments. Un énorme remerciement à Nicholas, mon « buddy » de course du samedi et de salon de thé qui m'a permis de développer mon anglais mais qui surtout a su m'aider lors de périodes plus creuses et pour cela il restera un ami très cher peu importe les années et les distances. Félicitations et bonne continuation à Sami Fadlallah (aka Samitraillette). La kawaii Elodie Louisy toujours prête à se dévouer pour finir les gâteaux. Ainsi que les permanents Audrey Favrelle, la jeune brocanteuse, Yohan Champouret, mon camarade du matin, Fanny Bonnet, Philippe Zinc et Thomas Chenal. De nombreux chercheurs ont rythmés la vie du laboratoire et méritent d'être remerciés pour leur aide : Till Bousquet, Lydie Pelinski, Isabelle Suisse, Christophe Michon, Sylvain Pellegrini ainsi que tous les chercheurs de l'UCCS que j'ai pu croiser.

J'aimerais remercier la patience de Claudine Butticaz, pour toujours avoir eu l'amabilité de me réexpliquer les procédures administratives maintes et maintes fois malgré tout le travail qui lui incombe. Merci à Céline Delabre, pour sa bonne humeur et pour m'avoir transmis son expertise sur les nombreux appareils d'analyse à sa charge.

L'une des principales techniques de caractérisation que j'ai utilisée pendant ma thèse a été la RMN solide. Pour ce point, de nombreuses personnes sont à remercier et notamment les personnes qui font vivre le plateau technique et qui ont su toujours se montrer disponible pour (très souvent) m'épauler et pour répondre à mes questions. Merci donc à Marc Bria, Bertrand Revel, Bertrand Doumert, Julien Trebosc et Xavier Trivelli.

J'ai eu la chance lors de cette thèse de réaliser un échange d'un mois au Brésil et pour cela je tiens à remercier grandement Michèle Oberson De Souza pour m'avoir encadré durant cette période. Un énorme merci à Bruno Lenz, Gabriel Pereira pour leur amitié et tout le temps qu'ils m'ont consacré pour me faire découvrir ce superbe pays où je promets d'y retourner. Muito obrigado à toutes les personnes rencontrées à l'UFRGS pour leurs explications et leur gentillesse : Anna, Luiza, Bruna, Casca, Yuri, Laura, Tiago. Je tiens spécialement à montrer toute ma gratitude à Rodrigo Fuscaldo, toujours prêt à rendre service et à me faire découvrir des nouvelles bières brésiliennes.

Finalement, je remercie Laure pour avoir réussi à supporter mon sale caractère durant cette rédaction malgré ses propres révisions, d'avoir pris sur son temps pour être avec moi et pour tous ses bons petits plats. Et merci à ma famille qui a su m'encourager sans même comprendre l'intérêt de ma thèse. Pour finir j'aimerai remercier ma mère qui m'a transmis son esprit critique et sa volonté de comprendre les choses qui nous entourent. Je continuerai de vivre ma vie en suivant son héritage.

Table of contents

1. Preamble

The aim of this thesis is the development of well-defined supported complexes onto silica for an enhancement of catalytic properties compared to their molecular counterparts. We selected potentially highly active molecular electrophilic complexes and thus grafted them onto a silica surface to induce enhanced properties as increased activity or selectivity, recycling of the catalyst or even new catalytic pathways.

To generate such efficient materials, a full understanding of the behavior of the species during the immobilization is needed. This can be achieved thanks to combination of several characterization techniques as infra-red, elemental analysis and solid state NMR. We used the knowledge developed in the laboratory to the preparation of several well-defined materials that have been applied to catalytic reactions in both polymerizations and fine chemistry reactions.

The first chapter will present the state of the art in surface organometallic chemistry and also describe the basics of solid state NMR with a focus on quadrupolar nuclei, which is strongly connected to the research developed here.

The second chapter is devoted to the preparation of supported rare-earth metal catalysts, their full characterization with a focus on solid state NMR and the investigation of their catalytic properties towards C-C bond formation or polymerization reactions.

The third chapter was devoted to aluminum surface chemistry, with the application of (supported) aluminum centers as cocatalysts for ethylene polymerization and oligomerization, and also in carbonatation of epoxide, with a focus on ^{27}Al NMR as a powerful characterization tool.

The last chapter present our attempts at the generation of new silica-based material featuring an amine ligand grafted in the immediate vicinity of a silanol site, which can behave as a bidentate, monoanionic chelate upon reaction with a metal center.

2. Bibliographic study

2.1. Introduction

The development of organometallic chemistry and the accompanying progress in homogeneous catalysts have led to systems able to perform an impressive library of reactions for the synthesis and conversion of chemical species. However, when considering industrial applications, heterogeneous catalysis is the dominating tool, accounting for the vast majority of catalyzed industrial processes. This is the case, despite that, when comparing activity per metal site, homogeneous catalysts are most often more active and selective. Some of the reasons are technological in nature: heterogeneous catalysts are easy to implement in solid-gas phase processes, and also, easier to separate from the reaction mixture, which has an impact on product purification and/or contamination by catalyst's residues. On the other hand, heterogeneous catalysts suffer from several drawbacks. They may require high temperature, have a too short lifetime or be not selective. In addition, the determination of the active site(s) structure can most often be out of reach, due inter alia to the fact that the fraction of active center may be very small within a given material. This induces major difficulties such as no structure-relationship establishment, and empirical developments mostly by trial-and-error processes, as rationalization of catalytic performances of a given material is most often not possible. Ideally speaking, it would be highly interesting to develop preparation methodology reconciling the strength of homogenous catalysis (in short, control over active sites structure, with high activity and selectivity) and of heterogeneous catalysis (easy separation and recyclability of catalysts, thermal robustness).

2.2. Principle of surface organometallic chemistry (SOMC)

Considering these preparation issues, the chemist devoted to the development of catalytic materials must consider the possibility offered by organometallic chemistry, in terms of active site tuning. Based on the assumption that the concept of organometallic chemistry (structure and reactivity) can be transferred to surface chemistry, Basset introduced the concept of surface chemistry (SOMC): this allows, in principle, the design of tailor-made supported catalysts, provided that both the structure and the reactivity of the incoming organometallic complex and of the inorganic support are either mastered, or understood. Obviously, this goes hand in hand with the application of analytical and spectroscopic techniques, aiming at reaching a degree of understanding comparable to what is achieved in molecular organometallic chemistry.

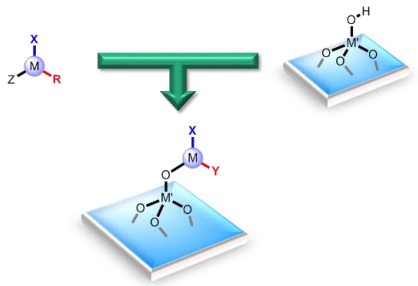

Scheme 2.2.1 Surface organometallic principe

Thus, surface organometallic chemistry (SOMC) focuses on the grafting of organometallic catalyst onto a surface. This surface can be an inorganic oxide like alumina, ceria or silica, but metallic (nano)particles, carbon nanotubes or polymers are also good candidates depending of the envisioned

application. Due to their availability, wide range of types and thermal robustness, inorganic oxides are mostly used. With this kind of surface, the generation of single site catalytic centers can be achieved be controlling the type and the amount of anchoring groups on the inorganic support. Structural and chemical characterization of the material allows to investigate on the thus-generated surface-moieties. Powerful tools have been developed or adapted to meet this goal. Infra-red, solid state NMR, EXAFS and elemental analysis are usually combined to fully characterize these heterogeneous catalysts and assess their structure.

2.3. Historical background of SOMC

The first reports on surface organometallic chemistry were issued by Yermakov in 1976[1], when he reported on the hydrogenolysis of ethane using a supported mixture of molybdenum and platinum supported onto silica, with molybdenum being introduced as the homoleptic tetra allyl derivative. However, the tools required in the full understanding of the underlying chemistry had still to be developed: use of probe molecules to highlight the coordination on the surface[2], in situ EXAFS, solid state NMR or IR[3], and so forth.

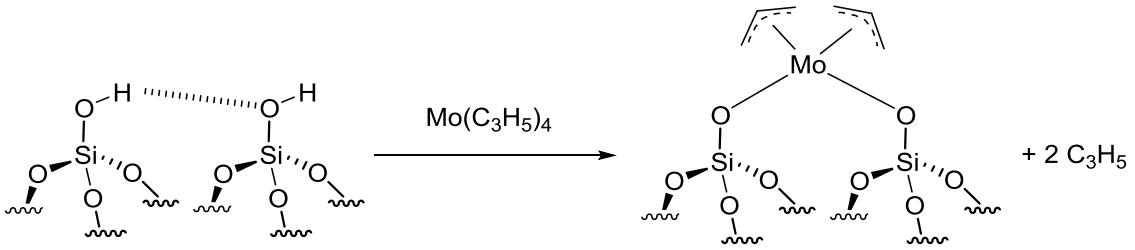

Scheme 2.3.1 First example of SOMC developed by Yermakov

With these methodological developments established, surface organometallic chemistry grew rapidly with various applications. The literature about SOMC is abundant and several reviews have been published on the topic[4,5]. We focus here on silica-grafted species, as this oxide is rather easily tunable and has been used as a support for a very wide range of metals.

An early example can be found in the literature from the Basset group in 1988[6]. In this paper the comparison is made between a molecular catalyst $(\mu\text{-OPh})Os_3(\mu\text{-H})(CO)_{10}$ and its silica-supported equivalent $[(\mu\text{-OSi}\equiv)Os_3(\mu\text{-H})(CO)_{10}$. Both were applied for ethylene hydrogenation and authors reported a stabilizing effect of the silica grafting which allows to achieve better conversion than the molecular catalyst.

A typical early example on the influence of the grafting mode of a surface-supported species on the reactivity was demonstrated in 1994[7] , using carbon monoxide as a probe molecule with bis(allyl)rhodium immobilized onto several oxides (silica, titania and alumina). Authors showed that with low content hydroxyl group on the surface, an active catalyst for the formation of 1,5-hexadiene (using the allyl from the catalyst) is obtained. In the presence of high concentration of silanols ($SiO_{2\text{-}200}$) two reactions occurred. One involving the formation of propene from the allyl ligand and the second one being the insertion of CO into the metal-

carbon bond. This behavior highlights the influence of the silanol surface content onto the formation of various products.

2.4. SOMC applied with silica as a support

2.4.1. Characteristics of silica

Silica is widely used as an inorganic support for the immobilization of metals. Amongst the various types of silica available in terms of texture (ordered, amorphous, porous etc.), flame silica is the preferred support for SOMC. Flame silica (or fumed silica) is made from pyrolysis at 3000 °C of silicon tetrachloride ($SiCl_4$) or from quartz sand. Mainly produced by Evonik (under the name of Aerosil), OCI (Konasil) or by Cabot Corporation (Cab-O-Sil), it is made of spherical particles of diameter a size comprised between 5 to 50 µm, thus with a high specific surface area. Two main surface groups can be found in fumed silica: siloxane (≡Si-O-Si≡) and silanol (≡Si-OH). Siloxane is the core structural unit of silica and is found both inside the particle and on its surface, whereas the silanol are in their vast majority on the surface, being the species of interest regarding the grafting properties of the silica. Three types of silanols can be observed (Figure 2.4.1). The geminal silanol has two reactive oxygen atoms linked on the same silicon center, and is theoretically highly reactive but less common than the vicinal silanol. This last type of silanol bears a single hydroxyl group, and is close to a neighboring silanol with which it establishes a hydrogen bond. These groups can exist as clusters, depending on the surface density. If the silanol moieties are too far one from each other, no interaction takes place, resulting in non-interacting or isolated silanol groups.

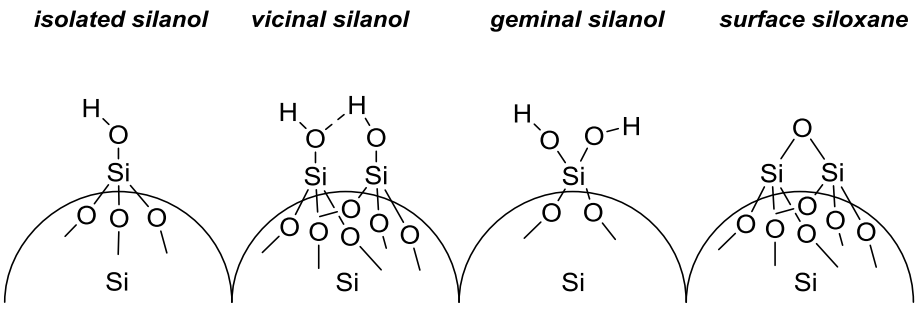

Figure 2.4.1 The silanols and siloxane from the silica

The several silanol types possess different reactivity towards the metal complexes (Scheme 2.4.1). Tuning the amount of it on the surface is the most appropriate way to obtain well defined sites. To achieve this, the silica is heated in order to condensate the silanols into siloxane bridges, thus releasing water and reducing the quantity of silanols available on the surface[8]. The Figure 2.4.2 presents the decrease of OH on the surface depending on the temperature8. From infrared spectroscopy (see below), it has been shown that heating the silica at 700 °C for 15 h will result in the sole presence of non-interacting silanols on the surface.

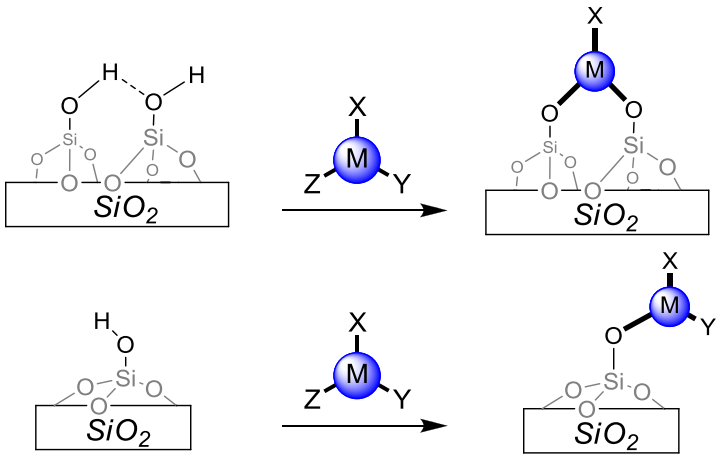

Scheme 2.4.1 Influence of the silanol type toward the grafting of organometallics

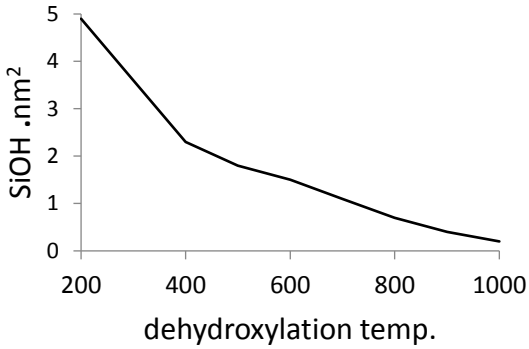

Figure 2.4.2 Concentration of SiOH.nm^{-2}depending of the temperature

The influence of the thermal treatment is evidence by the infrared spectrum of thermally treated silica, thanks to the specific elongations bands of the SiO-H function. The Figure 2.4.3 presents the differences between a silica heated at several dehydroxylation temperatures and confirms the influence of this treatment on quantity and nature of surface silanol groups.

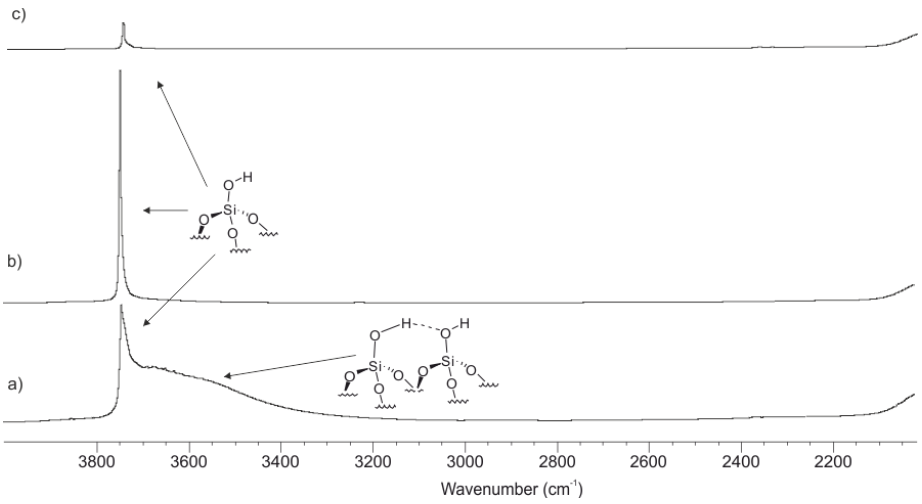

Figure 2.4.3 DRIFT spectra of a) $SiO_{2\text{-}200}$, b) $SiO_{2\text{-}700}$ and c) $SiO_{2\text{-}1000}$

Thus, with conveniently dehydroxylated silica at hand, the immobilization of metal species can be performed by reacting these two components, followed by washing of the resulting material to remove the unreacted products along with potential by-products, and by drying to obtain the material as illustrated in the Scheme 2.4.25

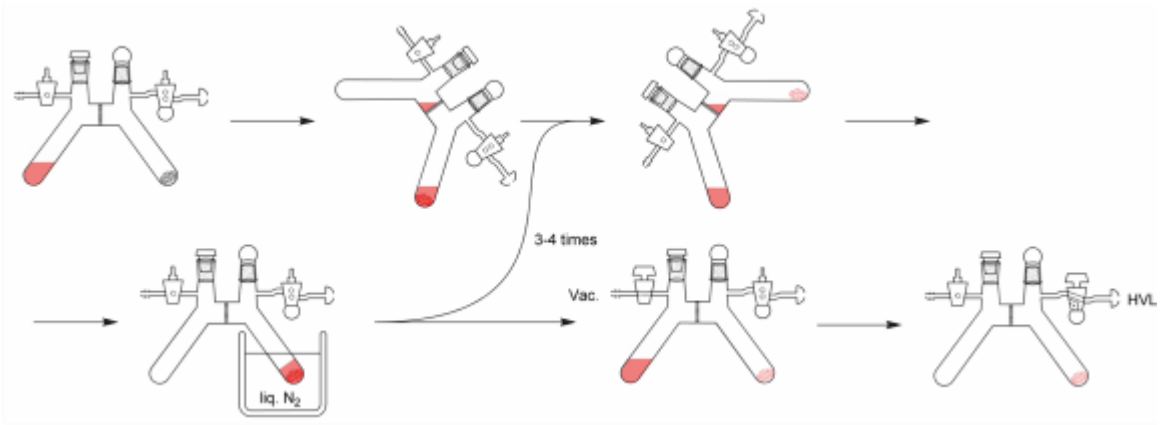

Scheme 2.4.2 Grafting procedure of an organometallic onto a dehydroxylated silica

2.5. Rare-earth metal silica-supported single site catalyst

Rare-earth metals have generated significant interest thanks to their applications in catalysis. Indeed, they present good activity for ring-opening polymerization of ε-caprolactone[9], lactone or even polymerization of methylmethacrylate[10].

In the specific case of rare-earth metals, the immobilization of alkyl species is not a practical option, as these species are significantly sensitive to oxygen and moisture, which is a severe drawback for the handling and synthesis of the resulting materials.

As described above, in order to generate well-defined moieties on the surface several options are available. In a fist place, the direct reaction of one silanol with the rare-earth complex involving at least one X ligand per hydroxyl group to react with, that will be released during the reaction to form SiO[Ln] bonds[11]

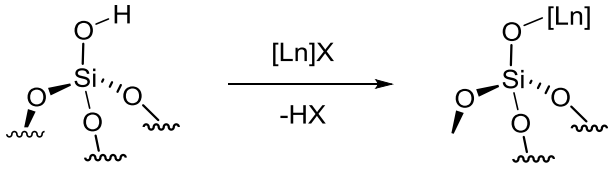

Scheme 2.5.1 Direct reaction of lanthanide complex with silanol from the surface

Alternatively, two step reactions is also an option if the catalyst present some restrictions regarding the reactivity of the silanol. A pre-grafting is made using reagents such as aluminum alkyl species (AlR_3, MAO etc.), magnesium alkyl derivatives (Grignard compounds), etc.[12] Then the lanthanide complex reacts easily with the new surface species, generating alkylating species.

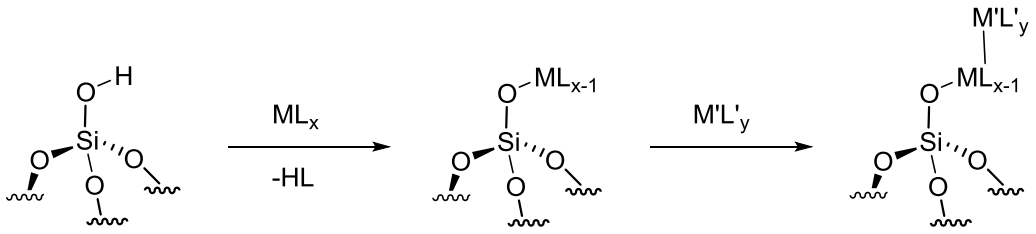

M= Al, Mg
L,L'= monoanionic ligand

Scheme 2.5.2. Two-step grafting of lanthanide complex onto silica

Several types of rare-earth supported catalysts were developed along the years. The main groups are detailed below:

- Rare earth alkoxide

Metal alkoxide [$M(OR_x)_y$] are mainly used in the development of complex ceramic materials (i.e., electroceramics, superconductors, and computer memories), and have also been described as good catalysts for polymerization[13] and fine chemistry reactions[14]. Immobilization of neodymium alkoxide $Nd(Otriox)_3$ (triox= tris-*tert*-butylmethoxide) onto a mesoporous material MCM-41, it is characterized by a large surface and a large pore volume (heated at 250°C) to obtain well-defined site was made by Anwander in 1998, tested for reduction of 4-tert-butylcyclohexanone to a primary alcohol with the Meerwein-Ponndorf-Verley reduction[15]. He showed the formation of bipodal species, based FTIR, elemental analysis and nitrogen physisorption explained by the presence of vicinal silanols (Scheme 2.5.3.)

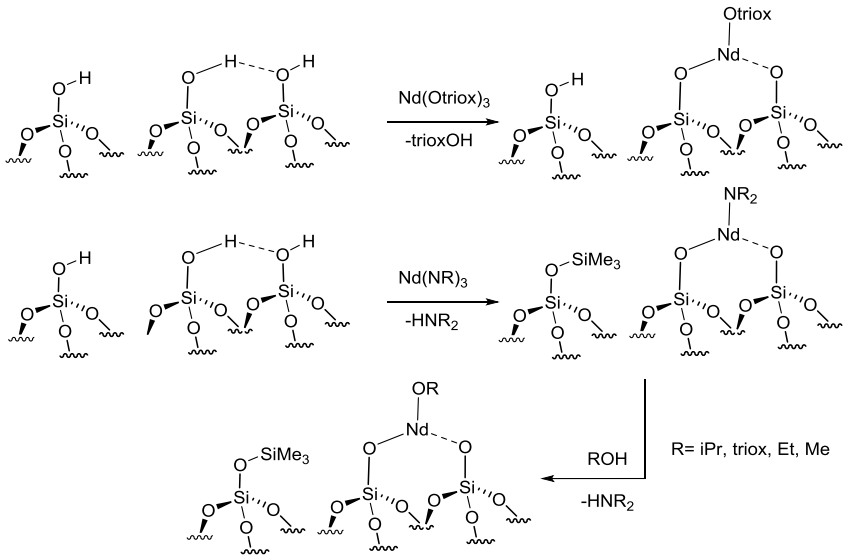

Scheme 2.5.3. Immobilization of $Nd(OR)_3$ onto silica

A further pathway to formation of surface alkoxides was investigated, using in a first step a neodymium silylamide as reactant for the MCM-41, which was then subjected to alcoholysis to generate the alkoxide sites (allowing the generation of several $Nd(OR)_x$ depending of the

alcohol used for the second step). This second route to generate the supported species illustrates one of the inconvenient of using $Ln(OR)_3$ for SOMC. Indeed, the direct grafting of this catalyst is always incomplete and induces the release of alcohol that will interact with the surface.

Alkoxide yttrium complexes were immobilized onto several support (zirconia, silica and alumina)[16] and are active initiators for the ring-opening polymerization of 2,2-dimethyltrimethylene carbonate. Another drawbacks is described in this paper, where rare-earth metal aggregates are observed on the surface, preventing precise design of surface sites (Scheme 2.5.4).

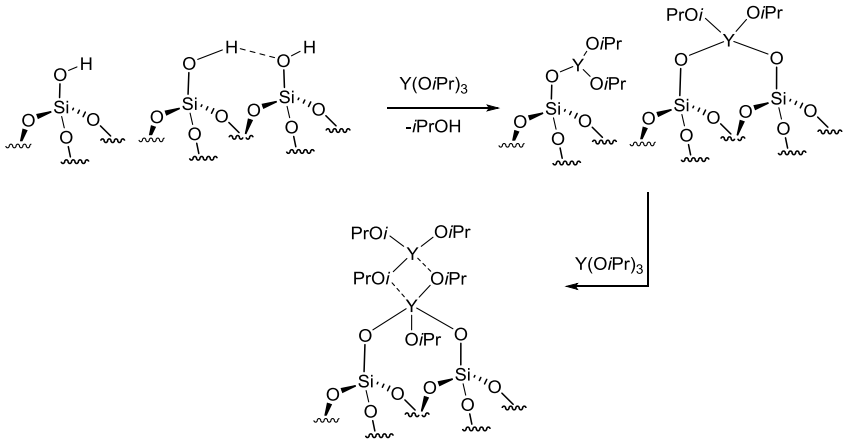

Scheme 2.5.4. Grafting of $Y(OR)_3$ and its aggregation onto silica support

Other examples can be found in the literature showing the activity of rare-earth metal alkoxide catalysts compared to their heterogeneous equivalent[17] showing that the grafting of the metal onto the silica can lead to new catalytic properties.

- Rare-earth (silyl)amides

In order to solve the difficulties encountered with the alkoxide precursors, silylamide rare earth species have been successfully immobilized onto surfaces. The silylamide complexes present several advantages like high reactivity towards protonolysis, better stability that the alkyl precursors and the release of silylamine that can silylate the unoccupied silanols (favorable atom economy and lipophilicity of the modified support). One of the first example was presented by Anwander producing various species using $N(SiMe_3)_2$ or $N(iPr)_2$[18] derivatives onto MCM-41. Contrary to alkyl oxides the consumption of surface silanol is fast and complete and the only side-products of the surface reaction are a non-coordinating amine and NH_3, which can easily be removed under high vacuum at 80°C.[19] Mono- and bipodal species are observed depending of the abundance of interacting and non-interacting silanols on the surface. Indeed, our group and others showed how to control the ratio of mono- and bipodal species by dehydroxylation temperature, which has an important influence on the resulting catalytic performances[20,21]. Once the efficiency of the generation of well-defined sites has been shown, several examples have been developed. A non-

exhaustive list was made in *Modern Surface Organometallic Chemistry*4 and highlight the numerous examples for these materials.

The applications are numerous for supported rare-earth metal silylamides: for instance, these are highly active for the polymerization of ε-caprolactone,[22] as well as in other polymerization reactions[11]. Moreover, examples showed good results in fine chemistry (90% of benzaldehyde conversion with $Y[N(SiMe_3)_2]_3$ for Tischenko reaction, complete conversion and high selectivity (82% for one product) in alkyne dimerization, etc.)[22]

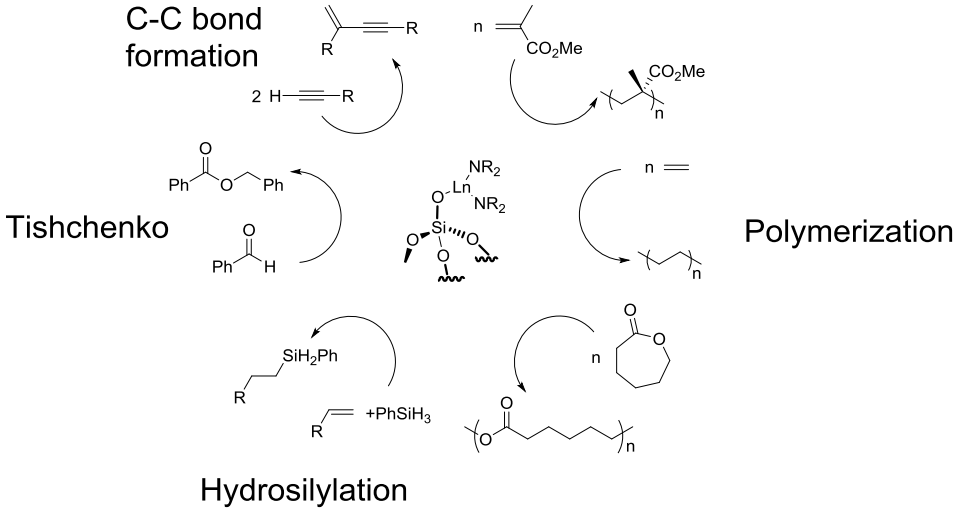

Scheme 2.5.5. Examples of catalytic reactions available for silica-grafted rare-earth metals

Unfortunately, these materials are highly sensitive to air and moisture which makes the recycle of the material after one cycle difficult. However, researchers showed activity for 2 or 3 cycles, with rigorously controlled experimental conditions[11].

-Ln alkyl and hydride species

As mentioned above, less employed that the silylamide compounds, the alkyl and hydrido rare-earth catalysts are known to be highly reactive but in the same time sensitive to moisture. Regarding the alkyl ligand the cyclopentadienyl (Cp) derivatives proved to be ligands of choice to solve this problem. Moreover the Cp*, C_5Me_5, showed even more stability than the Cp[23]. First examples of immobilization of rare-earth metal alkyl complexes were developed in industrial laboratories of Mazuren and of Showa Denko, when they immobilized species such as $[Cp_2*Sm(\mu\text{-}H)_2]$[24], $[Me_2Si[C_5H_2(SiMe_3)_2]_2]LnCH(SiMe_3)_2$ (Ln = Y and Sm) or $Cp_2*NdCH(SiMe_3)_2$onto inorganic supports, as described in patents[25]. These catalysts are highly active for olefin polymerization. Moreover, in 2004 a $Cp_2*SmMe(THF)$ complex was immobilized onto a silica modified with alkylaluminum, and applied in polymerization of methylmethacrylate with total conversion to polymethylmethacrylate unfortunately with a poor control of the system (polydispersity = 1.45 instead of 1.03 with the homogeneous version but higher M_n : 16.4 x 10^5 and 0.5 x 10^5 for the grafted catalyst and the homogenous one respectively) [26]. The polymerization of isoprene can be performed

with $Nd(AlMe_4)_3$ and Et_2AlCl immobilized onto several types of silica support using 2 pathways to generate the materials (Scheme 2.5.6)[27].

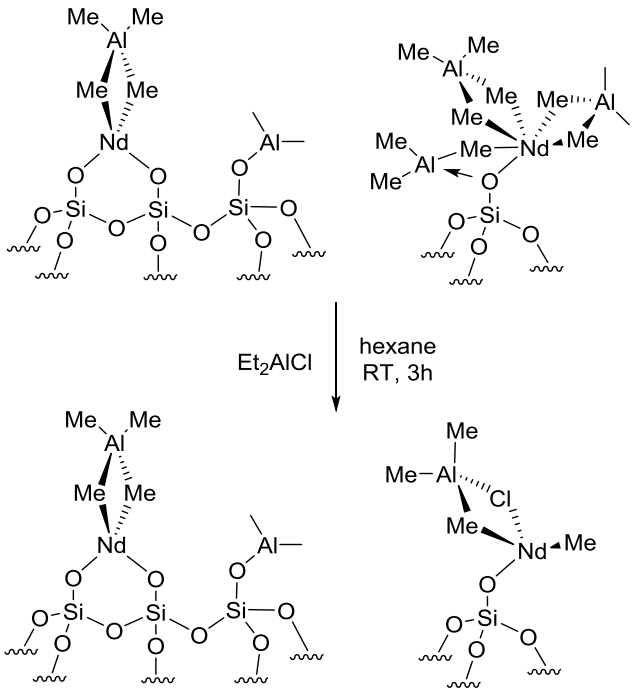

Scheme 2.5.6. Proposed surface species of hybrid materials after the immobilization of $Nd(AlMe_4)$ and Et_2AlCl on mesoporous silica.[27]

Supported Ziegler-type neodymium surface species have been prepared by reacting molecular components composed of $[Nd(naph)_3]$ and alkyl aluminium reagents such as $Al_2Et_3Cl_3$, $Al(i\text{Bu})_3$ and/or $Al(i\text{Bu})_2H$ with silica[28]. These materials display interesting properties in butadiene polymerization, though improved properties may be expected provided that rigorous synthetic control would be applied to generate well-defined active sites.

2.6. Silica-supported single-site aluminum species

In literature a wide range of examples can be found about the use of aluminum in SOMC, mostly as alkyl derivatives. This owes much to the fact that aluminum alkyls (and chloroalkyls) are commercially available and highly reactive towards protonolysis. Their synthesis and early use was pioneered by the Ziegler group in Mülheim, in the aftermath of WW2. Thus, Ziegler and coworkers reported on the Aufbau reaction, where aluminum alkyl species perform oligomerization of ethylene under forceful conditions, affording longer chain alkyls which can undergo further functionalization into valuable products[29].

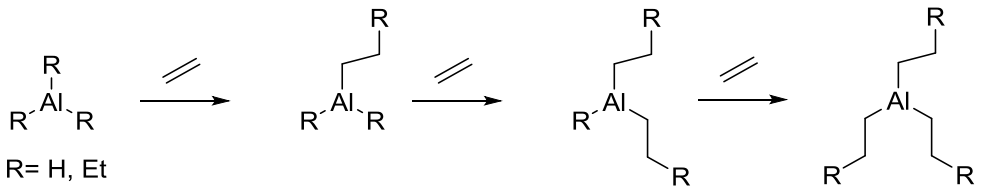

Scheme 2.6.1 Aufbau reaction for the oligomerization of ethylene

In the same line, aluminum species were used from the early 1950's as co-catalysts for (alkylating agent) for ethylene polymerization. The so-called heterogeneous Ziegler–Natta catalysts are probably the most known example for such catalytic process[29]. In 1953, Ziegler showed that $TiCl_3$, prepared by reduction of $TiCl_4$ with Et_3Al, polymerizes ethylene and propylene to high molecular weight polymers at low pressure[30]. In this system, the aluminum alkyl alkylates the transition metal to promote initial alkene insertion and subsequent chain propagation.

Further developments were brought by Kaminsky in 1980[31], when he reported the serendipitous discovery of methylaluminoxane (MAO), of general formula $[AlMe(O)]_n$. This cocatalyst is extremely efficient in activating molecular group 4 complexes, most particularly metallocenes, which initiated an incredible quantity of academic and industrial research efforts. The outcome was the development of catalysts able to achieve efficient industrial production of tailor-made polyolefins (control of molecular weight, of tacticity, of comonomer incorporation etc.). Nowadays, industrial processes rely on MAO supported on silica (or various supports) as a solid activator for alkene polymerization in gas phase or slurry processes[32]. However, the complex structure of (molecular or supported) MAO still raises a challenge in the full understanding of this peculiar reactivity.

The industrial importance of silica-supported aluminum alkyls has induced several research groups to investigate the corresponding surface chemistry.

For instance, Anwander[33] described the grafting of trimethylaluminum onto MCM-41. He studied the capacity of the silicate material to immobilize various amounts of the organoaluminum. Several techniques (elemental analysis, FTIR nitrogen physisorption and multinuclear solid-state NMR) were employed and revealed a $SiCH_3/AlCH_3$ ratio of approximately 0.45 which indicates a highly distorted geometry and polarized charge density, respectively, at the aluminum centers (Scheme 2.6.2).

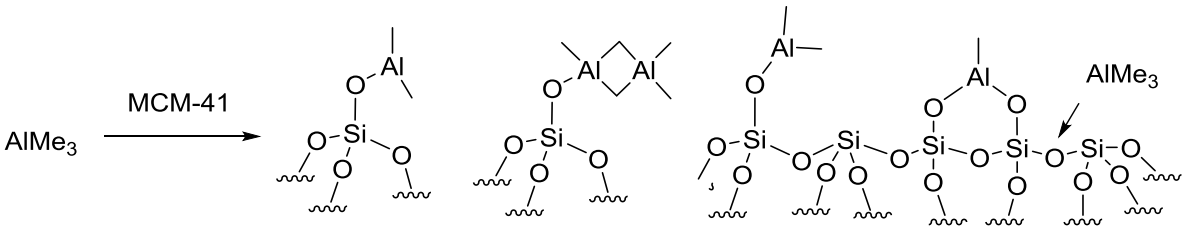

Scheme 2.6.2 Possible surface species of the immobilization of $AlMe_3$ on MCM-41

Maciel also investigated the surface chemistry of $AlMe_3$ thanks to combination of mass balance analysis, infrared and NMR spectroscopy[34]. He concluded that the aluminum on the surface exists predominantly as a five-coordinate species and detailed the formation of all the sites founded on the surface.

Concerning the challenge to design of a well-defined aluminum alkyl species, Taoufik and collaborators reported in 2011 that Al*i*Bu_3(THF) reacts very selectively with the silica surface (dehydroxylated at 700 °C), to afford a single type of species, [(≡SiO)$_2$Al(*i*Bu) (THF)] through consecutive protonolysis and transfer of an alkyl group onto the surface[35]. This material was used as a scaffold for the anchoring of various types of cocatalysts, prepared via a further functionalization of the Al center by introduction of a phenolic moiety. This allowed access to catalysts for olefin metathesis[36], olefin polymerization[37], or to alkyne semi-hydrogenation using frustrated Lewis pairs[38]. The same groups also described the reaction of Al*i*Bu_3 with gamma-Al_2O_3 and its subsequent hydrogenolysis. Whereas the reaction of the trisalkyl species with the support resulted in a complex mixture, the hydrogenolysis afforded well-defined aluminum hydride centers, as demonstrated by advanced solid state NMR[39]. This material is active in ethylene polymerization and hydrogenation.

In addition, the surface chemistry of triethyl aluminum was investigated by Coperet, using a high specific area silica that has been dehydroxylated at 700 °C[40].

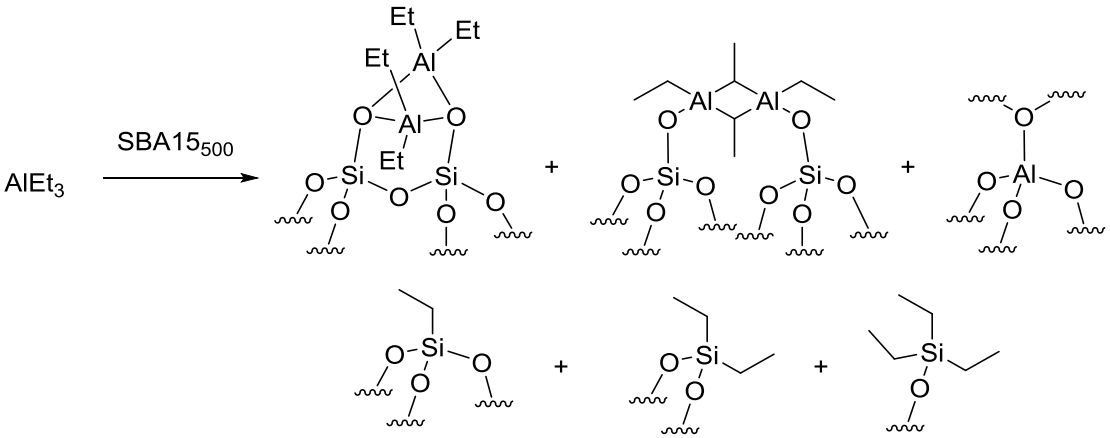

Scheme 2.6.3 Grafting of $AlEt_3$ onto $SBA15_{500}$

As was already described in the literature, a complex mixture of species was obtained, and authors proposed that these consist of mostly by dinuclear, tetracoordinated aluminum sites. These conclusions were reached by combination of experimental (mostly ^{27}Al NMR) and theoretical investigations.

These studies were extended to uncomplexed Al*i*Bu_3 by both Basset[41] and Coperet[42]. The same conclusions about the uncontrolled reactivity towards the silica surface were reached, with as a difference the fact that β-H elimination from the *i*-butyl group was a side-reaction causing formation of aluminum hydrides as transient species, or as species with limited stability Scheme 2.6.4.

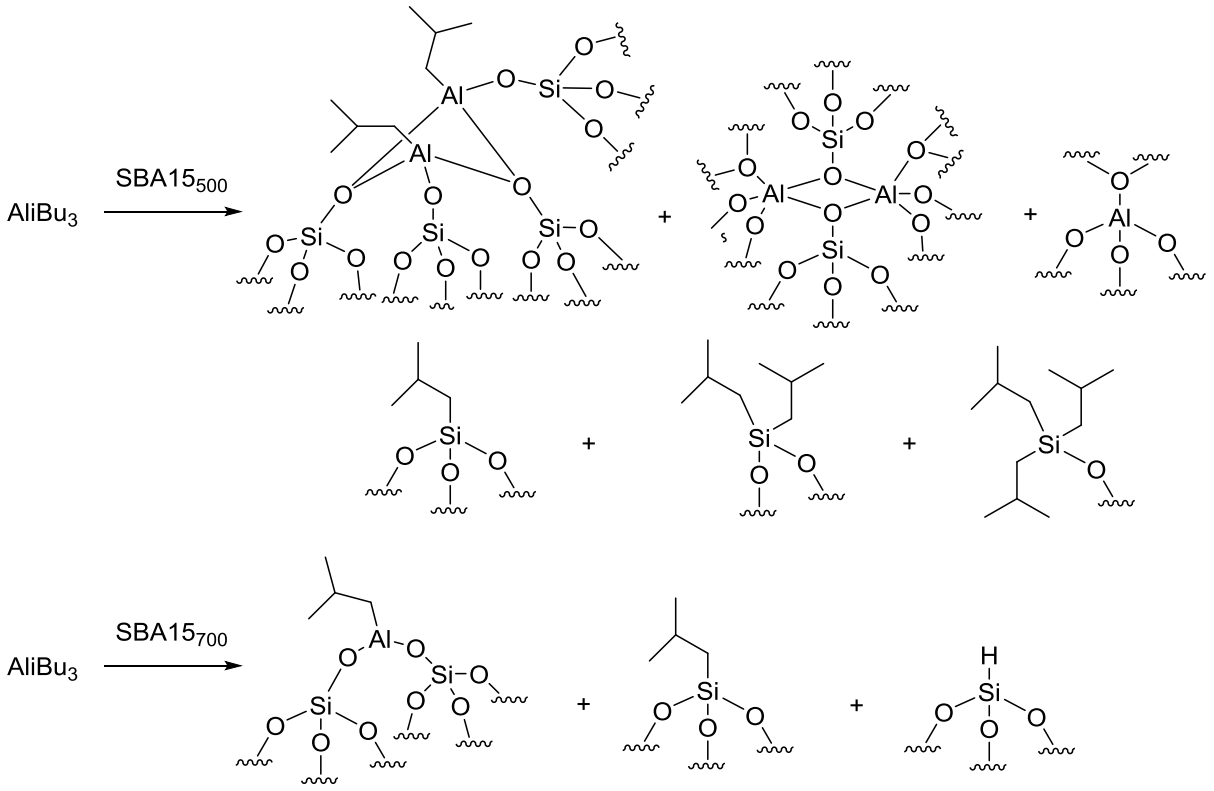

Scheme 2.6.4 Grafting of Al*i*Bu$_3$ onto SBA15$_{500}$ and SBA15$_{700}$

Another class of reaction catalyzed by aluminum is the Meerwein–Ponndorf–Verley (MPV) reduction of ketones and aldehydes (Scheme 2.6.5).

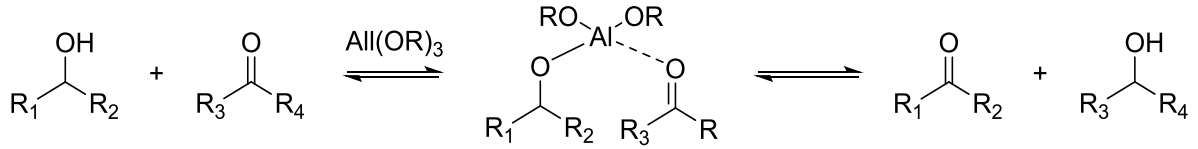

Scheme 2.6.5 Meerwein-Ponndorf-Verley reduction of ketones and aldehydes

Indeed, Al(O*i*Pr)$_3$ has been successfully grafted onto mesoporous silica[43] (Scheme 2.6.6) and has been applied for cyclohexanone derivatives reduction. However, the precise definition of the grafted sites remains unreported.

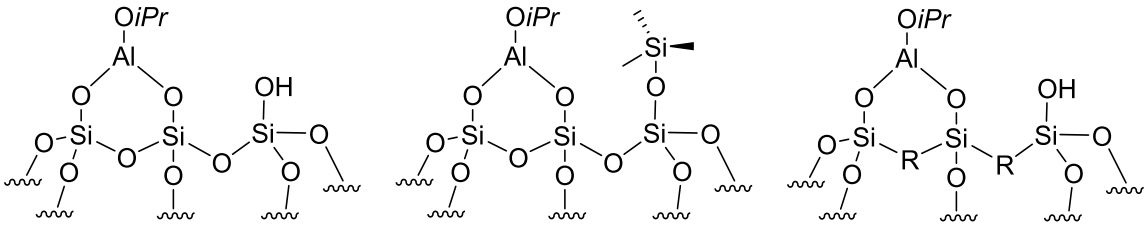

Scheme 2.6.6 Grafting of Al(O*i*Pr)$_3$ onto mesoporous silica

Thus, as a conclusion, the surface chemistry of aluminum is quite complex, and strongly depends on the nature of the grafted species. Indeed, the propensity of aluminum to form

bridges and thus polynuclear entities has to be taken into account. Also, it has been shown that the high reactivity of alkyl species towards inorganic support induces side-reactions such as insertion into the inorganic network and therefore, loss of a reactive moiety from the aluminum center. To help in the understanding of these materials, in particular in the case of aluminum which features an NMR active, spin 7/2 isotope (^{27}Al), solid state NMR offers exciting possibilities for detailed understanding. This will be reviewed in the next session.

2.7. Solid state NMR of spin ½ and quadrupolar nucleus as a probe for structural properties

2.7.1. Introduction to NMR principles

Nuclear Magnetic Resonance, or NMR spectroscopy is a non-destructive analytical technique used in both academia and industry to determine the structure of a compound or a material, to analyze its composition or also to probe its purity. NMR uses the ability of a magnetic field to disturb the fundamental energy of nuclei that possess a nuclear spin (Scheme 2.7.1). Indeed, many nuclei have a spin I (I≠0) and are electrically charged which means that when a magnetic field is applied, the magnetic moment, μ, associated to the nucleus can take 2I+1 orientations. The magnetic moment of a spin I is proportional to the gyromagnetic ratio of a nucleus, γ, an intrinsic property of a spin I≠0 nucleus. In the presence of a magnetic field B_0, the magnetic moment precesses about the B_0 field at a frequency $\omega_0 = -\gamma B_0$, called the Larmor frequency. If the orientation of the magnetic moment is in the same direction than the magnetic field (B_0) the energy level will be higher. It is lower if they are in opposite direction. An NMR experiment consists in a pulse excitation at the Larmor frequency of a given nucleus. An energy transfer is possible between different energy levels, generally a single energy gap. When the spin returns to its fundamental level, under the effect of the magnetic field B_0, the transverse relaxation that is measured into an FID (Free induction Decay) can be influenced by the local interactions of the nucleus with its environment. This frequency can be measured in many ways and further processed in order to obtain a NMR spectrum (Scheme 2.7.2). The interactions of interest in solid-state NMR are the chemical shift, the chemical shift anisotropy, the dipolar coupling and the quadrupolar interactions (spin I > ½).

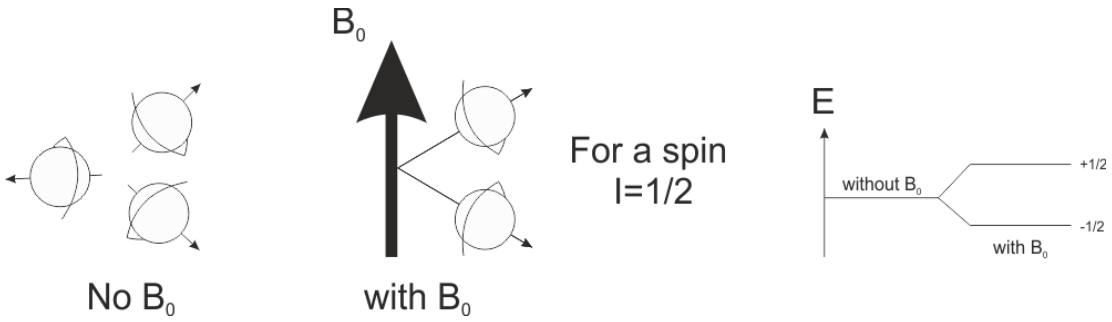

Scheme 2.7.1 Effect of magnetic field (B_0) on nuclei energy

The most important interaction in NMR (liquid- and solid-state) is the one corresponding to the interaction of the electronic structure with the magnetic field. The electronic structure acts as a shielding around the nucleus, which is in turn dependent of the chemical environment. For example, a general law is to consider that for a given nucleus, the more electron-poor the nucleus is, the higher the frequency will be. Other interactions that can influence the NMR signal will be discussed later. It is important to note that the frequency recorded will be also directly influenced by the magnetic field applied on the sample (B_0). To allow comparison between two spectra recorded at different fields, a non-magnetic field-dependent unit is used: the chemical shift. Noted as δ or CS, it is expressed in parts per million (ppm) and is the result of the equation: $\delta = \frac{\nu - \nu 0}{\nu 0} \times 10^6$, where ν is the considered frequency within the sample and ν_0 is the reference frequency for the considered nucleus (TMS for ^{1}H, ^{13}C and phosphoric acid for ^{31}P for example).

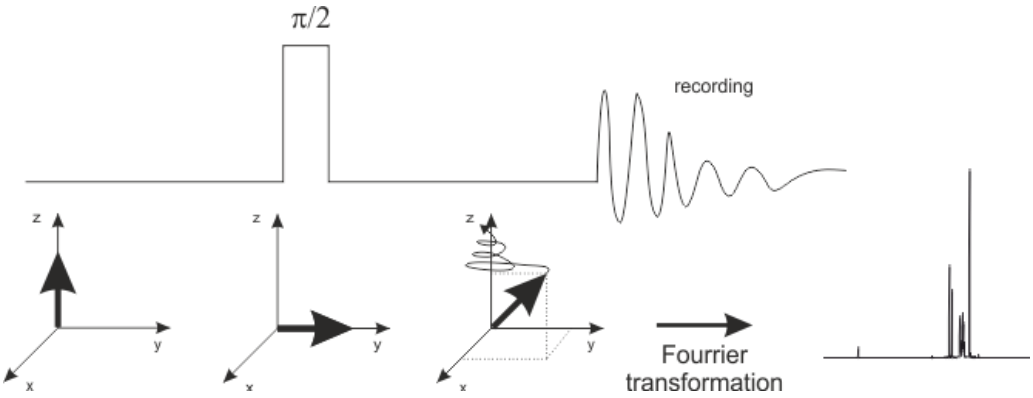

Scheme 2.7.2 Typical of NMR sequence

For each nucleus a frequency will be recorded and a signal will correspond to a species.

The electrons around the nucleus move within the magnetic field and creates a second one. It opposes the applied field: atoms with higher induced fields (i.e., higher electron density) are designated as “shielded”, relative to those with lower electron density, thus designated as “deshielded”. The variation of the chemical shift can be explained from varying degree of shielding or deshielding. For example, a proton near to an electronegative atom will be deshielded and will resonate at a frequency higher than otherwise expected. The main factors that can influence the chemical shift are the electronic density of a nucleus, the electronegativity of the environment around the nucleus and the anisotropy of the induced magnetic field (depending on the geometry of the molecule).

The relaxation frequency of a given nucleus A, will be affected by the state of a neighboring nucleus X, covalently bound. This effect is known as spin-spin coupling (J) which can cause splitting of the signal for each type of nucleus into several lines (Scheme 2.7.3). In liquid NMR, tables of coupling constants can be found and help to identify the connectivites around the observed nucleus. Its magnitude depends on the considered nuclei, varying between 0 and 100 Hz. They are often ignored in solid-state NMR studies as their magnitude is much lower than that of other interactions.

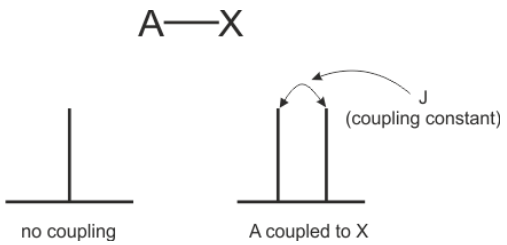

Scheme 2.7.3 Coupling constant effect

2.7.2. Specificities of Solid state NMR

Liquid state NMR is a cornerstone in the synthetic chemistry analytical toolbox. Its counterpart, solid-state NMR is also nowadays routinely used for a wide range of applications.

Solid-state NMR, compared to liquid NMR, presents some pros and cons. For the synthetic chemist, the main advantage is the study of insoluble materials that cannot be analyzed otherwise. The other interest is to determine the structure of a compound in its solid form and not in solution, where solvents and other physical perturbations can lead to distorted information (especially when the sample is designed to be used in its solid state). In the solid state, there are other interactions (that are averaged in liquid) that can prevent a direct interpretation and lead to broad NMR lineshape. For spin ½ nuclei (^{1}H, ^{13}C, ^{31}P, etc.), these additional interactions are the dipolar coupling and the chemical shift anisotropy. In the case of a powdered samples, the amplitude of the interaction will be dependent on the orientation of each crystallite with respect to the magnetic field B0. This anisotropic characteristic of the dipolar and CSA interactions generally leads to a broadening of the NMR resonances in the solid-state. The dipolar interaction is the direct interaction between two magnetic dipoles (two nuclei of spin $I \neq 0$) through space. If the dipolar interaction is averaged out in the liquid state, thanks to fast Brownian movements, it is a dominant interaction in solid-state NMR, with values that can exceed several kilohertz of magnitude. This is illustrated in Figure 2.7.1, which shows a much broader resonance for the ^{31}P signal in the solid-state than in the liquid-state.

In order to average out the dipolar interaction or at least to reduce its effect on the spectrum, one may spin the sample at high speed about a rotational axis inclined at an angle of 54.7°, the so-called Magic Angle Spinning or MAS)[44]. The MAS method is nowadays routinely used in most solid-state NMR experiments and technical improvement in the last decades allows for MAS speeds up to 100 kHz and beyond to be reached.

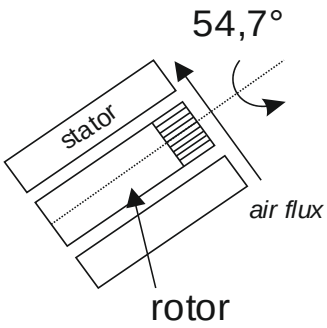

Scheme 2.7.4 Magic angle spinning (MAS)

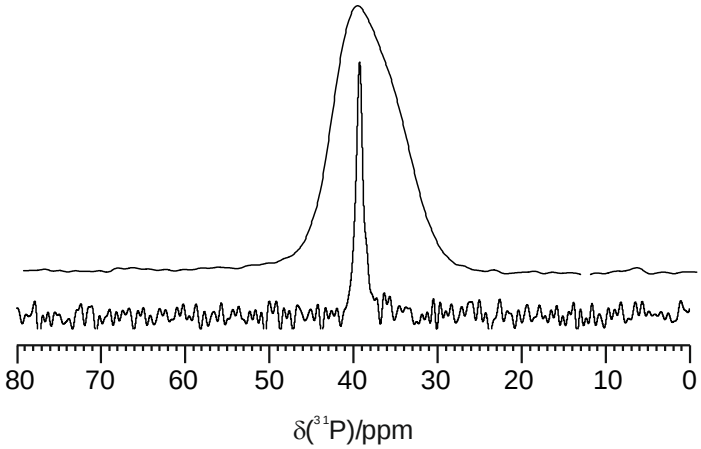

Figure 2.7.1 Comparison between MAS solid state (top spectrum) and liquid (bottom spectrum) ^{31}P NMR of $Sc[N(SiMe_3)_2)_3(OPPh_3)$.

Moreover, for each crystallite orientation within the magnetic field, the chemical shift will have a different value. This means that in a sample we see all the orientations taken by the crystallite, which results in a broader signal. This phenomenon is characterized by a physical parameter called chemical shift anisotropy (CSA). Once again, the high speed rotation at MAS will reduce this interaction. If the rotation is not fast enough, spinning side bands will be observed in addition to the main band. The study of CSA can give precious information about the geometry of the molecule. In fact, if the asymmetry around the nucleus is high the CSA will be increased and the side bands will be more intense. The intensity of the signal is distributed within the ensemble of the central signal and the spinning side bands. A consequence of this is that when increasing spinning speed, the spinning side bands are stretched further apart which thus emphasizes the main signal. It is also important to remind that the CSA interaction is directly proportional to the magnetic field B_0. As a consequence, increasing the magnetic field B_0, will lead to an increase of the anisotropic part of the CSA interaction. As the distance between the spinning side bands is the rotation frequency in Hz, when increasing the magnetic field intensity, the spinning side band manifold will be more intense as spacing in ppm is smaller. Thus, in the case of systems (or nuclei) featuring high CSA such as ^{51}V, it may be counterproductive to increase the magnetic field (i.e to switch to a spectrometer with higher B_0).

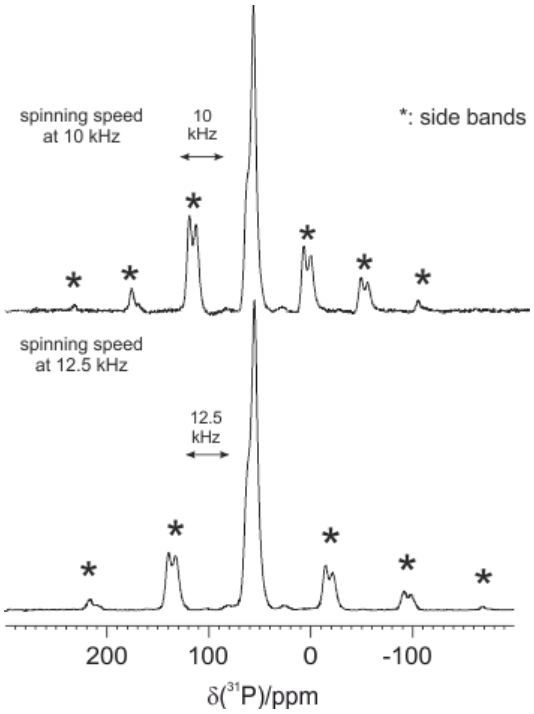

Figure 2.7.2.Influence of the spinning speed onto the observed spectrum

2.7.3. Solid-state NMR with ½ spin nuclei

Despite the broadening of signals, nuclei typically analyzed in liquid state NMR can be used in solid-state NMR affording spectra with rather good spectral line-width. In fact, due to physical properties the excitation of spins in solid state requires higher electric power which in the same time allows to observe nuclei that are not commonly investigated in liquid as they need high power (mostly 100 W amplifiers are used in liquid instead of 1000 W in solid). However, if the principle remains the same, specific sequences have been designed to resolve inherent problems encountered in solid state NMR.

2.7.3.1. Direct acquisition

This basic sequence[45] is composed by a simple 90° pulse then the relaxation is recorded. It affords a 1D NMR spectrum without any enhancement of the signal or any improvements. If needed, a better sequence will be use later on.

2.7.3.2. Cross-Polarization (CP)-MAS

The CPMAS sequence, for Cross Polarization Magic Angle Spinning was proposed by Pines and coworkers in 1973[46], and the first ^{13}C NMR spectra was presented by Schaefer in 1977[47]. The aim of the sequence is to transfer the polarization of a high receptive nucleus (almost always ^{1}H) to a less abundant and less responsive nucleus. It helps enhancing the signal/noise ratio and leads to a faster recording of spectra. The main disadvantage of this technique is that the intensity of the signal that will be observed is directly linked to the close environment of the site. If a nucleus is surrounded by many protons, its intensity will be enhanced much more than that with a few protons around. Thus, the CPMAS sequence

cannot be used for quantitative measurements, even more when considering that the polarization pulse may not totally transfer the whole magnetization because of relaxation phenomena. Figure 2.7.3 illustrates this effect with an example of a silica material featuring 3 different environments. Using direct acquisition (MAS), the spectrum was acquired in 15 h in order to get a decent signal/noise ratio. Using the CPMAS sequence, the spectrum is obtained within 4h only. The information about the existence of 3 main sites is the same for both spectra. However, the intensity of each peak is different and only the MAS spectrum, obtained with a direct acquisition pulse sequence (a) can be used for quantitative measurements.

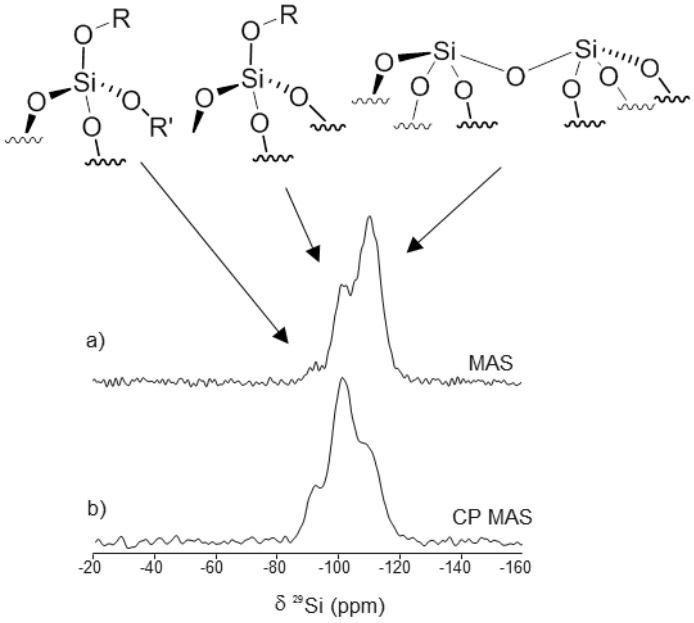

Figure 2.7.3. (a) ^{29}Si MAS spectrum and (b) $^{1}H \rightarrow {}^{29}Si$ CPMAS NMR of a silica-type material.

2.7.3.3. DQ-SQ

The Double-Quanta Single-Quantum experiment, developed by Spiess' group, leads to a two-dimensional homonuclear correlation spectrum, which gives information about spatial proximities by using the dipolar interaction[48]. As illustrated in Figure 2.7.4, self-correlation signals on the diagonal reveal proximities between sites of the same kind (A-A for example), in opposition to off-diagonal signals which result from the spatial proximities between two different chemical environments (A-B or B-C in Figure 2.7.4 or signal 1, 2 and 3 on the Figure 2.7.5). It is a very important experiment for the characterization of surface catalysts as it uses the high NMR sensitivity of ^{1}H to probe the proximity between the different sites, as illustrated in Figure 2.7.5.

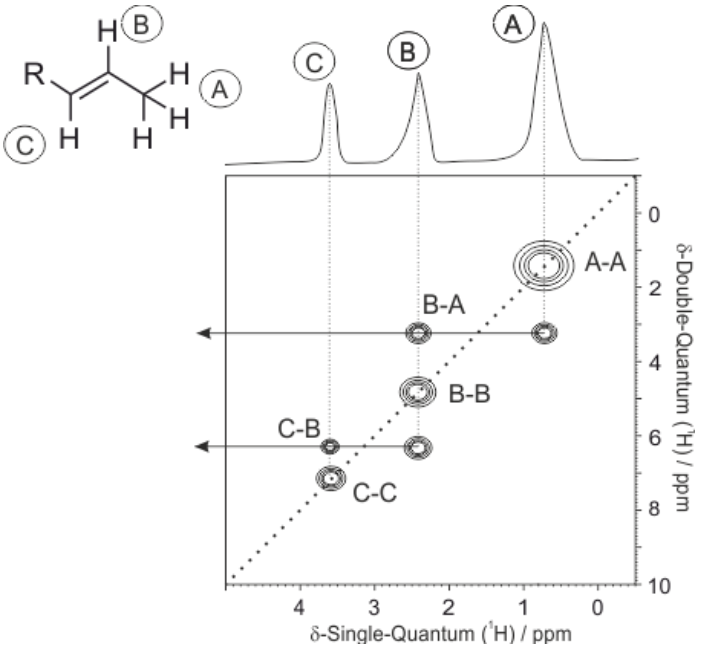

Figure 2.7.4 Simulated DQSQ experiment

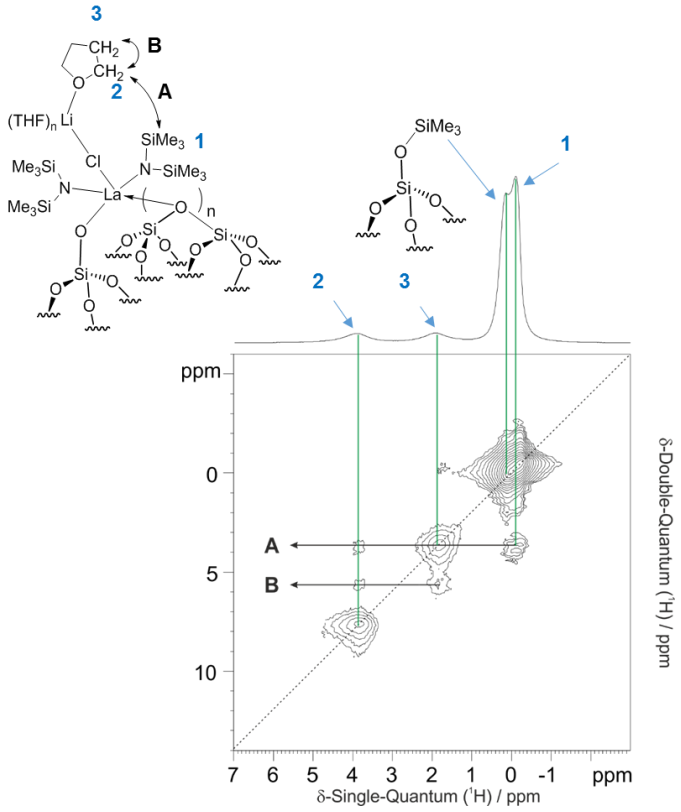

Figure 2.7.5 ^{1}H-^{1}H DQ-SQ MAS experiment of $Li(THF)_3[La\{N(SiMe_3)_2\}_3(Cl)]$

2.7.3.4. HETCOR

In solid-state NMR, the heteronuclear correlation experiment, denoted HETCOR, is a 2D NMR experiment where two different types of nuclei are correlated through space (i.e. using the dipolar interaction) by adding a CP transfer at the beginning of the pulse sequence. The

so-called CP-HETCOR pulse sequence leads to a 2D spectrum where the ^{1}H spectrum in the indirect dimension is correlated to the CPMAS 13C spectrum in the detection dimension (Figure 2.7.6). In the present case, the cross-polarization is used not only to enhance the ^{13}C signal/noise ratio but also to probe the local proton environment of each ^{13}C site. It is to note that the dipolar recoupling time (contact time in the CP sequence) between ^{1}H and ^{13}C must be chosen in order to probe the very local environment of the ^{13}C sites.

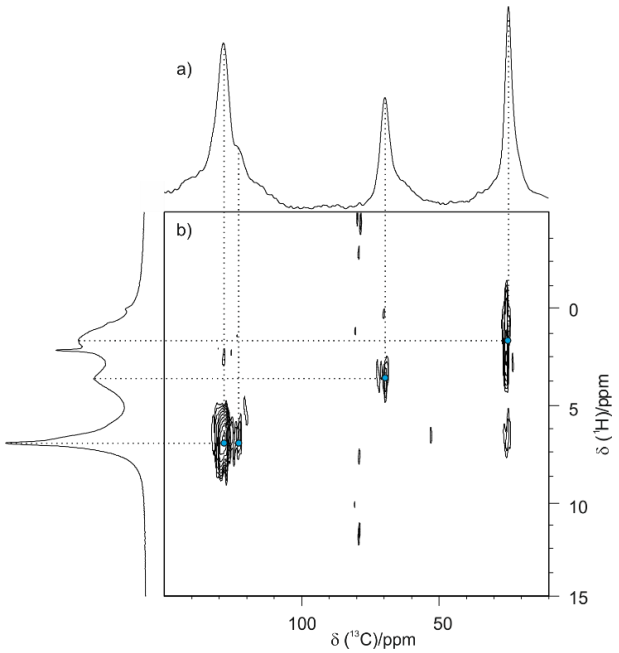

Figure 2.7.6. a) ^{13}C MAS spectrum, b) ^{13}C-^{1}H CP-HETCOR MAS experiment

2.7.4. Solid-state NMR with quadrupolar nuclei

Nuclei featuring spin greater than ½, namely quadrupolar nuclei, constitute the majority of the periodic table. Most of the catalytically-relevant atoms fall in this category. The recording of their NMR spectra is obviously of high interest. However, if for spin ½ nuclei, the distribution of charges within the nucleus is homogenous, it is different for quadrupolar nuclei. In the latter case, the non-homogeneous charge distribution is quantified by the quadrupolar moment, *Q*, a parameter intrinsic to quadrupolar nuclei (Scheme 2.7.5). To make it short, the interaction of the quadrupolar moment with the surrounding electric field gradient, *q* (as a result of the electronic distribution around the nucleus), called the quadrupolar interaction, leads to large distortions and broadenings of the NMR signal (Figure 2.7.7).

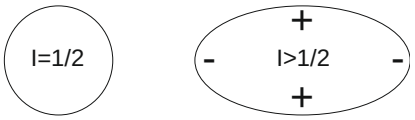

Scheme 2.7.5. Charge distribution of non quadrupolar (left) and quadrupolar nucleus (right).

Sometimes, the quadrupolar broadening is such that it prevents us from any interpretation. In many cases though, it is possible to deduce NMR parameters that are further used to

characterize the local environment of quadrupolar nucleus. In order to help in the interpretation of NMR spectrum of quadrupolar nuclei, specific sequences have been developed and will be presented later. In the following, we will limit the explanation to half-integer quadrupolar nuclei, omitting the few integer quadrupolar nuclei of the periodic table (^{2}D, ^{14}N, ^{6}Li) of limited interest in our study. Nowadays, thanks to the emergence of very high magnetic field, new methods and technical developments (probes and electronics), NMR of quadrupolar nuclei is routinely used for the investigation of many types of materials, including in the field of catalysis.

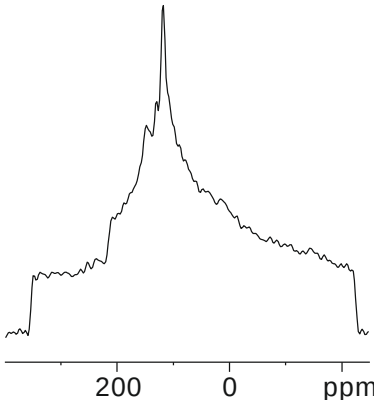

Figure 2.7.7 Example of ^{27}Al spectrum showing a typical quadrupolar lineshape

Reducing the quadrupolar broadening of the NMR spectrum is simply obtained (like for dipolar and CSA interactions) by using the MAS technique. However, under MAS conditions, even at a high spinning speed, the quadrupolar interaction is not completely averaged out. The use of the MQMAS experiment (see below section 2.7.4.2) is required to obtain a high resolution spectrum of a half-integer quadrupolar nucleus.

A total of two parameters (C_Q, η_Q) are required to characterize the strength of the quadrupolar interaction for a given environment. They are the result of the coupling between the quadrupolar moment eQ, and the electric field gradient, eq. Their effect on the NMR spectrum is illustrated in the following sections. The CSA contribution to the quadrupolar lineshape will also be explained at both interactions can be present simultaneously for some nuclei of interest.

- The quadrupolar coupling constant, C_Q

The quadrupolar coupling constant, C_Q=e^2qQ/h, h being the Planck constant, affects the width of the signal. For a given nucleus, characterized by an intrinsic quadrupole moment Q, the higher the electric field gradient, eq, the higher the C_Q (Figure 2.7.8). Thus, in systems featuring strained environment, or a mixed coordination sphere, high values of C_Q are expected. Notice in Figure 2.7.8, the effect of the C_Q values on the quadrupolar lineshape.

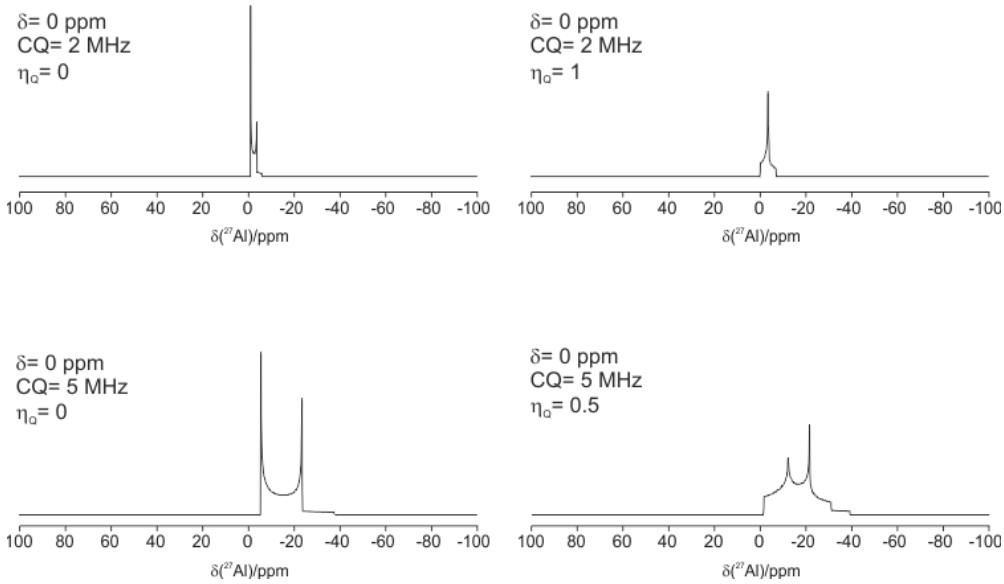

Figure 2.7.8 Simulated MAS spectra of ^{27}Al with variation of C_Q and η_Q.

- The quadrupolar asymmetry parameter

Noted η_Q, the quadrupolar asymmetry parameter (comprised between 0 and 1) affects the shape of the signal and is related to the geometry of the molecule. If the species possesses a high geometry, the η_Q value will be close to 0. On the opposite, if no plane or axis of symmetry can be found in the molecule, the η_Q value will be close to 1. Lineshape modification depending of η_Q can be observed within the simulated spectra of Figure 2.7.8.

- Chemical shift anisotropy

As explained above, the effect of the CSA interaction may add up to the quadrupolar interaction to modify the signal, especially if the MAS rate is not high enough to completely average out the CSA interaction. Therefore, if the CSA is too large (with respect to the MAS rate), it will drastically affect the signal lineshape (Figure 2.7.9), and in order to best fit to the experimental spectrum two additional parameters need to be taken into account: Δ_{CSA}, the amplitude of the CSA (similar to C_Q for quadrupolar nuclei) and the η_{csa} (equivalent of the η_Q).

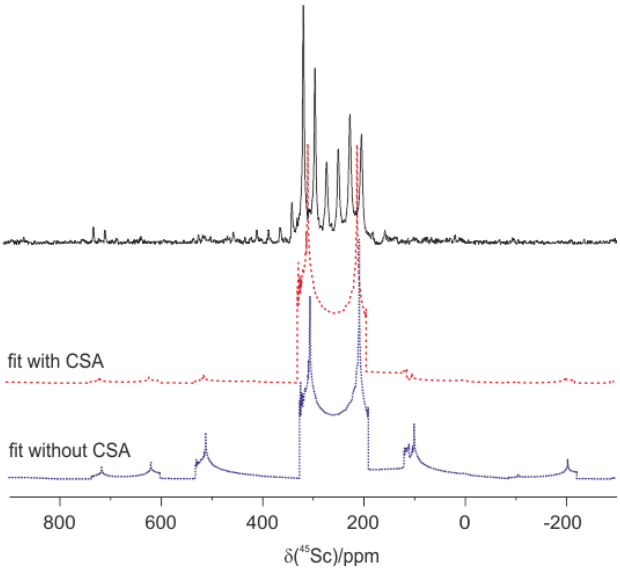

Figure 2.7.9 Influence of CSA onto the ^{45}Sc MAS spectrum.

When the CSA is too large and that the MAS rotation is not sufficient to average out the interaction, it may be interesting to acquire the spectrum under static conditions (no MAS conditions). The sequence must be chosen adequately, as discussed in section 2.7.4, and the magnetic field B_0 must be high enough to reduce the quadrupolar broadening.

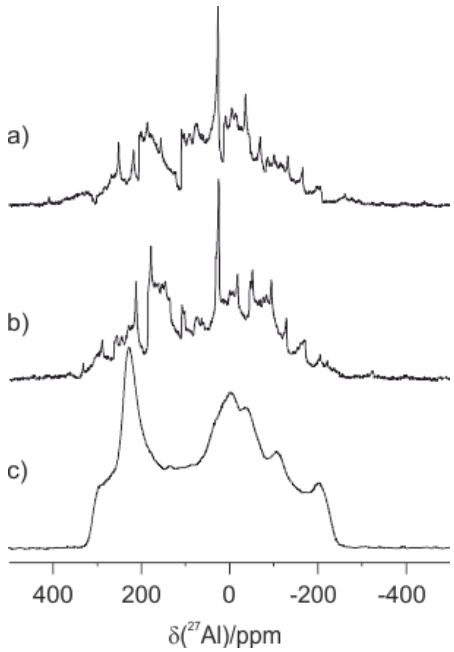

Figure 2.7.10 Comparison between rotation at a) 20 kHz, b) 16 kHz and c) under static conditions for ^{45}Sc MAS NMR

As a side note, the field dependency of the signal line-shape for quadrupolar nuclei is huge: the spectral line width is strongly dependent on the magnetic field intensity, the higher the B_0, the narrower the line-shape will be (and thus, the better the signal-to-noise ratio). For specific case such as spectra of nuclei featuring high CQ values, recording on high magnetic field spectrometers is mandatory. Indeed, if we compare spectra recorded at 9.4 T and at

18.8 T, the signal for the higher magnetic field will thinner than the one at 9.4 T (Figure 2.7.11).

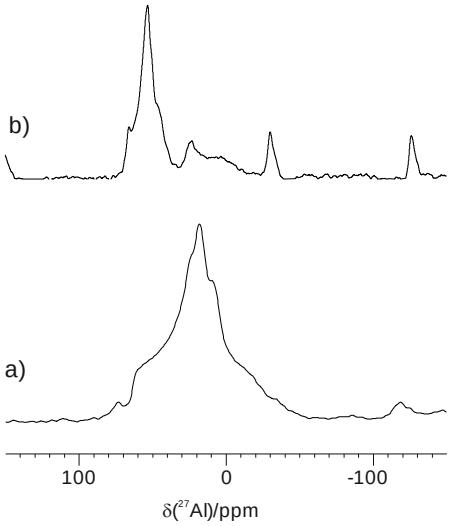

Figure 2.7.11 ^{27}Al MAS NMR spectrum recorded at a) 9.4T and b) 18.8T.

In the case of broad NMR signals, a single pulse acquisition might be insufficient to get proper phased spectrum. In the 1950'[49], Erwin Hahn showed that an echo sequence, composed of a 90° pulse and a 180° pulse, with adequate phase cycling, separated by a delay τ, can provide pure absorption spectra with no line distortion. In this experiment, the delay is an integer multiple of the rotor period, and this is thus designated as "rotor-synchronized".

2.7.4.1. QCPMG

The QCPMG (Quadrupolar Carr-Purcell Meiboom-Gill), applied to quadrupolar nuclei, is an extension of a pulse sequence[50] developed in 1954. It is composed by a series of 180° pulses that refocus the magnetization. It is now used routinely to get NMR spectra that are strongly broadened by the quadrupolar coupling (often in static consitions). As it is a series of echoes with interleaved acquisition, the resulting FID leads after Fourier Transformation, to a multitude of spikelets where the signal intensity is focused (Figure 2.7.122). The acquisition time is strongly reduced while the total envelop of the quadrupolar lineshape is maintained.

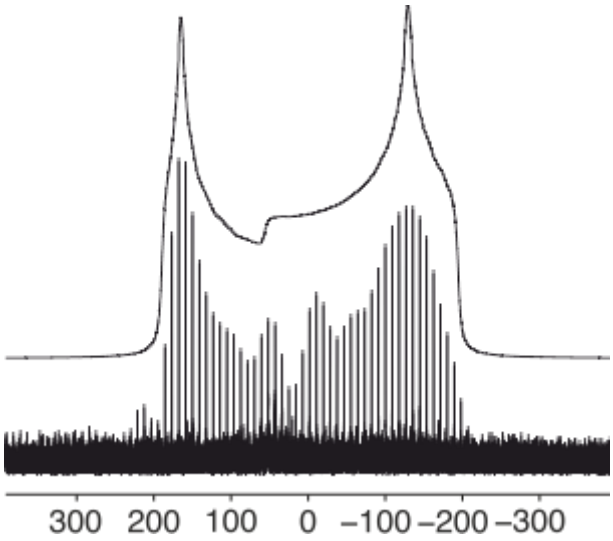

Figure 2.7.12. QCPMG spectrum of a ^{35}Cl spectrum under static conditions[51]

2.7.4.2. MQMAS

The MQ-MAS experiment presented by Frydman and Harwood was designed to provide high resolution 2D NMR of a half-integer quadrupolar nucleus[52]. The 2D spectrum provides an isotropic spectrum in the indirect dimension and a MAS spectrum, broadened by a part of the quadrupolar interaction (the second-order terms) in the acquisition dimension. This 2D experiment is really useful to identify several species hidden a broad MAS spectrum by a projection onto the indirect dimension. Each 1D slice, extracted from the 2D spectrum, can be fitted independently to deduce the quadrupolar parameters and the chemical shift for the different sites within the sample.

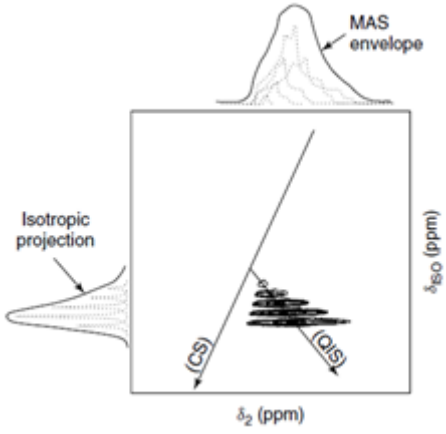

The chemical shift information can be found on the diagonal line while the quadrupolar interaction shift is the deviation between this diagonal and the observed signal (Scheme 2.7.6). The extracted rows can be simulated to extract with precision the several parameters (Figure 2.7.13).

Scheme 2.7.6 MQMAS principle

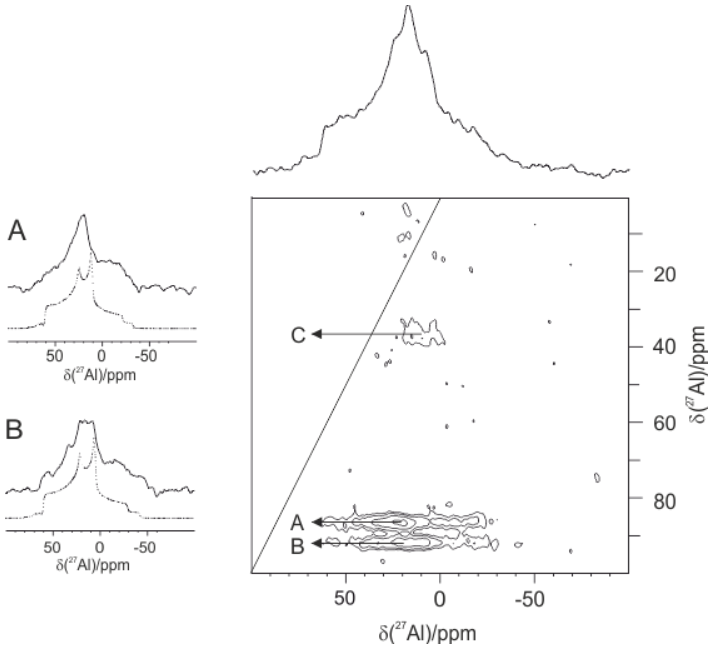

Figure 2.7.13. ^{27}Al MQMAS (9.4 T) spectrum revealing three sites hidden in the broad lineshape

2.7.4.3. HMQC

The 2D HMQC (Heteronuclear Multiple-Quantum Correlation) sequence is another (more recent) heteronuclear correlation, such as the 2D HETCOR previously explained. The HMQC pulse sequence was developed to avoid the drawbacks of the 2D CP-HETCOR applied to a quadrupolar nucleus. It offers more robustness for quadrupolar nucleus than the CP-HETCOR sequence and it allows observation of a nucleus (most of the time ^{1}H) directly bonded to another type of NMR-active quadrupolar nucleus (Figure 2.7.14). In this example, correlations are observed with the proton around 0 ppm and the signal for the aluminum showing the presence of protons close to the metal center.

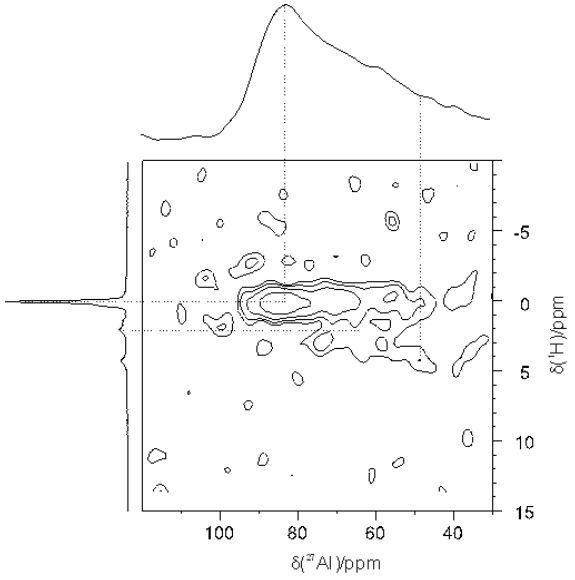

Figure 2.7.14. ^{1}H-^{27}Al HMQC experiment

2.8. Conclusion

In this chapter, we presented the background of our research, namely surface organometallic chemistry. This domain relies on the use of molecular species that present high activity for catalytic transformations (or that can be precatalysts) and graft them onto a surface to generate a novel material that can feature benefits compared to molecular counterparts (enhanced activity or selectivity, recyclability, etc.). Many types of supports can be employed and we highlighted silica as an efficient and versatile oxide, which makes it a most convenient support of choice. We have briefly described the state of the art for rare-earth metals and aluminum applied to SOMC. These two classes of metals are good candidates for immobilization, thanks to their high affinity towards oxygen, thus forming strong bonds with the surface. However, in both cases, precise control over the surface chemistry must be exerted, in order to generate well-defined grafted sites. This is a pre-requisite for rationalization and for establishment of structure-activity relationships. To meet this goal, solid state NMR is a key characterization tool. Most particularly, when applied to the study of quadrupolar nuclei, it can afford precious structural information down to the molecular level.

Thus, in the next chapters, we will describe some examples of SOMC strongly backed-up with solid-state NMR, with a focus on quadrupolar nuclei. Thus, the first chapter will be devoted to rare-earth metals surface chemistry: use of amido derivatives for alkyne dimerization, specific input from ^{45}Sc solid state NMR and development of a grafted lanthanum benzyl for several types of reactions will be presented. In the second chapter will be gathered our research efforts devoted to aluminum surface organometallic chemistry and related problematics, such as grafted salen derivatives for carbonatation of epoxides, molecular and supported alkyl cocatalysts for polymerization or oligomerization of ethylene, and understanding of chloroamido aluminum species reactivity towards the silica surface. Finally, in the third chapter, a novel approach to the design of chelating, LX type surface ligands will be introduced

---

[1] Y.I. Yermakov, B.N. Kuznetsov, Y.A. Ryndin, *J. Catal*, 1976, **42**, 73-78

[2] M. Primet, J.M. Basset, M.V. Mathieu, M. Prettre, *J. Catal.*, 1973, **29** ,213-23

[3] a) F. Hugues, J.M. Basset, Y. Ben Taarit, A. Choplin, M. Primet, D. Rojas, A.K. Smith, *J. Am. Chem. Soc.*, 1982, **104**, 7020-4 b) G.M. Zanderighi, C. Dossi, R. Ugo, R. Psaro, A. Theolier, A. Choplin, L. D'Ornela, J.M. Basset, *J. Org. Chem.*, 1985, **196**, 127-146

[4] J.-M. Basset, R. Psaro, D. Roberto, R. Ugo, *Modern Surface Organometallic Chemistry*, 2009,Wiley

[5] C. Coperet, A. Comas-Vives, M.P. Conley, D.P. Estes, A. Fedorov, V. Mougel,H. Nagae, F. Núñez-Zarur, P.A. Zhizhko, *Chem. Rev.*, 2016, **116** , 323–421

[6] A. Choplin, B. Besson, L. D'Ornelas, R. Sanchez-Delgado, J.M. Basset, *J. Am. Chem. Soc.*, 1988, **110** ,2783-7

[7] P. Dufour, S.L. Scott, C.C. Santini, F. Lefebvre, J.M. Basset, *J. Am. Chem. Soc.,* 1994, **13**, 2509-2511

[8] L. T. Zhuravlev, *Langmuir,* 1987, **3**, 316

[9] Y. Shen, Z. Shen, Y. Zhang, *Polym. Bull.*, 1996, **37**

[10] N. Barros, M. Schappacher, P. Dessuge, L. Maron, SM. Guillaume, *Chem. Eur. J.* 2008, **14**, 1881-90.

[11] R. Anwander, C. Palm, *Stud. Sci. Catal.*, 1998, **117**, 413.

[12]a) C. Coperet, M. Chabanas, R. Petroff Saint-Arroman, J.-M. Basset, *Angew. Chem. Int. Ed.,* 2003, **42**, 156–181. b) P. Leyrit, C. McGill, F. Quignard, A. Choplin, *J. Mol. Cat. A: Chemical*, 1996, **112,** 395-400
[13] Z. Zhong, P.J. Dijkstra, J. Feijen, *Macromol. Chem. Phys*.,2000, **201,**1329-1333
[14] A. Lebrun, J.-L. Namy, H.B. Kagan, *Tetrahedron Lett*., 1991, **20**, 2355-2358
[15] R. Anwander, C. Palm, *Stud. Surf. Sci. Catal.,* 1998,**177**
[16] E. Colomb, C. Novat, T. Hamaide, *Macromol. Chem. Phys.,* 1999, **200**, 2525-2532
[17] G. Gerstberger, C. Palm, R. Anwander, *Chem. Eur. J.,* 1999, **5**,997
[18] R. Anwander, R. Roesky, *J. Chem. Soc.*, 1997, **137**
[19] R.M. Gauvin, L. Delevoye, R.A. Hassan, J. Keldenich, A. Mortreux, *Inorg. Chem.,* 2007, **46**
[20] N. Ajellal, G. Durieux, L. Delevoye, G. Tricot, C. Dujardin, C.M. Thomas, R.M. Gauvin, *Chem. Commun.*, 2010, **46**, 1032
[21] Y. Liang, R. Anwander, *Dalton Trans.*,2013, **42**, 12521
[22] R. M. Gauvin, T. Chenal, R. A. Hassan, A. Addad, A. Mortreux, *J. Mol. Cat. A: Chem.*, 2006, **257**, 31–40.
[23] H. Schumann, J.A. Meese-Marktscheffel, L. Esser, *Chem. Rev.*, 1995, **95**, 865–986
[24] G. Jeske, H. Lauke, H. Mauermann, H. Schumann, T.J. Marks, *J. Am. Chem. Soc.,* 1985, **107**, 8111-8118
[25] a) Y. Satake, S. Myake, N. Kibino, Y. Sasaki, S. Inasawa, 1995, Showa Denko Kk, Japan. JP07258330. b) K. Soga, S. Yamamoto, K. Inematsu, 1997, Maruzen Oil Co., Ltd., Japan. JP09272710
[26] H. Yasuda, Y. Nakayama, Y. Satoh, Z. Shen, X. Ni, M. Inoue, S. Namba, *Polym. Int.*, 2004, **53**, 1682
[27] A. Fischbach, M.G. Klimpel, M. Widenmeyer, E. Herdtweck, W. Scherer, R. Anwander, *Angew. Chem.*, 2004, **116**, 2284 – 2289
[28] X. Ni, J. Li, Y. Zhang, Z. Shen, *J. Appl. Polym. Sci.,* 2004, **92**, 1945–1949
[29] G. Wilke, *Angew. Chem. Int. Ed*. 2003, **42**, 5000–5008
[30] S. S. Reddy, S. Sivaram, *Prog. Polym. Sci.*, 1995, **20**, 309
[31] a) W. Kaminsky, *J. Chem. Soc., Dalton Trans.,* 1998, 1413–1418. b) H. Sinn, W. Kaminsky, H.-J. Vollmer, R. Woldt, *Angew. Chem. Int. Ed.* 1980, **19**, 390-392
[32] a) E. Y.-X. Chen, T. J. Marks, *Chem. Rev.*, 2000, **100**, 1391. b) G. G. Hlatky, *Chem. Rev*., 2000, **100**, 1347.
[33] R. Anwander, C. Palm, O. Groeger, G. Engelhardt, *Organometallics*, 1998, **17**, 10, 2029
[34] J. H. Li, J. A. DiVerdi, G. E. Maciel, *J. Am. Chem. Soc.*, 2006, **128**, 17093.
[35] J. Pelletier, J. Espinas, N. Vu, S. Norsic, A. Baudouin, L. Delevoye, J.Trebosc, E. Le Roux, C. Santini, J-M. Basset, R.M. Gauvin, M. Taoufik, C*hem. Commun.,* 2011, **47**, 2979–2981
[36] a) N. Popoff, J. Espinas, J. Pelletier, K. C. Szeto, L. Delevoye, R. M. Gauvin, M. Taoufik, *ChemCatChem*, 2013, **5**, 1971-1977. b) N. Popoff, N. Merle, K. Szeto, F. Lefebvre, L. Delevoye, R. M. Gauvin, M. Taoufik, *Catal. Today*, 2014, **235**, 41-48.
[37] N. Popoff, B. Macqueron, W. Sayhoun, J. Espinas, J. Pelletier, O. Boyron, C. Boisson, N. Merle, K. C. Szeto, R. M. Gauvin, A. De Mallmann, M. Taoufik, *Eur. J. Inorg. Chem.*, 2014, 888-895
[38] K. C. Szeto, W. Sahyoun, N. Merle, J. Llop Castelbou, N. Popoff, F. Lefebvre, J. Raynaud, C. Godard, C. Claver, L. Delevoye, R. M. Gauvin, M. Taoufik, *Cat. Sci. Tech.,* 2016, **6**, 882-889.
[39] E. Mazoyer, J. Trébosc, A. Baudouin, O. Boyron, J.-M. Basset, J. Pelletier, M. J. Vitorino, C. P. Nicholas, R. M. Gauvin, M. Taoufik, L. Delevoye. *Angew. Chem., Int. Ed.* 2010, **49**, 9854-9858.
[40] R. N. Kerber, A. Kermagoret, E. Callens, P. Florian, D. Massiot, A. Lesage, C. Coperet, F. Delbecq, X. Rozanska, P. Sautet, *J. Am. Chem. Soc.* 2012, **134**, 6767−6775.
[41] a) B. Werghi, A. Bendjeriou-Sedjerari, J. Sofack-Kreutzer, A. Jedidi, E. Abou-Hamad, L. Cavallo, J.-M. Basset, *Chem. Sci*, 2015, **6**, 5456. b) B. Werghi, A. Bendjeriou-Sedjerari, A. Jedidi, E. Abou-Hamad, L. Cavallo, J.-M. Basset, *Organometallics,* **35**, 3288-3294
[42] A. Kermagoret, R. N. Kerber, M.P. Conley, E. Callens, P.Florian, D. Massiot, C. Coperet, F. Delbecq, X. Rozanska, P.Sautet, *Dalton Trans*, 2013, **42**, 12681
[43] S. Shylesha, M.P. Kapoor, L.R. Juneja, P.P. Samuel, C. Srilakshmi, A.P. Singh, *J. Mol. Cat. A. Chem.*, 2009, **301**, 118–126
[44] E. R. Andrew; A. Bradbury; R. G. Eades, *Nature*., 1958, **182**, 1659
[45] R. R. Ernst, W. A. Anderson, *Rev. Sci. Inst*., 1966, **37**, 93
[46] A. Pinest, M. G. Gibbyt, J. S. Waugh, *J. Chem. Phys.*, 1973, **59**, 569
[47]J. Schaefer, E.O. Stejskal, R. Buchdahl, *Macromolecules*, 1977, **10**, 2,
[48] I. Schnell, S. P. Brown, H. Y. Low, H. Ishida, H. W. Spiess, *J. Am. Chem. Soc.*, 1998, **120**, 11784.
[49] E. L. Hahn, *Phys. Rev.*, 1950, **80**, 580
[50] H.Y., Carr; E.M. Purcell, *Phys. Rev.,* 1954, **94**, 630-638.
[51] K.E. Johnston, C.A. OKeefe, R.M. Gauvin, J. Trebosc,.L. Delevoye, J.-P. Amoureux, N. Popoff, M. Taoufik,.K. Oudatchin, R.W. Schurko, *Chem. Eur. J* , 2013, **19**, 12396
[52] L. Frydman, J.S. Harwood, *J. Am. Chem. Soc.,* 1995, **117**, 5367-5368

3. Surface organometallic chemistry of rare-earths

3.1. Introduction

As briefly described above in the bibliographic, rare-earth metals species can be readily grafted onto silica and thus offer efficient access to potentially highly catalytically-active materials. We present in this chapter our contributions in the field, first with the immobilization onto silica of a lanthanum trisbenzyl species, with detailed investigations on the grafting process and with applications in various catalytic reactions. The second part will focus on the application of rare-earth metals trisamides grafted onto dehydroxylated silica, with applications in C-C bond formation and related mechanistic investigations. In the last part, we looked in detail into the structure of molecular and supported scandium amide-functionalized material using ^{45}Sc solid state NMR, which provides information on the coordination sphere of the metal centers (either as isolated molecules or grafted on silica).

These results have been published in:

"Silica-grafted lanthanum benzyl species: synthesis, characterization and catalytic applications." T. Vancompernolle, A. Valente, T. Chenal, P. Zinck, I. Del Rosal, L. Maron, S. Harder, R. M. Gauvin, *Organometallics*, DOI: 10.1021/acs.organomet.7b00538

3.2. Silica-grafted lanthanum benzyl species: synthesis, characterization and catalytic applications

3.2.1. Abstract

The grafting of a lanthanum *tris*-benzyl derivative onto dehydroxylated silica affords a mixture of $[(\equiv SiO)_2La(CH_2Ph)(THF)_n]$ and $[(\equiv SiO)La(CH_2Ph)_2(THF)_m]$ surface sites, in respective proportions of 80 and 20%, as evidenced from mass balance analyses, IR and ^{1}H, ^{13}C and ^{29}Si 1D and 2D solid state NMR spectroscopy. Significant transfer of alkyl groups from lanthanum to the surface was demonstrated. The grafting mechanism was also probed by DFT calculations, which confirm that benzyl group transfer from the lanthanum to the surface (via Si-O-Si cleavage) occurs readily. This material proved to be active in alkyne dimerization, and in ethylene, styrene and ε-caprolactone homopolymerizations

3.2.2. Introduction

Rare-earth metals have attracted constant attention in catalysis thanks to their remarkable properties, mostly owing to their high Lewis acidity.[1] Impressive early examples of lanthanide alkyls' reactivity include C-H activation chemistry or cocatalyst-free ethylene polymerization.[2] However, this high reactivity (and thus, high sensitivity) of rare-earth alkyl derivatives has hampered their widespread use, which was partly addressed as high yield syntheses of LnR_3 species (occasionally as Lewis base adducts) were proposed for such starting materials.[3] Among the reported solvated *tris*-alkyl species, the benzyl derivatives

have been described by the Harder and Hessen groups, who reported simple and efficient access route to benzyllanthanide reagents.[4] These are available to a wide range of metals and are thermally stable (contrary to neosilyl derivatives). Furthermore, contrary to the *bis*(trimethylsilyl)methyl derivatives, these compounds retain a high reactivity towards protic reagents.

On the other hand, heterogenization of molecular complexes onto inorganic supports is of high interest in the view of their use in industrially-relevant processes (mostly related to polymerization), or to generate site-isolated highly reactive organometallic species. One of the most efficient methods to meet this goal is the use of surface organometallic chemistry, which allows the precise synthesis of supported species.[5] In this context, following the pioneering work from Anwander,[6] we have developed well-defined silica-grafted amide and borohydride rare-earth metals derivatives.[7] These display interesting properties, affording for instance systems with enhanced selectivity in specific polymerization reactions.**7**[a,c]

There are very few reported examples of immobilization of lanthanide alkyl derivatives onto inorganic supports, namely grafting of $[Lu\{CH(SiMe_3)_2\}_3]$ onto dehydroxylated silica,[8] or formation of scandium methyl complexes by metalation of silica-supported scandium amides.[9] No catalytic application of these materials was described. In related approaches, lanthanide alkyl aluminates have been immobilized onto mesostructured supports by Anwander and applied in diene polymerization.[10]

In this contribution, we describe the study of the reaction of $[La(CH_2Ph)_3(THF)_3]$ (**1**) with silica dehydroxylated at 700°C, along with theoretical investigations on the grafting pathway. Additionally, we discuss the performances of this material in four types of catalytic reactions, namely alkyne dimerization, polymerization of styrene, polymerization of ethylene and ring opening polymerization of ε-caprolactone.

3.2.3. Results and discussions

Starting from $[La(CH_2Ph)_3(THF)_3]$ (**1**), our initial goal was the design of well-defined lanthanum alkyl surface sites bearing a single surface-to-metal bond (**2a**, Scheme 3.2.1), which would leave two reactive alkyl moieties. This would offer the possibility for further generation of cationic monosiloxy monoalkyl species using cationizing agents, a step toward enhanced reactivity.[11] To achieve this, we have selected highly dehydroxylated silica, namely Aerosil 380 silica from Evonik, treated under vacuum at 700°C. This support features a specific surface area of 350 $m^2.g^{-1}$. As evidenced by infrared spectroscopy, this dehydroxylated silica bears only non-interacting silanol groups on its surface (Figure 3.2.1a). Grafting of inorganics and organometallics on such a support typically generates monosiloxide surface species.5

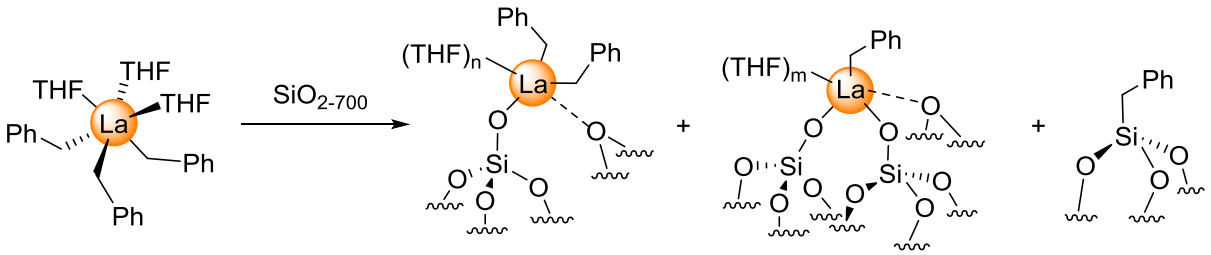

1 **2a**, 20% **2b**, 80%

Scheme 3.2.1. Grafting of $[La(CH_2Ph)_3(THF)_3]$ (**1**) on $SiO_{2\text{-}700}$.

Reaction of **1** with $SiO_{2\text{-}700}$ in THF affords a deep orange material (**2**). Elemental analysis indicates La and C loading of 5.48 and 9.58 w%, respectively. The La loading corresponds to 0.39 mmol.g^{-1} of material. The corresponding C/La atom ratio is 20.2. Infrared spectroscopy reveals full consumption of the silanols, as shown by the lack of SiOH signal in the DRIFT spectrum of **2**, notably of the 3747 cm^{-1} $\nu_{(O\text{-}H)}$ band (Figure 3.2.1b). We also observe new signals at 3061-3027 and 2983-2885 cm^{-1}, accounting respectively for $\nu_{(sp^2\ C\text{-}H)}$ and $\nu_{(sp^3\ C\text{-}H)}$. In addition, bands at 1588 cm^{-1} (characteristic for C=C aromatic-ring-stretching vibrations) and 1494 cm^{-1} (δ(C-H) vibration of the methylene groups) are also present.

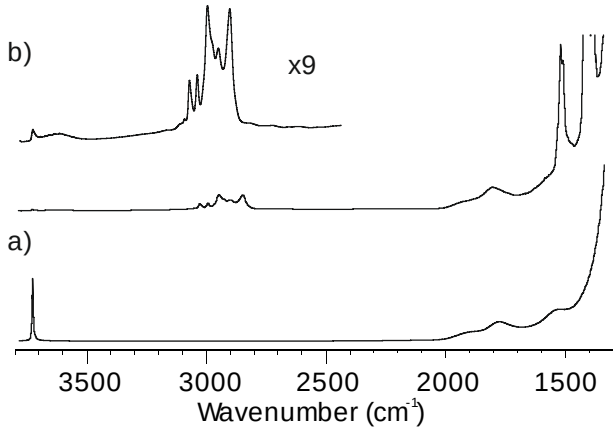

Figure 3.2.1. DRIFT of a) $SiO_{2\text{-}700}$, b) $[La(CH_2Ph)_3(THF)_3]$ over $SiO_{2\text{-}700}$ (**2**).

Solid state NMR was used to get further insight into the structure of **2**. ^{1}H MAS NMR features broad signals even at high magnetic field (18.8 T) (Figure 3.2.2a). Thus, signals at 7.1, 3.7 and 1.6 ppm are observed, accounting respectively for aromatic C-H groups, OCH_2 from lanthanum-bound THF and both La-CH_2 and OCH_2CH_2 protons.4 The overlap of the signals in the 2.5-1 ppm region prevents precise assignment, however, the intensity of the considered signal compared to that of OCH_2 is fully in line with the presence of overlapping La-CH_2 and OCH_2CH_2 signals.

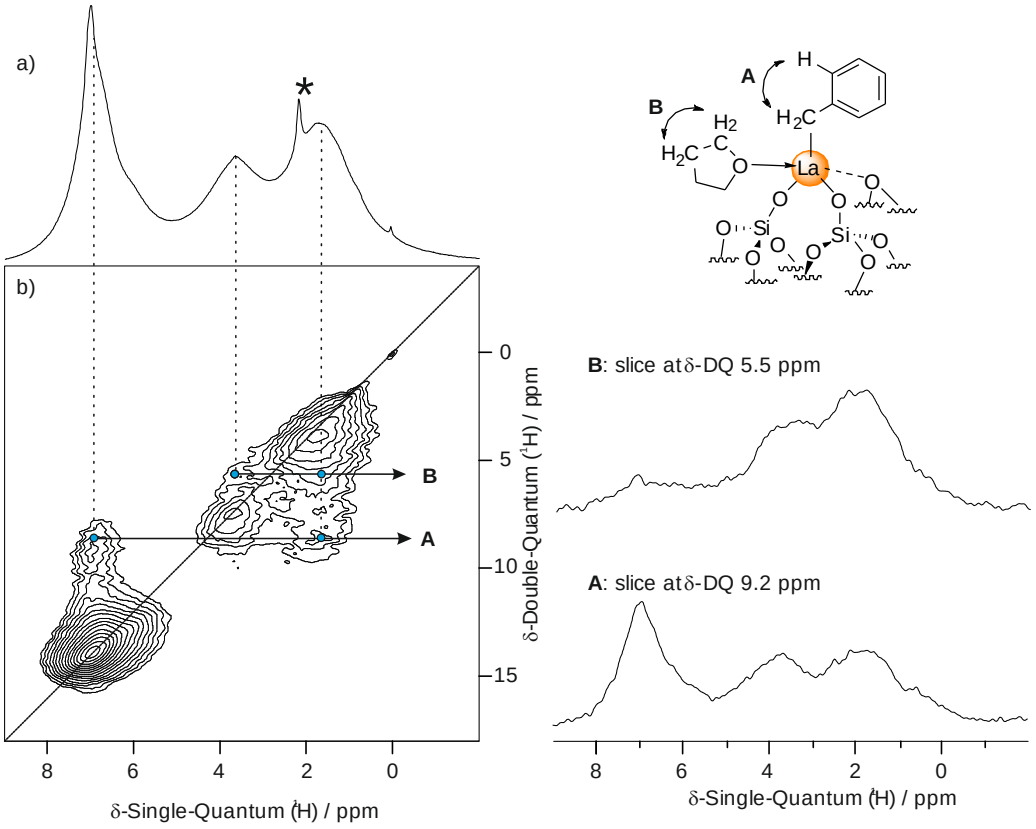

Figure 3.2.2. ^{1}H (a) and ^{1}H-^{1}H DQ-SQ (b) MAS NMR spectra of **2** (18.8 T, spinning speed 20 kHz).

Noteworthy, the width of the signals is reminiscent of that of the group 4 benzyl derivatives (Ti, Zr) on the same support.[12] In this case, this was assigned to occurrence of η^2 and/or η^3 coordination mode of the benzyl ligand.[13] To further probe the structure of the supported species, we resorted to a two-dimensional ^{1}H-^{1}H DQ-SQ MAS NMR experiment. This technique relies on dipolar interactions and gives information on spatial proximities[14] (Figure 3.2.2b). Each signal in the ^{1}H spectrum gives rise to an on-diagonal correlation, in line with the presence of CH_2 moieties (from $LaCH_2$ and THF) or with neighboring protons with similar chemical shift (aromatic C-H protons). Two off-diagonal signals are observed: The first one (tagged as interaction A in Figure 3.2.2) associates aromatic CHs at 7.1 ppm and protons at 1.6 ppm, which would be best assigned to interaction within the benzylic fragments, namely between methylenic and aromatic protons of $LaCH_2Ph$. A second set of less intense cross-peaks (tagged as interaction B in Figure 3.2.2) associates the OCH_2 OCH_2CH_2 protons from THF (at respectively 3.7 and 1.6 ppm). The ^{13}C CP MAS NMR of **2** features 3 major sets of signals at 128, 69 and 24 ppm, characteristic for aromatic, OCH_2 and OCH_2CH_2 carbons (Figure 3.2.3).

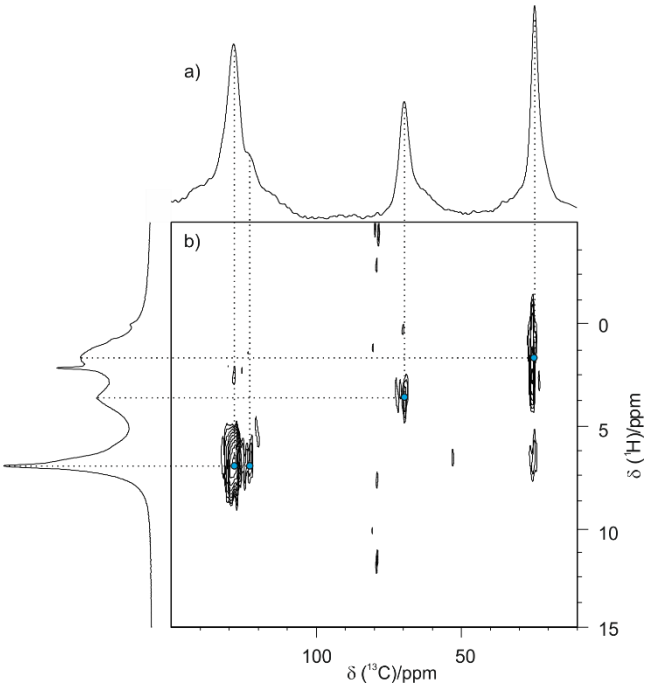

Figure 3.2.3. ^{13}C (a) and ^{1}H-^{13}C HETCOR (b) CP MAS NMR spectra of **2** (^{13}C: 100.6 MHz, ^{1}H: 400 MHz, spinning speed 14 kHz)

A shoulder at 62 ppm on the 69 ppm peak is assigned to the $LaCH_2$ group.4[15]. These assignments were confirmed by a 2D ^{1}H-^{13}C CP HETCOR MAS NMR spectrum (Figure 3.2.3b). Indeed, the aromatic moieties gives rise to a ^{1}H signal at 7.1 ppm and ^{13}C signals at 128-120 ppm, while the THF OCH_2 feature ^{1}H and ^{13}C resonances at 3.6 and 69 ppm, respectively. Accordingly, the THF OCH_2CH_2 groups give rise to a correlation associating signals at 1.5 (^{1}H) and 24 ppm (^{13}C). A further long range correlation involves the OCH_2CH_2 protons and the OCH_2 carbons. However, no ^{1}H-^{13}C correlation was observed for the $LaCH_2$ moiety under our conditions. Benzyl ligands are known to be involved in dynamic processes and generally show a rich coordination behavior that varies from η^1 to η^3 coordination4[,13]. This could prevent efficient dipolar coupling to take place and thus hinder observation of heteronuclear interactions.

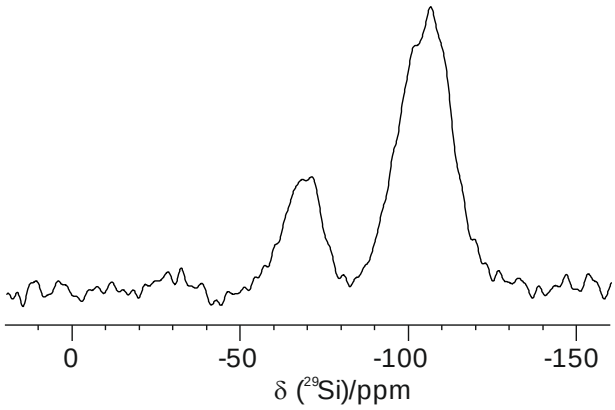

Figure 3.2.4.^{29}Si CP MAS NMR spectrum of **2** (79.5 MHz, spinning speed 6 kHz)

^{29}Si CP MAS NMR (Figure 3.2.4) features an intense signal characteristic for T_3 groups (≡$SiCH_2Ph$) at -66 ppm,[16] along with the signal from the Q-type (SiO_4) sites at -103 ppm. This indicates that significant benzyl group transfer onto the silica support occurred, as observed during the grafting of electrophilic metal complexes on (very) highly dehydroxylated silica supports.[17]

This prompted us to assess the stoichiometry of the grafting reaction and the precise structure of the surface organometallic centers in **2**, most noteworthy through mass balance analysis. The lanthanum loading (5.48 w%, 0.39 mmol.g^{-1}) is higher than what would be expected from a grafting mode involving only protonolysis of **1** by silanols, which would afford 0.27 mmol(La).g^{-1}. Thus, other reaction pathways must be operative, such as grafting by siloxane opening, forming ≡SiO-La and ≡$SiCH_2Ph$ sites. When comparing the expected and observed lanthanum loading (0.27 and 0.39 mmol.g^{-1}, respectively), this shows that about 70% of grafting proceeds with protonolysis as the first step, and that about 30% results from initial nucleophilic cleavage of (strained) Si-O-Si fragments.

We reacted **2** with excess (5 eq) *n*-butanol in C_6D_6, and we quantified by ^{1}H NMR the released organic compounds (THF and toluene), using ferrocene as an internal standard. The toluene and THF detected after alcoholysis of **2** amount to 0.47 and 0.51 mmol.g^{-1}, respectively (average of 4 different runs). Thus, the average number of benzyl ligand moiety per lanthanum center is 1.2, which is significantly different from the ratio of 2.0 expected for species **2a**. On the same line, the average number of THF molecules per lanthanum center is 1.3 (if considering that excess butanol fully displaces THF from grafted centers). Thus, the average formulation for the surface species is [(≡$SiO)_{1.8}La(CH_2Ph)_{1.2}(THF)_{1.30}$]. This means that grafted species consist of 20% [(≡SiO)$La(CH_2Ph)_2(THF)_n$] (**2a**) and 80% [(≡$SiO)_2La(CH_2Ph)(THF)_m$] (**2b**), signifying that alkyl transfer plays a significant role in the surface chemistry of **1** on $SiO_{2\text{-}700}$ (Scheme 3.2.1). If one considers that THF is fully released upon alcohol addition, the residual C content (accounting for silica-transferred benzyl groups) after removing the benzyl and THF contribution (13.6 C/La) is 6.6 C/La. This corresponds to 0.9 equivalent of [≡$SiCH_2Ph$] per surface La center.[18] This significant amount of alkyl → Si transfer is in sharp contrast with the surface chemistry of [Lu{$CH(SiMe_3)_2$}$_3$] on silica,8 where grafting proceeds only via protonolysis of the Lu-C by silanols, most probably due to the bulk of the alkyl moieties which could hinder attack of siloxane bridges.

To confirm and further refine the understanding of the formation of **2a** and **2b**, DFT calculations have been carried out at the DFT-B3PW91 level of theory. Thus, the grafting reaction of **1** onto a silica surface treated at 700°C has been studied using a polyoligosilsesquioxane derivative-type surface model (called **c** model), successfully used to study both the grafting reaction of several d/f metal complexes [19] and their catalytic activity.[20] The Gibbs free-energy profile for the grafting reaction leading to **2a** is given in Figure 3.2.5.

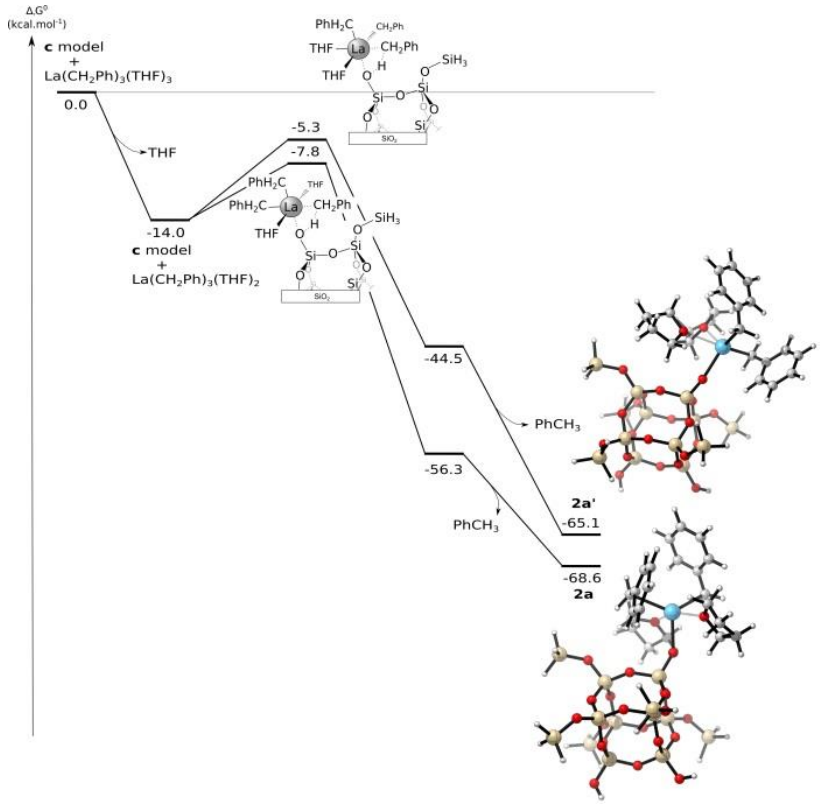

Figure 3.2.5 Calculated Gibbs free-energy profile (in kcal/mol) for the grafting reaction of **1** onto the **c** model.

The reaction sequence starts by the loss of one THF molecule leading to a complex in which the lanthanum center exhibits a distorted trigonal bipyramidal environment with two THF molecules in axial positions and three benzyl ligands in the equatorial plane. From an energy point of view, the formation of this complex is exergonic by -14.0 kcal.mol^{-1} relative to the starting point. The reaction continues by the grafting of this intermediate onto the silica surface through a protonolysis of a La – C bond by a surface silanol, leading to two possible mono-grafted ≡Si-O-La(THF)$_2$(CH$_2$Ph)$_2$ isomers with benzyl and THF ligands in a *cis* (**2a'**) or *trans* (**2a**) configuration with the concomitant formation of a free toluene molecule. The formation of these two isomers it is, in both cases, computed to be exergonic, by -65.1 kcal.mol^{-1} for the *cis* isomer and by -68.6 kcal.mol^{-1} for the *trans* configuration, and kinetically accessible (highest barrier of 8.7 kcal.mol^{-1}). It is interesting to note that in both isomers the two benzyl groups are η^2 coordinated to the metal center. Thus, these complexes are stabilized by the formation of an interaction between the *ipso*-carbon atom and the metal center, *i. e.*, by a donation from the CH$_2$ – C$_{ipso}$ bond to an empty *d*-orbital of lanthanum as indicated by the second-order perturbation natural bond order (NBO) analysis. We can therefore conclude that, according to the slight stability difference between both isomers and the small activation energies needed for formation, these two isomers can coexist on the silica surface. DFT calculation also have been used to consolidate the above-proposed spectroscopic assignment (Table 3.2.1, Table 3.2.2). Good agreement was observed between calculated and experimental ^{13}C NMR and ^{1}H NMR chemical shifts. The

spectral signatures of both isomers are very close implying that they cannot be distinguished by NMR which argues for the coexistence of the two complexes on the silica surface. It is also noteworthy that, from **2a** and **2a'**, loss or addition of a THF molecule are both endergonic processes (circa 11.0 kcal.mol^{-1}) that presumably would not occur.

	$C\underline{H}_2Ph$	$C\underline{H}_2Ph$			$OC\underline{H}_2$	$OCH_2C\underline{H}_2$
		H_{ortho}	H_{meta}	H_{para}		
2 (exp.)	1.6	7.1	7.1	7.1	3.7	1.6
2a	2.0	6.5	7.1	6.4	3.9	1.8
2a'	1.8	6.7	7.3	6.4	3.9	1.8
2b	2.2	6.8	7.1	6.4	3.6	1.7
2b'	2.1	6.8	7.1	6.2	3.7	1.7
CH_2Ph (Transf)	2.7	7.6	7.3	7.2	-	-

Table 3.2.1 Experimental and calculated ^{1} NMR data for silica-supported lanthanum benzyl complexes

	$\underline{C}H_2Ph$	$CH_2\underline{Ph}$				$O\underline{C}H_2$	$OCH_2\underline{C}H_2$
		C_{ipso}	C_{ortho}	C_{meta}	C_{para}		
2 (exp.)	62	-	128			69	24
2a	55.9	144.1	118.4	127.6	113.5	70.2	28.8
2a'	56.3	146.3	117.8	128.7	112.9	70.2	28.8
2b	59.9	145.5	118.7	127.2	114.1	70.2	28.6
2b'	56.7	149.2	116.6	129.2	112.5	68.9	28.4
CH_2Ph (Transf)	24.9	134.7	126.2	124.1	120.1	-	-

Table 3.2.2 Experimental and calculated ^{13}NMR data for silica-supported lanthanum benzyl complexes

Next, we focused on the mechanism leading to the formation of a doubly grafted complex (**2b**) through the transfer of a benzyl group to the silica surface. The Gibbs free-energy profile for the alkyl transfer is given in Figure 3.2.6. The formation of **2b** takes place through a concerted mechanism in which the transfer of the benzyl group from lanthanum to a neighboring silicon atom is concomitant to the activation of a Si–O bond and the formation of a La–O bond. Starting from **2a** and **2a'**, two different doubly grafted complexes can be obtained, depending on the silicon center onto which the alkyl group is transferred (namely if it is linked by a siloxane bridge or not to the silanol group on which the lanthanide complex is grafted). In both cases, the reaction starts by an endergonic isomerization of **2a** and **2a'**, by 10.0 and 6.5 kcal.mol^{-1}, respectively. This leads to an isomer exhibiting a trigonal-bipyramidal geometry around the metal center, with the oxygen atom of the silanol group and one THF ligand in axial positions and the two benzyl groups and the second THF ligand in the equatorial plane. From this intermediate, the benzyl transfer to a silicon atom linked by a siloxane bridge to the silanol group on which the lanthanide complex is grafted leads to the formation of a doubly grafted complex on the same silanol group (**2b'**). The alkyl transfer reaction proceeds with an accessible energy barrier of 28.7 kcal.mol^{-1} with respect to **2a** and

25.2 kcal.mol^{-1} with respect to **2a'**. From a thermodynamic point of view, the formation of **2b'** is found to be an athermic process with respect to **2a** and **2a'**, which is in agreement with the coexistence of both mono and bi-grafted complexes onto the silica surface as experimentally observed. In this case, the Si–O and La–C bond breaking is counterbalanced by the formation of a strong La–O bond and Si–C bond. However, this complex is destabilized by the ring constraint of the grafting mode which explains the athermicity of this reaction. On the other hand, the transfer of a benzyl group to a silicon atom not linked by a siloxane bridge to the siloxyde bearing the lanthanum center leads to the formation of a bi-grafted complex on two vicinal silanol groups (**2b**). The alkyl transfer reaction take place via a high energy process with activation barriers of 61.8 kcal.mol^{-1} and 58.3 kcal.mol^{-1} for **2a** and **2a'**, respectively. Thus, even though the formation of **2b** and **2b'** is found to be exergonic by 7.6 kcal.mol^{-1} and 4.1 kcal.mol^{-1}, respectively, these reactions would not occur on account of the high activation energies needed. Thus, the benzyl transfer can only be carried out on silicon atoms close to the initial grafting site.

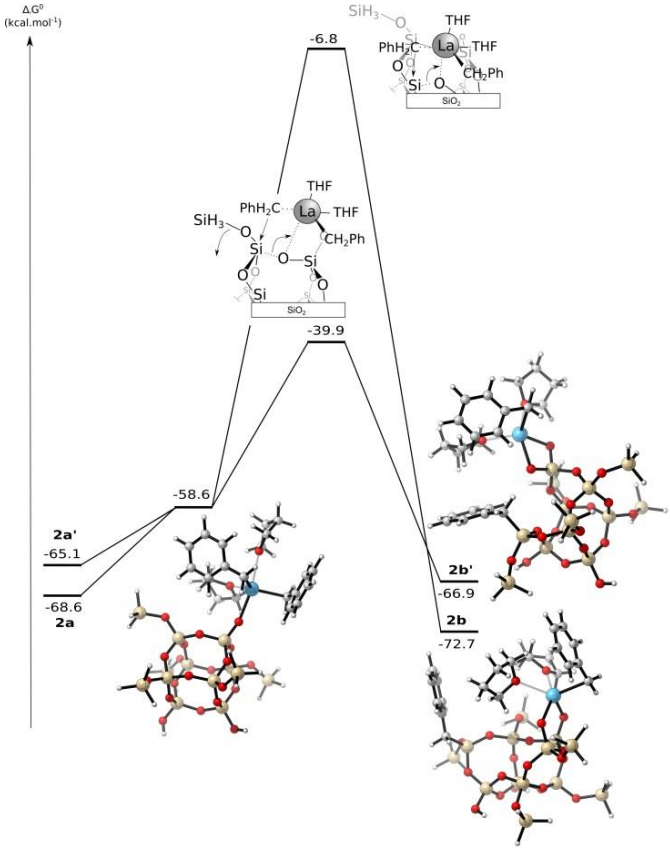

Figure 3.2.6 Calculated Gibbs free-energy profile (in kcal/mol) for the alkyl transfer mechanism leading to **2b** and **2b'**.

With this material at hand, we proceeded to probe its performances in catalytic reactions that are typically catalyzed by rare-earth molecular species, i.e alkyne dimerization as well as ethylene, styrene and ε–caprolactone homo-polymerization.

Alkyne dimerization catalyzed by rare-earth metal derivatives was first described by the Teuben group,[21] originally with *bis*-pentamethylcyclopentadienyl systems. The reaction starts with the deprotonation of the acidic C-H from the alkyne substrate by the La-C bond which is followed by alkyne insertion into the La-C≡C bond and protonolysis by the C-H from a further substrate molecule. Thus, this C-C bond formation transforms two terminal alkyne substrate molecules into an enyne product (Scheme 3.2.2). It can afford either branched, head-to-tail (**3a**) or linear, head-to-head (**3b**) dimers. Trimers (**4**) can also be produced. We have previously reported that grafted amides can catalyze this reaction.7[b,22] Analogous, in the presence of **2** (1% catalytic loading) after 4 hours at 100°C, 1-hexyne is converted into a mixture of dimers with 40% conversion. The major species is the head-to-tail isomer **3a** (90%), while the tail-to-tail **3b** species accounts for 8% (Scheme 3.2.2). Only traces (2%) of trimer **4** were detected. Longer reaction times (up to 15 h) did not improve the conversion.

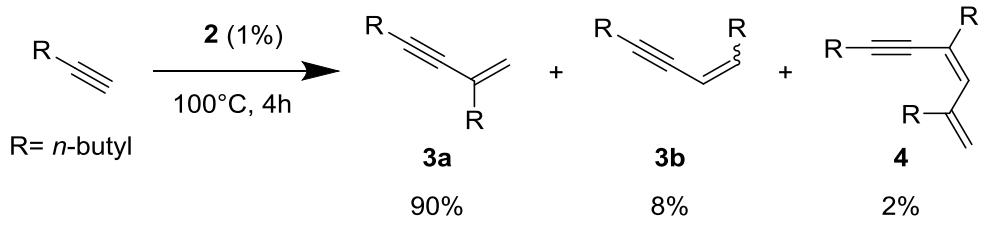

Scheme 3.2.2.Dimerization of 1-hexyne catalyzed by **2**.

The presence of La-C bonds within **2** also opens up the possibility to use it as an ethylene polymerization catalyst, as, in contrast with group 4 catalysts, rare-earth species do not necessarily require cationizing activators to achieve ethylene polymerization.[23] Indeed, under mild reaction conditions (90°C, 1.5 bar), **2** afforded linear polyethylene, though with modest activity (activity of 1.9 $kg_{PE}.mol_{La}^{-1}.bar^{-1}.h^{-1}$ after 1h). This is within the same range as that of silica-supported lanthanum silylamides activated by *tris*-isobutyl aluminum.[22,24] Use of 1 eq. of $[Ph_3C^+][(C_6F_5)_4B^-]$ per La as cationizing agent slightly reduced the activity (1.0 $kg_{PE}.mol_{La}^{-1}.bar^{-1}.h^{-1}$ after 1h). This can be related to the fact that, as we have shown above, 80% of the lanthanum centers bear a single alkyl group (**2b**): Alkyl abstraction would lead to a catalytically inert system. Thus, only the 20% of *bis*-alkyl species (**2a**) could react and afford a cationic alkyl entity able to polymerize ethylene.

Material **2** is also able to polymerize styrene in the absence of activator. Reacting 100 equivalent of monomer per lanthanum center at 80°C afforded high molecular weight polystyrene (M_w 4.1 10^5 g/mol, with a substantial dispersity of 5.7) in an isolated yield of 42%. This moderate activity and the lack of mass control indicate poor initiation control of the polymerization process. However, ^{13}C NMR analysis revealed a syndiotacticity of 85%, showing that grafting induced some degree of stereocontrol over the polymerization process, as previously observed in the case of silica-supported calcium benzyl surface species.[25]

Finally, ε-caprolactone is efficiently polymerized by **2**: conversion of 89% for 650 equivalents of monomer per lanthanum center was readily achieved at room temperature within 2

hours, affording a white solid upon precipitation in methanol. SEC analysis shows that polymerization is rather controlled (M_w 1.8 10^5 g.mol^{-1}, Đ = 1.64).

3.2.4. Conclusion

We have described here the surface chemistry of a lanthanum *tris*-benzyl derivative onto dehydroxylated silica. This highly reactive organometallic species reacts not only with silanols, but also with (strained) siloxane moieties, affording as major surface site the doubly grafted surface species, along with [$SiCH_2Ph$] groups, as shown by a combination of mass balance analysis and spectroscopic techniques. These conclusions are in agreement with DFT calculations which in particular show that siloxane bridge opening occurs readily on a neighboring siloxane site after a first protonolysis step. Furthermore, this material catalyzes a range of reactions, however with modest activity. Further investigations aim to study the influence of the nature of the metal center by grafting various [$Ln(CH_2Ph_2)(THF)_n$] complexes on silica. As reactivity is known to depend on the nature of the rare-earth metal (ionic radius, Lewis acidity),[24,26] this should give a relationship between catalytic performances and metal choice.

3.2.5. Experimental section

General considerations. Experiments were carried out under an argon atmosphere in an M-Braun glove-box or by using Schlenk techniques. Solvents and reactants were dried by using conventional reagents and stored in the glove-box over 3A molecular sieves. Aerosil 380 silica (Degussa, specific area 380 m^2 g^{-1}, prior to heat treatment) was subjected to heating under secondary vacuum (10^{-6} mbar) for 15 h at 500 °C, followed by 4 h at 700 °C, and stored in a glovebox. Liquid-state NMR spectroscopic analyses were run on a Bruker Avance 300 spectrometer. Solid-state MAS NMR spectra were recorded on Bruker Avance 400 and 800 spectrometers. Chemical shifts are given with respect to adamantane, glycine and TMS as external references for ^{1}H, ^{13}C and ^{29}Si NMR spectroscopy, respectively. The two-dimensional homonuclear experiment (DQ-MAS) was obtained at a spinning frequency of 20 kHz by using excitation and reconversion pulse blocks of two rotor periods each (200 µs). The 90° pulse length was 2.25 µs, the recycle delay was 30 s, and 16 scans were collected for each slice (128 in total). The ^{1}H-^{13}C CP MAS NMR experiment (HETCOR) was obtained at a spinning frequency of 14 kHz. The 90° pulse length was 4 µs, the recycle delay was 5 s, and 512 scans were collected for the 32 slices. For the CP step, a ramped radio frequency (RF) field centered at 45 kHz was applied on protons, and the contact time was set to 1 ms. The ^{29}Si CP MAS spectrum was recorded at a spinning frequency of 6 kHz, with a recycling delay of 3 s.

Diffuse reflectance infrared spectra were collected with a Harrick cell on a Nicolet Avatar spectrometer fitted with a MCT detector. Typically, 64 scans were accumulated for each spectrum (resolution 4 cm^{-1}). Elemental analyses were conducted in at the Service d'Analyse Elémentaire, LSEO, Université de Bourgogne (CHN) and in the Service Central d'Analyse du CNRS (La).

The weight - and number–average molar masses (M_w and M_n) and dispersities ($Đ = M_w/M_n$) of the polymers were determined by size exclusion chromatography (SEC) in THF at 40 °C (1 mL/min) with a triple detection system, equipped with an Alliance Waters e2695, a multiangle light scattering detector (MALS, Wyatt Technology mini DAWN TREOS), and a refractive index detector (Waters 2414). The SEC system was equipped with three Waters Styragel (HT1, HT3 and HT4) columns. The refractometer was used to determine the molar masses against polystyrene standards with the corrections Mn(SEC)= 0.56x M(obs) for polycaprolactone.[27] Samples were prepared by dissolving the product (10 mg) in 4 mL of THF. The solutions were then filtered with 0.45 µm filters. For alkyne dimerization, reaction mixtures were analysed using a Shimadzu GC2010 chromatograph fitted with a CP-Sil5CB column (25m× 0.25mm× 0.2 µm), argon as carrier gas, and both injector and detector temperature at 250 °C. Heating program: starting at 50 °C then a ramp of 10 °C/min up to 250°C, hold for 10 min is applied (more details in supplementary information about conversion and selectivity calculations).

Grafting of 1 onto SiO_{2-700}. In a glovebox, a double-Schlenk vessel was loaded with **1** (655 mg, 1.04 mmol) dissolved in 20 mL of THF in one compartment and with **SiO_{2-700}** (1.5 g) suspended in 20 mL of toluene in the other compartment. The orange complex solution was added at room temperature to the support by filtering through the sintered glass separating the two Schlenk tubes, and the reaction mixture was stirred for 15 h. The supernatant liquid was then separated by filtration into the other compartment, from which the solvent was gas-phase transferred by trap-to-trap distillation back into the compartment containing the modified support in order to wash away the residual molecular precursor. This operation was repeated thrice (resulting in colorless washing fractions). The resulting material (**2**) was then dried under secondary vacuum (10^{-6} mbar) at room temperature for 14 h.

Alkyne dimerization. In the glove box, a glass reactor is filled with **2** (100 mg, 0.039 mmol La), 3ml of toluene and 1-hexyne (325 mg, 3.9 mmol, 100 mol eq. per La). The reaction mixture is heated at 100°C. After 4 hours, the reaction is quenched by exposure to air. The supernatant is analysed by GC using *n*-decane as a standard (added after quenching). See Figure 3.2.7 and Figure 3.2.8.

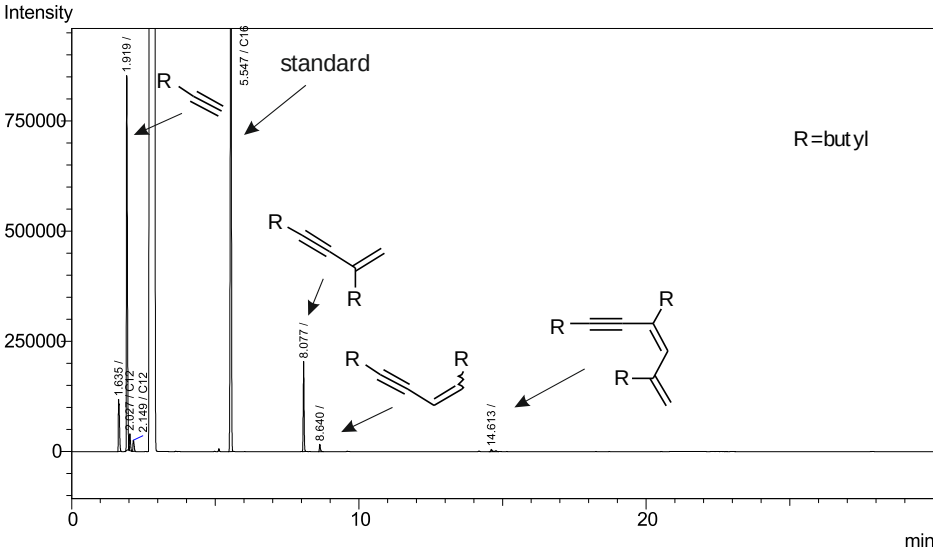

Figure 3.2.7 GC trace from dimerization of 1-hexyne with **2**

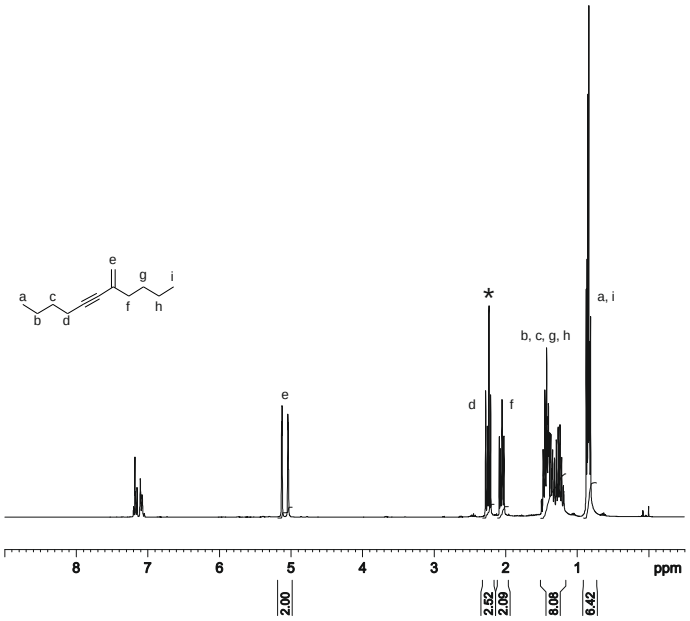

Figure 3.2.8 ^{1}H NMR spectrum (300 MHz, C_7D_8) of 7-methylenundexc-5-yne

Polymerization of ethylene. A solution of Al(*i*Bu)$_3$ scavenger (300 mg) in 18 mL of toluene was introduced in a thermostated (90°C) glass reactor equipped with a powerful mechanical stirrer. The reactor was pressurized and continuously fed with 1.5 bar ethylene. A suspension of **2** (253 mg containing 5.48% La, 100 µmol) in 2 mL toluene was prepared in the glove box and injected through a septum into the polymerisation reactor. The ethylene consumption was then monitored with a mass flow meter. The polymerisation was stopped after 2 h by hydrolysis with acidic methanol (100 mL with 1 mL concentrated HCl). The solid material was recovered by filtration, washed with pure methanol, dried and weighed (580 mg). Integration of the mass flow meter signal indicated consumption of 350 mg of ethylene. ^{13}C CP MAS NMR shows that the produced polymer is linear polyethylene (Figure 3.2.9).

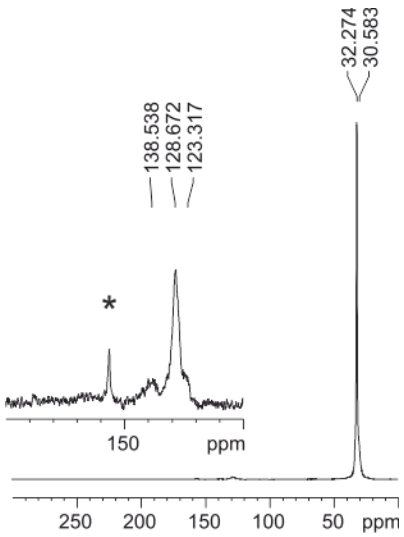

Figure 3.2.9 ^{13}C CP MAS NMR spectrum (100.6 MHz) of polyethylene produced by **2**. *: spinning side band. Inset shows the presence of Ph end-groups from benzyl initiating moieties.

Polymerization of styrene. In the glove box, a glass reactor is filled with **2** (128 mg, 0.05 mmol La) and 0.575 ml of toluene Then freshly distilled styrene (0.52 g, 5.0 mmol, 100 eq. per La) is added dropwise while the reaction mixture is vigorously stirred. The reaction mixture is heated at 80°C. After 2h, the reaction is quenched with a methanol/water mixture and polystyrene is precipitated from methanol and dried under vacuum, affording 0.22 g of white polymer (42% yield). Tacticity was determined by analyzing ^{13}C signal of the C_{ipso} from the phenyl ring (Figure 3.2.10).

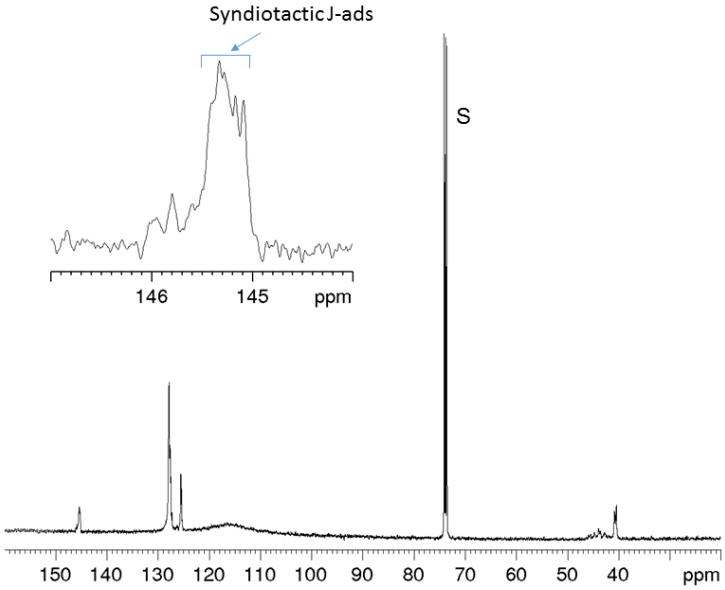

Figure 3.2.10 ^{13}C NMR signal for the C_{ipso} atom in polystyrene obtained by polymerization using **2** as an initiator (100.6 MHz, $C_2D_2Cl_4$, 363 K). S: solvent signal. For assignments of the J-ads see reference 1.

Ring-opening polymerization of ε-caprolactone. In the glove box, a glass reactor is filled with **2** (50 mg, 0.020 mmol La) and 3 ml of toluene. Then, a freshly distilled -caprolactone solution in 2 mL toluene (1.48 g, 13.0 mmol, 650 eq. per La) is added dropwise while the reaction mixture is vigorously stirred. Exothermicity is observed and formation of a gel occurred within about an hour. After 2 hours, the reaction mixture was exposed to air, and extracted with THF. The poly--caprolactone was precipitated from methanol and dried under vacuum, affording 1.32 g of white polymer (89% isolated yield). ^{1}H and ^{13}C NMR features are consistent with reported data (Figure 3.2.11 and Figure 3.2.12).[28]

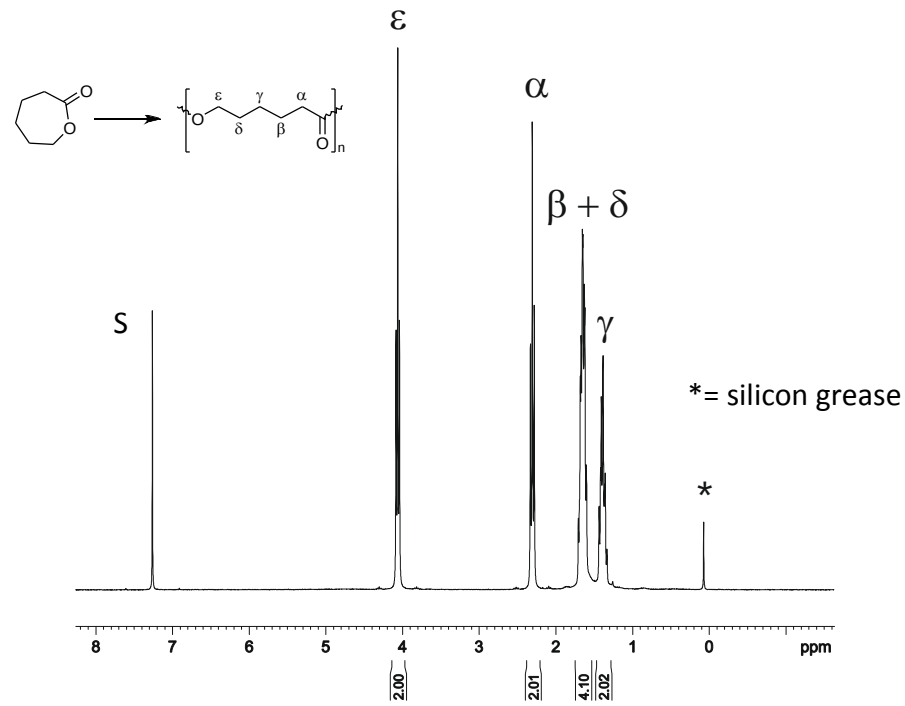

Figure 3.2.11 ^{1}H NMR spectrum (300 MHz, $CDCl_3$) of poly-ε-(caprolactone) produced by **2**

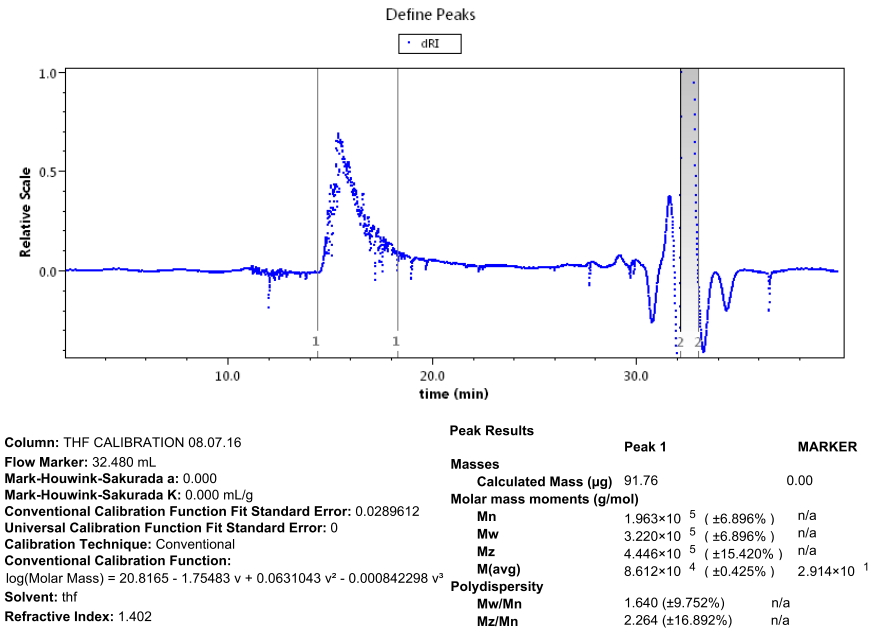

Column: THF CALIBRATION 08.07.16
Flow Marker: 32.480 mL
Mark-Houwink-Sakurada a: 0.000
Mark-Houwink-Sakurada K: 0.000 mL/g
Conventional Calibration Function Fit Standard Error: 0.0289612
Universal Calibration Function Fit Standard Error: 0
Calibration Technique: Conventional
Conventional Calibration Function:
log(Molar Mass) = 20.8165 - 1.75483 v + 0.0631043 v² - 0.000842298 v³
Solvent: thf
Refractive Index: 1.402

Peak Results

	Peak 1	MARKER
Masses		
Calculated Mass (µg)	91.76	0.00
Molar mass moments (g/mol)		
Mn	1.963×10^{5} (±6.896%)	n/a
Mw	3.220×10^{5} (±6.896%)	n/a
Mz	4.446×10^{5} (±15.420%)	n/a
M(avg)	8.612×10^{4} (±0.425%)	2.914×10^{1}
Polydispersity		
Mw/Mn	1.640 (±9.752%)	n/a
Mz/Mn	2.264 (±16.892%)	n/a

Figure 3.2.12. SEC trace of poly-ε-caprolactone obtained with **2**

DFT calculations. All DFT calculations were performed with Gaussian 09.[29] Geometries were fully optimized in gas phase without symmetry constraints, employing the B_3PW_{91} functional[30] and the Stuttgart effective core potential for La and Si[31] augmented with a polarization function (ζ_d = 0,284 for Si and ζ_f = 1.000 for La). For the other elements (H, C and O), Pople's double-ζ basis set 6-31G(d,p)[32] was used. Calculations of vibrational frequencies were systematically done in order to characterize the nature of stationary points. Calculating a theoretical chemical shift requires the knowledge of the chemical shielding of a reference, since it is explicitly calculated as $\delta = (\sigma_{ref} - \sigma)$, in ppm, where σ_{ref} is the isotropic ^1H and ^{13}C chemical shielding of a molecule of tetramethylsilane (calculated at the same level as the studied systems): $\sigma_{ref}(C)$ = 196.1148 ppm, $\sigma_{ref}(H)$ = 31.6435 ppm. Among the various theories available to compute chemical shielding tensors, the gauge including atomic orbital (GIAO) method has been adopted for the numerous advantages it presents.[33] The same methodology was used in previous studies involving grafted systems, showing that theoretical results are fairly accurate with respect to experimental values with an error lower than 15% for ^{29}Si,[19a] 10% for ^{31}P [34] and ^{17}O [19b-1d] and 5% for ^1H [12] and ^{13}C.[12] The electron density and partial charge distribution were examined in terms of localized electron-pair bonding units using the NBO program[35] available in Gaussian 09.

---

[1] Y. Yao; K. Nue, D. A. Ed. Atwood, *the Rare Earth Elements: Fundamentals and Applications,* 2012 Wiley, 459-474.

[2] a) P. L. Watson; G. W. Parshall, *Acc. Chem. Res.* 1985, **18**, 51-56; b) G. Jeske, H. Lauke, H.P. Mauermann, N. Swepston, H. Schumann, T. J. Marks, *J. Am. Chem. Soc.*, 1985, **107**, 8091-8103.

[3] S. A. Cotton, D. A. Ed. Atwood, the Rare Earth Elements: Fundamentals and Applications, 2012, Wiley, 299.

[4]. a) S. Harder, *Organometallics,* 2005, **24**, 373-379; b) S. Bambirra, A. Meetsma, B. Hessen, *Organometallics*, 2006, **25**, 3454-3462

[5] a) J.-M. Basset, R. Psaro, D. Roberto, R. Ugo, *Modern Surface Organometallic Chemistry*, 2009, Wiley. b) C. Coperet, A. Comas-Vives, M. P. Conley, D. P. Estes, A. Fedorov, V. Mougel, H. Nagae, F. Núñez-Zarur, P. A. Zhizhko, *Chem. Rev.*, 2016, **116**, 323-421.

[6] a) R. Anwander, H. W. Roesky, *J. Chem. Soc., Dalton Trans.* 1997, 137-138. b) R. Anwander, O. Runte, J. Eppinger, G. Gestberger, E. Herdtweck, M. Spiegler, *J. Chem. Soc., Dalton Trans.* 1998, 847-858 c) I. Nagl, M. Widenmeyer, E. Herdtweck, G. Raudaschl-Sieber, R. Anwander, *Micropor. Mesopor. Mat.,* 2001, **44**, 311-319

[7] a) R. M. Gauvin, A. Mortreux, *Chem. Commun.* 2005, 1146-1148; b) R. M. Gauvin, L. Delevoye, R. Ali Hassan, J. Keldenich, A. Mortreux, *Inorg. Chem.* 2007, **46**, 1062-1070, c) N. Ajellal, G. Durieux, L. Delevoye, G. Tricot, C. Dujardin, C. M. Thomas, R. M. Gauvin, *Chem. Commun.* 2010, **46**, 1032-1034.

[8] M. P Conley, G. Lapadula, K. Sanders, D. Gajan, A. Lesage, I. Del Rosal, L. Maron, W. W. Lukens, C. Coperet, R. A. Andersen, *J. Am. Chem. Soc.*, 2016, **138**, 3831-3843.

[9] I. Nagl, M. Widenmeyer, E. Herdtweck, G. Raudaschl, R. Anwander, *Microporous Mesoporous Mater.* 2001, **44**, 311-319.

[10] a) A. Fischbach, M. G. Klimpel, M. Widenmeyer, E. Herdtweck, W. Scherer, R. Anwander, *Angew. Chem., Int. Ed.* 2004, **43**, 2234-2239; b) E. Le Roux, Y. Liang, K. W. Törnroos, F. Nief, R. Anwander, *Organometallics,* 2012, **31**, 6526-6537.

[11] S. Arndt, J. Okuda, *Adv. Synth. Catal.* 2005, **347**, 339-354.

[12] N. Popoff, J. Espinas, J. Pelletier, B. Macqueron, K.C. Szeto, O. Boyron, C. Boisson, I. Del Rosal, L. Maron, A. De Mallmann, R.M. Gauvin, M. Taoufik, *Chem. Eur. J.*, 2013, **19**, 964-973.

[13] a) C. Pellechia, A. Grassi, A. Zambelli, *Chem. Commun.* 1993, 947-949. b) C. Pellechia, A. Grassi, A. Zambelli, *Organometallics* 1994, **13**, 298-302.

[14] I. Schnell, S. P. Brown, H. Y. Low, H. Ishida, H. W. Spiess, *J. Am. Chem. Soc.*, 1998, **120**, 11784-11795.

[15] S. Bambirra, F. Perazzolo, S. J. Boot, T. J. J. Sciarone, A. Meetsma, B. Hessen, *Organometallics*, 2008, **27**, 704-712.

[16] F. J. Feher, T. A. Budzichowski, *J. Organomet. Chem.* 1989, **373**, 153-164.

[17] a) H. Ahn, T. J. Marks, *J. Am. Chem. Soc.* 2002, **124**, 7103-7110; b) C. P. Nicholas, H. Ahn, T. J. Marks, *J. Am. Chem. Soc.* 2003, **125**, 4325-4331; c) J. Pelletier, J. Espinas, N. Vu, S. Norsic, L. Delevoye, J. Trebosc, E. Le Roux, C. Santini, J.-M. Basset, R. M. Gauvin, M. Taoufik, *Chem. Commun.* 2011, **47**, 2979-2981.

[18] P.J. Toscano, T.J. Marks, *Langmuir*, 1986, **2**, 820-823

[19] (a) I. del Rosal, I. C. Gerber, R. Poteau, L. Maron, *J. Phys. Chem*. A, 2010, **114**, 6322-6330; (b) N. Merle, J. Trebosc, A. Baudouin, I. Del Rosal, L. Maron, K.C. Szeto, M. Genelot, A. Mortreux, M. Taoufik, L. Delevoye, R. M. Gauvin, *J. Am. Chem. Soc.,* 2012, **134**, 9263-9275; (c) N. Merle, G. Girard, N. Popoff, A. De Mallmann, Y. Bouhoute, J. Trebosc, E. Berrier, J.-F. Paul, C. P. Nicholas, I. Del Rosal, L. Maron, R. M. Gauvin, L. Delevoye, M. Taoufik, *Inorg. Chem.* 2013, **52**, 10119-10130; (d) Y. Bouhoute, A. Garron, D. Grekov, N. Merle, K. C. Szeto, A. De Mallmann, I. Del Rosal, L. Maron, G. Girard, R. M. Gauvin, L. Delevoye, M. Taoufik, *ACS Catal*. 2014, **4**, 4232-4241; (e) I. del Rosal, I. C. Gerber, R. Poteau, L. Maron, *New J. Chem*., 2015, **39**, 7703-7715; (f) Y. Bouhoute, D. Grekov, K. C. Szeto, N. Merle, A. De Mallmann, F. Lefebvre, G. Raffa, I. del Rosal, L. Maron, R. M. Gauvin, L. Delevoye, M. Taoufik, *ACS Catal.* 2016, **6**, 1-18; (g) Y. Bouhoute, I. Del Rosal, K. C. Szeto, N. Merle, D. Grekov, A. De Mallmann, E. Le Roux, L. Delevoye, R. M. Gauvin, L. Maron, M. Taoufik, *Catal. Sci. Technol*. 2016, **6**, 8532-8539.

[20] (a) I. Del Rosal, R. Poteau, L. Maron. *Dalton Trans*. 2011*,* **40***,* 11211-11227; (b) I. Del Rosal, R. Poteau, L. Maron. *Dalton Trans*. 2011*,* **40***,* 11228-11240; (c) I. Del Rosal, M. J.-L. Tschan, R. M. Gauvin, L. Maron, C. M. Thomas, *Polym. Chem.* 2012*,* **3**, 1730-1739; (d) I. Del Rosal, A. Yahia, L. Maron, *Inorg. Chem*. 2016, **55**, 10024-10033.

[21] K.H. den Haan, Y. Wielstra, J. H. Teuben, *Organometallics*, 1987, **6**, 2053-2060.

[22] R.M. Gauvin, T. Chenal, R. Ali Hassan, A. Addad, A. Mortreux, *J. Mol. Cat. A. Chem.*, 2006, **257**, 31-40.

[23] J. Gromada, J.-F. Carpentier, A. Mortreux, *Coord. Chem. Rev.* 2004, **248**, 397-410.

[24] T. J. Woodman, Y. Sarazin, G. Fink, K. Hauschild, M. Bochmann, *Macromolecules* 2005, **38**, 3060-3067.

[25] R. M. Gauvin, F. Buch, L. Delevoye, S. Harder, *Chem. Eur. J.* 2009, **15**, 4382-4393

[26] a) S. Bambirra, M. W. Bouwkamp, A. Meetsma, B. Hessen, *J. Am. Chem. Soc.* 2004, **126**, 9182-9183; b) M. Zimmermann, N. A. Froystein, A. Fischbach, P. Sirsch, H. M. Dietrich, K. W. Törnroos, E. Herdtweck, R. Anwander, *Chem. Eur. J.* 2007, **13**, 8784-8800.

[27] S. M. Guillaume, M. Schappacher, A. Soum, *Macromolecules*, 2003, 36, 54-60.

[28] R. Lapenta, M. Mazzeo, F. Grisi, *RSC Adv.* 2015, 87635-87644.

[29] Gaussian 09, Revision D.01, M.J. Frisch, G.W. Trucks, H.B. Schlegel, G.E. Scuseria, M. A. Robb, J. R. Cheeseman, G. Scalmani, V. Barone, G. A. Petersson, H. Nakatsuji, X. Li, M. Caricato, A. Marenich, J. Bloino, B.G. Janesko, R. Gomperts, B. Mennucci, H. P. Hratchian, J. V. Ortiz, A. F. Izmaylov, J. L. Sonnenberg, D. Williams-Young, F. Ding, F. Lipparini, F. Egidi, J. Goings, B. Peng, A. Petrone, T. Henderson, D. Ranasinghe, V. G. Zakrzewski, J. Gao, N. Rega, G. Zheng, W. Liang, M. Hada, M. Ehara, K. Toyota, R. Fukuda, J. Hasegawa, M. Ishida, T. Nakajima, Y. Honda, O. Kitao, H. Nakai, T. Vreven, K. Throssell, J. A. Jr. Montgomery, J.E. Peralta, F. Ogliaro, M. Bearpark, J. J. Heyd, E. Brothers, K.N. Kudin, V. N. Staroverov, T. Keith, R. Kobayashi, J. Normand, K. Raghavachari, A. Rendell, J. C. Burant, S. S. Iyengar, J. Tomasi, M. Cossi, J. M. Millam, M. Klene, C. Adamo, R. Cammi, J.W. Ochterski, R.L. Martin, K. Morokuma, O. Farkas,. J. B. Foresman, D. J. Fox, Gaussian, Inc., Wallingford CT, 2016.

[30] A. D. Becke, *J. Chem. Phys.*, 1993, **98**, 5648-5652 and references therein.

[31] (a) M. Dolg, H. Stoll, H. J. Preuss, *J. Chem. Phys.*, 1989, **90**, 1730-1734. (b) X. Cao, M. Dolg, *THEOCHEM*, 2002, **581**, 139-147.

[32] (a) P. C. Hariharan, J. A. Pople, *Theor. Chem. Acc*., 1973, **28**, 213-222. (b) W.J. Hehre, R. Ditchfield, J. A. Pople*, J. Chem. Phys*., 1972, **56**, 2257-2261

[33] (a) F. J. London, *J. Phys. Radium*, 1937, **8**, 397-409; (b) R. McWeeny, *Phys. Rev.*, 1962, **126**, 1028-1034; (c) R. Ditchfield, *Mol. Phys*., 1974, **27**, 789-807; (d) J.L. Dodds, R. McWeeny, A. Sadlej, *J. Mol. Phys*., 1977, **34**, 1779-1791

[34] H. Staub, I. Del Rosal, L. Maron, F. Kleitz, F.-G. Fontaine*, J. Phys. Chem. C*, 2012, **116**, 25919-25927

[35] (a) A. E. Reed, F. Weinhold, *J. Chem. Phys*. 1983, **78**, 4066-4073; (b) A. E. Reed, L. A. Curtiss, F. Weinhold, *Chem. Rev.*, 1988, **88**, 899-926.

3.3. Grafted rare-earth metal catalysts for C-C bond formation: Synthesis, characterization and application

3.3.1. Introduction

The development of more efficient catalysts is one of the main challenge to solve both environmental and economic issues. A way to achieve this is the generation of well-defined heterogeneous catalysts. Indeed, grafting molecular catalysts on a material is a most promising approach which allows access to a wealth of potential new catalytic systems. Technically, the preparation of materials that combine both advantages of homogenous catalyst (high selectivity and activity) and heterogeneous ones (recyclability and easy separation from products) is of high interest. To achieve this, precise conditions are required to form well-defined species that are bound to the surface in a controlled fashion, to generate active sites that are as precisely understood as their molecular counterparts. In the present work, we present the immobilization of rare-earth metal trisamide species on a highly dehydroxylated silica and their use for C-C bond formation, namely in dimerization of terminal alkynes.

Originally used for its lipophilicity and its simple signature in ^{1}H NMR the bis-trimethylsilylamido ligands (-$N(SiMe_3)_2$) has been proved to be useful for organometallic chemistry, especially due to the absence of beta-hydrogen atoms that might lead to decomposition of transition element complexes. Preliminary studies were carried out by Bürger and Wannagat[1] who described the synthesis of several 4th period transition metal complexes bis- or tris-amides $M(N(SiMe_3)_2)_3$ (M= Cr, Mn, Cu and Ni). The development of a tin complex by Lappert and Zuckerman initiated the widespread use of $N(SiMe_3)_2$ in coordination chemistry[2]. Regarding application in the rare-elements, the $Ln(N(SiMe_3)_2)_3$ species were first reported by Bradley in 1973[3]. In this paper, he presented the synthesis of nearly all the lanthanide complexes (lanthanum from lutetium). These feature a triscoordinated coordination mode, due to the bulk of the bissilylamide ligands, which even more remarkable when considering the ability of the rare-earth metals to accommodate a number of ligands larger than transition metals (Figure 3.3.1).

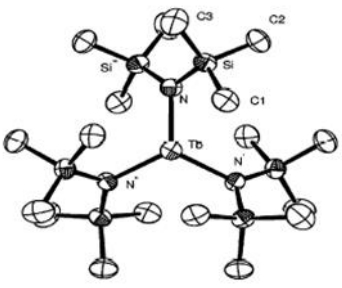

Figure 3.3.1 Structure of $Tb(N(SiMe_3)_2)_3$ from reference 3

These homoleptic compounds have been applied in several reactions as polymerization of ε-caprolactone[4], butadiene[5] or methylmethacrylate[6]. Moreover, they are also active for

dimerization of aldehydes into esters (Tishchenko reaction)[7], hydrosilylation[8] hydroamination[9] and alkyne dimerization[10]. We have selected the last reaction for our studies, as it affords different products, with a selectivity depending on catalysts and reaction conditions. This is thus a well-suited tool to probe, for instance, the influence of grafting of the molecular catalyst. These experimental investigations will be combined in the near future with theoretical calculations on the mechanism by the team of L. Maron (LPCNO).

3.3.2. Results and Discussion

Thanks to the reactivity of NR_2 ligands towards protonolysis and to the lanthanides' ability to form strong bond with oxygen, these catalysts are perfect for immobilization onto inorganic supports such like silica. Upon grafting, several surface species can be obtained with direct reaction of $Ln(NR_2)_3$ with partially dehydroxylated silica[10,11] (Scheme 3.3.1).

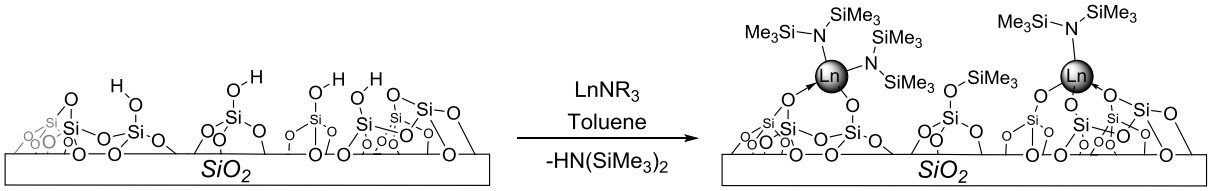

Scheme 3.3.1 Generation of $\equiv SiOLn(NR_2)_x$ using silica and $LnNR_3$

Thus, depending on the presence of interacting and non-interacting silanols, both mono-grafted (bearing two bis(trimethylsilylamido) ligands) and bis-grafted (bearing one bis(trimethylsilylamido) ligand) species can be formed. As these reactions release hexamethyldisilazane, a well-known silylating agent, the grafting occurs concomitantly to silanol capping by trimethylsilyl groups and NH_3 release. After first studies from Anwander on surface chemistry of lanthanide trisamide on several supports,[12] it was shown in the UCSC that monografted species could be selectively prepared using silica treated at 700 °C, which comprises only non-interacting silanols[11,13]. Further examples of grafting using amido species have been reviewed by Liang and Anwander. [14]

The synthesis of $Ln(NR_2)_3$ was performed by following literature procedure.[15] It involves reaction of 3 equivalent of hexamethyldisilazane lithium salt (LiHMDS) with 1 equivalent of $LnCl_3$ in THF (Ln= Sc, Y, La, Yb, Nd, Scheme 3.3.2). The products are purified by sublimation under vacuum (10^{-5} mbar) at 100°C. In the case of diamagnetic species (Sc, Y, La), the single peak (different from the pro-ligand) in ^1H NMR confirms the formation of the pure product (Figure 3.3.2).

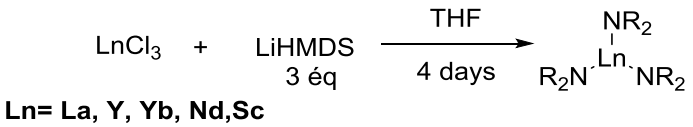

Scheme 3.3.2 Synthesis of $Ln(NR_2)_3$

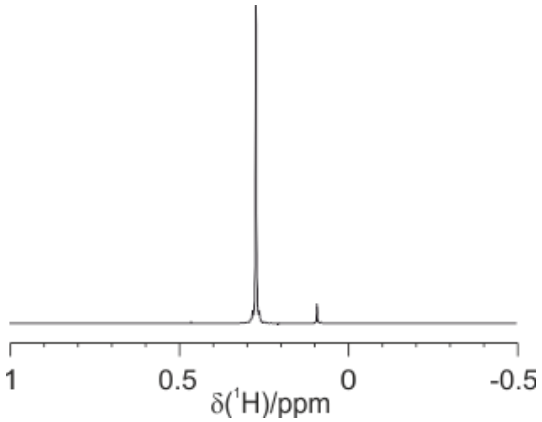

Figure 3.3.2 ^{1}H NMR spectrum of La(N(SiMe$_3$)$_2$)$_3$ **La** (C_6D_6, 300 MHz)

Immobilization of these species onto $SiO_{2\text{-}700}$ was then performed following the reported procedure[11]. The sole presence of non-interacting silanols on the pristine support is checked by IR (sharp signal at 3747 cm^{-1}, Figure 3.3.3). Reaction with a small excess of complex **Ln** (1.3 eq.) with respect to silanols affords materials **Ln-700** (Scheme 3.3.3) after 15 h in pentane and several washing to remove the unreacted precursor. A further drying step is carried out at 80 °C to remove traces of bound ammonia.

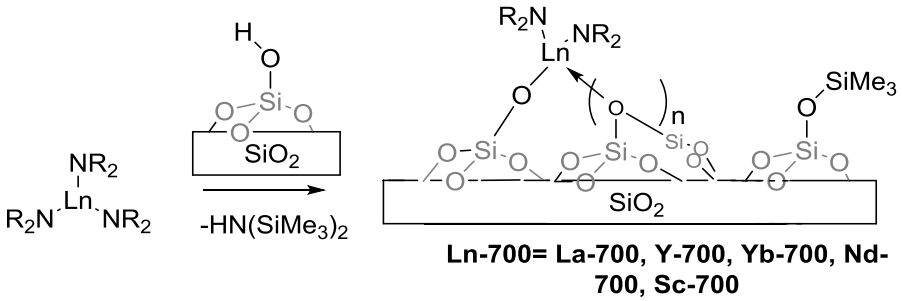

Scheme 3.3.3 Grafting **Ln** over highly dehydroxylated silica to generate **Ln-700**

The full consumption of silanols is compared to the starting material in infrared spectroscopy (Figure 3.3.3). The disappearance of $\nu_{(O\text{-}H)}$ band at 3747 cm^{-}1 and new signals at 3000-2950 and 2950-2900 cm^{-1}, accounting for $\nu_{(\ sp^3\ C\text{-}H)}$ reveal both catalyst and silylated silanols formation. Elementals analysis are consigned in Table 3.3.1. The ratio N/Ln is in line with the structure. The loading of metal per gram is in accordance with the previous results of our team[16], and indicates a maximum loading. ^{1}H MAS solid state NMR presents one signal at 0.1 ppm with a shoulder at 0.4 corresponding to ≡SiOSiMe$_3$ moieties creates during the release of hexamethyldisilazane while grafting (Figure 3.3.4). Interestingly, the synthesis with THF coordinated Li(HMDS) instead of the Li(HMDS) alone gives the ate Ln corresponding catalyst (Figure 3.3.6 top caption). It has been confirmed with a ^{1}H-^{1}H DQSQ experiment which relies on dipolar interactions, and thus that gives information on spatial proximities (Figure 3.3.6). Thus, both signals at 3.9 and 1.9 ppm can be attributed to THF species, α-CH$_2$ and β-CH$_2$ respectively and is confirmed by the correlation (Figure 3.3.6 -site B). Interaction with the signal at -0.1 ppm (Figure 3.3.6 -site A) and with the signal at 3.9 ppm (α-CH$_2$) probe spatial

proximity between THF and $NSiMe_3$ ligand. In addition, the shoulder at 0.2 ppm showing no correlation and can be attributed to $\equiv SiOSiMe_3$ species as observed with DRIFT experiment.

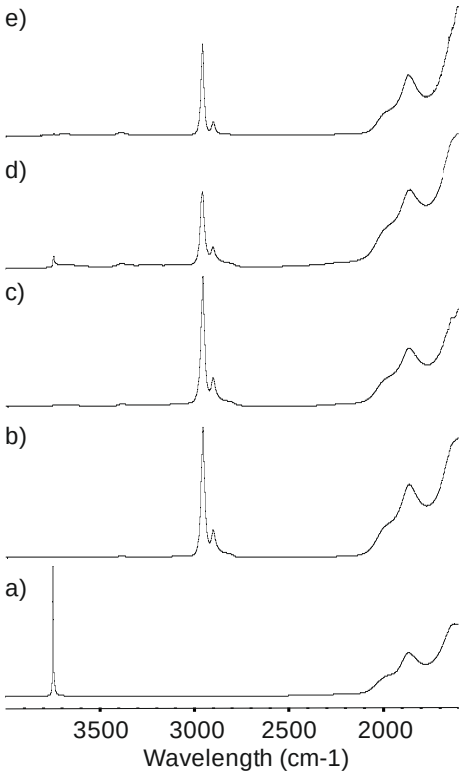

Figure 3.3.3 DRIFT spectra of a) $SiO_{2\text{-}700}$, b) **La-700**, c) **Y-700**, d) **Sc-700**, e) **Nd-700**.

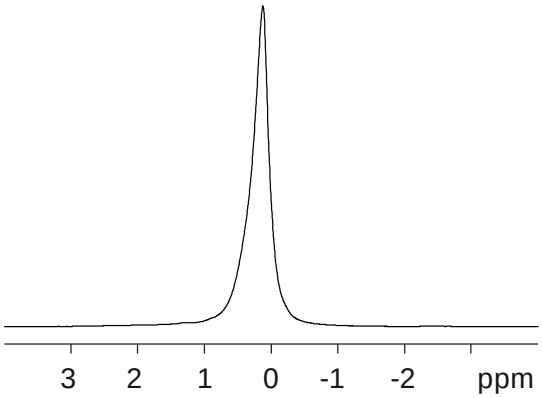

Figure 3.3.4 ^{1}H MAS NMR of **La-700**

Ln-700	%C	%H	%N	%Ln	C/N	N/Ln
La-700	4.1	0.8	0.8	3.3	5.9	2.45
Y-700				2.6		
Nd-700	4	0.9	0.5		9.4	
Sc-700	3.4	0.8	0.7	1.04	5.7	2.1

Table 3.3.1 Elemental Analysis of **Ln-700**.

Interestingly, in the case of lanthanum and yttrium, carrying out the synthesis with THF-coordinated Li(HMDS) instead of Li(HMDS) gives the known ate-species

$Li(THF)_3[Ln\{N(SiMe_3)_2\}_3(Cl)]$ (Ln= Y, La) (Scheme 3.3.4). ^1H NMR confirms the structure described in the literature.[17]

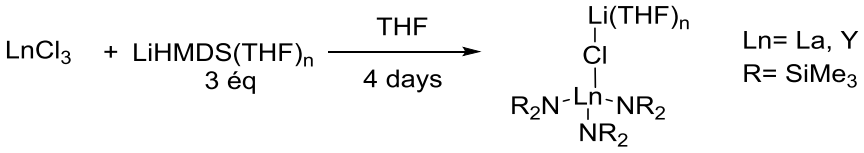

Scheme 3.3.4 Synthesis of **Ln-LiCl**

The lanthanum derivative was grafted onto $SiO_{2\text{-}700}$, affording material **La-LiCl-700**, which was characterized by MAS NMR, infrared and elemental analysis.

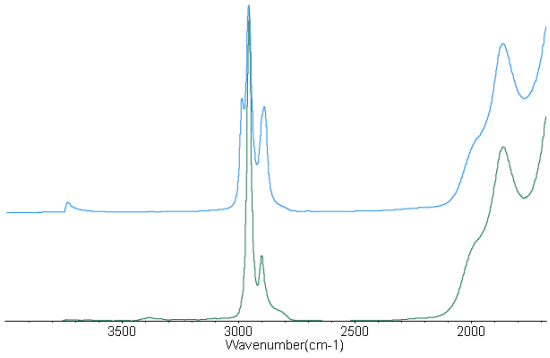

Figure 3.3.5 DRIFT spectra of **La-700** (bottom) and **La-LiCl-700** (top)

The comparison of the DRIFT spectra of **La-700** and **La-LiCl-700** shows the presence of a new signal at 2982 cm^{-1} that can be attributed to CH_2 from THF (Figure 3.3.5). The same bands at 2951 and 2887 cm^{-1} than with **La-700** corresponding to the elongation of sp^3 C-H bonds are also observed. Some residual silanols are still present on the material.

The structure of **La-LiCl-700** was studied with a ^1H-^1H DQSQ NMR experiment which relies on dipolar interactions, and thus that gives information on spatial proximities (Figure 3.3.6). Thus, both signals at 3.9 and 1.9 ppm can be attributed to bound THF, α-CH_2 and β-CH_2 respectively as confirmed by the off-diagonal correlation (Figure 3.3.6–correlation B). Interaction between protons at -0.1 and at 3.9 ppm (Figure 3.3.6 – correlation A) stems from spatial proximity between α-CH_2 from the THF ligand and $NSiMe_3$ moieties. In addition, the shoulder at 0.2 ppm showing no correlation can be attributed to $\equiv SiOSiMe_3$ species as observed previously[11].

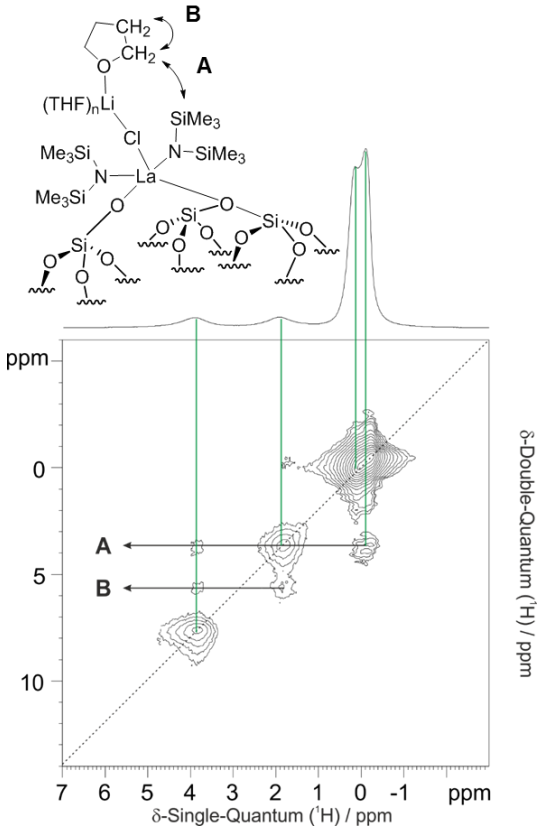

Figure 3.3.6 ^{1}H MAS NMR (top) and ^{1}H-^{1}H DQ-SQ MAS NMR spectrum of **La-LiCl-700** (18.8 T, spinning speed 20 kHz).

The molecular species (**Ln**) and the corresponding materials (**Ln-700**) were applied to the formation of C-C bonds by dimerization of terminal alkynes. This reaction, described in the same year by the Bercaw and Teuben group[18], allows to obtain ene-yne type molecules. Results can be found in Table 3.3.3. The proposed mechanism of this reaction[19] is detailed in the Scheme 3.3.6 for the homoleptic molecular species as starting precatalyst. The first step consists of the protonolysis of one equivalent of the terminal alkyne, forming an alkynyl species. Then, after coordination of the alkyne, insertion into the C-C triple bound occur, either in 1,2 or 1,1 fashion, affording two distinct alkenyl species (**1a** and **1b** on Scheme 3.3.5). Then, protonolysis of the Ln-C(sp^2) by the more acidic sp^3 C-H releases the enyne, either as head-to-tail (from **1a**) or as head-to-head (from **1b**) dimers. Influence of reaction conditions on the outcome in terms of selectivity is a key issue of this study. Furthermore, it also has been observed that once the dimer is formed, it can also enter a catalytic cycle, to form trimers (pathway **2**), which is also a factor to be taken in account.

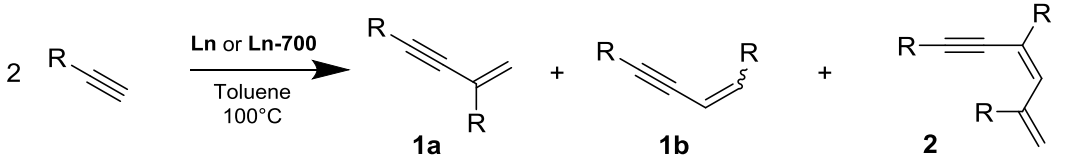

Scheme 3.3.5 Alkyne dimerization with homogeneous or heterogeneous catalysts

Entry	**Ln**	Ionic radius	Conversion	Selectivity **1a/1b/2**
1	**La**	103	92	82/13/5
2	La(μ-Cl)Li(THF)$_3$(HMDS)$_3$	103	0	0
3	**Y**	90	65	99/1/0
4	**Sc**	75	91	99/1/0
5	**La$_{700}$**	103	70	68/2/30
6	**Y$_{700}$**	90	78	93/1/6
7	**Nd$_{700}$**	98	74	67/2/31
8	**Yb$_{700}$**	78	76	96/1/3
9	**Sc$_{700}$**	75	47	93/1/6

Conditions: 1% of catalyst, 3 mL of toluene, 4h at 100°C, quantification by GC

Table 3.3.2. Dimerization of 1-hexyne

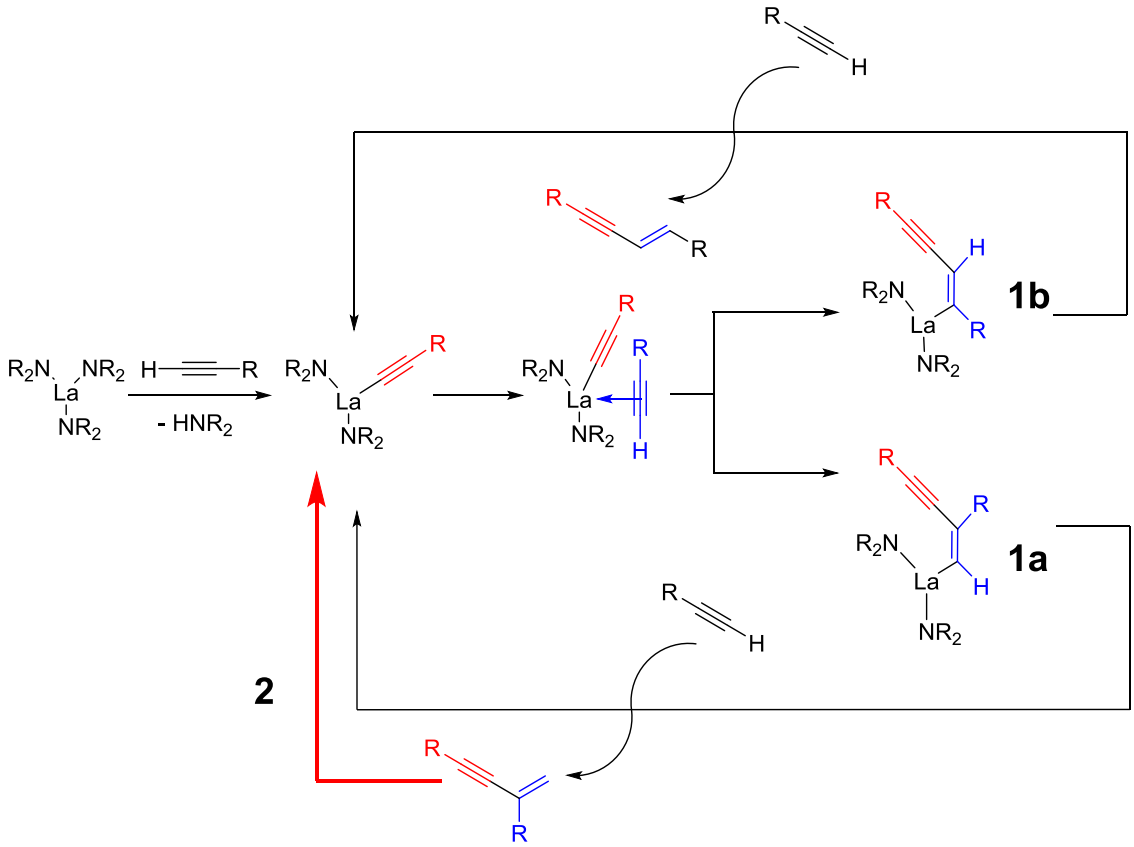

Scheme 3.3.6 Proposed mechanism of dimerization of terminal alkyne

The results from catalysis are reported on Table 3.3.2. A first catalytic test with **La** gave good results (Entry 1, 92% of conversion, in line with previous reports[10]), which validates our experimental conditions (Scheme 3.3.5). The analysis of the products reveals the presence of dimers **1a** and **1b**, and of trimer species **2**. The latter accounts for about 5% of the products. Regarding the dimers, **1a** is the major one (82%), indicating that some degree of regioselectivity is reached with this system (see Scheme 3.3.7). The comparison of the ^{1}H NMR in Figure 3.3.7 (the dimer and the mix of trimer and dimer were obtained using the

experimental conditions of the entry 3 and 5 respectively from Table 3.3.2) reveals that major trimer (the resolution is not enough to see if another one is formed) is of type **2**, though analysis is complexified by the low quantity of material. This is evidenced by the presence of a singlet at 6.05 ppm (assigned to H_b in 2, Scheme 3.3.7) and not of a triplet in the case of **3** (accounting for H_c, Scheme 3.3.7).

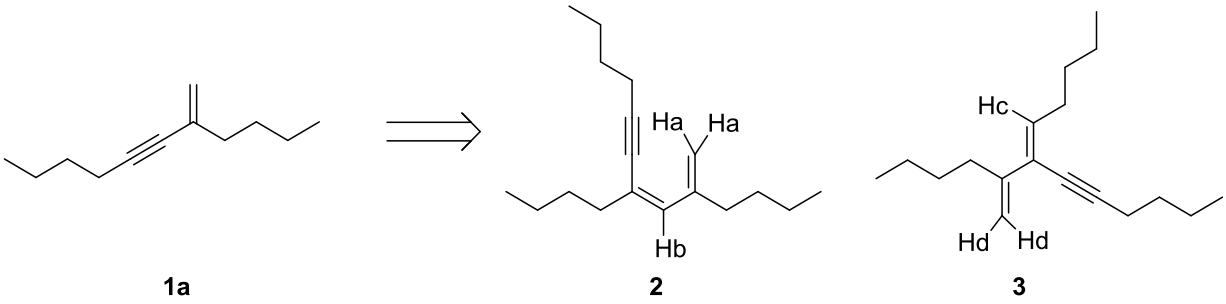

Scheme 3.3.7 Possible products formed by the addition of a terminal alkyne onto the head-to-tail dimer

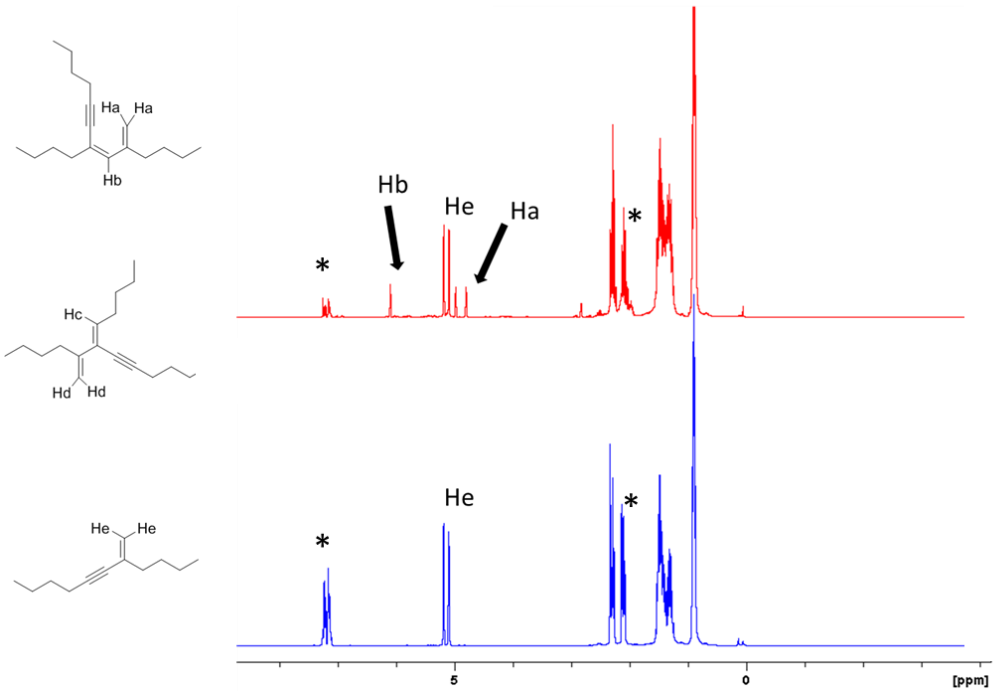

Figure 3.3.7 Comparison in ^{1}H NMR spectra of **1a** dimer (bottom) and of mixture of **1a** and trimer **2** (top). *: solvent

Once the products were clearly identified, the influence of the nature of the metal was probed (Table 3.3.2). Yttrium is less active than lanthanum and scandium (that display comparable activity after 15 h. However, the selectivity towards **1a** is almost complete in the case of the smaller metals Sc and Y (Table 3.3.2, entries 1, 3 and 4). A link between the ionic radius and the activity or selectivity may be proposed, but further studies would be

necessary to confirm this point. Interestingly, the ate-complex (the LiCl adduct of **La**) was shown to be inactive for this transformation.

Supported catalysts were also probed, for Sc, Y, La, Nd and Yb species. Conversion rates after 15 hours were correct overall, with only scandium affording poor results. The larger lanthanum and neodymium derivatives proved to be less selective toward dimer formation, resulting both in about 30 % of **2**. However, the selectivity towards **1a** formation remained high, though less than what was observed with molecular catalysts.

In order to better understand these systems, we carried out a comparative study with both homogenous and heterogeneous catalysts based on lanthanum and yttrium metal (Figure 3.3.8). In these cases, each result for a given reaction time corresponds to two separate experiments, to ensure reproducibility and accuracy.

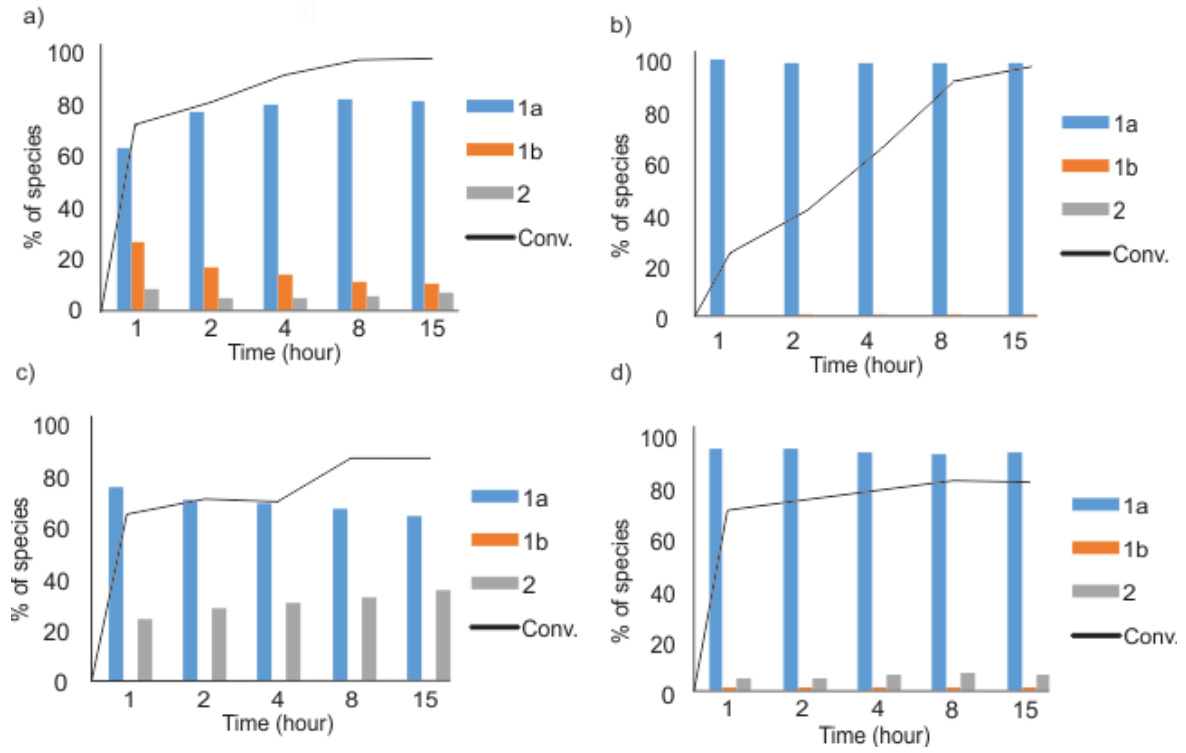

Figure 3.3.8 Kinetic studies of dimerization of 1-hexyne with a) **La**, b) **Y**, c) **La$_{700}$**, d) **Y$_{700}$.**
*Conditions: 1% of **Ln**, 3 mL of toluene* , quantified by GC.

All the catalysts afforded high conversion (80% minimum) with a strong selectivity towards dimer **1a** that can be explained by the steric hindrance that drive the system toward the 1,2 insertion. The comparison between molecular **La** and **Y** reveals a higher activity with lanthanum, reaching the maximum of conversion (99%) after 8h (instead of 15h for the **Y**). This takes place with lesser selectivity than **Y**, as both dimer **1b** and trimer **2** are obtained. Interestingly, in the case of **La**, the **1a**/**1b** ratio evolves over time, showing initial lesser selectivity toward 1a. This may be due to change in active species, which may correspond to gradual substitution of two amido ligands by acetylides, instead of one, initially. The materials **La-700** and **Y-700** behave differently from their molecular counterparts. The **La**

derivative is slightly slower in its grafted version, whereas very fast intial reaction is observed for the yttrium derivative (90% at 15h for **La-700** and 82% at 15h for **Y-700**, see conversion vs. time in Figure 3.3.8). Interestingly, the grafted catalysts display a different selectivity than the corresponding molecular ones. Indeed, the supported lanthanum species is less selective towards dimer vs. trimer formation, but very selective regarding the **1a** vs. **1b** dimer selectivity, as only **1a** is detected. It may be that grafting increases the electrophilicity of the metal center on one hand, thus increasing the rate of trimerization, and one the other hand, the bulk from the surface may be at the origin of the higher head-to-tail product selectivity. Additionally, we observed that the grafted ate-species, **La-LiCl-700**, was inactive.

To go further, and assess the nature of the catalyst resting state, a deuterolysis was performed on the **La-700** system after 4h of catalysis under the same reaction conditions as above. Thus, solvent and products were removed from the reactor in the glove box, and the resultant material was washed 3 times with pentane. Deuterated methanol was added and the released species were analyzed by GC and NMR. 99% of the species is the deuterated alkyne (Scheme 3.3.8). We can confirm that the resting state of the catalytic cycle is the alkynyl derivative, and thus not the enynyl one. The limiting step could thus be the insertion of the La-C into the triple bond. As a comment, one should mention that upon coordination on the lanthanum alkynyl species, the reaction can proceed along two directions (if one excepts decoordination): 1) either insertion to for the enynyl by nucleophilic attack on the triple bond, or 2) protonolysis of the La-C by the C-H from the coordinated alkyne. The last option would then consist in unproductive scrambling of substrate around the metal. Further studies would be necessary to assess this.

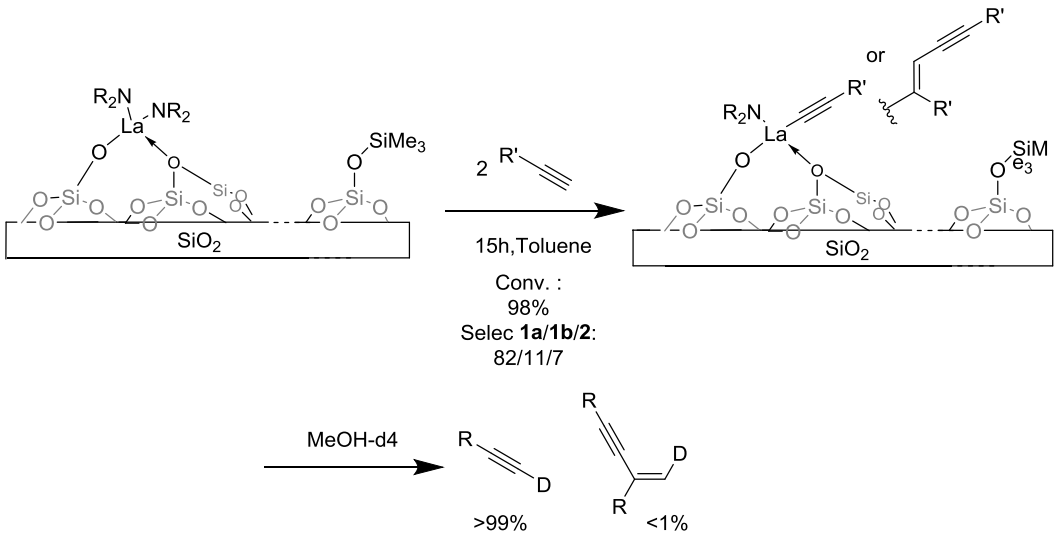

Scheme 3.3.8 Deuterolysis of **La-700** after catalysis

We also aimed at determining the comparative rate of reaction between the substrate and dimer **1a**. As the trimer species is formed with longer reaction time, we designed an experiment involving equimolar ratio of dimer and alkyne. Specific experiments were carried out by mixing 1-heptyne with pure **1a** dimer derived from 1-hexyne (named $\mathbf{1a_{hex}}$, prepared

specifically from the molecular **Y** catalyst and rigorously purified prior to use), assuming that 1-heptyne feature quasi-identical reactivity compared to 1-hexyne. The goal was to probe the relative rate of formation of 1) the dimer from 1-heptyne (**1a**$_{hep}$) **2**) the trimer from 1-heptyne (**2**$_{hep}$) and **3**) the mixed trimer resulting from reaction of dimer **1a**$_{hex}$ and 1-heptyne (designated as **2** $_{hex\text{-}hept}$). We chose the **La-700** catalyst for this peculiar study based on its low selectivity towards dimer vs. trimer (tests with **Y**$_{700}$ showed only products from 1-hexyne). After 15h, staring from an equimolar reaction mixture, the conversion reaches 49 and 15 % for of 1-heptyne and **1a**$_{hex}$, respectively. The selectivity in products is 56%, 42% and 2% for **1a**$_{hept}$,**2**$_{hex\text{-}hept}$ and **2a**$_{hept}$ respectively. As the conversion is higher with the 1-heptyne, the insertion of an alkyne is thus faster than with the dimer (independently of its origin).

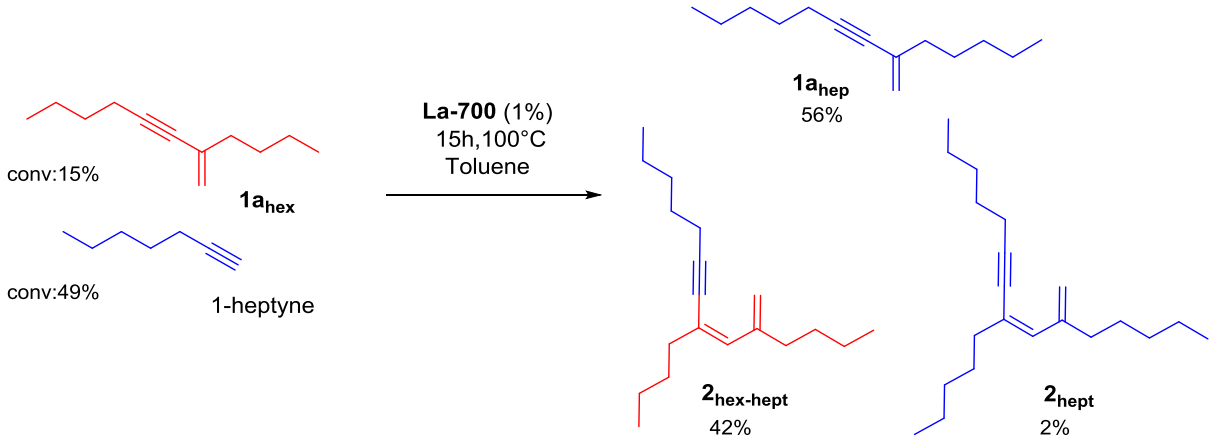

Scheme 3.3.9 Cross-experiment between **1a**$_{hex}$ and 1-heptyne

The substrate scope of this transformation was extended to several alkynes (Table 3.3.3). Moderate to high conversion rates were reached, with overall good selectivity, excepted for specific case involving La and Nd derivatives (Table 3.3.3, entries 5, 11 and 13). We used 1,8-nonadiyne, a dialkyne molecule, to check the possibility of the generation of cyclic species, oligomer or polymers but only the typical dimer/trimer couple was observed in GC, with a disappointing conversion.

Entry	Alkyne	Catalyst	Time	Conv.	Selec. 1a/1b/2
1	1-hexyne	La	4	92	82/13/5
2	1-hexyne	La-700	4	70	68/2/30
3	1-hexyne	Y	4	65	99/1/0
4	1-hexyne	Y-700	4	78	93/1/6
5	1-hexyne	Nd-700	4	74	67/2/31
6	1-hexyne	Sc-700	4	47	93/1//6
7	1-heptyne	La	4	89	82/15/3
8	1-heptyne	La-700	4	59	80/1/19
9	1-heptyne	Y	4	68	99/1/0
10	1-heptyne	Y-700	4	49	97/1/2

11	Cyclopropyl-acetylene	La	4	97	76/11/13
12	Cyclopropyl-acetylene	La-700	4	76	82/4/14
13	3-cyclohexyl-1-propyne	La-700	4	78	64/4/32
14	3-cyclohexyl-1-propyne	Y-700	4	40	93/3/4
15	1,8-nonadiyne	Y-700	4	26	92/2/6

Table 3.3.3 Alkyne dimerization with **Ln** or **Ln-700**

3.3.1. Conclusion

We have described here the use of a series of well-defined silica-supported rare-earth metal amides in terminal alkyne dimerization. The reactivity of the supported species was compared to that of molecular counterparts. Slightly lower activity was most often observed for the silica-grafted amides, with significant differences in chemio- and regioselectivity. In terms of chemioselectivity, part of the differences arises from the higher electrophilicity of the surface-bound species, which causes higher proportion of species resulting from trimerization (namely, from enhanced reactivity towards the dimerization product compared to that of molecular counterparts). We also showed that the resting state of the catalyst was as an alkynyl product, and we concluded that the rate determining step was the insertion of the Ln-C into the substrate's triple bond. We also showed that the enyne formed as primary product is less reactive than the alkyne substrate towards addition of a further substrate molecule, showing that trimerization occurs at a slower rate than dimerization, when present in similar concentration. The scope was also explored, demonstrating the applicability of the grafted amides in the conversion of a range of alkynes. DFT calculations performed by the Maron team from LPCNO (INSA Toulouse) are currently in progress to help and rationalize these results. Most unfortunately, these studies were not completed at the time of the writing of this manuscript. Once available, these will complement these experimental studies and help in a better understanding of this catalytic reaction.

3.3.2. Experimental Section

All experiments were carried out under an argon atmosphere in a M-Braun glove box or by using standard Schlenk techniques. Lanthanide chlorides were purchased from Strem Chemicals. Solvents, reactants were dried under argon using conventional reagents, degassed by freeze–pump–thaw cycles and stored in the glove box over 3A molecular sieves. Alkynes were obtained from Aldrich. Aerosil 380 silica (Degussa, specific area 380 $m^2\ g^{-1}$, prior to heat treatment) was subjected to heating under secondary vacuum (10^{-6} mbar) for 15 h at 500 °C, followed by 4 h at 700 °C, and stored in a glovebox. Elemental analyses were carried out at London Metropolitan University (CHN) and at LASIR (Ln). Diffuse reflectance infrared spectra were collected with a Harrick cell on a Nicolet Avatar spectrometer fitted with a MCT detector. Typically, 64 scans were accumulated for each spectrum (resolution 4 cm^{-1}). Liquid-state NMR analyses were run on a Bruker Avance 300 spectrometer. Solid-state MAS NMR spectra were recorded on Bruker Avance 400 and 800 spectrometers. Chemical shifts are given with respect to adamantane as external reference. The ^1H MAS NMR was

recorded with a spinning speed at 20MHz. The 90° pulse length was 3 µs, the recycle delay was 10 s for 16 scans. The two-dimensional homonuclear experiment (DQ-MAS) was obtained at a spinning frequency of 20 kHz by using excitation and reconversion pulse blocks of two rotor periods each (200 µs). The 90° pulse length was 3.25 µs, the recycle delay was 2 s, and 16 scans were collected for each slice (1024 in total). Gas chromatography analyses were performed on a Shimadzu GC2010 gas chromatograph under argon flow with a CP-Sil5CB column (25 m length, 0.25 mm diameter, 0.2 µm film thickness). Both injector and detector temperature are set at 250 °C. Heating program: starting at 50 °C then a ramp of 10 °C/min up to 250°C, hold for 10 min is applied (more details in supplementary information about conversion and selectivity calculations).

Synthesis of trisamido derivatives: A solution of $LnCl_{3\ I}$ is prepared with THF (1eq, 2.07 mmol) and stirred for 2 days. Then a LiHMDS solution (3eq, 6.22 mmol) in THF (15mL) in added under argon at 0°C. The mixture is stirred for 3 days more at room temperature. The solvent is removed and the solid is heated at 100°C under vacuum for 3h. The solid extracted with pentane and the washing fractions were filtered over celite. Volatiles were evacuated. Sublimation under high vacuum (10^{-5} bar) afforded white crystals in 54 % yield. Analytical data are identical to literature values.

Grafting of Ln onto $SiO_{2\text{-}700}$ to afford Ln-700: In a glovebox, a double-Schlenk vessel was loaded with **Ln** (0.3 mmol) dissolved in 20 mL of pentane in one compartment and with $SiO_{2\text{-}700}$ (1 g) suspended in 20 mL of pentane in the other compartment. The complex solution was added at room temperature to the support by filtering through the sintered glass separating the two Schlenk tubes, and the reaction mixture was stirred for 15 h. The supernatant liquid was then separated by filtration into the other compartment, from which the solvent was gas-phase transferred by trap-to-trap distillation back into the compartment containing the modified support in order to wash away the residual molecular precursor. This operation was repeated thrice (resulting in color-less washing fractions). The resulting material **Ln-700** was then dried under secondary vacuum (10^{-6} mbar) at 80°C for 5h.

Alkyne dimerization: In the glove box, a glass reactor is filled with the catalyst (0.05 mmol), 3ml of toluene and 1-hexyne (5 mmol, 100 mol eq. per metal). The reaction mixture is heated at 100°C. After 4 hours, the reaction is quenched by exposure to air. The supernatant is analyzed by GC using n-decane as a standard (added after quenching).

---

[1] a) H. Bürger, U. Wannagat, *Monatshefte für Chemie*, 1964, 95-1099. b) H. Bürger, U. Wannagat, *Monatshefte für Chemie*, 1963, 93-1007

[2] C.D. Schaeffer Jr., J.J. Zuckerman, *J. Am. Chem. Soc.,* 1974, **96**, 7160–7162

[3] D.C. Bradley, J.S. Ghotra, F.A. Hart, *J.C.S. Dalton,* 1973, 1166–1172.

[4] a) E. Martin, P. Dubois, R. Jerome, *Macromolecules,* 2000, **33**, 1530-1535. b) K.C. Hultsch, T.P. Spaniol, J. Okuda, *Organometallics*, 1997, **16**, 4845-4846

[5] C. Boisson, F. Barbotin, R. Spitz, *Macromol. Chem. Phys.,* 1999, **200**, 1163-1166

[6] R.M. Gauvin, A. Mortreux, *Chem. Commun,* 2005, 1146-1148
[7] H. Berberich, P.W. Roesky, *Angew. Chem.,* 1998, **110**, 1618-1620
[8] M.L. Mays, T.P. Hanus, T.A. Nile, *J. Organometal. Chem.,* 1996, **514**, 73.
[9] M. R. Bürgstein, H. Berberich, P.W. Roesky, *Chem. Eur. J.,* 2001*, **7**, 3078-3085*
[10] R.M. Gauvin, T. Chenal, R. A. Hassan, A. Addad and A. Mortreux, *J. Mol. Cat. A. ;* 2006, **257**, 31-40.
[11] R.M. Gauvin, L. Delevoye, R.A. Hassan, J. Keldenich, A. Mortreux, *Inorg. Chem.,* 2007, **46**
[12] R. Anwander, R. Roesky, *J. Chem. Soc.*, 1997, **137**
[13] R.M. Gauvin, A. Mortreux, *Chem. Commun*., 2005, 1146–1148
[14] Y. Liang, R. Anwander, *Dalton Trans.*, 2013, ***42***, 12521
[15] T.Woodman, Y. Sarazin, G. Fink, *Macromolecules*, 2005, **38**, 8
[16] R.M. Gauvin, T; Chenal, R.A. Hassan, A. Addad, A. Mortreux, *J. Mol. Cat. A: Chemical*, **257**, 2006, 31-40
[17] S.-L. Zhou, S.-W. Wang, G.-S. Yang, X.-Y. Liu, E.-H. Sheng, K-H. Zhang, L. Cheng, Z.-X. Huang, *Polyhedron*, 2003, **22**, 1019-1024
[18] a) M.E. Thompson, S.M. Baxter, A.R. Bulls, B.J. Burger, M.C. Nolan, B.D. Santasiero, W.P. Schaefer, J.E. Bercaw, *J. Am. Chem. Soc.* 1987, **109**, 203–219. b) K.H. Den Haan, Y. Wielstra, J.H. Teuben, *Organometallics*, 1987, **6**, 2053–2060
[19] S. Ge, F. Victor, Q. Norambuena, B. Hessen, *Organometallics*, 2007, **26**

3.4. On the use of solid-state ^{45}Sc NMR for structural investigations on molecular and silica-supported scandium amide catalysts.

This work was published in:

"On the use of solid-state ^{45}Sc NMR for structural investigations of molecular and silica-supported scandium amide catalysts.", T. Vancompernolle, X. Trivelli, L. Delevoye, F. Pourpoint, R. M. Gauvin, *Dalton Transactions*, 2017, **46**, 13176 - 13179.

It was selected by the Editor for the thematic issue: "Frontiers in Spectroscopic Techniques in Inorganic Chemistry"

3.4.1. Abstract

Tris- and tetra-coordinated scandium amides were grafted onto silica and probed as catalysts for alkyne dimerization. ^{45}Sc NMR studies were carried out, providing information on the metal coordination sphere. The increasing number of coordinated ligands was correlated with decreased catalytic activity.

3.4.2. Introduction

The development of supported organometallic and inorganic catalysts is driven by the advantages expected from heterogenization, such as the possibility to efficiently separate reactants, products and catalytic material, to operate under flow conditions or to be able to recycle the systems. The control of the synthesis of heterogenized catalysts is of key importance when considering the importance of the nature of a metal coordination sphere on the resulting catalytic performances. One of the most successful approaches, when considering the grafting onto silica, is surface organometallic chemistry, where an organometallic complex reacts directly with conveniently dehydroxylated silica support, which allows for fine tuning of the anchoring mode of the surface organometallic species.[1] In this context, we and other have developed (well-defined) rare-earth metal surface species,[2,3] which displayed interesting catalytic properties compared to their molecular counterparts, such as increase in activity or in selectivity.2 The understanding of such materials (and thus, their rational development) critically depends on thorough characterization. One of the most efficient methods to assess molecular level structure of grafted sites is solid state NMR, thanks to which not only identification of functional groups but also proximities can be inferred. On the top of that, when relying the grafted metal center itself as a probe, one may directly access information on the catalytic center configuration. This is particularly efficient when considering quadrupolar nuclei, for which not only isotropic (chemical shift, δ_{iso}) but also anisotropic parameters (quadrupolar coupling constant C_Q, asymmetry parameter η) can be extracted. This provides a further level of structural information. For instance, a rare-earth metal such as scandium, commonly used in catalysis, [4] features a NMR active isotope, ^{45}Sc (I= 7/2), with interesting NMR properties. Indeed, its isotropic chemical shift, which can

found over a wide range, is highly sensitive to the metal coordination number, bond angles and bond distances. Furthermore, its moderate quadrupolar moment allows for efficient recording of spectroscopic data within very reasonable time.[5] Thus, in the context of grafted rare-earth metals catalysts, we studied the possibility to use ^{45}Sc NMR to investigate on coordination sphere of such grafted scandium catalysts.

We have previously reported that the grafting of [Ln(NR_2)$_3$] (Ln = Y, La, Nd, Sm, R= $SiMe_3$) onto silica dehydroxylated at 700 °C (Evonik Aerosil 380, $SiO_{2\text{-}700}$, specific area 350 $m^2.g^{-1}$) which only features non interacting silanols) affords materials with [(≡SiO)Ln(NR_2)$_2$], with most probably coordination of siloxane entities from the surface coordinating the metal center.2 In order to access the Sc analogous species, we reacted the known trisamide scandium derivative [6] with $SiO_{2\text{-}700}$ (Scheme 3.4.1).

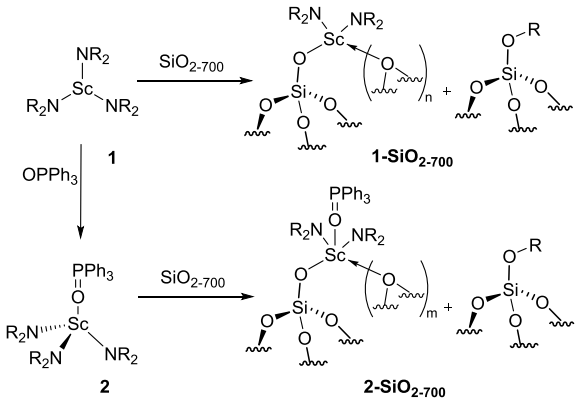

Scheme 3.4.1 Synthesis of molecular and silica-grafted scandium amides (R= $SiMe_3$)

3.4.3. Results and discussion

Infrared spectroscopy confirms that the reaction with the support took place (Figure 3.4.1, a and b): full consumption of surface silanols is evidenced by the lack of $\nu_{(O\text{-}H)}$ band from non-interacting silanols at 3746 cm^{-1} after the grafting, and new signals appear at 2959 and 2901 cm^{-1}, accounting for $\nu_{(sp^3\ C\text{-}H)}$ from $SiMe_3$ moieties.

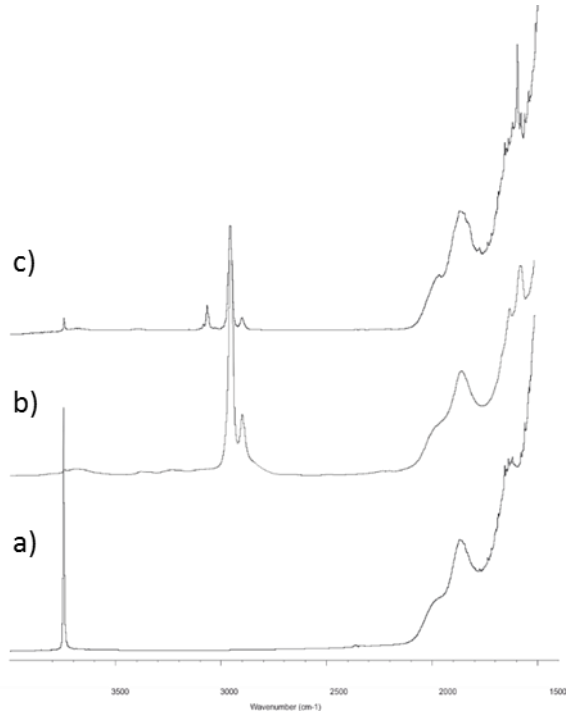

Figure 3.4.1. DRIFT of a) $SiO_{2\text{-}700}$, b) **1-$SiO_{2\text{-}700}$**, and c) **2-$SiO_{2\text{-}700}$**

Elemental analysis indicates a Sc loading of 1.04 w%, which corresponds to 0.23 mmol.g^{-1}. This is slightly lower than the loading of larger rare-earth metal derivatives (Y, La, Sm, Nd), which are of about 0.28 mmol.g^{-1}. As all silanols from $SiO_{2\text{-}700}$ have reacted (from infrared data), the difference in metalated SiOH groups comes from concomitant silylation by hexamethyldisilazane, affording ≡$SiOSiMe_3$ groups.2,3 Furthermore, when taking into account the N loading of 0.69 w%, the N/Sc molar ratio is of 2.13, which is in line with formation of [(≡SiO)Sc(NR_2)$_2$] species. Combined to ^{1}H and ^{13}C NMR data (see Figure 3.4.2, Figure 3.4.3, Figure 3.4.4), these results are fully in line with the previously reported surface chemistry of trisamide rare-earth metal species.2

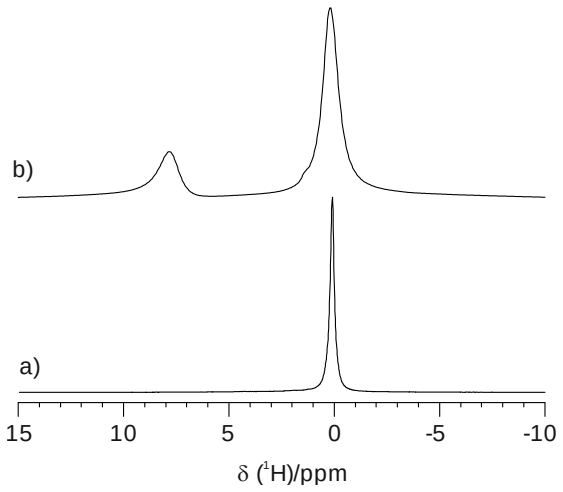

Figure 3.4.2. ^{1}H MAS NMR spectra (400 MHz) of a) **1-$SiO_{2\text{-}700}$**, b) **2-$SiO_{2\text{-}700}$**

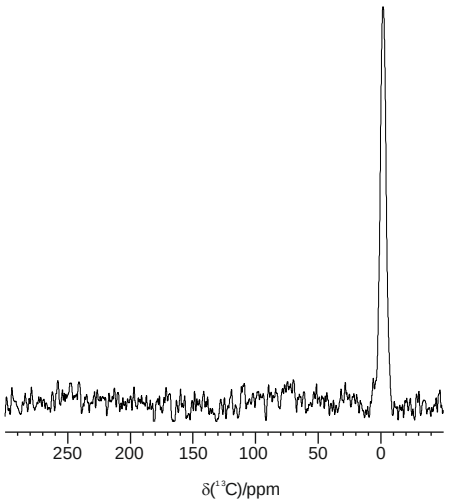

Figure 3.4.3. ^{13}C CPMAS NMR spectrum of (100.6 MHz) of **1-SiO$_{2\text{-}700}$**

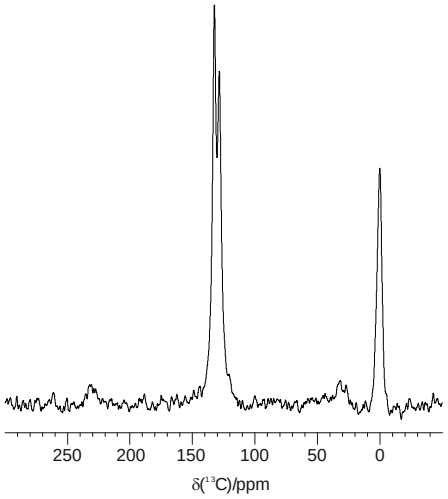

Figure 3.4.4. ^{13}C CPMAS NMR spectrum (100.6 MHz) of **2-SiO$_{2\text{-}700}$**

In order to generate surface scandium derivatives with different coordination spheres, we grafted the triphenylphosphine oxide adduct, $[Sc(NR_2)_2(OPPh_3)]$ (2), which was prepared following the procedure of Aspinall et al. (Scheme 3.4.1).[7] Reaction with $SiO_{2\text{-}700}$ was performed similarly than with the parent trisamide, affording **2-SiO$_{2\text{-}700}$**. The DRIFT spectrum of this material confirms the immobilization of **2** on the support (Figure 3.4.1): the very weak residual non-interacting silanols band indicates their quasi-quantitative consumption, peaks at 3083, 3066 cm-^{1} and at 2959, 2901 cm^{-1} account for $\nu_{(\ sp^2\ C\text{-}H)}$ and $\nu_{(\ sp^3\ C\text{-}H)}$ elongation vibrations, respectively, while bands characteristic of aromatic C=C vibrations are observed at 1594, 1485, 1440 cm^{-1}, as expected from the presence of the $OPPh_3$ ligand. The scandium loading in **2-SiO$_{2\text{-}700}$** is significantly lower than that in **1-SiO$_{2\text{-}700}$** (0.67 and 1.04 w%, respectively), as expected from the higher steric hindrance within the metal coordination sphere which inhibits reactivity with surface silanols.

The ^{1}H and ^{13}C MAS NMR spectra are in agreement with expected structure, showing signals characteristic for both aromatic C-H and $SiMe_3$ groups. Accordingly, ^{31}P CP MAS NMR features a broad signal at a δ_{iso} of 40 ppm, which is close to that of **2** (39.8 ppm) (see Figure 3.4.5).

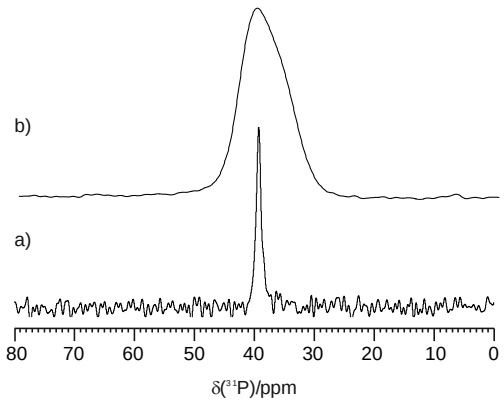

Figure 3.4.5. ^{31}P NMR spectrum (161.9 MHz) of a) **2** (C_6D_6, 300 K), b) **2-SiO$_{2\text{-}700}$** (CPMAS)

These molecular and supported scandium derivative were probed as catalyst for the dimerization of terminal alkyne (Scheme 3.4.2, Conditions: Sc (0.05 mmol), 100 eq of 1-hexyne, 3 ml toluene, 4h, 100°C

Table 3.4.1).[8] **1** proceeds rather efficiently, converting 91 equivalents of 1-hexyne selectively into head-to-tail dimer **3a**. Neither the head-to-head dimer **3b** nor trimer **4** are formed in significant quantity. The grafted analogue **1-SiO$_{2\text{-}700}$** is less reactive, as under similar conditions 47 equivalents of substrate are converted. Interestingly, the selectivity of the reaction is different, as both dimer **3a** and trimer **4** are obtained in respective selectivity of 94 and 6%. The higher selectivity towards trimer formation may be due to adsorption of the dimer on the surface (rather than desorption into the supernatant) in the vicinity of the surface active sites. On the other hand the $OPPh_3$-adducts **2** and **2-SiO$_{2\text{-}700}$** did not afford any conversion of 1-hexyne.

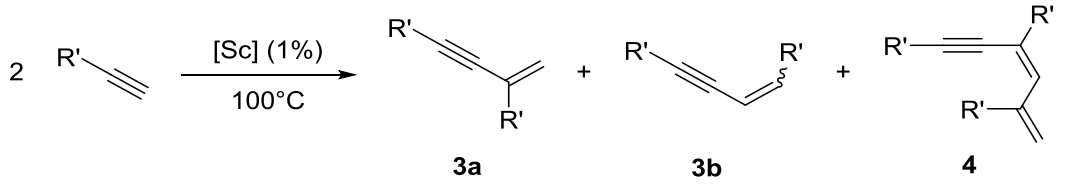

Scheme 3.4.2 Scandium-catalyzed alkyne dimerization (R' = *n*-hex)

Entry	Catalyst	Conv. (%)	Selec. 3a/3b	Selec. 3a,3b/4
1	1	91	99	>99
2	2	-	-	-
3	1-SiO$_{2\text{-}700}$	47	99	94/6
4	2-SiO$_{2\text{-}700}$	-	-	-

Conditions: Sc (0.05 mmol), 100 eq of 1-hexyne, 3 ml toluene, 4h, 100°C

Table 3.4.1 Scandium-catalysed 1-hexyne dimerization

These markedly distinct reactivity patterns between the molecular and supported amido species, and with their respective phosphine oxide adducts, illustrate the importance of the coordination sphere of the metal center when considering catalytic performances. This prompted us to further investigate structural aspects by probing the metal center itself, namely by resorting to ^{45}Sc NMR.

As ^{45}Sc is a quadrupolar nucleus, the use of high magnetic field is highly beneficial, as sensitivity is increased, while narrower lineshapes are obtained, thus facilitating detection and interpretation.

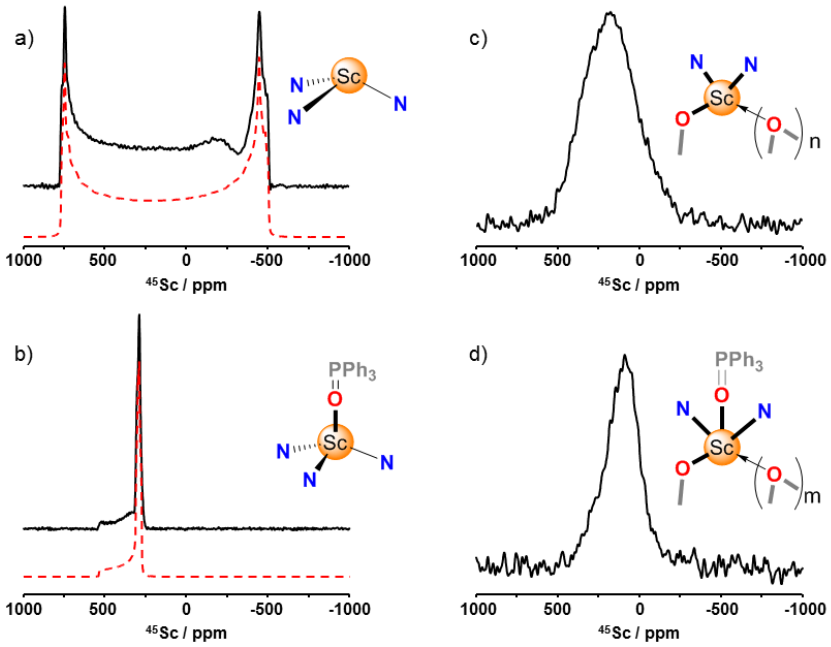

Figure 3.4.6.[45]Sc NMR spectra of (a) **1**, (b) **2**, (c) **1-SiO$_{2\text{-}700}$** and (d) **2-SiO$_{2\text{-}700}$** recorded under static condition at 18.8 T. Deconvolution of the spectra (a) and (b) are displayed in red dashed lines.

	δ_{iso}[a](ppm)	Δ_{iso}[a](ppm)	η_{csa}	C_Q (MHz)	η_Q
1	396 ± 20	383 ± 20	0	66.2 ± 0.5	0.03 ± 0.02
2	350 ± 10	187 ± 10	0.05	19.0 ± 0.5	0.06 ± 0.02
1-SiO$_{2\text{-}700}$	180 ± 10	N/A	N/A	N/A	N/A
2-SiO$_{2\text{-}700}$	90 ± 10	N/A	N/A	N/A	N/A

Table 3.4.2 [45]Sc NMR parameters

Figure 3.4.6 displays the [45]Sc NMR spectra of molecular compounds **1** and **2** along with that of their grafted analogues (**1-SiO$_{2\text{-}700}$** and **2-SiO$_{2\text{-}700}$**) recorded under static conditions at 18.8 T. **1** (Figure 3.4.6-a) features a single resonance with a broad lineshape and a large quadrupolar coupling constant value of 66.2 MHz (Table 3.4.2) suggesting a highly distorted environment. **2** (Figure 3.4.6-b) experiences a smaller, albeit relatively high, quadrupolar interaction than **1** with C_Q= 19.0 MHz. The difference in C_Q value between these two samples is induced by changes in the local environment of the scandium center. Indeed, the scandium nucleus features a trigonal pyramidal configuration in **1**6, and a more symmetrical tetrahedral environment in **2**.7As expected from their axial symmetry, an asymmetry parameter of η_Q close to 0 is found for both samples. Interestingly, best fit simulations (red-dashed lines in Figure 1) were obtained when adding a substantial contribution of chemical shift anisotropy, as confirmed by recording the spectra at lower magnetic field (see Table 3.4.2 and Figure 3.3.7-10). The isotropic chemical shift of **1** and **2** is 396 and 350 ppm, respectively (the latter being confirmed by solution NMR studies). This agrees with previous studies demonstrating that δ_{iso} of [45]Sc nuclei increases for lower coordination number.[5, 9]

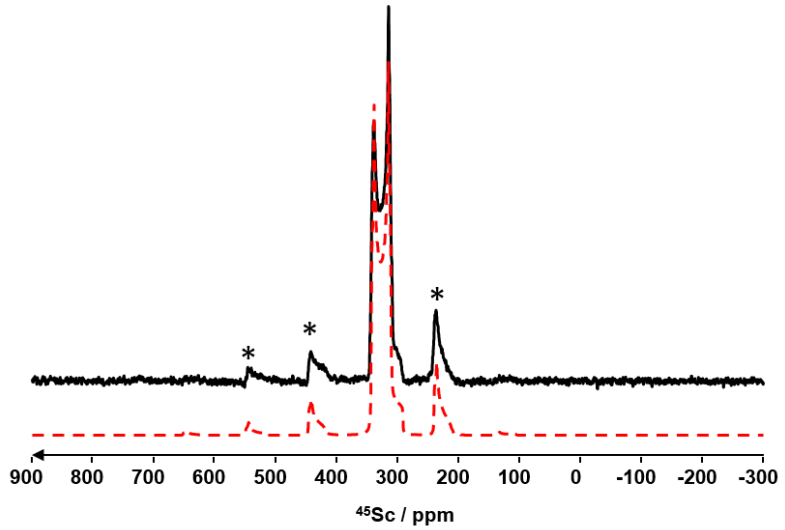

Figure 3.4.7.^{45}Sc NMR spectrum of **2** recorded using a Hahn echo experiment at 18.8 T and a spinning speed of 20 kHz. The simulations (red dashed line spectrum) lead to the NMR parameters given in Table 3.4.2.

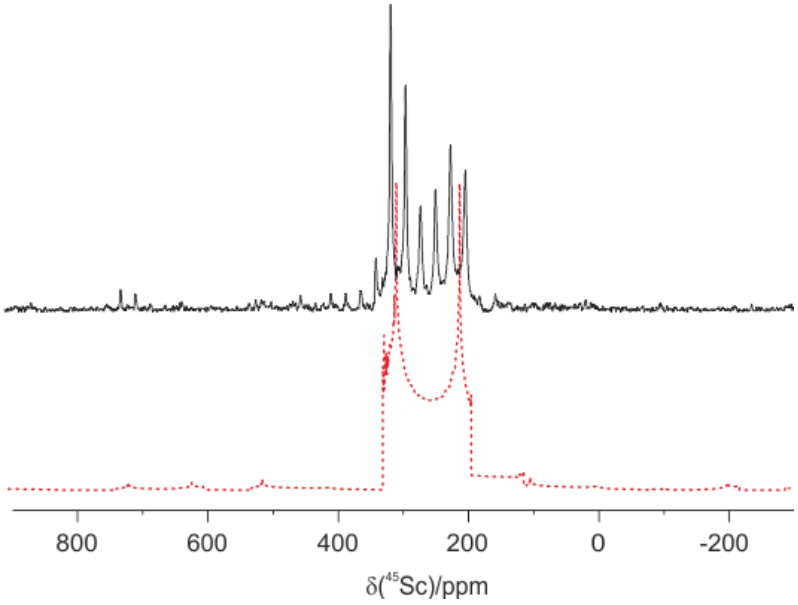

Figure 3.4.8.^{45}Sc NMR spectrum of **2** recorded using a QCPMG experiment at 9.4T and a spinning speed of 20 kHz. The simulation (red dashed line spectrum) was done with the NMR parameters given in Table 3.3.1.

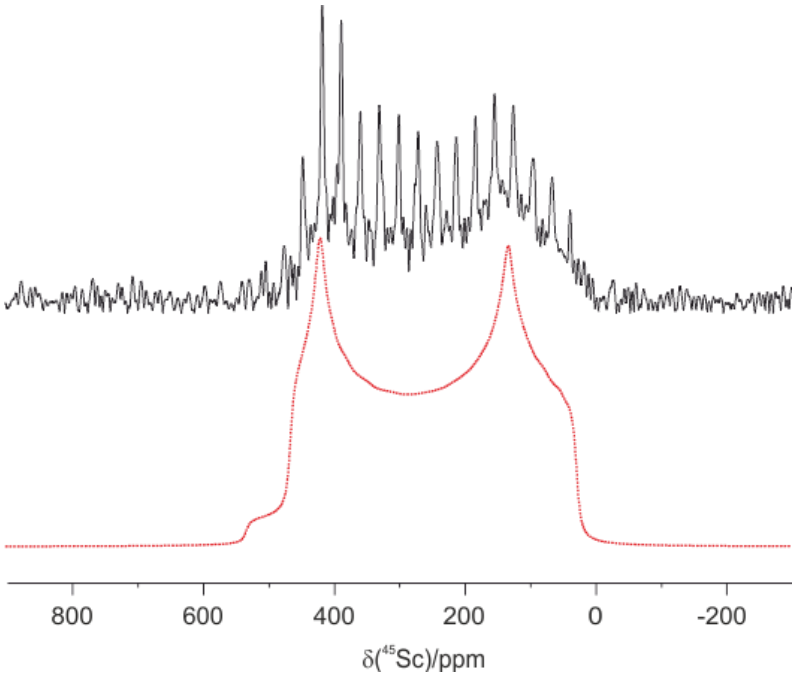

Figure 3.4.9.[45]Sc NMR spectrum of **2** recorded using a QCPMG experiment at 9.4T under static conditions. The simulation (red dashed line spectrum) was done with the NMR parameters given in Table 3.3.1.

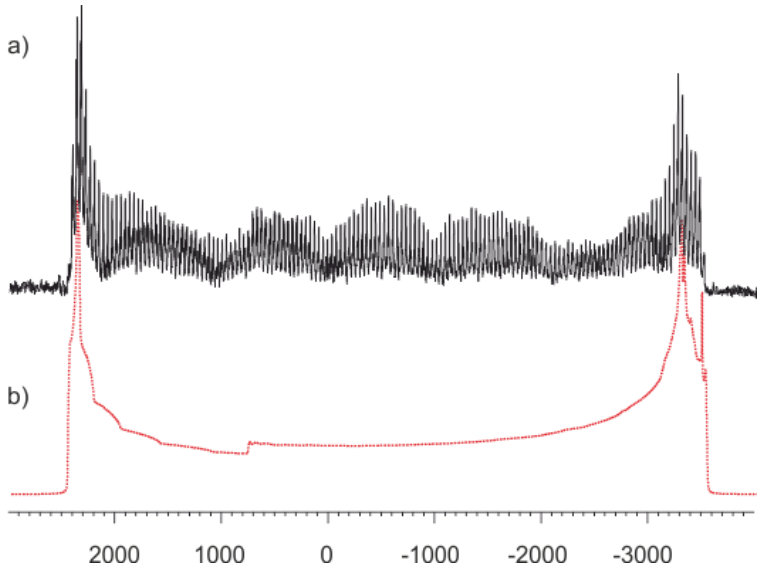

Figure 3.4.10.[45]Sc NMR spectrum of **1** recorded using a QCPMG experiment at 9.4T under static conditions (a). The simulation (red dashed line spectrum) was done with the NMR parameters given in Table 3.3.1 (b).

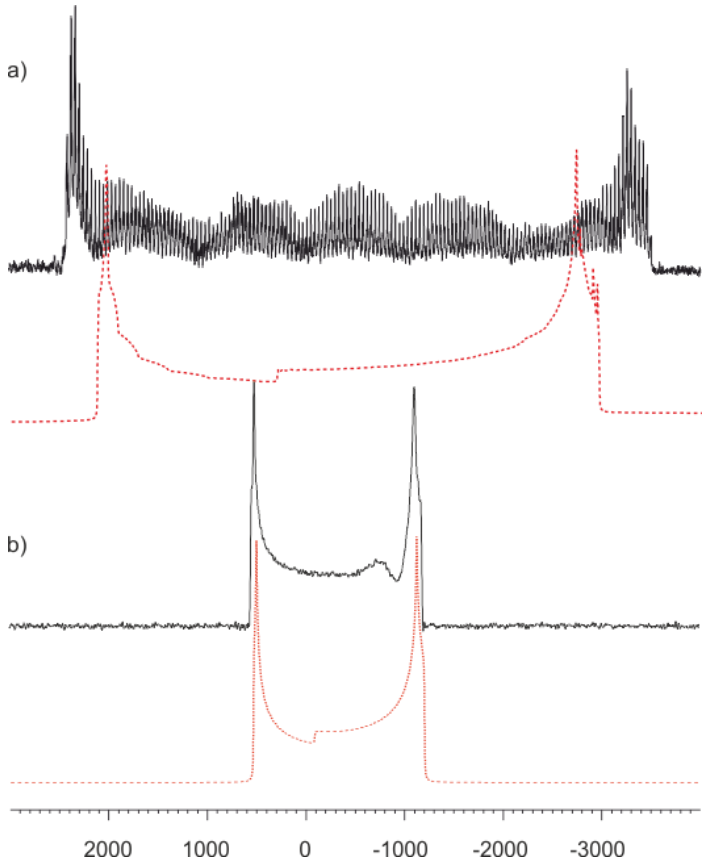

Figure 3.4.11.^{45}Sc NMR spectrum of **1** recorded using a QCPMG experiment at 9.4 (a) and at 18.8 T (b) under static conditions. The simulations (red dashed line spectra) use the NMR parameters obtained by best-fit simulation of the spectrum at 18.8 T, considering no CSA contribution.

The grafted samples **1-SiO$_{2\text{-}700}$** (Scheme 3.4.1-c) and **2-SiO$_{2\text{-}700}$** (Scheme 3.4.1-d) ^{45}Sc NMR spectra exhibit featureless broad resonance, with respective maxima values of 180 and 90 ppm (Table 3.4.2). Unfortunately, this precludes the precise determination of the quadrupolar and anisotropy parameters. The dramatic change compared to the parent molecular compounds, which display very typical quadrupolar lineshape, is attributed to major changes in the metal coordination sphere upon grafting: 1) substitution of an amido ligand by a siloxide group, 2) coordination of several Si-O-Si moieties onto the Sc center, thereby increasing the number of oxygen within the Sc coordination sphere (labelled as n and m in Scheme 1 and Figure 1), and 3) large distribution of bond lengths and angles within local environment, stemming from the intrinsic heterogeneity of the non-crystalline silica surface.

Interestingly, the FWHM (full-width of half maximum) of **1-SiO$_{2\text{-}700}$** is roughly twice higher than that of **2-SiO$_{2\text{-}700}$** probably due to a greater distortion and distribution. As shown above, **2-SiO$_{2\text{-}700}$** comprises a phosphine oxide ligand, which narrows ^{45}Sc NMR spectrum by inducing increase in symmetry of the local environment.

When considering the isotropic chemical shift decrease at higher coordination number (CN), we can also comment on the observed tendency within our series of materials. As we can range those as: δ_{iso} (**1**, CN= 3) > δ_{iso} (**2**, CN= 4) > δ_{iso} (**1-SiO$_{2\text{-}700}$**, CN>4)> δ_{iso} (**2-SiO$_{2\text{-}700}$**), we can conclude that **2-SiO$_{2\text{-}700}$** features a higher degree of bonded oxygen atoms than **1-SiO$_{2\text{-}700}$**, most probably from the phosphine oxide ligand coordination.

It is worth mentioning that the reactivity trends in alkyne dimerization are inversely correlated with the scandium coordination number (as probed by the isotropic chemical shift), namely that lower coordination number induces higher activity. Even if this is expected (unsaturation at the metal center is beneficial for the binding of incoming substrate and this for its conversion), this link between catalytic performances and spectroscopic features demonstrates the interest of our approach. Furthermore, in these examples, ^{45}Sc NMR data clearly illustrates the complex nature of the interaction of silica surface with the grafted metal entities when investigating their molecular level structure, which impacts on the catalytic potential of the considered material. Extension of these studies to related materials and to other catalytic reactions, along with input from DFT calculations of NMR parameters, will be targeted in our next endeavors.

3.4.4. Supporting information

General considerations

Experiments were carried out under an argon atmosphere in an M-Braun glovebox or by using Schlenk techniques. Solvents and reactants were dried by using conventional reagents and stored in the glovebox over 3A molecular sieves. Aerosil 380 silica (Degussa, specific area 380 $m^2\ g^{-1}$, prior to heat treatment) was subjected to heating under secondary vacuum (10^{-6} mbar) for 15 h at 500 °C, followed by 4 h at 700 °C, and stored in a glovebox for limited time. Liquid-state NMR spectroscopic analyses were run at 7 T (300 MHz for ^{1}H) using a Bruker Avance-II spectrometer. The 1D-^{45}Sc solution NMR experiments were recorded at 97.3 MHz and 300 K on a Bruker AVANCE II 400 spectrometer equipped with a 5 mm broad-band probe using the following parameters: a 8.8 µs pulse calibrated on a 0.18 M $Sc(NO_3)_3$ solution in D_2O, a 0.5 s recycling delay, a 6 ms acquisition time, a 60 kHz spectral width and 2048 scans. Solid-state MAS NMR spectra were recorded either (i) at 9.4 T (400 MHz for ^{1}H, 161.9 MHz for ^{31}P) using a Bruker AVANCE-II console equipped with a 4 mm probe spinning at 10 kHz or (ii) at 18.8 T (800 MHz) using a Bruker AVANCE-III console equipped with a 3.2 mm probe spinning at 20 kHz or used under static conditions. Chemical shifts for ^{1}H, ^{45}Sc, ^{31}P are given with respect to adamantane, $Sc(NO_3)_3.3H_2O$ and H_3PO_4 respectively as external references. For the ^{31}P CP MAS experiment, the spinning frequency was 10 kHz, the recycle delay was 5 s, and 11264 scans were collected with a pulse lasting 5 µs. 1D ^{45}Sc static spectra were recorded using a Hahn echo experiment with a QCPMG detection[10] (Quadrupolar Carr-Purcell Meiboom-Gill) using a train of refocusing pulses of echoes. The Hahn echo experiment used rf pulses lasting 0.80 µs and 1.60 µs for the 90° and the 180° pulses respectively and a rf amplitude of 78 kHz and the delay between the two pulses is 5 ms. A

total of 22 echoes was recorded in the CPMG experiment. A 4 ms hyperbolic secant[11] (HS) inversion pulse was used initially in order to enhance the polarization of ^{45}Sc central transition. The optimal HS enhancement was obtained with an rf field of 12 kHz and an offset frequency of 180 kHz. A SPINAL-64 (small phase Incremental alternation with 64-steps[12]) proton decoupling of 78 kHz was used during the acquisition. The recycle delay was 1 s, the number of scans was 1024 and the experiments lasted for 17 minutes for samples **1** and **2**. The recycle delay was 0.5 s, the number of scans was 614400 and the experiments lasted for 3 days and 12 hours for samples 1-$SiO_{2\text{-}700}$ and 2-$SiO_{2\text{-}700}$. 1D ^{45}Sc MAS spectrum of 2 was recorded using Hahn echo experiment with rf pulses lasting 1.4 µs and 2.80 µs for the 90° and the 180° pulses respectively and a rf amplitude of 45 kHz. The delay between the two pulses is rotor synchronized to 0.5 ms (one rotor period). The recycle delay was 1 s, the number of scans was 1024 and the experiment lasted for 17 minutes. The chemical shift parameters are defined according to the Haeberlen notation[13]: $\boldsymbol{\delta_{iso}} = {}^{\mathbf{1}}\!/_{\mathbf{3}}\,(\boldsymbol{\delta_{XX}} + \boldsymbol{\delta_{YY}} + \boldsymbol{\delta_{ZZ}})$ and $\Delta_{\boldsymbol{CSA}} = \boldsymbol{\delta_{ZZ}} - \boldsymbol{\delta_{iso}}$. Where $\boldsymbol{\delta_{iso}}$ denotes the isotropic chemical shift; $\boldsymbol{\delta_{XX}}$, $\boldsymbol{\delta_{YY}}$, and $\boldsymbol{\delta_{ZZ}}$ are the principal components of the Chemical Shift Anisotropy (CSA) tensor ordered as $|\boldsymbol{\delta_{YY}} - \boldsymbol{\delta_{iso}}| \leq |\boldsymbol{\delta_{XX}} - \boldsymbol{\delta_{iso}}| \leq |\boldsymbol{\delta_{ZZ}} - \boldsymbol{\delta_{iso}}|$; and $\Delta_{\boldsymbol{CSA}}$ is the anisotropic chemical shift. Simulation of the spectra were performed using TOPSPIN Bruker® software. Diffuse reflectance infrared spectra were collected with a Harrick cell on a Nicolet Avatar spectrometer fitted with a MCT detector. Typically, 64 scans were accumulated for each spectrum (resolution of 4 cm^{-1}). Elemental analyses were conducted at London Metropolitan University (CHN) and at LASIR, University of Lille (Ln). For alkyne dimerization, reaction mixtures were analysed using a Shimadzu GC2010 chromatograph fitted with a CP-Sil 5CB column (25m× 0.25mm× 0.2 µm), argon as carrier gas, and both injector and detector temperature at 250 °C. Heating program: starting at 50 °C then a ramp of 10 °C/min up to 250°C, hold for 10 min.

Synthesis of $Sc[N(SiMe_3)_2]_3$ (1)[14]: In a Schlenk tube a solution of $ScCl_3$ (120 mg, 0.8 mmol) in THF (20 mL) was stirred for 2 days then LiHMDS (412 mg, 2.4 mmol) in solution in THF (10 mL) was slowly added. The mixture was stirred further for 3 days then the solvent is removed under vacuum for 3h at 100°C. The solid extracted with pentane and the washing fractions were filtered over celite. Volatiles were evacuated. Sublimation under high vacuum (10^{-5}bar) afforded white crystals in 54 % yield (210 mg). Analytical data are identical to literature values.

Synthesis of $Sc[N(SiMe_3)_2]_3(OPPh_3)$ (2)[15]: In glovebox, a Schlenk tube was filled with 1 (75 mg, 0.143 mmol) and freshly sublimed triphenylphosphine (44 mg, 0.157 mmol), dissolved in 5 mL of toluene. After 3 h of stirring at room temperature, the solution was filtered over Celite and washed 3 times with pentane. Crystallization from pentane afforded 2 as white solid (109 mg, 95% yield). ^{1}H NMR (300 MHz, C_6D_6): δ 7.7 (m, 6H, PPh_3), 7.0 (m, 9H, PPh_3), 0.52 (s, 54H, $N(Si(CH_3)_3)$. $^{31}P\{^1H\}$ NMR (121.5 MHz, C_6D_6) δ 39.8 (s, $OPPh_3$). δ(^{45}Sc) 360 ppm (C_6D_6, 300 K, FWHM: 4500 Hz).

General procedure for grafting (1) or (2) onto $SiO_{2\text{-}700}$ to form (1-$SiO_{2\text{-}700}$) or (2-$SiO_{2\text{-}700}$)

In a glovebox, a double-Schlenk vessel was loaded with the tri or tetra-coordinated scandium precursor (0.3 mmol) dissolved in 20 ml of pentane in one compartment and with $SiO_{2\text{-}700}$ (1 g) suspended in 20 mL of pentane in the other compartment. The colourless complex solution was added at room temperature to the support by filtering through the sintered glass separating the two Schlenk tubes, and the reaction mixture was stirred for 15 h. The supernatant liquid was then separated by filtration into the other compartment, from which the solvent was gas-phase transferred by trap-to-trap distillation back into the compartment containing the modified support in order to wash away the residual molecular precursor. This operation was repeated thrice. The resulting material (**1-$SiO_{2\text{-}700}$**) or (**2-$SiO_{2\text{-}700}$**) was then dried under secondary vacuum (10^{-6} mbar) at 80°C for 5 h. Elemental analysis (w%): **1**: Sc 1.04, C 3.35, H 0.77, N 0.69, **2**: Sc: 0.67, C 6.29, H 0.50, N 0.58.

Alkyne dimerization procedure

In the glove box, a glass reactor is filled with the catalyst (0.05 mmol), 3 ml of toluene and terminal alkyne (5 mmol, 100 mol eq. per Sc). The reaction mixture is heated at 100 °C. After the desired time, the reaction is quenched by exposure to air. The supernatant is analyzed by GC using *n*-decane (10 mg) as a standard (added after quenching).

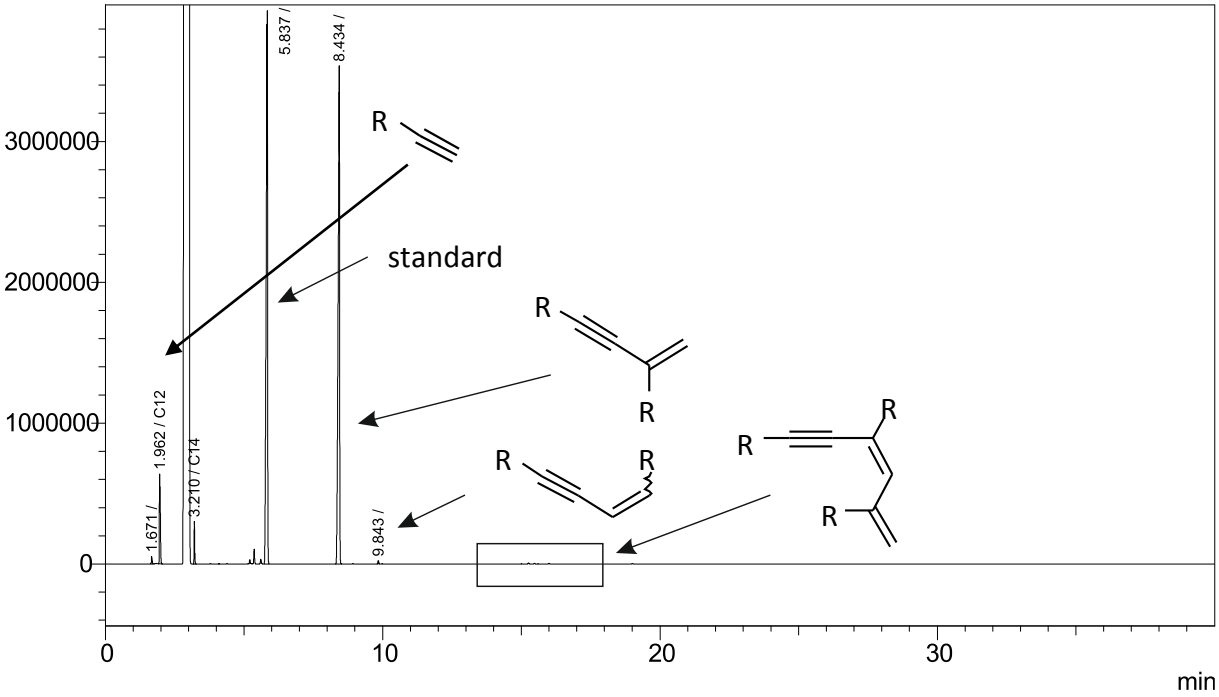

Figure 3.4.12 GC trace from dimerization of 1-hexyne with **1**

3.5. Conclusion

This chapter showed the synthesis of several rare-earth metal-based materials that have been employed for reaction of polymerization of polar and non-polar monomers as well as in fine chemistry reactions such as alkyne dimerization. In the case of the grafting of a trisbenzyl derivative, we have demonstrated that the grafting reaction proceeds via distinct pathways involving the La-C bond, namely protonolysis by silanol, or insertion into Si-O-Si

groups on the surface, as confirmed by DFT calculations. The resulting material catalyzes efficiently a range of reactions typical for rare-earth metals. Perspectives to this work are the extension of this chemistry to the $[Ln(CH_2Ph)_3(THF)_n]$ family, which would demonstrate the effect of the nature of the rare-earth metal (ionic radius, Lewis acidity) onto the catalysis properties.

In a separate effort, we prepared well-defined silica-grafted rare-earth amide species and used these in terminal alkyne dimerization, focusing not only on conversion rate but also on selectivity, which was different from that of analogous molecular species. Most particularly, the exacerbated electrophilicity of the grafted metal center induces increased formation of trimer from subsequent reaction of the primary product. DFT studies are still in progress to account for these phenomena. Furthermore, specific investigations on the scandium derivatives were carried out using ^{45}Sc NMR. The modification within the metal coordination sphere were shown to impact on the NMR parameters. This opens options for the use of this spectroscopic tool for future studies on molecular and supported scandium species, though in the case of grafted metal centers, distribution effects and low quantity of NMR active are a severe problems, for which solutions must be sought to conveniently model those and increase signal-to-noise ratio, respectively.

---

[1]J.-M. Basset, R. Psaro and D. Roberto, R. Ugo, *Modern Surface Organometallic Chemistry*; Wiley-VCH: Weinheim, Germany, 2009; C. Copéret, A. Comas-Vives, M. P. Conley, D. P. Estes, A. Fedorov, V. Mougel, H. Nagae, F. Núñez-Zarur and P. A. Zhizhko, *Chem. Rev.*, 2016, **116**, 323.

[2] a) R.M. Gauvin, T. Chenal, R. A. Hassan, A. Addad and A. Mortreux, *J. Mol. Cat. A. ;* 2006, **257**, 31-40. b) I. Del Rosal, M. Tschan,R. M. Gauvin, L. Maron and M. Thomas, *Polym. Chem*. 2012, **3**, 1730-1739. R. Anwander, R. Roesky, *J. Chem. Soc. Dalton Trans.*, 1997, **137**

[3] a) Y. Liang and R. Anwander, *Dalton Trans.* 2013, **42**, 12521. b) C. Coperet, M. Chabanas, R. Petroff Saint-Arroman and J.-M Basset, *Angew. Chem. Int. Ed.*, 2003, **42**, 156

[4] a) A.E. Nako, J. Oyamada, M. Nishiura and Z. Hou, *Chem. Sci.* 2016, **7**, 6429. b) F. Lauterwasser, P.G. Hayes, S. Bräse, W.E. Piers and L.L. Schafer, *Organometallics*, 2004, **23**, 2234-2237

[5] N. Kim, C.-H Hsieh and J.F. Stebbins, *Chem Mater*, 2006, **18**, 3855-3859; A.J. Rossini and R. W. Schurko, *J. Am. Chem. Soc*, 2006, **128**, 10391-10402 ; M.D. Alba, P. Chain, P. Florian and D. Massiot, *J. Phys. Chem. C*, 2010, **114**, 12125-12132 ; R. Giovine, C. Volkringer, S.E. Ashbrook, J. Trebosc, D. McKay, T. Loiseau, J.-P. Amoureux, O. Lafon and F. Pourpoint, *Chem Eur. J*, 2017, **23**, 1-11.

[6] D.C. Bradley, J.S. Ghotra and F.A. Hart, J.C.S. Dalton, 1973,1166–1172 ; D. H. Woen, G.P. Chen, J.W. Ziller, T.J. Boyle, F. Furche and W.J. Evans, *Angew. Chem. Int. Ed.* 2017, **56**, 2050 –2053.

[7] H. C. Aspinall, D. C. Bradley and K. D. Sales, *J. Chem. Soc., Dalton Trans.* 1988, 2211-2213

[8] R. Anwander, O. Runte, J. Eppinger, G. Gerstberger, E. Herdtweck and M. Spiegler, *J. Chem. Soc. Dalton Trans* ,1998, 847-858. R.M. Gauvin, L. Delevoye, R. A. Hassan, J. Keldenich and A. Mortreux, *Inorg. Chem.*, 2007, **46**, 1062-1070.

[9] T. Brauniger et al., *Solid state Science*, 2006, **51**, 1-7

[10] H.Y., Carr; E.M. Purcell, *Phys. Rev.* 1954, **94**, 630-638.

[11] R. Siegel, *Chem. Phys. Lett*., 2004, **388**, 441-445.

[12] B. M. Fung, A. K. Khitrin, K. Ermolaev, *J. Magn. Reson*. 2000, **142,** 97-101.

[13] K. Schmidt-Rohhr, H. W. Spiess, Multidimensional Solid-State NMR and Polymers. Hartcourt Brace & Company: London 1999.

[14] D.C. Bradley, J.S. Ghotra, F.A. Hart, *J. Chem. Soc. Dalton*, 1973, 1166–1172; D. H. Woen, G.P. Chen, J.W. Ziller, T.J. Boyle, F. Furche, W.J. Evans, *Angew. Chem. Int. Ed.* 2017, **56**, 2050 –2053.

[15] H. C. Aspinall, D. C. Bradley, K. D. Sales, *J. Chem. Soc., Dalton Trans.* 1988, 2211-2213.

4. Surface organometallic chemistry of aluminum

4.1. Introduction

This chapter focuses on the use of aluminum derivatives as (co)catalysts for several applications. In a first instance, we performed the immobilization of mono- and binuclear aluminum salen species onto silica for carbonation of epoxides into cyclic carbonates. This part will describe the synthesis and characterization of the corresponding materials, with a focus on ^{27}Al MAS NMR, along with their behavior as supported catalysts for the carbonation of several epoxides. The next part describes the synthesis of a new aluminum amidochloro derivative, [Al{(N(SiMe$_3$)$_2$}$_2$(Cl)THF)], and its grafting onto silica, which results in a mixture of species, as shown by advanced solid state NMR thanks to the use of specific sequences. The third part derives from a collaboration with researchers from the C2P2 laboratory, that concerns the influence of the dehydroxylation temperature of the silica onto the grafting of methyl aluminum oxide (MAO) and on the outcome in polymerization of ethylene. A detailed solid state NMR was performed in the UCCS, demonstrated for the first time some theoretically-postulated structural patterns in MAO. Finally, we will present the development of silica-supported alkyl and chloroalkyl silica-grafted aluminum cocatalysts, which were used in the framework of a collaboration with the De Souza group (University of Porto Alegre, Brazil) devoted to cobalt-mediated olefin oligomerization.

4.2. Immobilization of mono- and bimetallic aluminum salen derivatives on silica: spectroscopic investigations and application in the synthesis of carbonates

4.2.1. Introduction

The valorization of CO_2 has become nowadays an important topic in the view of developing greener chemical processes[1]. While already being widely used as a solvent in super critical conditions[2], carbon dioxide can be used as an alternative C1 synthon for introducing carbonyl group in organic molecules[3]. One of the most successful reactions to date is the synthesis of cyclic carbonates from epoxides, which proceeds with full atom economy.

In this contribution, we focus on mono- and binuclear complexes featuring a salen-type ligand. Since its first synthesis by Pfeiffer in 1933[4] this ubiquitous ligand, complexed onto a considerable number of metal complexes, has known extraordinarily wide range applications. For instance, in asymmetric catalysis, the Jacobsen's catalyst allows to reach excellent enantiomeric excess for epoxidation of alkenes[5]. In the case of aluminum derivatives, efficient catalytic opening of propylene oxide[6] or carbonatation of epoxide[7] were reported. North[8] showed that better activity for cyclic carbonate formation could be achieved with binuclear aluminum catalyst, thanks to cooperative mechanism, which illustrate how this type of system can be efficiently tuned.

The preparation of salen aluminum complexes has been studied in detail in the literature[9]. The selective synthesis of monometallic {Salen}[AlX] (X=Me, Cl or OiPr) or bimetallic {Salen}[AlR_2]$_2$ (R=Me) species has been achieved, resulting from adjustment of experimental conditions, as shown by Thomas and Carpentier[10]. It is therefore possible to generate at will either type of complex. Furthermore, in order to improve the catalytic performances of this type of system, their immobilization onto an inorganic support can be performed, to generate a catalytic material than can be recycled and might also features new properties. Several examples already describe the grafting of salen-based species onto a surface to obtain efficient catalytic materials[11]. Following our efforts in the development of aluminum-phenoxyimine derivatives[12] and on the immobilization of aluminum organometallic derivatives[13], we decided to focus on the immobilization of aluminum salen derivatives onto silica surface. As described in literature, use of flame silica with high specific surface area (such as Aerosil from Evonik) allows high metal loading and appropriate thermal treatment can lead to a good control of the nature of the surface species generated upon grafting. Indeed, controlling the dehydroxylation of the surface of the silica is a key point to generate well-defined species. This is an important point, as some examples[14] demonstrate that bis- or mono-silica-grafted species can influence the catalytic performances. In this view, we have designed our experimental conditions in order to obtain only mono-grafted organometallic entities. We present here grafting of aluminum alkyl salen derivatives on dehydroxylated silica via surface organometallic chemistry, along with detailed solid state NMR investigations and preliminary investigations on their potential as catalysts for the carbonatation of epoxides.

4.2.2. Results and discussion

Synthesis and characterization of alkyl derivatives

The reaction between trimethylaluminum and salen ligand **1** featuring an enantio-pure cyclohexanediamine backbone has been reported to lead to 2 different products: **2-Me** or **3-Me**, depending on the experimental conditions (Scheme 4.2.1). The formation of bimetallic species can be attributed to the fact that, thermodynamically, insertion of a new aluminum is easier than the intramolecular reaction. Thomas and Carpentier[10] showed that 3 parameters influence the chemioselectivity: reaction temperature, ligand/Al ratio and order of addition of compounds. Indeed, to selectively obtain monometallic **2-Me**, it is necessary to heat the reaction mixture at 110 °C (binuclear **3-Me** is also formed, with a **2-Me**:**3-Me** ratio of 9:1). In the view of preparing silica-grafted mono- and binuclear aluminum salen frameworks, we chose to selectively prepare both **2-Me** and **3-Me**. To help in the understanding of the (surface) chemistry involved in our studies, we resorted to ^{27}Al solid state NMR, which proved to be a most valuable spectroscopic tool for these species.

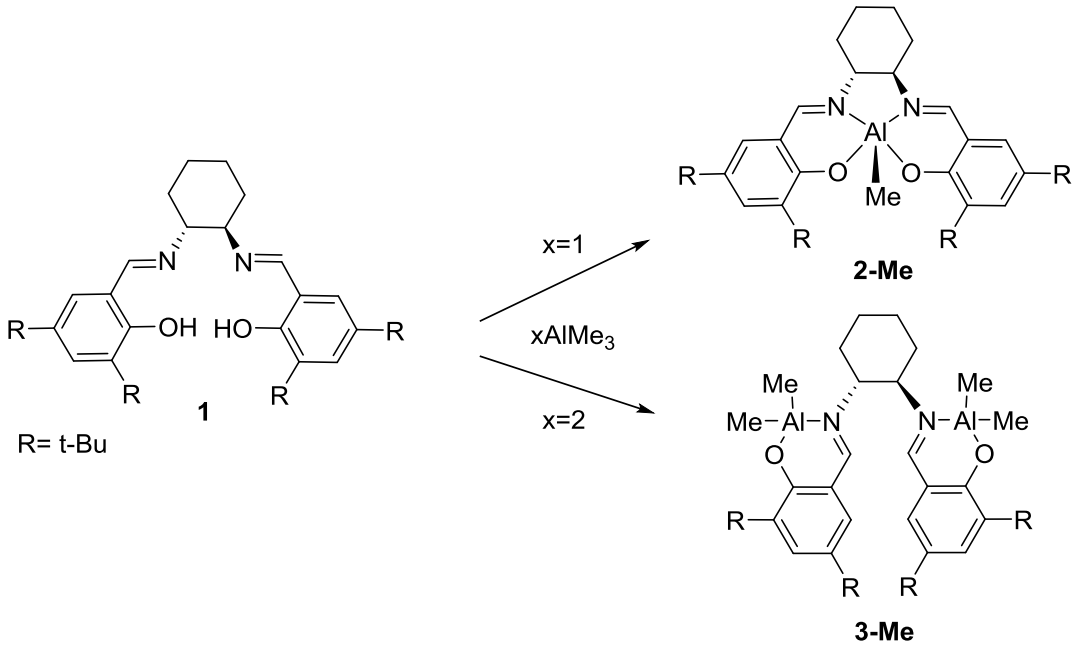

Scheme 4.2.1 Synthesis of **2-Me** and **3-Me**

Indeed, the quadrupolar ^{27}Al nucleus features a nuclear spin of 5/2, a good sensibility and its chemical shift is strongly dependent on the metal coordination sphere. Furthermore, for quadrupolar nuclei, not only isotropic (chemical shift, δ_{iso}) but also anisotropic parameters (quadrupolar coupling constant C_Q, asymmetry parameter η) can be extracted from spectroscopic data, thus providing additional parameters that can help in providing further structural information. Moreover, in complexes involving non-alkyl ligands (O, N, or halide) the tetra-, penta- and hexa-coordinated aluminum nucleus present chemical shift at about 60, 30 and 0 ppm, respectively[15].

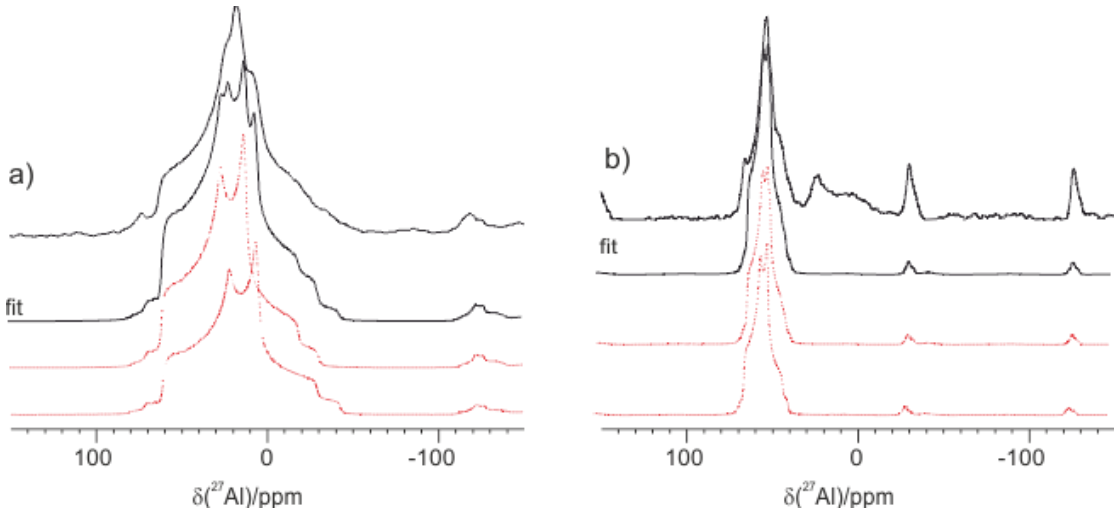

Figure 4.2.1 ^{27}Al MAS NMR of a) **2-Me**, 104 MHz, b) **2-Me**, 208 MHz

The ^{27}Al MAS NMR spectrum of **2-Me** has been recorded at 2 magnetic fields, namely 9.4 and 18.8 T (Figure 4.2.1-a and b, respectively). The signal lineshape is indicative of the

presence of several species within the sample. In order to ease interpretation, we resorted to a high resolution method such as MQ MAS[16] experiment. This method provides 2D high resolution NMR spectra for quadrupole nuclei where one dimension presents the isotropic spectrum and the second one, the second order lineshapes. Thus, the MQ MAS spectrum of **2-Me** comprises 3 resonances: two strongly quadrupolarly coupled signals at 62.0 and 62.3 ppm, and a third one at about 24 ppm (Figure 4.2.2).

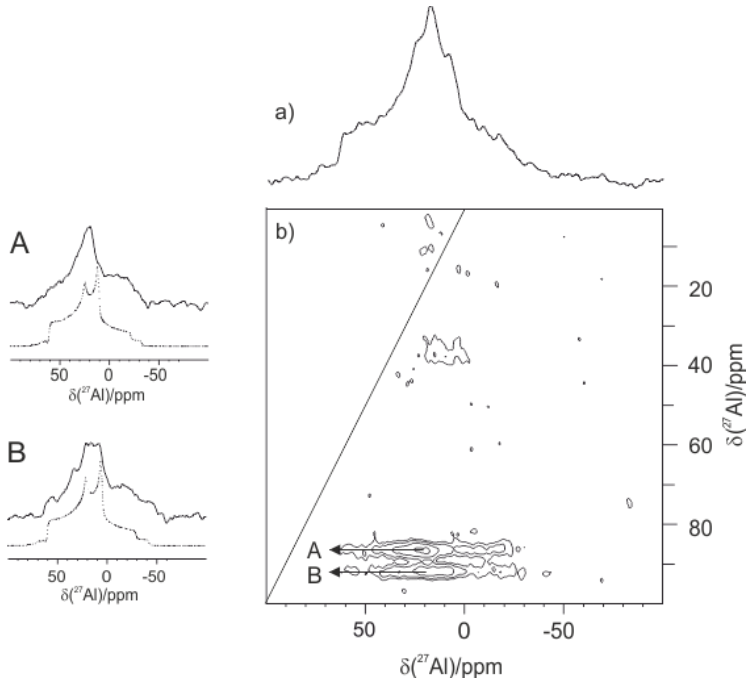

Figure 4.2.2 ^{27}Al MAS (104 MHz) (a) and ^{27}Al MQMAS (b) of **2-Me**.

The corresponding parameters for the first 2 signals are given on Table 4.2.1. These correspond to aluminum alkyl derivatives in pentahedral configuration, where the presence of the alkyl moiety induces a downfield shift of the CS compared to AlO_5 configuration. The occurrence of 2 signals can be explained by the fact that 2 sites are present in the crystallographic cell[10]. Furthermore, the close NMR parameters (site A: CS = 62.1 ppm and C_Q = 7.9 MHz, site B: CS = 62.3 ppm and CQ = 8.4 MHz) are in line with similar structure for both sites. The nature of the species fiving rise to a signal at about 24 ppm is most probably a dimer of the type [{Al(salen)}O], in line with the Al centers being in AlN_2O_3 configurations.

	δ (ppm)	C_Q (MHz)	η
2-Me	62.1	7.9	0.7
	62.3	8.4	0.7
2-OSiPh3	30.6	5.1	0.3
	31.8	4.7	0.2
3-Me	158.2	20.4	1
2-$SiO_{2\text{-}700}$	26.3	4400	-
3-$SiO_{2\text{-}700}$	nd	nd	

Table 4.2.1 NMR experimental chemical shift and simulated values

The synthesis of bimetallic **3-Me** was performed according to literature procedure[10]. When compared with monoalkyl, pentacoordinated **2-Me**, the bisalkyl, tetracoordinated **3-Me** is expected to feature higher chemical shift and C_Q values, due respectively to the nature of their coordination sphere and higher electrical field gradient. Indeed, preliminary ^{27}Al MAS NMR studies indicated that the signal was too broad to be recorded under spinning conditions (namely, the resonances were larger that the spinning rate, causing signal distortion which prevents interpretation). Thus, the ^{27}Al solid-state NMR spectrum was carried under static conditions with a QCPMG[17] sequence to enhance the signal-to-noise ratio (Figure 4.2.3). Indeed, the QCPMG technique can generate an order of magnitude sensitivity enhancement when compared to echo experiments, thanks to the discretization of the signal. The best fit is obtain using CSA contribution (δ_{csa}= -34 ppm, η_{csa}= 0.8). Both the chemical shift (158 ppm) and quadrupolar coupling constant (20.4 MHz) are in line with the proposed Al(N,O)R_2 structure. However, it is difficult to go in further assignment with the present set of data.

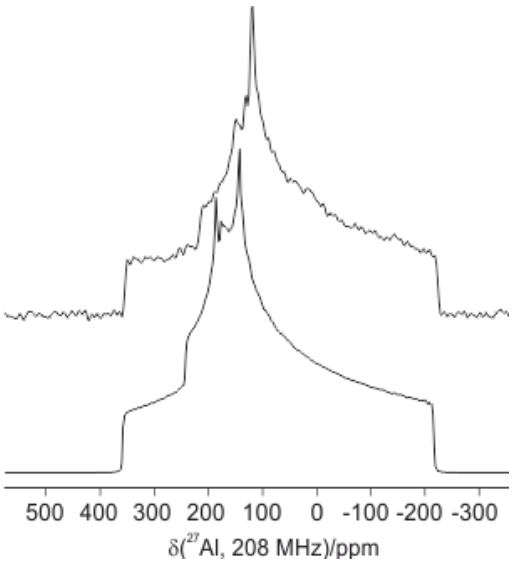

Figure 4.2.3 ^{27}Al (208 MHz) QCPMG of **3-Me**

Studies on a model silanolate compound

The detailed spectroscopic study of supported organometallic catalysts is a challenging task, due to several aspects: grafting induces low concentration of surface species, structural distribution strongly affects the signal and presence of different sites may also interfere with full understanding. This latter point can be addressed by controlling grafting chemistry. Provided that a single type of surface species can be prepared, specific molecular models can be independently synthetized. Thus, when targeting [{salen}Al(OSi≡)], a suitable model species is the triphenylsilanolate derivative, for which spectroscopic investigations can be easily performed to be, in a later stage, compared to those of the grafted material. Thus, the synthesis of **2-OSiPh$_3$** was carried out by mixing 1:1 ratio of Ph_3SiOH and **2-Me**[18]. Further characterization of known **2-OSiPh$_3$** was performed by ^{27}Al MAS NMR. It reveals the presence of 2 sites (similarly to **2-Me**), as confirmed with MQ MAS (Figure 4.2.4-a and Figure 4.2.5).

The NMR parameters extracted from these spectra can be found in Table 4.2.1. The CS (about 31 ppm) are in line with the AlO_5 coordination sphere, while the C_Q values (4.7 and 5.1 MHz) are lower than that of **2-Me**, as expected from the formal substitution of an alkyl ligand by a silanolate. Interestingly, this compares very well with the data obtained in the case of **2-SiO$_{2\text{-}700}$**, validating this structural hypothesis for the nature of the surface grafted aluminum centers (see below).

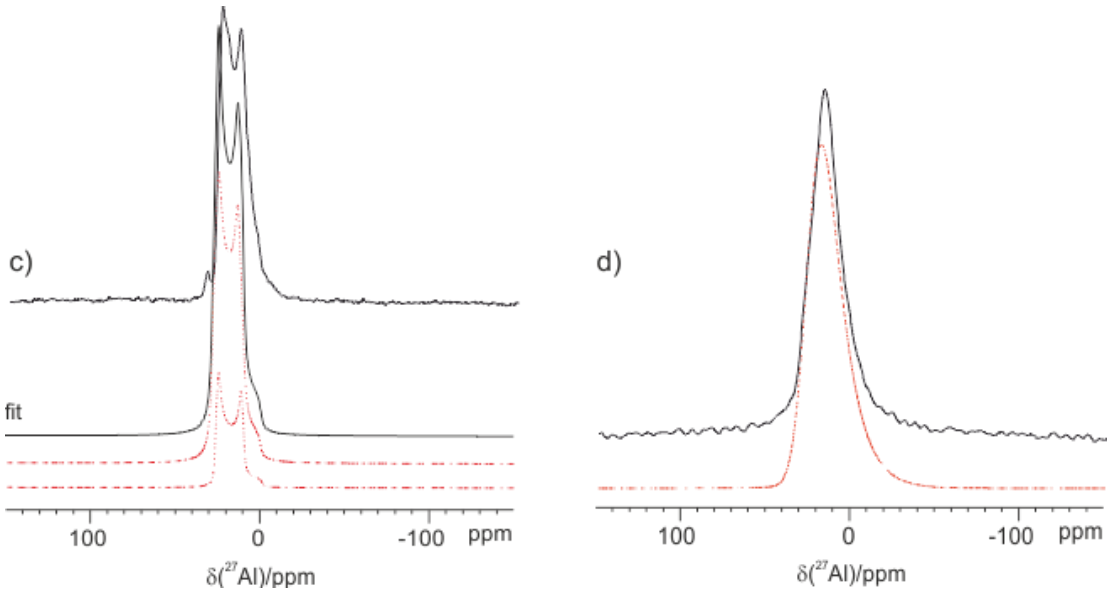

Figure 4.2.4 ^{27}Al MAS NMR of a) **2-OSiPh$_3$**, 104 MHz, b) **2-SiO$_{2\text{-}700}$**, 104 MHz.

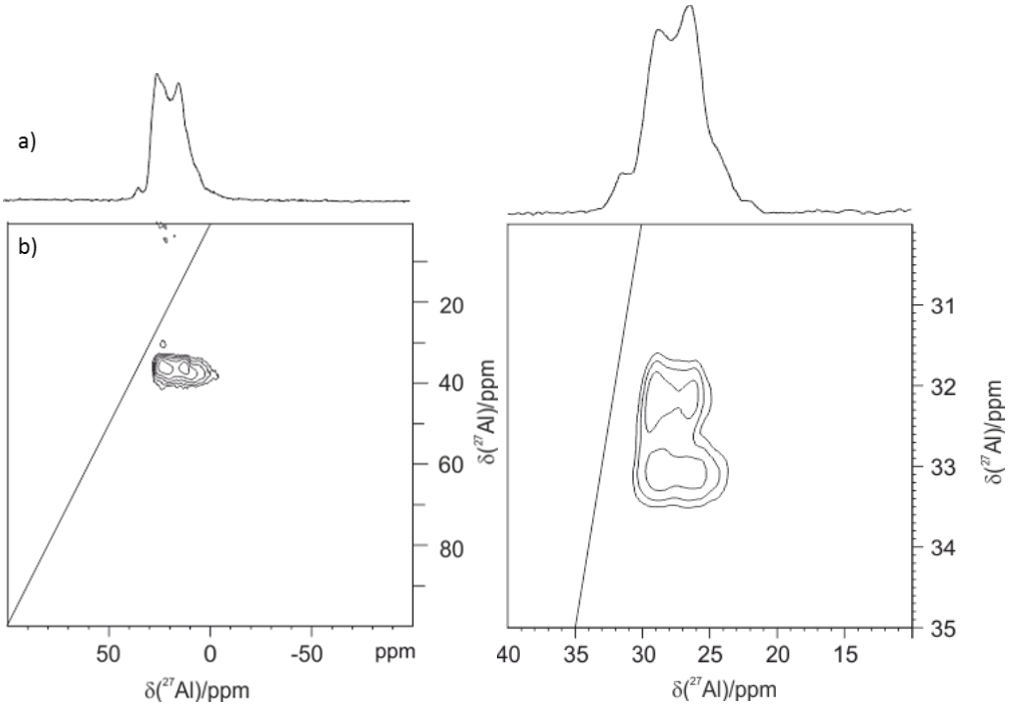

Figure 4.2.5 . ^{27}Al MAS (104 MHz-left, 208 MHz-right) (a) and ^{27}Al MQMAS (b) of **2-OSiPh$_3$**.

Grafting of 2-Me and 3-Me onto silica dehydroxylated at 700 °C

In order to immobilize the salen derivatives onto silica with high degree of control over the resulting species structure, we selected as the inorganic carrier a flame silica, namely Evonik Aerosil 380, which was treated at 700°C under vacuum ($SiO_{2\text{-}700}$), thus affording a surface bearing only non-interacting silanols (see the ν(OH) band at 3747 cm^{-1} on the IR spectrum on Figure 4.2.6-a). This support is routinely used in surface organometallic chemistry, as it has been shown to afford well-defined monografted species is several cases. It is therefore ideally suited to afford our targeted grafted species.

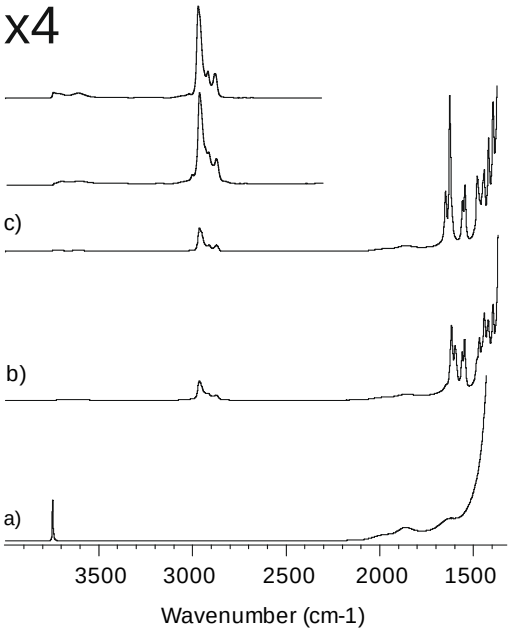

Figure 4.2.6 DRIFT of a) $SiO_{2\text{-}700}$, b) **2-$SiO_{2\text{-}700}$**, c) **3-$SiO_{2\text{-}700}$**

The grafting of **2-Me** on $SiO_{2\text{-}700}$ was performed by reacting silica with the aluminum complex in toluene (1.3 eq of Al per silanol), affording a yellow material, **2-$SiO_{2\text{-}700}$** (Scheme 4.2.2).

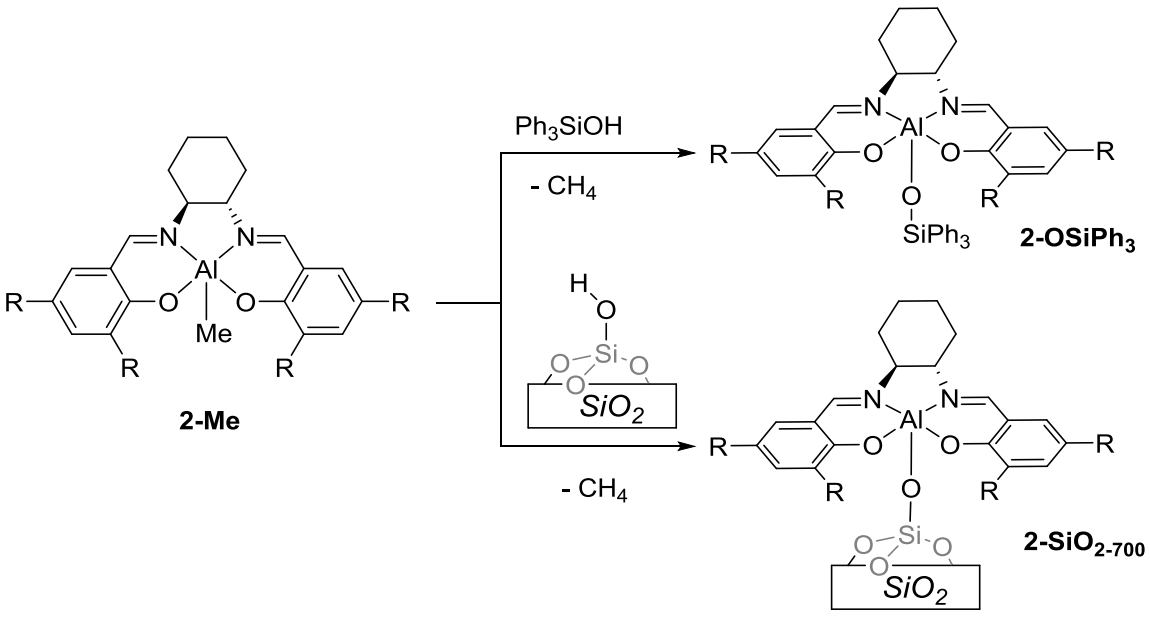

Scheme 4.2.2 Synthesis of **2-OSiPh$_3$** and **2-SiO$_{2\text{-}700}$**

Comparison of DRIFT spectra of $SiO_{2\text{-}700}$ and **2-SiO$_{2\text{-}700}$** evidences the consumption of silanol from the surface, as shown by the lack of non-interacting SiOH's signal on the DRIFT spectrum of **2-SiO$_{2\text{-}700}$**, notably of the 3747 cm^{-1} $\nu_{(O\text{-}H)}$ band (Figure 4.2.6-a, b). New, broad signals corresponding to interacting silanols are observed at 3606 cm^{-1}. New signals at 3004 and 2962-2872 cm^{-1}, correspond to sp^2 and sp^3 C-H elongations, respectively. In addition, a band at 1617 cm^{-1} is in accordance with the stretching band of C=N from imine group. Also, several bands are present between 1600 cm^{-1} and 1540 cm$^{-.1}$, that are characteristic for C=C aromatic-ring-stretching vibrations). The loading of aluminum in **2-SiO$_{2\text{-}700}$** is of 0.18 mmol.g^{-1} which corresponds to a two-third of the theoretical complete grafting onto the silica (0.27 mmol of OH per gram of $SiO_{2\text{-}700}$[19]). The steric hindrance of the catalyst can be an explanation of the non-fully occupation of SiOH group. The ratio N/Al is 2.5, close to the expected value of 2.0.

The resolution of ^{1}H MAS NMR is not enough to fully describe the catalyst however 2 zones are observed (Figure 4.2.7-a). The one at 7.5 ppm corresponds to the ensemble of the aromatic protons and the other one around 1 ppm is for the *t*-butyl and methyl groups.

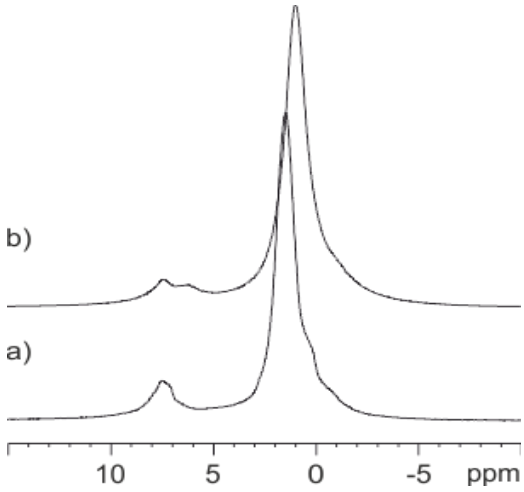

Figure 4.2.7 ^{1}H MAS NMR (400 MHz) of a) **2-SiO$_{2\text{-}700}$**, b) **3-SiO$_{2\text{-}700}$**

The ^{27}Al MAS NMR of **2-SiO$_{2\text{-}700}$** (9.4 T) consists of a featureless signal with a maximum at 16.9 ppm (Figure 4.2.4-b). This may be due to the structural distribution of moieties on the surface (in terms of bond length and angle variations due to the heterogeneity of the silica surface) which quenches quadrupolar coupling, as observed in several related cases[20,21,22]. From best fit simulations using Czjzeck model, chemical shift of about 26 ppm (with a distribution of 45 ppm) and C_Q of about 4.4 MHz can be inferred (Table 4.3.1), consistent with the AlO_5 coordination sphere. Additionally, the ^{27}Al MAS NMR spectrum shows no indication for coordination of an additional siloxane ligand from the surface, which would have given rise to signals at about 0 ppm (as expected from hexacoordination with a AlN_2O_4

environment). These NMR parameters are well in line with those of the model species **2-OSiPh$_3$** (CS and C_Q of about 31 ppm and 4.9 MHz, respectively).

Furthermore, the MQ MAS spectrum of **2-SiO$_{2\text{-}700}$** (Figure 4.2.8) comprises a single resonance, with a chemical distribution of 12 ppm from 35 to 47 ppm, which compares well with that extracted from best fit simulations. This is thus in line with the formation of a single type of aluminum species on the surface.

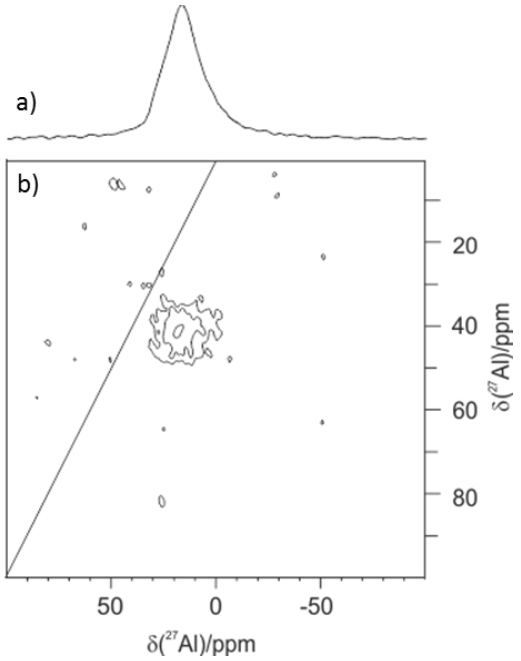

Figure 4.2.8 a) ^{27}Al MAS NMR and b) ^{27}Al MQMAS NMR spectra of **2-SiO$_{2\text{-}700}$** (18.8 T, spinning speed 20 kHz)

Reaction of **3-Me** with $SiO_{2\text{-}700}$ in similar conditions with a longer reaction time (15h) leads to formation of **3-SiO$_{2\text{-}700}$** (Scheme 4.2.3) (1.3 eq of Al per silanol). The DRIFT spectrum shows the consumption of silanol from the surface, as seen with **2-SiO$_{2\text{-}700}$**, notably of the 3747 cm^{-1} $\nu_{(O\text{-}H)}$ band (Figure 4.2.6 a, c). Residual signals from interaction SiOH groups are also observed (at 3735 and 3606 cm^{-1}). Again, sp^2 and sp^3 C-H elongations signals are observed at 2962, 2914 and 2872 cm^{-1}. The main difference is the relative intensity (higher in **3-SiO$_{2\text{-}700}$** than with **2-SiO$_{2\text{-}700}$**) which is easily explained regarding the structure of bimolecular catalyst featuring twice more salen ligand than the monomolecular one The Al loading (0.34 mmol.g^{-1}) corresponds to about 1.26 Al per silanol, while the N/Al ratio of 1.9 is in line with the expected structure (theoretical value 2.0).

Again, information obtained from the ^{1}H MAS NMR are scarce, as only 2 main signals are observed (Figure 4.2.7-b) at about 7.5 ppm for the aromatic part of the catalyst and at about 1 ppm is for the alkyl groups. The same observation was made for the ^{13}C CPMAS NMR spectrum (Figure 4.2.9). It features two broad signals centered at 169 and 133 ppm that are attributed to the carbon in alpha position of the imine and to the carbons from the aromatic ring, respectively. Signals around 65 ppm are assigned to carbon from the cyclohexyl

fragment, and the broad signal from 35 to 25 ppm can be assigned to the *t*-butyl groups. The sharp signal at about 0 ppm may be due to Al-Me groups, or to methyl groups transferred on the support.

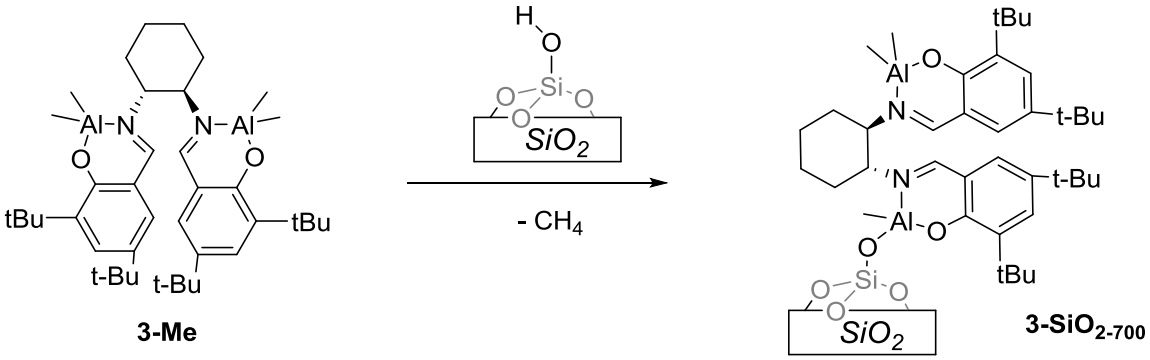

Scheme 4.2.3 Synthesis of **3-SiO$_{2\text{-}700}$**

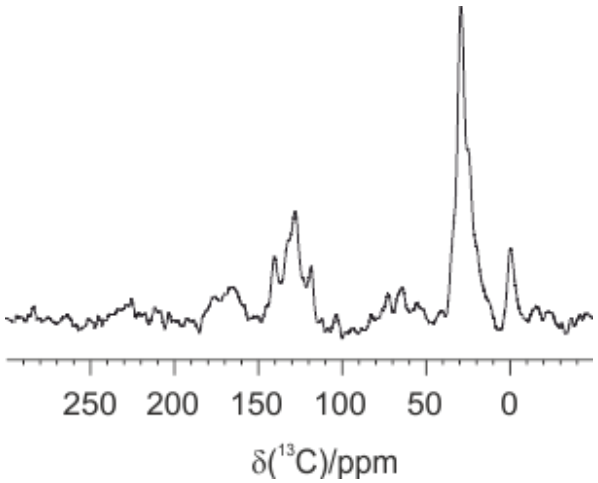

Figure 4.2.9 ^{13}C CPMAS NMR spectrum of **3-Me** (9.4 T, ro= 10 kHz)

The ^{27}Al solid-state NMR recorded under static conditions with the QCPMG technique is presented in Figure 4.2.10. A single, broad signal is observed, spanning from 400 to -100 ppm with a maximum around 0 ppm. However, assessment of NMR parameters from this signal is out of reach at this stage, due to the signal distribution that prevents any meaningful modeling to be performed.

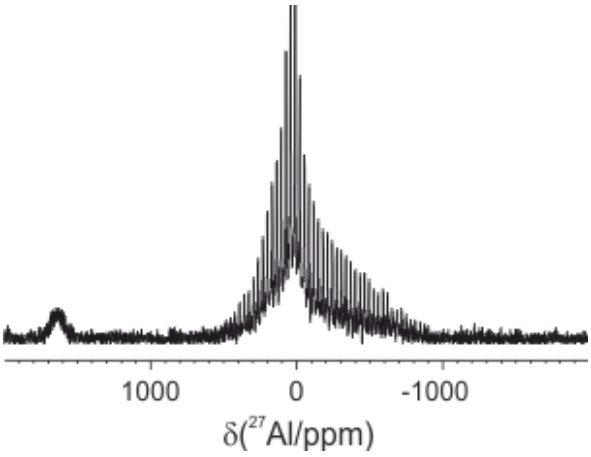

Figure 4.2.10 ^{27}Al (208 MHz) QCPMG of **3-SiO$_{2\text{-}700}$** (208 MHz)

Catalytic application in carbonate synthesis

The molecular and supported Al-salen derivatives **2-Me**, **3-Me**, **2-SiO$_{2\text{-}700}$** and **3-SiO$_{2\text{-}700}$** were probed for the carbonates synthesis with similar experimental conditions as described by Kleij[23] The catalyst amount is 0.1 mol% for mononuclear catalyst (**2-Me** and **2- Me-SiO$_{2\text{-}700}$**) and 0.05 mol% for binuclear species (**3-Me** and **3-Me-SiO$_{2\text{-}700}$**). In addition to the Lewis acidic aluminum catalyst, tetrabutylammonium iodide (TBAI) was added as a nucleophilic co-catalyst. Results are reported in Table 4.2.2

Entry	Reactant	Al-Cat	Conv. by NMR(%)
1		**2-Me**	32
2		**3-Me**	17
3		**2-SiO$_{2\text{-}700}$**	33
4		**3-SiO$_{2\text{-}700}$**	13
5	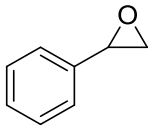	**2-Me**	54
6		**3-Me**	92
7		**2-SiO$_{2\text{-}700}$**	>99
8		**3-SiO$_{2\text{-}700}$**	>99
9		**SiO$_{2\text{-}700}$**	59
10	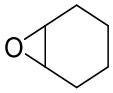	**2-Me**	13

Table 4.2.2 Catalytic results of carbonatation

Conditions: Al-cat = 0.1 mol%, Al$_2$-cat = 0.05 mol%, TBAI = 2eq, pCO$_2$ = 30 bar; T = 120 °C; t = 3 h

Comparable results between molecular and supported catalysts were reached with hexane oxide as a substrate, with modest conversion. Mononuclear species afford higher yield than binuclear ones, showing that in the present case, no significant beneficial bimetallic effect is operative.

The styrene oxide is the most reactive substrate. It reaches 100% conversion with the grafted catalyst. But the selectivity is not total and GC analysis shows 35% of phenylacetaldehyde, a degradation product of epoxide. No general pattern can be described for the activity of **2-Me** compared to that of **3-Me** (Table 4.2.2 entry 1, 2 and 5, 6) as it seems that is highly substrate dependent. Same observation for the grafted complexes (Table 4.2.2 entry 3, 4 and 7, 8). Grafted catalysts are more active for the styrene oxide but as observed with their molecular equivalent, their efficiency depend on the substrate. Blank tests cast some shadow over these results, as silica or TBAI alone afford respectively 59 and 81 % conversion. In the absence of cocatalyst, neither **2-SiO$_{2\text{-}700}$** nor **3-SiO$_{2\text{-}700}$** are active. Recycling the supported catalyst was not performed, as leaching into homogenous phase was

evidenced by the coloration of the supernatant. Cleavage of the Al-O bond from the surface could originate from reaction with TBAI, affording soluble [Al(salen)(I)] and [(≡SiO)(NBu_4)] species.

4.2.3. Conclusion.

In conclusion, mono- and binuclear aluminum salen alkyl complexes have been prepared and grafted on dehydroxylated silica. Spectroscopic investigation, mainly ^{27}Al MAS and MQ MAS NMR, combined with comparison to a molecular model of a mononuclear silica-supported species, have contributed to the assessment of the surface species' structure. In spite of positive catalytic results in epoxide carbonatation, both blank test and leaching studies cast doubt on the efficiency of the supported aluminum salen systems for this transformation.

4.2.4. Experimental

General Consideration: Unless specified, all manipulations were carried out under an argon atmosphere in an MBraun glovebox or using Schlenk techniques. Pre-purified solvents on a traditional solvent fountain are degassed through freeze-pump thaw cycles. Elemental Analysis were performed at London Metropolitan University and at LASIR, University of Lille (Al). DRIFT spectra were recorded with a Nicolet 6700 FTIR spectrometer by using airtight cells. GC analysis are performed on a Shimadzu. Solid state ^{1}H, ^{13}C, ^{27}Al and ^{29}Si MAS NMR spectra were obtained with a Bruker Avance 400 spectrometer with a conventional 3.2mm CP/MAS probe. The samples were loaded under argon in a zirconia rotor with airtight caps. The ^{27}Al MAS spectra at 18.8T were acquired at a spinning frequency of 20 kHz with a delay time at 0.5 s and a ¾ π pulse at 0.85 µs. The ^{27}Al MAS MQMAS spectra were collected using the Z-filter sequence, which consists of two hard pulses of 3.5 and 1.25 µs at an RF field of 70 kHz, for triple- quantum excitation and reconversion, respectively, followed by a soft pulse of 6 µs at an RF field of 10 kHz.

Synthesis of *{Salen}H_2:* In a 50 ml round bottom flask, 1,2-cyclohexanediamine (100 mg, 3mmol) and 3,5-di-ter-butyl-2-hydroxybenzaldehyde (412 mg, 6mmol) are introduced in solution with ethanol (10mL). After a night of refluxing at 80°C, all the solvent is removed under vacuum to obtain a yellow powder. ^{1}H (400 MHz, $CDCl_3$) δ(ppm): 1.23 (s, *t*-Bu, 9H); 1.42 (s, *t*-Bu, 9H); 1.72 (m, CH_2, 2H); 1.85 (m, CH_2, 2H); 3.32(m, CH-N, 2H); 6.98 (d, H_{arom}, 2H); 7.30 (d, H_{arom}, 2H);8.3 (s, imine, 2H); 13.7 (s, H_{PhOH}, 2H). DRIFT (NaCl, cm^{-1}): 3500 (large, ν $_{OH\ libre}$); 2962 (ν $_{C-H}$); 1630 (ν $_{C=N}$); 1592 (ν $_{C=C}$).

Synthesis of 2-Me[10]*:* In a Schlenk tube, a solution of $AlMe_3$ in toluene (0.14M, 2.5mL) is slowly added on a solution of {Salen}H_2 in toluene (200mg in 10mL of toluene). During addition, methane evolution is observed. The reaction mixture is heated at 110°C and stirred overnight. The solvent is removed under vacuum to afford a yellow powder that is washed several times with cold pentane. Yield: 85%. ^{1}H (400 MHz, $CDCl_3$) δ(ppm): -1.1 (s, CH_3-Al, 3H); 1.08 (s, CH_2, 2H); 1.3 (s, *t*Bu,9H); 1.31 (s, *t*Bu,9H) 1.35 (s, CH_2, 2H); 1.51 (s, *t*Bu, 9H); 1.52 (s,

*t*Bu, 9H); 3.06 (m, CH-N, 2H); 3.55 (m, CH-N, 2H); 6.55(d, H_{arom} 2H); 7.05 (d, $H_{arom,}$ 2H); 8.10 (d, imine, 1H); 8.28 (d, imine, 1H). DRIFT (KBr, cm^{-1}) 2957(ν_{C-H}), 1620 ($\nu_{C=N}$), 1620 ($\nu_{C=C}$).

Synthesis of 3-Me[10]: In a Schlenk tube, a solution of $AlMe_3$ in toluene (0.14M, 2.5mL) is slowly added to a solution of {Salen}H_2 in toluene (200mg in 10mL of toluene). During addition methane evolution is observed. The reaction mixture is stirred overnight. The solvent is removed under vacuum to afford a yellow powder that is washed several times with cold pentane, yield: 82%^{1}H (400MHz, $CDCl_3$) δ(ppm): -0.82 (s, CH_3-Al, 6H); -0.48 (s, CH_3-Al, 6H); 1.08 (s, *t*Bu, 18H); 1.35 (s, *t*Bu, 18H); 1.97 (m ,CH_2, 2H), 3.57 (d, CH-N, 2H); 6.55(d, $H_{arom,}$ 2H); 7.34 (d, H_{arom}, 2H); 7.8 (s, imine, 2H). DRIFT (KBr, cm^{-1}) 2954(ν_{C-H}), 1592 ($\nu_{C=N}$), 1543 ($\nu_{C=C}$).

Synthesis of 2-SiO_{2-700}: 1g of silica pre-heated at 700°C for 15h under high vacuum pump (0.27mmol of OH.g^{-1}) is added in a double-Schlenk vessel and suspended in 10 mL of pentane. A 10 mL solution of **2-Me** in pentane (1.3 eq, 0.351mmol) is added under argon. The reaction mixture is stirred for 90 minutes, the supernatant is removed and the yellow solid powder is washed 3 times with pentane in order to remove unreacted **2-Me**. The powder is dried at 80°C under high vacuum for 5 hours.

Synthesis of 3-SiO_{2-700}: 1g of silica pre-heated at 700°C for 15h under high vacuum pump (0.27mmol of OH.g^{-1}) is added in a double-Schlenk vessel and suspended in 10 mL of pentane. A 10 mL solution of **3-Me** in pentane (1.3 eq, 0.351mmol) is added under argon. The reaction mixture is stirred for 15 hours, the supernatant is removed and the yellow solid powder is washed 3 times with pentane in order to remove unreacted **3-Me**. The powder is dried at 80°C under high vacuum for 5 hours.

Carbonatation reaction: In the glovebox, a 40 mL stainless reactor with a magnetic stirrer is filled with the epoxide substrate (0.05 mol), aluminum catalyst and co-catalyst (ratio ½ for mononuclear system and ¼ for binuclear). Example: styrene oxide (5g, 0.05 mol), **2-Me** (25 mg, $5x10^{-2}$ mmol), TBAI (30.8 mg, 0.1 mmol) Then the reactor is charged with 30 bar of CO_2 and heated at 120°C for 3h. The pressure is then released and the reaction mixture is analyzed by ^{1}H NMR and gas chromatography.

---

[1] E.J. Beckman, *Ind. Eng. Chem. Res.* 2003, **42**, 1598-1602

[2] M.G. Hitzler, F.R. Smail, S.K. Ross and M. Poliakoff, *Chem. Commun.*, 1998, 359-360

[3] G. Yuan, C. Qi, W. Wu, H. Jiang, *Current Opinion in Green and Sustainable Chemistry*, 2017, **3**, 22-27

[4] P. Pfeiffer, E. Breith, E. Lübbe, T. Tsumaki., *Eur. J. Org. Chem.*, 1993, **503**, 84

[5] E. N. Jacobsen, W. Zhang, A. R. Muci, J. M. Ecker, L. Deng, *J. Am. Chem. Soc*, 1991, **113**, 706

[6] M. A Munoz-Hernandez, T.S. Keiser, P. Wei, S. Parkin, *Inorg. Chem.*, 2001, **40**, 6782

[7] W. Clegg, R. W. Harrington, M. North, R. Pasquale, *Chem. Eur. J. ,* 2010, **16**, 6828

[8] J. Meléndez, M. North, P. Villuendas, *Chem. Commun.,* 2009, 2577-2579

[9] D.A. Atwood, M.J. Harvey, *Chem. Rev.,* 2001, **101**, 1

[10] A. Alaaeddine, T. Roisnel, C. M. Thomas, J-F Carpentier., *Adv. Synth. Catal* ,2008, **350**, 731-740

[11] E.F. Murphy, L. Schmid, T. Bürgi, M. Maciejewski, A. Baiker, *Chem. Mater.,* 2001, **13**, 1296-1304

[12] a) J. Ternel, P. Roussel, F. Agbossou-Niedercorn, R. M. Gauvin, *Cat. Sci. Technol.*, 2013, **3**, 580-583 ; b) J. Ternel, F. Agbossou-Niedercorn, R. M. Gauvin, *Dalton Trans.*, 2014, **43**, 4530-4536

[13] a) J. Pelletier, J. Espinas, N. Vu, S. Norsic, L. Delevoye, J. Trebosc, E. Le Roux, C. Santini, J.-M. Basset, R. M. Gauvin, M. Taoufik, *Chem. Commun.* 2011, **47**, 2979-2981; b) D. W. Sauter, N. Popoff, M. A. Bashir, K. C. Szeto, R. M. Gauvin, L.

Delevoye, M. Taoufik, C. Boisson, *Chem. Commun.* 2016, **52**, 4776-4779 ; c) D. W. Sauter, V. Chiari, N. Aykac, S. Bouaouli, L. Perrin, L. Delevoye, R. M. Gauvin, K. C. Szeto, C. Boisson, M. Taoufik, *Dalton Trans.*, 2017, **46**, 11547–11551

[14] J. H. Z. dos Santos, C. Krug, M. B. da Rosa, F. C. Stedile, J. Dupont, M. de Camargo Forte, *J. Mol. Catal. A: Chem.*, 1999, **139**, 199–207

[15]C. Martineau, F. Taulelle, M. Haouas, 2016. *The Use of 27Al NMR to Study Aluminum Compounds: A Survey of the Last 25 Years. Patai's Chemistry of Functional Groups.* 1–51

[16] J. Kanellopoulos, D. Freude, and A. Kentgens, *Solid State NMR*, 2008, **32**, 99-108

[17] H.Y., Carr; E.M. Purcell, *Phys. Rev.,* 1954, **94**, 630-638

[18] R. Duchateau, U. Cremer, R.J. Harmsen, S.I. Mohamud, H.C.L. Abbenhuis, R.A. van Santen, A. Meetsma, S.K. - H. Thiele, M.F.H. van Tol, M. Kranenburg, *Organometallics* ,1999, **18**, 5447–59 .

[19] a) J.-M. Basset, R. Psaro, D. Roberto, R.Ugo, *Modern Surface Organochemistry*, Wiley, 2009. b) L.T. Zhuravlev, *Colloids Surf. A. Physicochem. Eng. Asp*, 2000, **173**, 1-38

[20] N. Merle, J. Trébosc, A. Baudouin, I. Del Rosal, L. Maron, K. Szeto, M. Genelot, A. Mortreux, M. Taoufik, L. Delevoye, R.M. Gauvin, *J. Am. Chem. Soc.,* 2012, **134** , 9263–9275

[21] T. Vancompernolle, X. Trivelli, L. Delevoye, F. Pourpoint, R.M. Gauvin, *Dalton Trans,* 2017, DOI: 10.1039/c7dt02415k

[22] D. W. Sauter, V. Chiari, N. Aykac, S. Bouaouli, L. Perrin, L. Delevoye, R. M. Gauvin, K. C. Szeto, C. Boisson, M. Taoufik *Dalton Trans.* 2017, **46**, 11547–11551

[23] Kleij, R. Martín and A.W., *ChemSusChem*, 2011, **4**, 1259-1263

4.3. Synthesis and grafting on silica of a bis-silylamido aluminum species

4.3.1. Abstract:

The new bisamido aluminum species [Al{(N(SiMe$_3$)$_2$}$_2$(Cl)THF)] (**1**) was prepared and fully characterized, including by ^{27}Al and ^{35}Cl solid state NMR, and by X-ray diffraction studies. These have shown that **1** is monomeric in the solid state, with a distorted tetrahedral geometry. **1** was grafted on silica dehydroxylated at 700°C, affording silica-supported Al species. The resulting material (**2**) was characterized by IR, elemental analysis and solid state NMR. The latter technique showed the occurrence of two main types of species, were the Al center adopts a tetracoordinated coordination sphere, with as additional coordinated Lewis base, either a THF ligand or a silica-surface siloxane moiety.

4.3.2. Introduction

Silylamides are a class of compounds which attracts attention for several decades. The use of NR_2 (R= $SiMe_3$) as ligand has been already proved to be an interesting choice for catalytic transformations[1]. Indeed, sodium, lithium and potassium salts are both easily synthesized and commercially available. Their stability, lipophilicity and unique signature in ^{1}H and ^{13}C NMR make them convenient ligands for organometallic chemistry. First examples and studies have been carried out by Bürger and Wannagat,[2] who described several bis- or tris-amido transition metal complexes (Cr, Mn, Cu, and Ni). More specifically, the -$NSiMe_3$ as a ligand has been proved to be a powerful asset for catalytic transformations. Indeed, originally the bis-trimethylsilylamido ligands use for its lipophilicity and the absence of beta hydrogen atoms that might lead to early decomposition of the catalyst. The development of tin complex by Zuckerman starts the widespread use of $N(SiMe_3)$[3]. Regarding structural issues, in 1961 Wanagat reported the crystal structure of the tris-amido aluminum derivative $Al[N(SiMe_3)_2]_3$[4] demonstrating the planarity of the ligand around the nitrogen atom. Since these pioneering studies, the silylamido ligand has been widely used in coordination chemistry, and with involvement of amido pre-catalysts in several reactions[5,6]. Furthermore, the amido moiety is well suited as reactive functionality for grafting onto silica, as demonstrated by the work of Anwander[7]. Silylamides have thus been employed as starting compounds for the preparation of hybrid materials via grafting onto dehydroxylated silica-type supports.

Silylamide aluminum derivatives derived from $AlCl_3$ and various equivalents of MNR_2 (1 to 3) have been used as BN-AlN ceramics precursors[8]. This work included the synthesis of $Al[N(SiMe_3)_2]_3$ with low yield (40%) and non-practical experimental techniques. In order to optimize these conditions, we performed several attempts to access the trisamide compound. In the course of these efforts, our investigations lead to a new tetra-coordinated aluminum complex with two amido functions, [Al{(N(SiMe$_3$)$_2$}$_2$(THF)Cl] (**1**). We present here

the full synthesis and characterization of this compound, along with its grafting onto silica, as a scaffold for further modification by protonolysis of the residual amido group.

4.3.3. Results and Discussion

In the course of attempts to prepare $Al[N(SiMe_3)_2]_3$8 from $AlCl_3$ with modification of the reported procedure, we obtained complex **1** when using $Li[N(SiMe_3)_2(THF)_x$ instead of unsolvated lithium bis(trimethylsilyl)amide. After filtration to separate LiCl salts and crystallization in pentane at -20 °C, colorless crystals are obtained in high yield (over 80%).

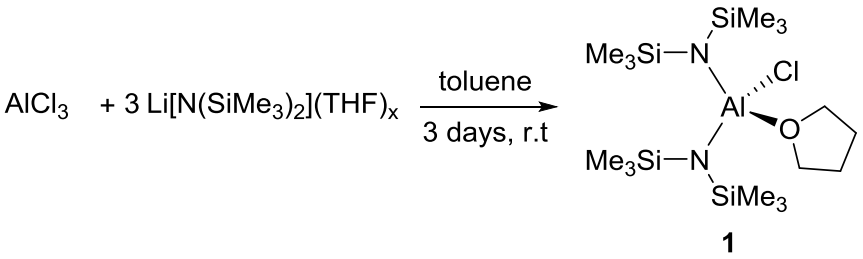

Scheme 4.3.1 Synthesis of **1**

Even in the presence of excess lithium amide excess, no further substitution leading to $[Al\{N(SiMe_3)_2\}_3]$ was observed.

Suitable samples for single crystal diffraction studies were obtained and the solid state structure is presented in Figure 4.3.1. The aluminum center features a distorted tetrahedral geometry, with two planar amido ligands as evidenced by the sum of angles around the N atoms N(1),Al(1),N(2): 357.8 °. The chloride ligand is in terminal configuration. Similar structure for the Y derivative $[Y\{(N(SiMe_3)_2\}_2(Cl)THF)]$ was recently reported by the Hayes group[9]. The ^1H NMR spectrum of **1** features 3 signals accounting for $SiMe_3$ (0.4 ppm) and THF (2 multiplets at 4.0 and 1.1 ppm for α- and β-CH_2 protons, respectively). Integration of the TMS and THF protons signals confirms the structure of **1**, as a THF mono-adduct. The ^{13}C NMR spectrum is also in line with the proposed structure of **1**, displaying 3 signals at 6.2 ppm ($SiMe_3$), 24.8 (β-CH_2 from THF) and 74.0 ppm (α-CH_2 from THF). Elemental analysis (C, H, N) is in line with these data.

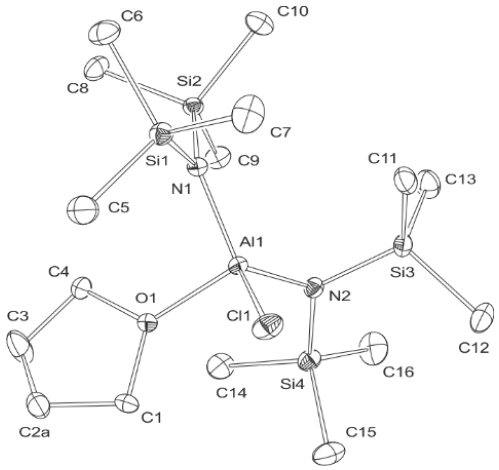

Figure 4.3.1 Solid-state structure of **1** (H atoms omitted for the sake of clarity). Selected bonds and angles: Al(1)-Cl(1) : 2.185 Å, Al(1)-N(1) : 1.833 Å, Al(1)-N(2) : 1.822 Å, Al(1)-O(1) : 1.901 Å, (Si(1)-N(1)-Si(2): 120.1°, Si(2)-N(1)-Al(1): 121.4°, Si(1)-N(1)-Al(1): 118.3°, Si(4)-N(2)-Si(3): 117.9°, Si(4)-N(2)-Al(1): 124.1°, Si(3)-N(2)-Al(1): 115.8°,N(1)-Al(1)-Cl(1): 112.9°, N(1)-Al(1)-N(2): 123.6°, N(2)-Al(1)-Cl(1): 107.4°, O(1)-Al(1)-Cl(1): 97.8°, N(2)-Al(1)-O(1): 110.6°.

Further characterization of this complex by ^{27}Al and ^{35}Cl solid state NMR was performed. Figure 4.3.2 presents the QCPMG ^{27}Al NMR spectrum; from which NMR parameters were extracted. The aluminum center features a very large quadrupolar coupling constant (*vide infra*), which motivated the recording of its spectrum under static conditions, as the width of the signal is significantly larger than the spacing of the spinning side bands (due to insufficient spinning speed), and as significant chemical shift anisotropy (CSA) was also observed. Thus, the isotropic chemical shift (δ_{iso}) is of 90 ppm and the quadrupolar coupling constant (C_Q) is of 20.7 MHz. The chemical shift value is in the upper range for aluminum centers in tetrahedral configuration[10]. Best fit simulation is obtained when considering chemical shift anisotropy (δ_{CSA}= -42 ppm). In addition, we were able to record the ^{35}Cl NMR spectrum of **1**. This nucleus was shown to be a convenient spectroscopic probe for studying organometallic and coordination compounds[11,12]. Figure 4.3.3 presents the static ^{35}Cl NMR spectrum recorded using the WURTS-QCMPG sequence which enables efficient recording for such ultra-wideline signals.[13] The best fit simulation corresponds to a δ_{iso} of 90 ppm and a C_Q value of 21.0 MHz. The similarity between the ^{27}Al and ^{35}Cl NMR parameters is entirely coincidental.

DFT calculations were performed as further evidence to strengthen our assessment of the quadrupolar nuclei NMR values. The ^{27}Al and ^{35}Cl chemical shift values of **1** were used to calibrate calculations (namely, the experimental value was selected as reference for ^{27}Al and ^{35}Cl chemical shift calibrations, used for calculations on silica-supported species). DFT calculations of anisotropic NMR parameters on **1** are fully in line with experimental results, which validates this combined experimental/theoretical approach.

	^{27}Al				^{35}Cl		
	δ_{iso}	C_Q	η_Q	δ_{CSA}	δ_{iso}	C_Q	η_Q
1	90	20.7		-42	90	21.0	
1$_{calc}$	90	20.7	0.92	-64.7	90	21.7	0.14
2	95-40	-	-	-	na	na	na
2$_{calc}$-a	70	21.1	0.69	-103.7	-	-	-
2$_{calc}$-b	81.0	16.5	0.88	-91.6	42.4	23.3	0.09
2$_{calc}$-c	107.7	36.7	0.47	-103.1	61.7	26.1	0.33
2$_{calc}$-d	83.9	25.9	0.92	-118.7	54.3	24.8	0.16

Table 4.3.1 Experimental and calculated ^{27}Al and ^{35}Cl NMR parameters.

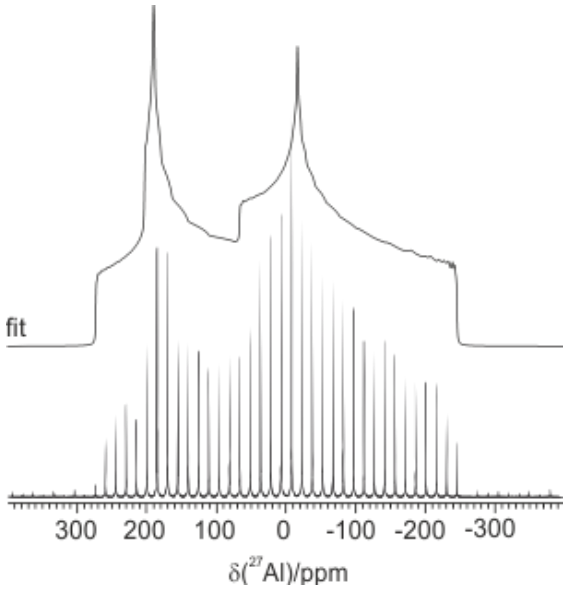

Figure 4.3.2 ^{27}Al QCPMG NMR spectrum (208.5 MHz) of **1**

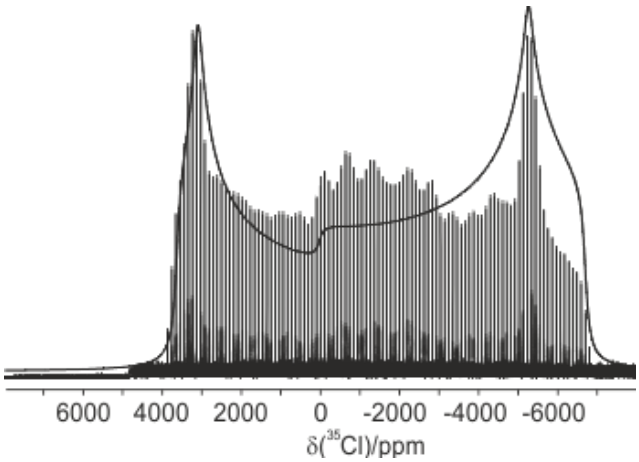

Figure 4.3.3 ^{35}Cl WURTS-QCPMG NMR spectrum of **1** (78.4 MHz).

Hybrid material **2** was prepared by reacting complex **1** with Aerosil 380 silica (Evonik, specific area of 380 $m^2.g^{-1}$). In order to generate preferentially well-defined, mono-grafted species, the support was treated at 700°C under high vacuum (10^{-5} mbar). Through condensation of silanols into siloxane with release of water, this treatment affords non-interacting silanols as sole type of silanol species, as confirmed by IR (Figure 4.3.4-b). Indeed, the spectrum comprises a sharp signal at 3747 cm^{-1} for $\nu_{(SiOH)}$. After stirring for 15 h in pentane at room temperature, washings to remove unreacted **1**, and drying under vacuum, **2** was obtained as a white material. The surface chemistry of **1** is expected to be very similar to that of lanthanide amides as studied by us and others[14], namely cleavage of M-N bonds release of hexamethyldisilazane (HMDS) and silylation of silanols.

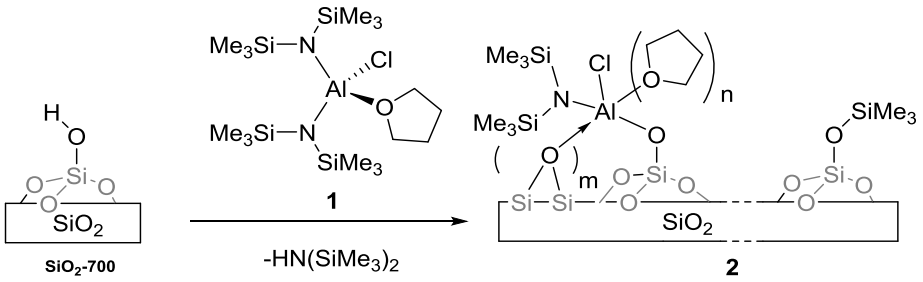

Scheme 4.3.2 Synthesis of **2**

Infrared spectra of **1**, $SiO_{2\text{-}700}$ and **2** are compared in Figure 4.3.4. The disappearance of the sharp signal at 3747 cm^{-1} for material **2** is in line with a total consumption of non-interacting silanols from $SiO_{2\text{-}700}$, either by reaction with **1** or with HMDS released upon reaction of the Al-N bond with SiO-H.[15] The signals between 3000 cm^{-1} and 2795 cm^{-1} can be attributed to $\nu_{(sp^3\ C\text{-}H)}$ elongation from $SiMe_3$ groups. The vibrations from the THF group can be observed as weak bands at 2984 and 2087 cm^{-1}. No $\nu_{(N\text{-}H)}$ is detected.

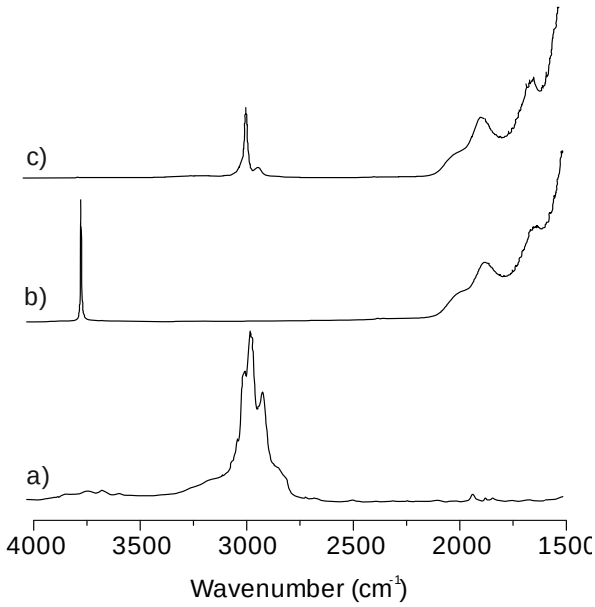

Figure 4.3.4 DRIFT of a) **1**, b) $SiO_{2\text{-}700}$ and c) **2.**

The loading in aluminum corresponds to an amount of 0.26 mmol of $Al.g^{-1}$ which is in line with results for Ln species[16] (Scheme 4.3.2). The N/Al ratio is 2.1 which is not in line with the cleavage of an aluminum-nitrogen bond by silanolysis. However, NMR tube experiments showed that upon mixing a silica slurry with **1**, only hexamethyldisilazane was detected, no ammonium nor HCl being observed, which is contradictory with the elemental analysis results and in agreement with the expected Al-N vs Al-Cl cleavage. Accordingly, in the case of HCl release during the grafting, formation of amine by reaction of amido with hydrochlorhydric acid would result in N-H signals, which are not detected by infrared spectroscopy. Current efforts are directed at reproducing the elemental analysis results, which are the outcome of the distinct determinations: ICP for Al content and combustion analysis for CHN.

Insights into the molecular structure of **2** was obtained thanks to high field solid state NMR. The ^{1}H MAS NMR spectrum (Figure 4.3.6-a) of **2** shows an intense peak at 0.1 ppm with a shoulder at 0.4 ppm, attributed to CH_3 from $SiMe_3$ group of $–N(SiMe_3)_2$ and $–OSiMe_3$, respectively. Two weaker signals at 4.2 and 2.0 ppm correspond to α- and β-CH_2 from the THF ligand. The significant shift of the α CH_2 signal in **2** compound compared to that in **1** (4.2 vs 3.65 ppm respectively) indicates coordination on a more electrophilic metal center. The ^{13}C MAS NMR (Figure 4.3.5) features 4 signals. The presence of the THF ligand is evidenced by the signals at 72.3 and 24.5 ppm which account respectively for $\alpha–$ and $\beta–$methylenic carbons. The signals at 2.1 and -1.2 ppm are assigned the methyl groups from the amido ligand and silylated silanols, respectively.

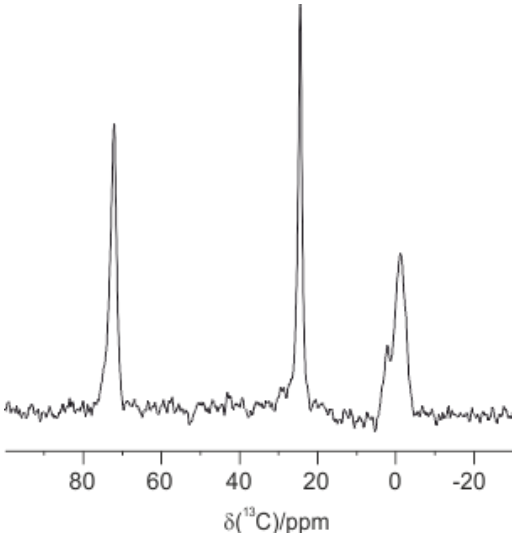

Figure 4.3.5. ^{13}C CPMAS NMR of **2**

In order to better understand the structure of **2** at the molecular level, a 2D ^{1}H-^{1}H DQSQ NMR spectrum was recorded. This experiment relies on dipolar interactions between neighboring protons and thus correlations on this spectrum are related to proximity. First of all, as expected from the structure, each signal on the 1D spectrum gives rise to self-correlation, as on-diagonal signals, as these originate from either methyl or methylene groups. Furthermore, three correlations are observed, noted as **A**, **B**, **C** on Figure 4.3.6-b. Correlation **A**, which associates signals at 4.2 and 2.0 ppm corresponds to the proximity between $\alpha–$ and $\beta–CH_2$ protons from THF. Interaction **B**, involving the signal at 4.2 with the signal at 0.1 ppm reveals proximity between α-CH_2 from THF and $AlNSiMe_3$ groups. The same type of interaction is also observed for **C** (of weaker intensity), which correlates peaks at 2.0 and 0.1 ppm (associating β CH_2 from THF and $AlNSiMe_3$ protons). No interaction is detected between $OSiMe_3$ groups at 0.4 ppm and THF protons, showing that correlations are restricted within the aluminum coordination sphere, as pictured on the structure on Figure 4.3.6's top caption.

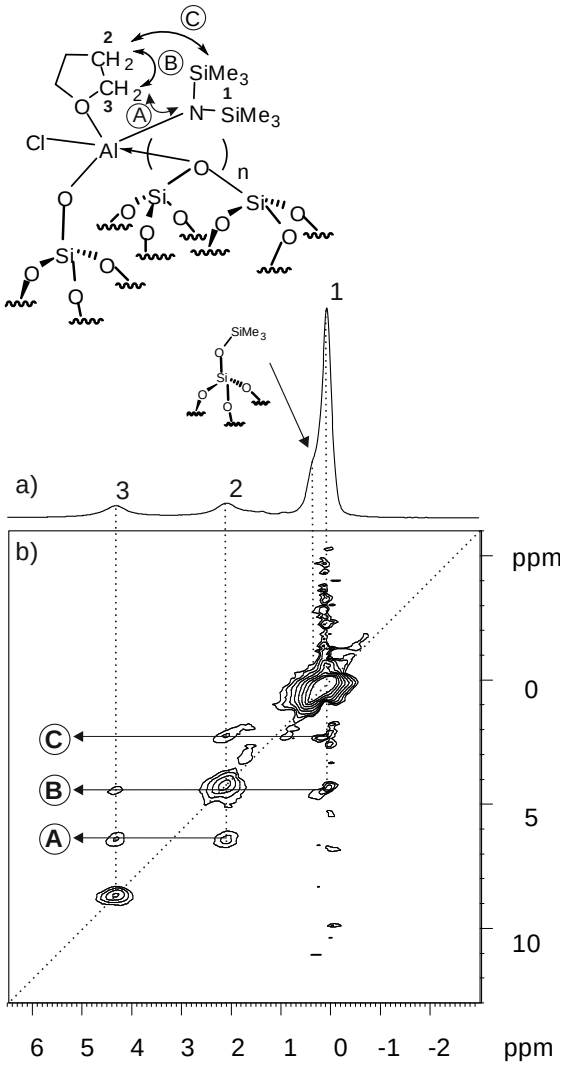

Figure 4.3.6 a) ^{1}H and b) ^{1}H-^{1}H DQ-SQ MAS NMR spectra of **2** (18.8 T, spinning speed 20 kHz).

The ^{27}Al MAS NMR spectrum of **2** at 18.8 T consists of a broad, complex signal spanning from 95 to 20 ppm, with maxima at about 90 and 65 ppm. If those chemical shift correspond to Al centers in tetracoordinated configuration, it remains unclear from this spectrum alone if the signal below 50 ppm stem from chemical shift distribution (and thus, from 5- and 6-coordinated species) or from broadening due to second-order coupling quadrupolar coupling (Figure 4.3.8). Nevertheless, recording the spectrum at lower field results in a signal of comparable width, which rules out the origin of broadening as due to quadrupolar coupling.

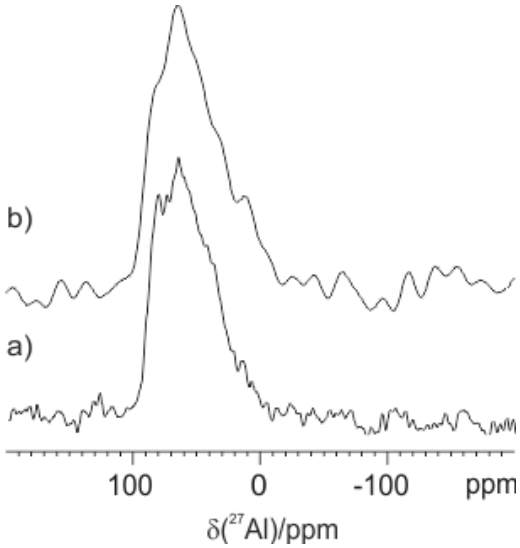

Figure 4.3.7. ^{27}Al MAS NMR of **2** at a) 18.8 T and b) 9.4 T

Further investigations were thus performed using a high resolution technique such as MQMAS[17]. This method provides 2D high resolution NMR spectra for quadrupolar nuclei, where the indirect dimension presents the isotropic spectrum and the direct one, the second order lineshapes. The MQMAS of **2** is presented on Figure 4.3.8. It comprises 2 different sites. The first one, noted **Site 2a**, corresponds to aluminum centers with a chemical shift distribution from 95 to 76 ppm (close to that of molecular precursor **1**, CS= 95 ppm), with a C_Q of 8.6 MHz. This is evidenced on extracted row on Figure 4.3.8-c. The second one, noted **Site 2b**, corresponds to aluminum centers with broader signal (see extracted row on Figure 4.3.8-d) starting from 85 to 55 ppm and a quadrupolar coupling constant of about 11.0 MHz. Both signals indicate a chemical shift distribution of about 5-10 ppm, resulting from structural distribution due to the heterogeneity of the silica surface. The signal from **Site 2b** does not span on the entire CS range from the ^{27}Al MAS NMR. This may be due to the lack of efficiency of the MQMAS experiment towards sites featuring large CQ values. Further studies using the ST MAS sequence, that is more robust towards excitation of sites featuring large C_Q, are planned in future endeavors.

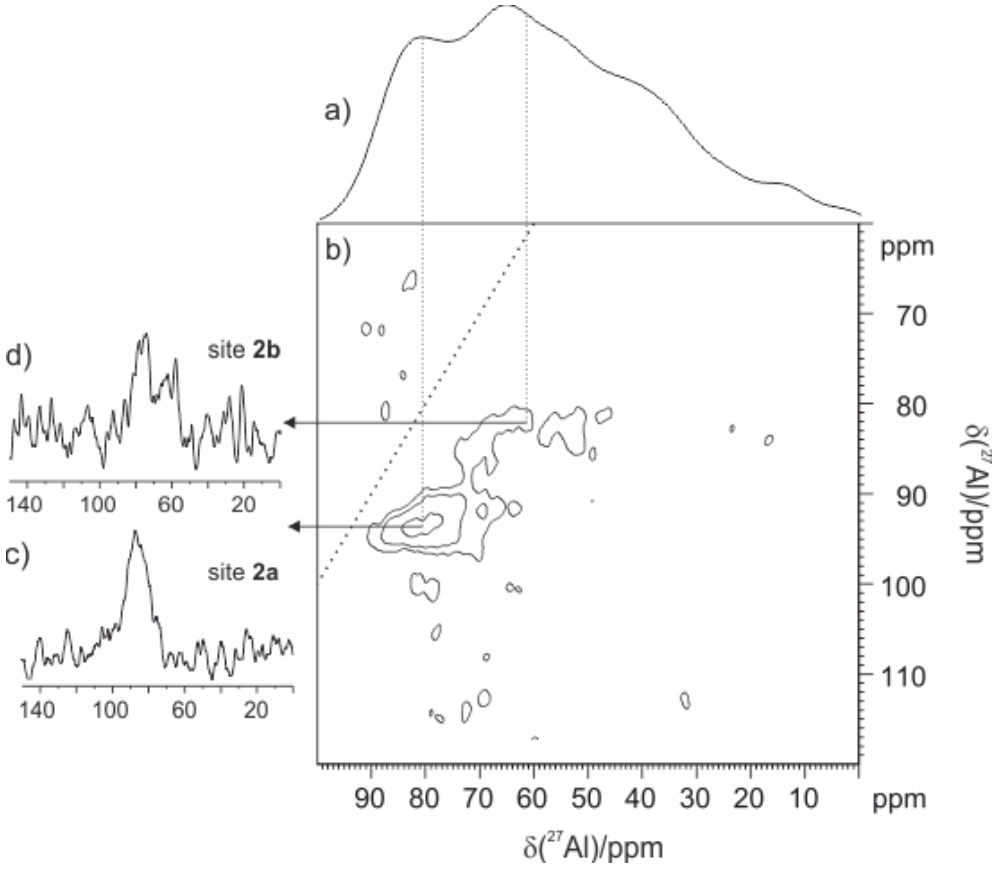

Figure 4.3.8. a) ^{27}Al MAS NMR and b) ^{27}Al MQ MAS NMR spectra of **2** , with representative slice for c) site **2a** and d) **2b** (18.8 T, spinning speed 20 kHz)

In order to help to further assignment of the experimental data, DFT calculations were performed on a series of potential surface species, built from non-interacting silanol model. Figure 4.3.9 presents the DFT-optimized structures used to calculate the corresponding NMR parameters listed in Table 4.3.1.

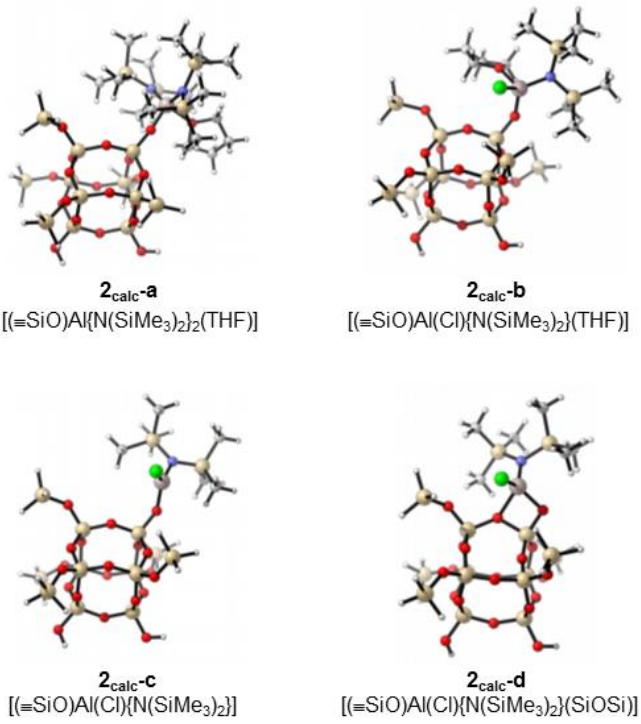

Figure 4.3.9 DFT-optimized models for the surface species in **2**.

Considering the data in Table 4.3.1, it appears that the chemical shift is rather dependent from the nature of the coordination sphere. The AlO_2NCl coordination sphere gives rise to chemical shift higher than that of AlO_2N2 (about 82 vs. 70 ppm), while the triscoordinate species would feature a higher CS value of about 110 ppm. When considering the quadrupolar coupling constants, they are all above 15 MHz, the lower stemming from the **2_{calc}-b** configuration, namely a monografted amido chloro THF-adduct (16.5 MHz). The bis amido THF-adduct (**2_{calc}-a**) and the amido-chloro siloxane (**2_{calc}-d**) feature C_Q values above 20 MHz (21.1 and 25.9 MHz, respectively). The triscoordinated species **2_{calc}-c** gives rise to a value of 36.7 MHz, as expected from the large electrical field gradient resulting from the trigonal planar configuration. Such values are not to be taken as such (as these C_Q values would result in non-observable signals), but should rather be used to estimate trends from which conclusions could be drawn to better understand our experimental results on the supported species.

Based on these elements, we propose that the major sites within material **2** both feature similar coordination sphere, namely tetracoordinated $[(\equiv SiO)Al(Cl)\{N(SiMe_3)_2\}(O_L)]$ site, where O_L is a L-type oxygen center from either SiOSi surface groups or from THF. Thus, for **site 2a**, where the C_Q value is the lowest (8.6 MHz), we propose the structure $[(\equiv SiO)Al(Cl)\{N(SiMe_3)_2\}(THF)]$. On the same line, **site 2b** (with higher C_Q value that **site 2a**, about 11 MHz), the corresponding structure would be $[(\equiv SiO)Al(Cl)\{N(SiMe_3)_2\}(SiOSi)]$ (Scheme 4.3.3).

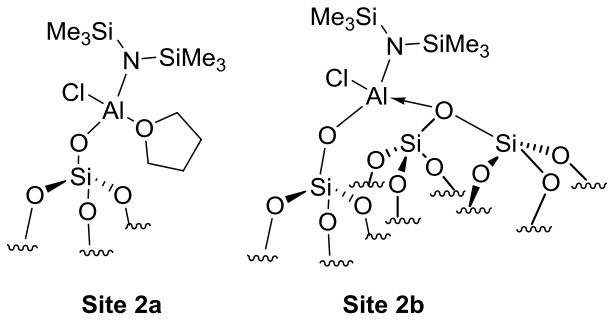

Scheme 4.3.3 Proposed structures for sites within material **2**

Further attempts at gathering detailed structural information on **2** were performed thanks to ^{1}H-^{27}Al D-HMQC NMR, which relies on dipolar interactions between protons and aluminum centers, thus providing information on the heteronuclear proximities within the sample (Figure 4.3.10). The only interaction observed concerns with protons at 0.1 ppm ($SiMe_3$) and both types of aluminum (**Sites 2a/2b**). No clear correlation could be detected between CH_2 protons from the THF ligand and either aluminum site.

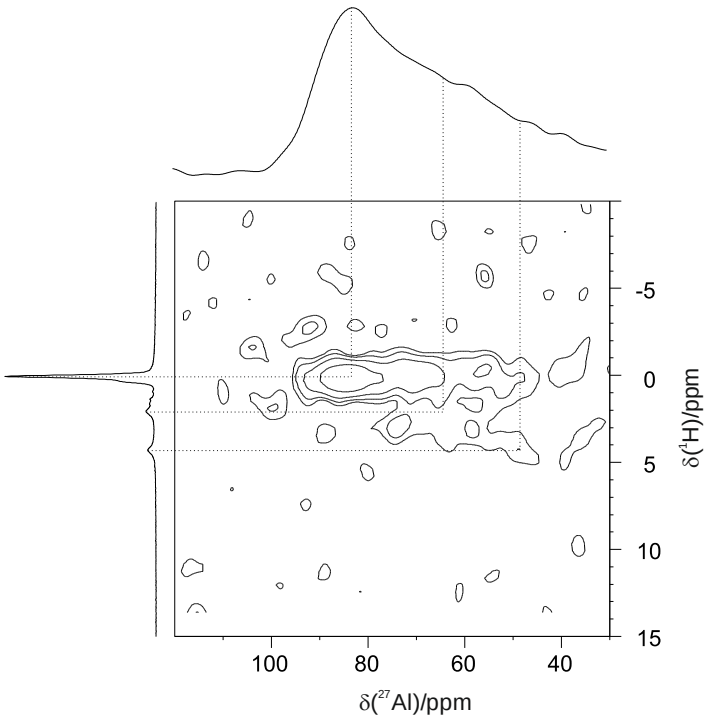

Figure 4.3.10 a) ^{27}Al MAS NMR, b) ^{1}H-^{27}Al D-HMQC NMR and c) ^{1}H MAS NMR spectra of **2** (18.8 T, spinning speed 20 kHz)

4.3.1. Conclusions

A new heteroleptic bis-amidochloro aluminum species was prepared and structurally characterized. Its grafting on dehydroxylated silica led to the formation of two main types of species, both featuring tetracoordinated coordination sphere, and differing in the nature of the oxygen-based donor ligand (THF or siloxane). These structural elements were determined thanks to mostly ^{27}Al MAS NMR, combined with DFT calculations. This study

thus shows how high field solid state NMR can bring deep insight into the structure of grafted species, especially when combined with DFT calculations.

4.3.2. Experimental Section

General Considerations: Manipulations were carried out under argon atmosphere in an M-Braun glove-box or by using Schlenk techniques. THF and pentane were dried by using conventional reagents and stored in the glove-box over 3Å molecular sieves. Liquid-state NMR spectroscopic analyses were run with a Bruker Avance 300 spectrometer. Solid-state MAS NMR spectra were recorded on a Bruker Avance 400 spectrometer (^{1} H: 400.12 MHz, ^{13}C: 100.63 MHz, ^{27}Al: 104.26 MHz) and on a Bruker Avance 800 spectrometer (^{1} H: 800.13 MHz, ^{27}Al: 208.49 MHz). For ^{1}H experiments, the spinning frequency was 20 kHz, the recycle delay was 10s and 16 scans were collected with a 90° pulse excitation of 3.5 µs. The two-dimensional homonuclear experiment (DQ-MAS) was obtained at a spinning frequency of 20 kHz by using excitation and reconversion pulse blocks of two rotor periods each (200 µs). The 90° pulse length was 2.25 µs, the recycle delay was 10 s, and 32 scans were collected for each slice (256 in total). The ^{1}H-^{27}Al HMQC experiment were set up with a ^{27}Al spin echo selective to the central transition, with pulse of 9 µs (RF = 10 kHz). The recoupling time was set at 500 µs (SR4 sequence for recoupling). The ^{1}H π/2 pulse of 3.5 µs on either side of the ^{27}Al π pulse (RF = 49 kHz). The number of scans for each t1 increment was set to 4090 with 53 slices and a delay of 1 s. The ^{27}Al MAS spectra at 18.8T were acquired at a spinning frequency of 20 kHz. The MQMAS spectra were collected using the Z-filter sequence, which consists of two hard pulses of 3.5 and 1.3 µs at an RF field of 70 kHz, for triple- quantum excitation and reconversion, respectively, followed by a soft pulse of 6 µs at an RF field of 10 kHz). The t1 step was set to the MAS period. 4800 scans with a delay of 1s was recorded for a total of 33 slices. The Chemical shifts were given in ppm with respect to TMS as external reference for ^{1}H NMR, and to $Al(H2O)_6^{3+}$ for ^{27}Al NMR. Diffuse reflectance infrared spectra were collected with a Harrick cell on a Nicolet Avatar spectrometer fitted with a MCT detector. Elemental analyses were conducted at London Metropolitan University (CHN) and at LASIR, University of Lille (Ln).

Synthesis of [Al{N(SiMe$_3$)$_2$}$_2$(THF)-Cl] with pre-formation of Li[N(SiMe$_3$)$_2$](THF) : A commercial solution of Li[N(SiMe$_3$)$_2$] (1M in THF) was dried under vacuum to obtain an orange anamorphous solid. Pentane was added and the solution cooled at -20 °C to form yellow crystals. Those crystals were purified by sublimation (10^{-5} mbar, 60 °C). The purity was checked by ^{1}H NMR. ^{1}H NMR (300 MHz, C_6D_6): δ 3.65 (4H, m, OCH_2), 1.26 (4H, m, OCH_2CH_2), 0.4 (36H, s, $SiMe_3$). Li[N(SiMe$_3$)$_2$](THF) (5 g, 31.5 mmol, 3 eq) was added to a solution of freshly sublimed $AlCl_3$ (1.4 g, 10.5 mmol) in toluene (30 mL). The clear light yellow solution was stirred for 3 days at room temperature. Formation of LiCl was observed while the solution became darker. Volatiles were removed by heating the mixture under vacuum for 3 h at 100 °C[18]. LiCl was removed by filtration with pentane then crystallization at -40 °C afforded white crystals. ^{1}H NMR (300 MHz, C_6D_6): δ 4.0 (4H, t, OCH_2), 1.1 (4H, t, OCH_2CH_2),

0.4 (36H, s, $SiMe_3$). ^{13}C NMR (75.5 MHz, C_6D_6): δ 74.0 (α–CH_2 from THF), 24.8 (β–CH_2 from THF), 6.2 ($SiMe_3$). Elemental analysis: C, 42.04; H, 9.58; N, 5.88. Theor: C, 42.21; H, 9.74; N, 6.15

Synthesis of material 2: A double-Schlenk vessel was loaded with a 10 mL pentane solution of **1** (160 mg, 0.35 mmol) in one compartment and with silica dehydroxylated at 700°C (1 g) with 10 mL of pentane in the other compartment (Scheme 2). After 15h of stirring, the supernatant liquid was then separated by filtration into the other compartment, from which the solvent was gas-phase transferred by trap-to-trap distillation back into the compartment containing the modified support in order to wash away the residual molecular precursor. This operation was repeated thrice and the resulting material **2** was then dried under secondary vacuum (10^{-6} mbar) at 80 °C for 5 h. ^1H MAS NMR: δ 4.28 (4H, t, OCH_2), 2.05 (4H, t, OCH_2CH_2), 0.33 (-$OSiMe_3$), 0.03 (36H, s, $NSiMe_3$). ^{13}C MAS NMR δ 72.3 (α–CH_2 from THF), 24.5 (β–CH_2 from THF), 2.1 (-$OSiMe_3$), 1.2 (-$NSiMe_3$). Elemental analysis shows: C, 3.64; H, 0.77; N, 0.77 Al 0.71.

---

[1] M. P. Coles, *Coord. Chem. Rev.*, 2015, **24**, 297-298
[2] a) H. Bürger, U. Wannagat, *Monatsh. Chem.*, 1964, 95-1099. b) H. Bürger, U. Wannagat, *Monatsh. Chem.*, 1963, 94-1007.
[3] C.D. Schaeffer Jr., J.J. Zuckerman, *J. Am. Chem. Soc.,* 1974, **96**, 7160–7162
[4] J. Pump, E.G. Rochow, U. Wannagat, *Angew. Chem. Int. Ed*, 1963, **75**, 374-375.
[5] a) E. Martin, P. Dubois, R. Jerome, *Macromol.* 2000, **33**, 1530-1535. b) K.C. Hultsch, T.P. Spaniol, J. Okuda, *Organometallics*, 1997, **16**, 4845-4846.
[6] H. Berberich, P.W. Roesky, *Angew. Chem.,* 1998, **110**, 1618-1620.
[7] R. Anwander, R. Roesky, *J. Chem. Soc. Dalton Trans.*, 1997, **137**
[8] K. J. L. Paciorek, J. H. Nakaharan, S. R. Masuda, *Inorg. Chem.,* 1990, **29**, 21.
[9] K.R.D. Johnson, P. G. Hayes, *Polyhedron*, 2016, **108**, 43-49
[10] R. Benn, E. Janssen, H. Lehmkuhl, Anna Rufihska, *J. Organomet. Chem.* 1987, **333**, 155-168.
[11] K.E. Johnston, C.A. O'Keefe, R.M. Gauvin, J. Trebosc, L. Delevoye, J-P. Amoureux, N. Popoff, M. Taoufik, K. Oudatchin, R.W. Schurko, *Chem. Eur. J.*, 2013, **19**, 12396-12414.
[12] J. Skibsted, H.J. Jakobsen, *Inorg. Chem*., 1999, **38**, 1806–1813
[13] L. O'Dell, R. Schurko, *Chem. Phys. Lett.*, 2008, **464**, 97-102
[14]] a) Y. Liang, R. Anwander, *Dalton Trans.,* 2013, **42**, 12521. b) C. Coperet, M. Chabanas, R. Petroff Saint-Arroman, J.-M Basset, *Angew. Chem. Int. Ed.,* 2003, **42**, 156.
[15] R. Anwander, P.W. Roesky, *J. Chem. Soc. Dalton Trans.,* 1997, **137**
[16] R.M. Gauvin, L. Delevoye, R.A. Hassan, J. Keldenich, A. Mortreux, *Inorg Chem.*, 2007, **46**, 1062-1070
[17] J. Kanellopoulos, D. Freude, A. Kentgens, *Solid State NMR*, 2008, **32**, 99-108
[18] T.Woodman, Y. Sarazin, G. Fink, *Macromol.*, 2005, **38**, 8

4.4. Investigations on the structure and silica surface reactivity of methylaluminoxane (MAO)

This work is the outcome of collaboration between the CASECO team in University of Lille 1 and the C2P2 laboratory in University of Lyon 1. This context of this study is the effect of the temperature of the silica used for grafting the MAO cocatalyst onto the activity in ethylene polymerization catalyzed by a zirconocene. My role in this project was the preparation and characterization of some of the samples for solid-state NMR analysis. Indeed, only this aspect will be presented in this section. The full paper is available online and be found with the reference below:

Silica/MAO/(*n*-BuCp)$_2$ZrCl$_2$ catalyst: effect of support dehydroxylation temperature on the grafting of MAO and ethylene polymerization. M. A. Bashir, T. Vancompernolle, R. M. Gauvin, L. Delevoye, V. Monteil, M. Taoufik, T. F. L. McKenna, C. Boisson, *Cat. Sci. Tech*., 2016, **6**, 2962-2974.

4.4.1. Abstract

The study in which this work takes place aimed to explore the link between the role of silica dehydroxylation temperature and the catalytic performance of an (*n*-BuCp)$_2$ZrCl$_2$ metallocene precursor supported on silica impregnated with methylaluminoxane (MAO) in ethylene homopolymerization. Diffuse Reflectance Fourier Transform Infrared Spectroscopy (FT-IR-DRIFT) and Solid State Nuclear Magnetic Resonance (SS NMR) were used to study the generation of different Al species on the surface of silica impregnated with MAO after calcination at temperatures of 200°, 450° and 600 °C. It was found that Si–CH$_3$ bonds can be formed when silica dihydroxylation temperature is ≥450 °C, and that three different types of aluminum species are generated on silica surface, the nature of which does not change significantly with the silica dehydroxylation temperature. Concerning the whole study, as described in the above-mentionned article, after grafting a metallocene precursor on the MAO-treated surfaces, increase in the zirconium loading, and in the intrinsic and average catalytic activities were observed with increasing silica dehydroxylation temperature. However, the molecular and physical properties of the high density polyethylene produced by using these catalysts were observed to be independent of the silica dehydroxylation temperature. These results indicated that the number of active sites on the surface of the catalyst increased with increasing dihydroxylation temperature, but the nature of the active sites does not.

4.4.2. Introduction

Amorphous silica is one of the most widely investigated and commonly used catalyst supports in the polyolefin industry. Metallocenes are anchored on pure, or methylaluminoxane (MAO)-modified amorphous silica to prepare supported (or heterogeneous) catalysts. Once supported, these catalysts can be employed in slurry or gas phase processes to produce different grades of polyolefins[1]. The benefits of using supported metallocenes (as opposed to homogenous catalysts) include the ease of their injection and removal of the final product in solid form, and the reduction of the risk of polymer film formation on the reactor walls which can in turn lead to poor heat removal from the reactor. A well-designed supported catalyst should offer good morphology control, high productivity, and ultimately, economic gains. One of the keys to obtaining these advantages is to ensure fine control of the surface chemistry of the support, and the procedure used to produce the MAO activated silica support (SMAO). Recent progress in deciphering MAO structure and its impact on the mechanism of metallocene activation leads us to believe that the cationic species $[AlMe_2]^+$ plays an important role in the activation process[2,3]. It is important to investigate the impact of the grafting of MAO on silica on the performance of this activator.

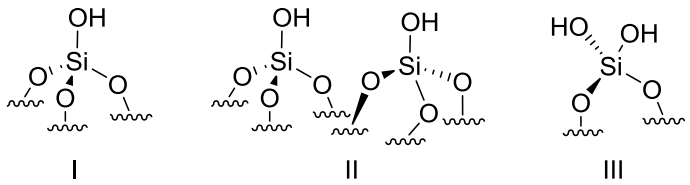

Scheme 4.4.1.Schematic representation of isolated (I), vicinal (II) and geminal (III) silanol groups on the surface of silica.

It is well-known that geminal, vicinal and isolated hydroxyl groups (OH), known collectively as silanols, and water can be found on the surface of untreated silica particles (Scheme 4.4.1). Furthermore, it has also been well established in the open literature that the surface concentration of these OH groups can be reduced by heating the silica, leaving only isolated silanol and siloxane (Si–O–Si) bridges at temperatures above 500 °C[4,5,6,7,8,9,10]. On the other hand, it is difficult to know a priori what type and concentration of silanol groups are optimal in terms of activating a given metallocene precursor. Depending on the size and shape of the metallocene, one needs to minimize the steric hindrance to the incoming catalyst precursor or co-catalyst molecule, to prevent bimolecular deactivation, and promote the generation of the active metallocenium cation, all of which contribute in determining the activity and performance of the catalyst. For example, $(n\text{-BuCp})_2ZrCl_2$ is one of the metallocenes that has found its application in industrial as well as academic research,[11,12,13] yet few studies have been carried out in order to understand the effect of silica dehydroxylation temperature on its activity[6,8,10,14]. Since it has been shown[1,14] different synthesis methods give different activities of the silica supported metallocenes, the most probable reason for this lack of clarity seems to be that different catalyst synthesis procedures were used in the previously cited studies, as discussed briefly in the next paragraph. It is therefore difficult to draw a clear conclusion on what, if any, relationship exists between the silica dehydroxylation temperature and the catalytic activity. In other words, whether or not a decrease in the concentration of OH groups on the silica surface helps to increase the activity of the supported catalyst. dos Santos et al.,6 analyzed the effect of silica dehydroxylation temperature on the metal loading on silica, catalytic activity in slurry ethylene polymerizations, the molecular weight distribution and crystallinity of the obtained polyethylenes. The catalysts were prepared by grafting $(n\text{-BuCp})_2ZrCl_2$ on Grace 948 silica dehydroxylated in the temperature range of 27 °C to 450 °C. MAO (10 wt% toluene solution) was added separately to the reactor in order to obtain Al/Zr molar ratio in the range of 100–5000, and the polymerizations were done at only 1 bar ethylene pressure. Using the same zirconocene, van Grieken et al.,[10] studied the effect of silica dehydroxylation temperature (in the range of 200 to 600 °C) on the catalytic activity by grafting a pre-mixed solution of MAO (30 wt% toluene solution) and $(n\text{-BuCp})_2ZrCl_2$ on the dehydroxylated silica in toluene slurry at room temperature for 3 h. Another study dedicated to the effect of silica dehydroxylation temperature on the catalytic activity of $(n\text{-BuCp})_2ZrCl_2$ was reported by Atiqullah et al.,8 who calcined the commercial ES-70 silica in the temperature range of 250 to 800 °C. The calcined

silica were functionalized by *n*-$BuSnCl_3$ at 130 °C before impregnation with MAO and grafting of the zirconocene at room temperature.

Given the diversity of the conditions used in these studies, it is difficult to identify a single silanol concentration which provides maximum catalytic activity for the silica supported (*n*-$BuCp)_2ZrCl_2$ in ethylene homopolymerization at conditions of industrial relevance, and to understand the reason due to which silica dehydroxylation temperature affects the catalytic activity. Furthermore, keeping in mind the fact that MAO has a significant effect on the catalytic performance of supported (*n*-$BuCp)_2ZrCl_2$, the effect of varying silanol concentration on the nature of aluminium species generated after the interaction of MAO with silica cannot be understood based on the above mentioned studies. Other works related to the influence of silica dehydroxylation temperature on the catalytic activity of supported metallocences in olefin polymerization focus catalysts different from (*n*-$BuCp)_2ZrCl_2$ and therefore report different results[15,16]. One of the goals of the present study is to investigate the influence of silica dehydroxylation temperature on the type(s) of aluminum specie(s) generated on the silica surface after impregnating MAO on silica dehydroxylated in the temperature range of 200 to 600 °C (i.e., by preparing SMAO). In order to achieve this, an optimized incipient wetness method has been selected to make SMAO samples and the final supported catalysts, prepared by the colleagues from C2P2 laboratory in University of Lyon 1. The catalysts were then evaluated by them in both slurry and gas phase ethylene homopolymerizations at conditions of industrial relevance. The benefit of using SMAO supported metallocene is twofold i.e., it allows one to study the interactions between hydroxyl groups of silica and the MAO molecule, and the leaching of the catalyst during polymerization is suppressed, thereby ensuring that the catalytic reaction takes place mainly on the silica surface (rather than in solution). In addition, Diffuse Reflectance Fourier Transform Infrared Spectroscopy (FT-IR-DRIFT) analysis of the SMAO coupled with a solid state NMR characterization of SMAO are reported. The results are used to provide unique information on the nature of chemical species formed on the surface of silica after impregnation of MAO which subsequently influences the catalytic activity of the resulting supported metallocene catalyst.

4.4.3. Experimental section

4.4.3.1. Materials

Grace 948 silica with a surface area of 290 $m^2\ g^{-1}$, average particle diameter of 58 μm and a pore volume of 1.7 mL g^{-1} was used as the catalyst support. The MAO solution 30 wt% in toluene used in this study was purchased from Albemarle with the following characteristics: 13.6 wt% Al, 5.24 wt% $AlMe_3$, gas/Al = 1.65.

4.4.3.2. Drying of MAO

White powder of dried MAO was obtained by first evaporating toluene from 30 wt% MAO commercial solution. Subsequently, the powder was dried under a dynamic vacuum of 10^{-3} to 10^{-5} mbar for 4 h at 80 °C. The dried MAO was then stored in a glove box.

4.4.3.3. Catalyst synthesis

For silica dehydroxylation, 3 g of Grace 948 silica were taken in a Schlenk tube and heated under dynamic vacuum of 10^{-3} to 10^{-5} mbar following the profiles shown in Figure 4.4.1.

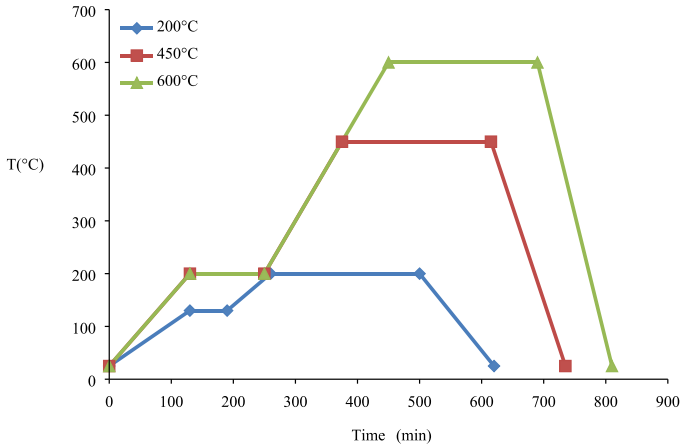

Figure 4.4.1.Temperature profiles used for silica dehydroxylation

The profiles for 450 °C and 600 °C are similar except the maximum temperatures. For 200 °C profile, silica was heated at 130 °C for 1 h in order to remove all the adsorbed water whereas for the other two profiles this was achieved by heating for 2 h at 200 °C. A time of 4 h was given at maximum temperature under vacuum for all profiles. After dehydroxylation, silica was kept in the glove box. The silica impregnated with MAO, named hereafter as SMAO, was prepared as follows. 2 g of dehydroxylated silica were placed in a three neck round bottom flask in the glove box under Argon. An amount of pure dry toluene equal to the pore volume of silica i.e., 1.7 $mL.g^{-1}$ was mixed with 3.5 mL of 30 wt% MAO solution in a separate vial at room temperature under argon and left for 30 min. This solution of MAO in toluene was then added to the silica drop-wise, which wetted the silica completely. The resulting thick slurry was heated at 80 °C for 4 h without any stirring under argon and the evaporating toluene was refluxed via a condenser. At the end of this process, the mixture was washed once with heptane, then dried under static vacuum at 80 °C. Dried SMAO, a free flowing white powder, was stored in a glove box.

4.4.3.4. Silica, MAO and SMAO characterization

Al content was measured using Inductively Coupled Plasma-Atomic Emission Spectroscopy (ICP-AES) at Mikroanalytisches Labor Pascher, Germany. Diffuse Reflectance Fourier Transform Infrared Spectroscopy (FT-IR-DRIFT) was used to characterize the as-received Grace 948 silica, the silica dehydroxylated at different temperatures, and MAO impregnated

silica (SMAO) prepared by using silica dehyroxylated at different temperatures and the final catalysts. A few milligrams of each sample were added to a DRIFT cell equipped with CaF_2 windows inside a glove box. For dried MAO, the sample was mixed with dry KBr (10 wt%). IR spectra were recorded on a Nicolet 6700 FT-IR spectrometer. Typically, 64 scans were accumulated for each spectrum (resolution 4 cm^{-1}). Solid-state NMR spectra were acquired on a Bruker Avance III 800 spectrometer (^1H: 800.13 MHz, ^{27}Al: 208.50 MHz). For ^1H experiments, the spinning frequency was 20 kHz, the recycle delay was 5 s and 128 scans were collected using a 90° pulse excitation of 2.25 µs. The ^{27}Al MAS NMR spectra at 18.8T were acquired at a spinning frequency of 20 kHz, using central transition – selective Hahn echo sequence. The D-HMQC experiments were set up with a ^{27}Al spin echo selective to the central transition, with pulses of 8 and 16 µs, with ^1H π/2 pulse of 3.3 µs on either side of the ^{27}Al π pulse. The number of scans for each t1 increment was set to 1280. The dipolar recoupling scheme ($SR4^2_1$) was applied for 600 µs[17]. Two-dimensional (2D) ^1H–^1H double quantum magic-angle spinning spectra were performed at 20 kHz spinning speed using the $R12_2^5$ symmetry-based recoupling scheme[18] applied for 133 µs at RF field strength of 65 kHz. The recycling delay was set to 2 s and 16 transients were added for each of the 100 t1 increments. The ^{27}Al MQMAS spectra were collected using the Z-filter sequence[19], which consists of two hard pulses of 3.5 and 1.3 µs at an RF field of 90 kHz, for triple quantum excitation and reconversion, respectively, followed by a soft pulse of 6 µs at an RF field of 15 kHz. The t1 step was set to the MAS period. Chemical shifts were given in ppm with respect to TMS as external reference for ^1H NMR, and to $Al(H_2O)_6^{3+}$ for ^{27}Al NMR. The samples analyzed by NMR were: dried MAO, SMAO-200 °C, SMAO-450 °C and SMAO-600 °C. The samples were prepared under strictly inert conditions in an argon-filled glovebox by packing into ZrO_2 rotors closed with Kel-F caps.

4.4.4. Results and discussion

The manner in which supported catalysts (metallocene or other) are prepared can eventually have an impact on the quantity and nature of the active species, and if so, this can influence the rate of polymerization, as well as the molecular and physical properties of the final polymer product. As we mentioned above, various routes for the preparation of silica-supported metallocenes have been proposed in the literature, and each synthesis procedure has specific advantages[6,8,10,14,20,21]. Supporting MAO on dehydroxylated silica before grafting the metallocene is one of the most common methods discussed in the open literature. However, the role of the dehydroxylation temperature of silica on the grafting of MAO, which in turn impacts the performance of the catalyst, has not been directly studied or clearly explained. In the present work three SMAO/(n-BuCp)$_2ZrCl_2$ catalysts were prepared using the Grace 948 silica treated at 200 °C, 450 °C or 600 °C. The dehydroxylation of silica was followed by the impregnation of a toluene solution of 30 wt% MAO (Albemarle) for 4 h at 80 °C. The chemical formula of the MAO can be determined from the analysis provided by the supplier (see Experimental part). In agreement with the work of Imhoff *et al.*,[22] the formula of MAO can be represented as $(Al(CH_3)_{1.42}O_{0.79})_n$ and free trimethylaluminium (TMA,

representing 14.4% of Al). The final product of this step was a white free flowing powder named as SMAO-200 °C, SMAO-450 °C or SMAO-600 °C depending upon the silica dehydroxylation temperature used. The nature of the silanol groups on silica support, which is controlled by the thermal treatment of the silica, impacts the structure of the supported MAO and consequently its ability to react with a metallocene precursor.

DRIFT and SS-NMR analyses of SMAO were performed for characterizing the SMAO and provided some information regarding the difference of reactivity between MAO and the Grace 948 silica treated, respectively, at 200 °C, 450 °C or 600 °C.

DRIFT analysis of silica, dried MAO and SMAO

Silica surface hydroxyl (OH) groups are characterized as isolated silanol (Scheme 4.4.1, I), vicinal silanol (Scheme 4.4.1, II), and geminal silanol (Scheme 4.4.1, III). These silanol groups act as fixation sites for the cocatalysts or metallocenes depending upon the method of catalyst synthesis, and their concentrations decrease with an increase in silica dehydroxylation temperature. DRIFT is an essential analytical tool for analyzing different type of chemical species present on silica surface and it has been used extensively to characterize different species present or generated on the silica surface before and after dehydroxylation, impregnation with MAO and metallocene grafting[4-7, 23,24].

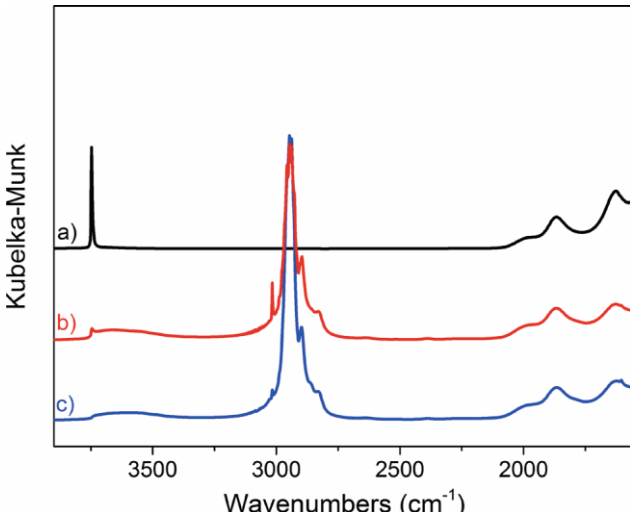

Figure 4.4.2.DRIFT spectra of silica-600°C (a), after reaction of MAO (SMAO-600°C) (b), after activation of (n-BuCp)$_2$ZrCl$_2$ (n-BuCp-600°C) (c)

The DRIFT spectra of 600 °C dehydroxylated Grace 948 silica, SMAO-600 °C and *n*-BuCp-600 °C are compared in Figure 4.4.2(see also Figure 4.4.3 and Figure 4.4.4. for silica treated at 200 °C and 450 °C, respectively). In addition to isolated silanol groups (peak at 3736 cm^{-1}), it can be observed that vicinal OH groups (peak at 3661 cm^{-1} and 3536 cm^{-1}) are also present after heat treatment at 200 °C, 6 whereas only isolated silanol groups remain on the silica after treatment at 450 °C and 600 °C. Broad bands at 1870 cm^{-1} and 1632 cm^{-1} are overtones and result from combination of intense Si–O fundamental modes. These results are in good agreement with available literature data[4-7]. After impregnation of each silica

with MAO, new peaks appear, especially in the range of 3100 to 2700 cm^{-1} due to the reaction of MAO with different silanol groups present on silica. Since, MAO is a mixture of oligomeric MAO and TMA, 5,25 it has been suggested that, depending on the dehydroxylation temperature, silanol (Si–OH) or siloxane (Si–O–Si) groups react with TMA, whereas MAO is physically adsorbed on the surface5,6,9.

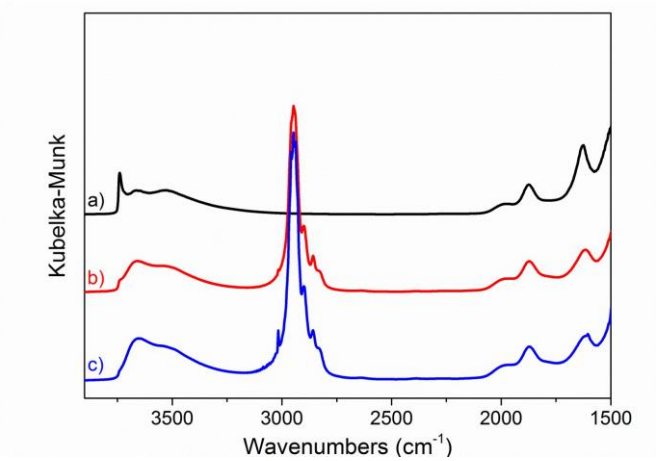

Figure 4.4.3 DRIFT spectra of silica-200°C (a), after reaction of MAO (SMAO-200°C) (b), after activation of $(n\text{-BuCp})_2ZrCl_2$ (n-BuCp-200°C) (c)

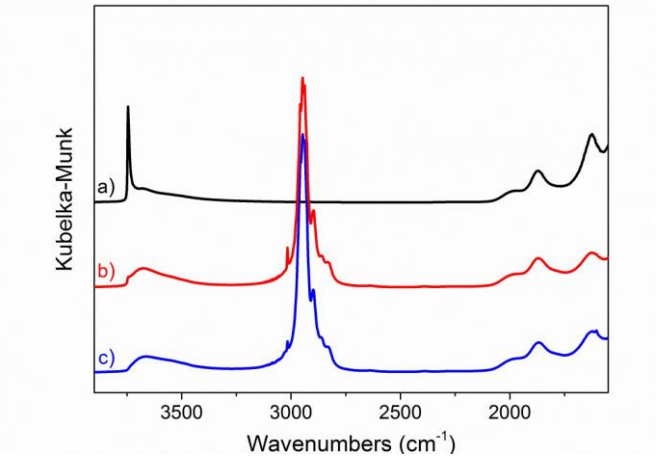

Figure 4.4.4. DRIFT spectra of silica-200°C (a), after reaction of MAO (SMAO-450°C) (b), after activation of $(n\text{-BuCp})_2ZrCl_2$ (n-BuCp-450°C) (c)

The reaction of TMA with OH groups generate –Si–O–Al–(CH_3) species, whereas, –Si–CH_3 moieties are produced by the reaction of Al–CH_3 species with siloxane groups (Si–O–Si) 5,25. For SMAO-200 °C and SMAO-450 °C, isolated silanols are totally consumed by reaction with MAO in contrast to SMAO-600 °C, as indicated by a small band at 3745 cm^{-1} in Figure 4.4.2 characteristic of isolated silanols. This peak totally disappeared after metallocene grafting. Hydrogen bonded OH groups can be observed in all the SMAO samples in the range of 3680 to 3660 cm^{-1}. Methyl groups of MAO can be observed in the region of 3000 to 2800 cm^{-1} with υ_a and υ_s of the terminal methyl groups in the range of 3050–2018 cm^{-1} and 2950–2750 cm^{-1} 4,5. In case of SMAO-450 °C and SMAO-600 °C, very similar peaks can be observed at

2957, 2947, 2940 and 2900 cm^{-1}. These peaks can be attributed to the stretching vibrations of methyl groups in Al–CH_3 species or Si–CH_3 species. Distinction between the two species (i.e., Al–CH_3 or Si–CH_3) based on DRIFT spectra is difficult because the stretching vibrations of methyl groups in both the species are very similar,[5,25] however, both Bianchini *et al*. 4 and Panchenko *et al*.5 attributed the peak at 2960 cm^{-1} to the presence of Si–CH_3 species. The DRIFT spectra of SMAO samples show the presence of this peak in SMAO-450 °C and SMAO-600 °C at 2957 cm^{-1}, whereas, no such peak is present in the SMAO-200 °C sample. This is due to the fact that reactive siloxane bonds (Si–O–Si) are formed only at higher dehydroxylation temperatures. The DRIFT spectrum of SMAO-200 °C (i.e.,Figure 4.4.3) showed peaks at 2949 and 2900 cm^{-1} due to the stretching vibrations of methyl groups in Al–CH_3 species.[4,5] In addition, the DRIFT spectrum of dried MAO (

Figure 4.4.5) showed peaks at 2947, 2937 and 2895 cm^{-1} for the stretching vibrations of methyl groups in Al–CH_3 species. This analysis confirms the assignment of peaks observed in the same region for SMAO. In summary DRIFT analyses of dehydroxylated silica, SMAO and supported metallocene showed that the nature of surface species is influenced by the reactivity of silanol and siloxane moieties, which depends on the thermal treatment of silica. DRIFT spectra of the final supported catalysts (i.e., after grafting the metallocene on SMAO) are also shown Figure 4.4.2, Figure 4.4.3, Figure 4.4.4. It is important to mention that characteristic absorption peaks of the aromatic and alkyl groups present in the (*n*-$BuCp)_2ZrCl_2$ molecule appear in the same region as that of MAO molecule i.e., 3100–2800 cm^{-1} (C–H stretching) and 1500–1300 cm^{-1} (methyl and methylene deformation modes).6 It is therefore difficult to differentiate between the DRIFT peaks coming from metallocene, MAO and toluene molecules. However, the peak at 1602 cm^{-1} can be attributed to –C=C– stretching of the Cp ring, whereas, the one at 1494 cm^{-1} can be attributed to bending vibrations δ(CH_3) of the butyl substituent of the Cp ligand[23,26] and appears in the DRIFT spectra of all the final supported catalysts only.

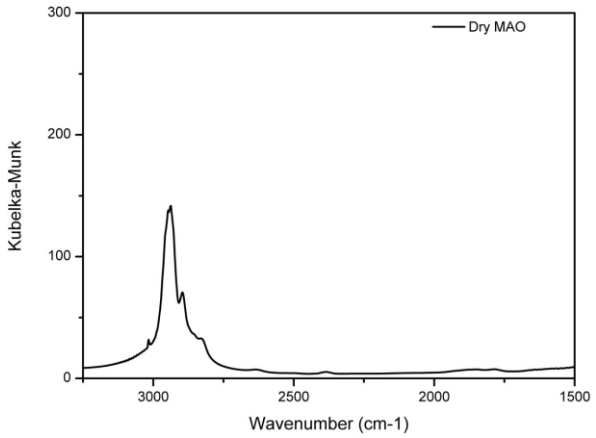

Figure 4.4.5. DRIFT spectra dried MAO at 100°C

The stretching vibrations at 3016 cm^{-1} have been attributed to the Cp ring by Bianchini *et al*.4 This peak was also observed in our spectra. However, it should be noted that residual toluene shows the same vibration (see SMAO spectra in Figure 4.4.2, Figure 4.4.3, Figure 4.4.4).

4.4.4.1. Solid state NMR analysis of dried MAO and SMAO samples

Liquid-state NMR studies on MAO and aluminoxanes have been previously reported in the literature.[27, 28, 29] In particular, given the possibility to determine the coordination number of aluminum alkyl from their chemical shift, ^{27}Al should be the most adequate tool to determine the structural features with MAO[30, 31]. However, since ^{27}Al is a quadrupolar nucleus (S = 5/2), the broad line width encountered in non-highly symmetrical environments prevents any detailed analysis. On the other hand, solid state NMR provides access to additional spectroscopic parameters other than chemical shift. Namely, it is possible to determine quadrupolar coupling constants that are characteristic for given structural types. One can also benefit from high resolution techniques such as MQMAS to disentangle complex 1D spectra (vide infra). Indeed, a few studies on MAO and molecular models have been performed, with mixed conclusions regarding the actual MAO structure[32,33] .It is therefore of interest to perform more detailed studies involving state of the art NMR methodology focused on structural investigations on MAO and on its grafting on silica. In the present study, we used high field NMR, combined with a high resolution method (MQMAS) for quadrupolar nuclei, as well as homo- and heteronuclear correlations to determine the main features of MAO and its silica-supported version along with the grafting reaction pathways. It is necessary to account for the fact that we will be studying materials (dried MAO and SMAO) that have been subjected to vacuum treatment. Thus in the case of dried MAO, its composition differs from that of commercial MAO solutions since $AlMe_3$ (either free or bound) is present in solution but the vacuum treatment causes $AlMe_3$ elimination from the product (Figure 4.4.6).

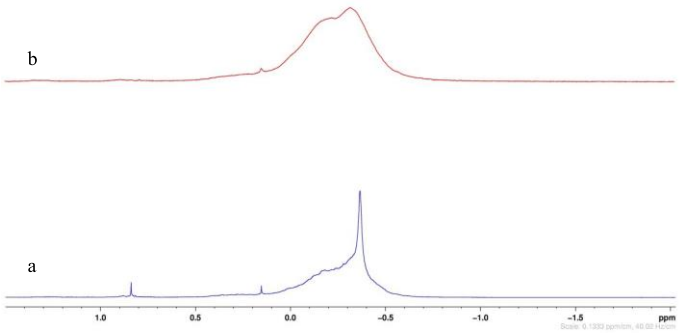

Figure 4.4.6. ^{1}H proton NMR spectrum of 30wt% MAO solution (a) dried MAO obtained by heating the 30wt% MAO solution at 80°C under vacuum for 4h (b). Benzene was used as solvent for both NMR spectra

^{1}H MAS NMR spectra of dried MAO and supported MAO (SMAO-200 °C, SMAO-450 °C and SMAO-600 °C) feature signals expected for Al–Me groups at a chemical shift (CS) of about −0.7 ppm (Figure 4.4.7, a–d)

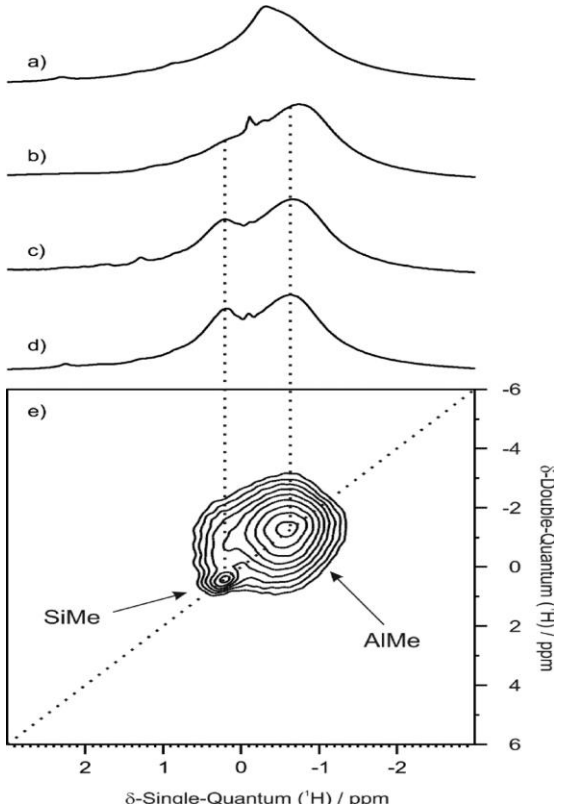

Figure 4.4.7. ^{1}H MAS NMR spectra of a) dried MAO, b) SMAO-200 °C, c) SMAO-450 °C and d) SMAO-600 °C; e) 1H–1H DQ MAS NMR spectrum of SMAO-600 °C (18.8 T, spinning speed 20 kHz)

A slight shift is observed in the position of the Al–Me signal upon grafting, from −0.4 ppm in dried MAO to about −0.7 ppm in the supported MAOs. Furthermore, when comparing spectra of SMAO-200 °C and SMAO-600 °C, one notices the increase of the 0.2 ppm signal assigned to Si–Me protons. This is in line with infrared studies described above. These groups arise from reaction of Al–Me with strained siloxane bridges, the proportion of which increases with silica dehydroxylation temperature (Scheme 4.4.2). Proximities between protons within a solid can be determined using ^{1}H–^{1}H two-dimensional (2D) Double-Quantum MAS NMR spectroscopy (DQ MAS), which relies on homonuclear dipolar recoupling methods[34]. The DQ MAS spectrum of SMAO-600 °C (Figure 4.4.7-e) shows that the Si–Me groups are close to some of the Al–Me moieties, as expected from the postulated reaction mechanism. This is highly reminiscent of the surface chemistry of $AlMe_3$, where similar spectra are obtained (see Figure 4.4.8 for comparison)[35,36]. This demonstrates that

grafting of MAO occurs not only via Al–Me protonolysis, but also from Si–O–Si opening, which results in spatially close Si–Me and Al–Me groups (Scheme 4.4.2).

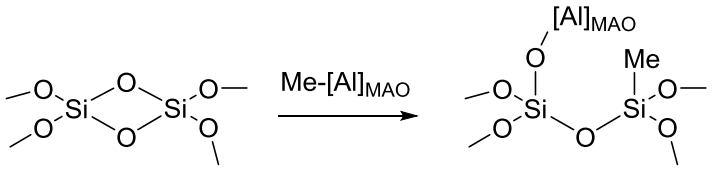

Scheme 4.4.2. Reaction of MAO with strained siloxanes

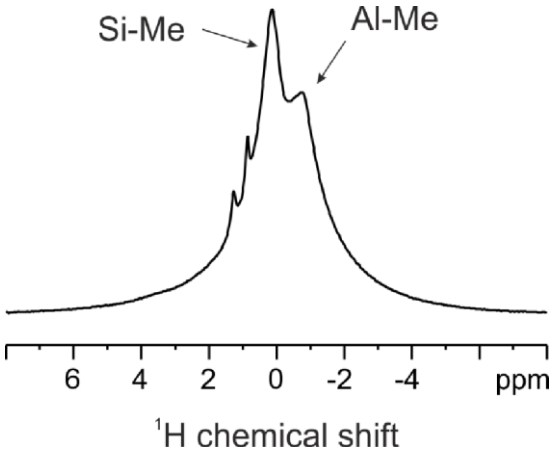

Figure 4.4.8. ^{1}H MAS NMR spectrum of $AlMe_3$ grafted on SiO2-600 (18.8 T, at spinning speed 20 kHz).

A further confirmation of proton signal assignment was brought by the ^{1}H–^{27}Al D-HMQC spectrum.[37] This technique probes the spatial proximity of heteronuclear pairs, within a given range. Using a short recoupling delay thus provides selective information on close spin pairs (below 4 to 5 Å).

In the case of SMAO-600 °C, the observed correlation with the ^{27}Al dimension (Figure 4.4.9) only concerns the −0.7 ppm ^{1}H signal, which confirms its assignment to Al–CH_3 group. Accordingly, no cross-peak is observed for the Si–Me site. The ^{27}Al Hahn echo MAS NMR spectra of dried MAO and supported MAO (Figure 4.4.10, a–c) are composed of a broad resonance as a consequence of a large second-order quadrupolar interaction, not averaged under MAS conditions. In an initial stage, the spectra look similar, with a featureless signal [20–110 ppm], most probably resulting from the overlapping of several Al sites. The observed CS values are in line with those reported by Talsi,[27] of about 110 ppm. In order to get a more precise insight into the dried MAO structure, we resorted to the 2D high resolution method MQ MAS.[38] The spectrum of the molecular sample of dried MAO has a good signal-to-noise ratio, but is rather complex, featuring peculiar line shapes due to large quadrupolar coupling associated with significant chemical shift anisotropy. This combination leads to a large number of highly distorted spinning side bands in the isotropic dimension ($\delta_1(^{27}Al)$).

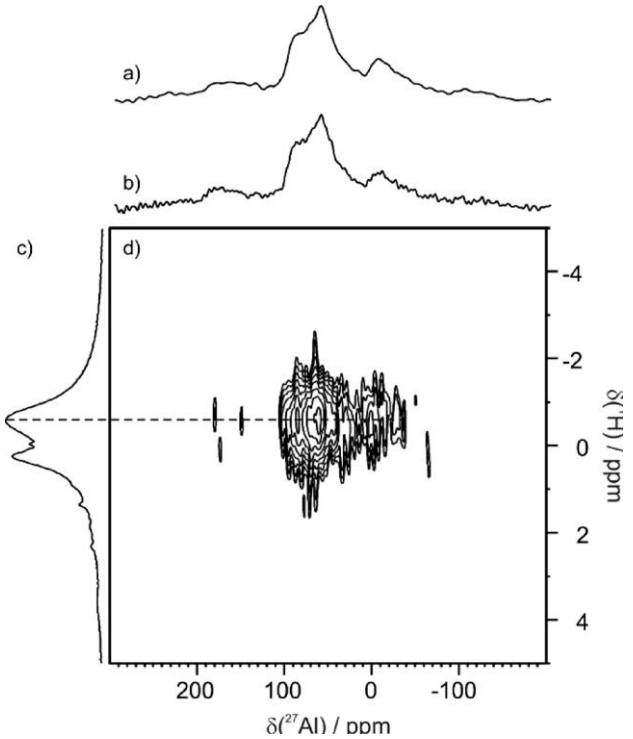

Figure 4.4.9. SMAO-600 °C: a) ^{27}Al Hahn-echo, b) ^{1}H-filtered ^{27}Al D-HMQC, c) ^{1}H and d) 2D ^{1}H–^{27}Al D-HMQC MAS NMR spectra (18.8 T, spinning speed 20 kHz)

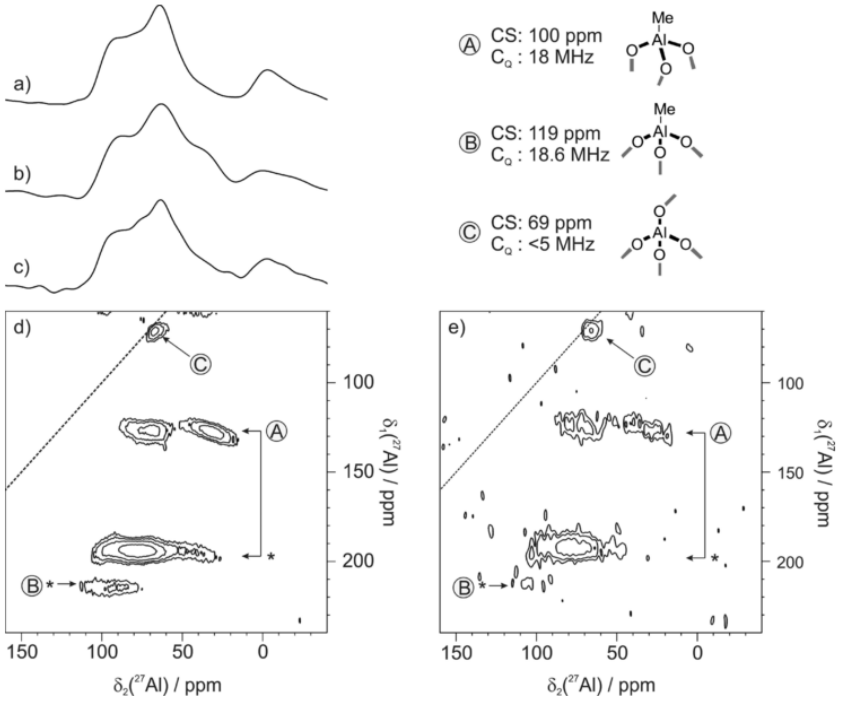

Figure 4.4.10. ^{27}Al Hahn Echo MAS spectrum of a) MAO, b) SMAO-200°C and c) SMAO-600°C and ^{27}Al MQ MAS spectrum of d) MAO and e) SMAO-600°C (18.8 T, spinning speed 20 kHz); on spectrum d), the B species is evidenced by its rotation band at 215 ppm in the isotropic dimension, while the chemical shift band expected at 146 ppm is not observed due to the

large anisotropic interactions associated with inhomogeneous MQ excitation conditions. Asterisks designate spinning side bands

This is reported in the literature for extreme cases such as ^{93}Nb MQ MAS NMR spectra of specific inorganic materials[39,40]. Remarkably, in the present case, the distortion is such that it can result in the quasi-negligible intensity of the isotropic signal, with maximized intensity in the spinning side bands. The position of the isotropic signals was unambiguously determined by recording the MQ MAS spectrum at 2 different spinning speed (Figure 4.4.11).

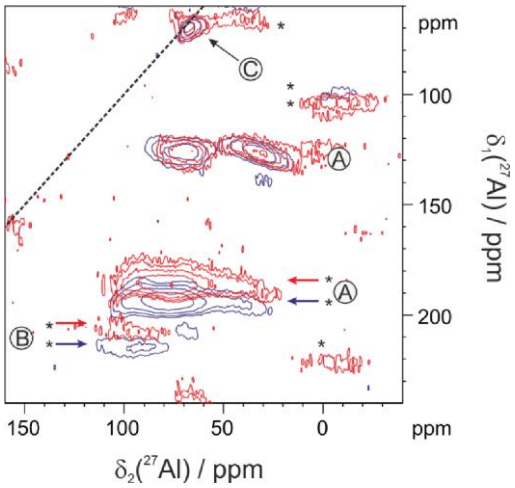

Figure 4.4.11. ^{27}Al MQ MAS of MAO (18.8 T), at spinning speed 20 kHz (blue) and 18 kHz (red); asterisks designate spinning side bands

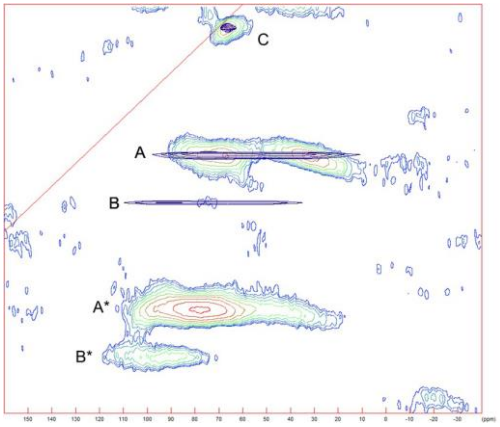

Figure 4.4.12. ^{27}Al MQ MAS spectrum of MAO (18.8 T), at spinning speed 20 kHz with simulated CS resonances. A: CS=100 ppm, CQ=18 MHz; B: CS=119 ppm, CQ=18.6 MHz; C: CS=69 ppm, CQ<5 MHz. Asterisks designate spinning side bands

Thus, three main sites emerge from the high resolution spectrum: a) the major site (site A, Figure 4.4.10) features a chemical shift of 100 ppm, with a large quadrupolar coupling, of about 18 MHz (calculated from the position and width of the isotropic signal in the 2D spectrum);[41] b) a second site of lesser intensity (site B, Figure 4.4.10) resonates at 119 ppm, with also quadrupolar coupling above 18.5 MHz, similar to that of site A; c) a third site appears as a minor component at 69 ppm, with a broadening dominated by chemical shift

distribution, and no apparent quadrupolar broadening (site C, Figure 4.4.10). These parameters have been used successfully to simulate the CS lines on the MQ MAS spectrum (Figure 4.4.12).

The reader's attention is drawn to the fact that in the case of spectra featuring quadrupolar lineshapes (as in the present cases), the isotropic chemical shift is not located in the center of the central transition signal, but on its lower frequency end. Thus, sites A and B feature rather similar chemical shift and quadrupolar coupling constant. The well-admitted main structural type within MAO is tetracoordinated $Al(Me)O_3$. Molecular species with similar aluminum coordination spheres indeed give rise to CS in the 120–80 ppm range, which is in agreement with both observed values for A and B.[28,42] The quadrupolar coupling constant is in the same range to that of MAO-related molecular species (where $Al(Me)O_3$ display a CQ value of 17.5 MHz[33] and of electronically comparable surface monohydride on tetra-coordinated aluminum ($Al(H)(O)_3$) which features a CQ value of about 15 MHz.[43] However, the rather well-separated lines for A and B in the MQ MAS and the lack of CS and CQ distribution are indicative of two slightly but definitively distinct types of environments. Interestingly, the theory group at Institut Français du Pétrole Energies Nouvelles (IFPEN) recently studied the structure of "pure" MAO cages, composed of $[AlOMe]_n$ units (with a 1:1 Al:Me ratio) arranged in either square or hexagonal faces, and computed the corresponding ^1H and ^{27}Al NMR chemical shifts.[44] They correlated the local environment of aluminum atoms in terms of nature of edge-sharing faces with 27Al chemical shift. Based on this, we propose that site A (CS of about 100 ppm) is on the edge of 1 square and 2 hexagonal faces (calculated range: 103–109 ppm) and that site B (CS of about 119 ppm) is on the edge of 2 square and 1 hexagonal faces (calculated range: 111–120 ppm).

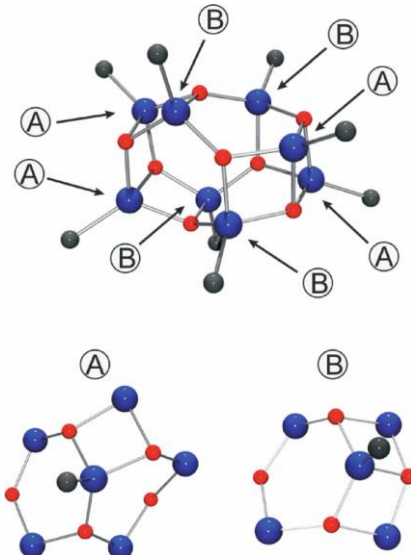

Figure 4.4.13. Example of [(AlMeO)8] MAO-cage and the two A and B structures

This is depicted in Figure 4.4.13, which features as an example a cage structure involving 8 Al atoms. This is the first experimental evidence of the topology and structure of MAO-cages that have been postulated by DFT calculations. Regarding site C, the low CS and CQ values plead for a purely oxygenated coordination sphere, of the $Al(O)_4$ type.[45]Most specifically, the low CQ (less than 5 MHz) rules out the hypothesis of $AlMeO_3$ sites on the edge of 3 hexagonal faces (calculated CS of 90 ppm). The low quantity of these sites may be an indication that they result from decomposition by hydrolysis or oxidation, although one cannot rule out that they are "buried" aluminum centers from larger structures within MAO. Unfortunately, unambiguous determination of the proportions of these sites (and thus assessment of the average

size of the oligomers based on DFT-calculated models) is out of reach, due to inhomogeneous site excitation for MQ MAS, to strong line shape overlapping of 1D spectra and to the occurrence of spectral components with fairly similar features (CS and CQ).

Furthermore, due to intrinsic NMR limitations, we cannot rule out the presence of aluminum centers featuring higher CQ, as was proposed in several MAO models,[30,33]or observed for silica-supported aluminum alkyls.[46] This means that bis- or tris-alkyl species such as $[Al(O)_nMe_m]$ (n,m = 2 or 3) that have been postulated in the literature may have escaped detection under our experimental conditions, and that we may not be observing all the aluminum centers present in the dried MAO sample. In particular, we did not observe oxygen-bound TMA in the above described spectra. This is a species postulated in the MAO structure that would give rise to signals in the 185–170 ppm range.[30,47] These elements can help to determine a range of possible structures with various nuclearity for the dried MAO. Indeed, in ref. 43, the most stable $(AlOMe)_n$ structures have been determined by theoretical calculations. It appears that for value "n" above 13, the number of hexagonal faces increases, while the number of square faces is constant. Thus, from thereon, the quantity of Al sitting on 3 hexagonal faces increases constantly with the nuclearity of the cages. Such Al centers give rise to an NMR signal expected at 90 ppm, which is not observed in the present case. On the other hand, below n = 12, the proportion of such sites is low (only 2 out of 10 and 2 out of 11 respectively for $(AlOMe)_{10}$ and $(AlOMe)_{11}$), below the detection limit of MQ MAS. Along the same line, the "n" values less than 6 can be excluded based on high proportion of square faces. Thus, we propose that the nuclearity of the $(AlOMe)_n$ is most probably between 6 and 12. This is much lower than reported values.[48] This discrepancy may be due to the thermal treatment of MAO upon its drying that affects the size of the cage. On the other hand, one can also propose that as NMR is sensitive to local parameters, as it gives evidence for low nuclearity, the larger MAO sizes determined in solution would be the result of aggregates formation by clustering of smaller entities.

The MQ MAS NMR spectrum of SMAO-600 °C was recorded (Figure 4.4.10-e). It features overall similar signals to that of dried MAO described above. This indicates that the structures present in the dried MAO are found in this material, obtained from reaction of MAO solution with silica followed by mild (80 °C) thermal treatment under vacuum. In spite of the low signal-to-noise ratio due to the low Al concentration in the silica-supported sample, it appears that the B sites are preferentially consumed upon grafting (see Figure 4.4.14 for the comparison of the isotropic projections of dried MAO and SMAO-600 °C).

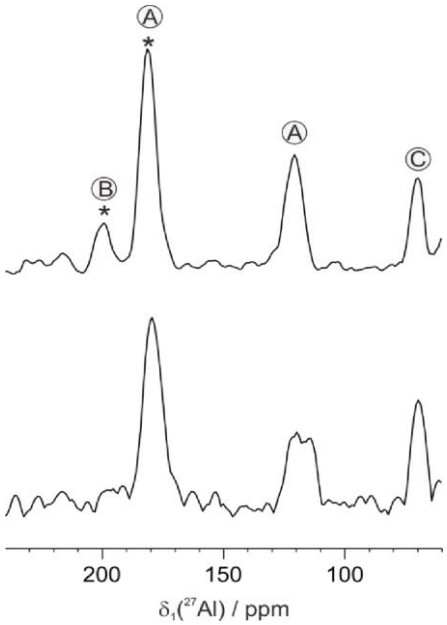

Figure 4.4.14. ^{27}Al MQ MAS isotropic projections of dried MAO (top) and SMAO-600 (bottom) (18.8 T). Asterisks designate spinning side bands

However, further discussion is not possible at this stage. In conclusion, both DRIFT and SS-NMR analysis of SMAO highlighted that the concentration and the nature of silanol and siloxane groups impact the reaction of MAO with silica. The analysis of SMAO obtained from silica thermally treated at elevated temperature (450–600 °C) showed the presence of Si–Me groups formed by opening of strained siloxane moieties. Thus, for silica treated at 200 °C the MAO reacts only with the silanol while for silica treated at higher temperature the MAO reacts first with the silanol and subsequently the surface Al–Me function opens siloxane moieties leading possibly to the formation of vicinal Si–CH3 sites. We can reasonably assume that the way the MAO reacts with silica impacts the structure of the activator, and thus the number of activating sites leading to different Zr content after impregnation of the metallocene precursor (see Table 4.3.1).

Silica T (°C)	Al (wt%)	Zr (wt%)	Al moles	Zr moles	Al/Zr
200	16.24	0.11	6.02×10^{-3}	1.21×10^{-5}	499
450	13.45	0.29	4.99×10^{-3}	3.18×10^{-5}	157
600	11.40	0.26	4.23×10^{-3}	2.85×10^{-5}	148

Table 4.4.1. Elemental analysis of the supported catalysts prepared by using different silica dehydroxylation temperature

Another important issue concerns the actual nature of the MAO compound that reacts with the silica surface. Indeed, MAO solution consists of a mixture of polymeric MAO fraction $(Al(CH_3)_{1.42}O_{0.79})_n$ and free trimethylaluminium (TMA). It is well accepted that the TMA reacts preferentially with silica due to its smaller size and its higher reactivity. However, we cannot rule out direct reaction of polymeric MAO, especially with silica treated at low temperature (200 °C) where a sub-stoichiometric amount of TMA (related to Si–OH concentration) was

introduced. The nature of the aluminum species that reacts can obviously impact the number of activating site on SMAO. It appears that a thermal treatment of silica at elevated temperature leading to a lower concentration of silanol group (isolated silanol) favored the grafting of the metallocene (n-BuCp)$_2$ZrCl$_2$. However, further discussion is not possible at this stage. Another observation is the fact that the structure of SMAO is close to that of dried MAO, namely consisting of cage structures.

4.4.5. Conclusion

The concentration and the nature of silanol (Si–OH) groups on the surface of silica support is an important chemical property of silica, and significantly affects the catalytic activity of supported (n-BuCp)$_2$ZrCl$_2$ metallocene complex in ethylene homopolymerizations. Increasing the dihydroxylation temperature from 200 °C to 600 °C decreases the OH concentration of silica and only isolated silanol groups remain on Grace 948 silica at 600 °C. After impregnation of the silica with MAO the aluminum content of these silica (dehydroxylated at different temperatures) decreased with increase in dehydroxylation temperature. DRIFT and SS-NMR analyses showed that the grafting of MAO was impacted by the nature and the concentration of silanol groups on the silica surface. MAO reacted on silica dehydroxylated at high temperature (i.e., ≥450 °C) with both silanol and siloxane groups which was evidenced by the formation of Si–Me. In addition, the presence of Al(Me)O$_3$ sites in different configuration was evidenced for the first time by SS-NMR in the present work. As a continuation of these structural investigations, the corresponding supported metallocene catalysts were evaluated in ethylene polymerization. The intrinsic and average activity of (n-BuCp)$_2$ZrCl$_2$ supported on MAO impregnated silica (SMAO) increases with increasing silica dehydroxylation temperature from 200 to 600 °C. Related to metal content in the supported catalysts, it was concluded that whatever the thermal treatment of silica is, the same active species are formed but more active sites are generated when silica is thermally treated at high temperature.

---

[1] J. R. Severn, J.C. Chadwick, *Tailor-Made Polymers,* 2008, Wiley, 98–138.
[2] F. Ghiotto, C. Pateraki, J. Tanskanen, J. R. Severn, N. Luehmann, A. Kusmin, J. Stellbrink, M. Linnolahti, M. Bochmann, *Organometallics*, 2013, **32**, 3354–3362.
[3] J. T. Hirvi, M. Bochmann, J. R. Severn, M. Linnolahti, *ChemPhysChem*, 2014, **15,** 2732–2742.
[4] D. Bianchini, J. H. Z. dos Santos, T. Uozumi, T. Sano, *J. Mol. Catal. A: Chem.,* 2002, **185**, 223–235.
[5] V. N. Panchenko, N. V. Semikolenova, I. G. Danilova, E. A. Paukshtis and V. A. Zakharov, *J. Mol. Catal. A: Chem.*, 1999, **142**, 27–37.
[6] J. H. Z. dos Santos, C. Krug, M. B. da Rosa, F. C. Stedile, J. Dupont and M. de Camargo Forte, *J. Mol. Catal. A: Chem.*, 1999, **139**, 199–207.
[7] D. Bianchini, F. C. Stedile and J. H. Z. dos Santos, Appl.Catal., A, 2004, **261**, 57–67.
[8] M. Atiqullah, M. N. Akhtar, A. A. Moman, A. H. Abu-Raqabah, S. J. Palackal, H. A. Al-Muallem, O. M. Hamed, *Appl. Catal.,* 2007, **320**, 134–143.
[9] M. J. D. Low, A. G. Severdia, J. Chan, *J. Catal.,* 1981, **69**, 384–391.
[10] R. van Grieken, A. Carrero, I. Suarez, B. Paredes, *Eur. Polym. J*., 2007, **43**, 1267–1277.
[11] B. Kou, K. B. McAuley, C. C. Hsu, D. W. Bacon, K. Z. Yao, *Ind. Eng. Chem. Res.,* 2005, **44**, 2443–2450.
[12] B. Paredes, R. V. Grieken, A. Carrero, I. Suarez, J. B. P. Soares, *Macromol. Chem. Phys.,* 2011, **212**, 1590–1599.

[13] J. M. Zhou, N. H. Li, N. Y. Bu, D. T. Lynch, S. E. Wanke, *J. Appl. Polym. Sci.*, 2003, **90,** 1319–1330.
[14] G. G. Hlatky, *Chem. Rev.,* 2000, **100,** 1347–1376.
[15] B.-Y. Lee, J.-S. Oh, *US Pat., 6469113 B1*, 1999.
[16] M. Smit, X. Zheng, J. Loos, J. C. Chadwick, C. E. Koning, *J. Polym. Sci. Part A: Polym. Chem*., 2005, **43**, 2734–2748.
[17] A. Brinkmann, A. P. M. Kentgens, *J. Am. Chem. Soc.,* 2006, **128**, 14758–14759
[18] M. Carravetta, M. Eden, X. Zhao, A. Brinkmann, M. H. Levitt, *Chem. Phys. Lett.,* 2000, **321**, 205–215.
[19] J. P. Amoureux, C. Fernandez, S. Steuernagel, *J. Magn. Reson. Ser. A*, 1996, **123**, 116–118.
[20] J. R. Severn, J. C. Chadwick, *Tailor-Made Polymers: Via Immobilization of Alpha-Olefin Polymerization Catalysts*, 2008, Wiley
[21] J. R. Severn, J. C. Chadwick, R. Duchateau, N. Friederichs, *Chem. Rev.,* 2005, **105**, 4073–4147.
[22] D. W. Imhoff, L. S. Simeral, S. A. Sangokoya, J. H. Peel, *Organometallics*, 1998, **17**, 1941–1945.
[23] M. Jezequel, V. Dufaud, M. J. Ruiz-Garcia, F. Carrillo-Hermosilla, U. Neugebauer, G. P. Niccolai, F. Lefebvre, F.Bayard, J. Corker, S. Fiddy, J. Evans, J. P. Broyer, J. Malinge, J. M. Basset, *J. Am. Chem. Soc.*, 2001, **123,** 3520–3540.
[24] V. N. Panchenko, L. G. Echevkaya, V. A. Zakharov, M. A.Matsko, *Appl. Catal. A.*, 2011, **404,** 47–53.
[25] I. Tritto, C. Mealares, M. C. Sacchi, P. Locatelli, *Macromol. Chem. Phys.*, 1997, **198**, 3963–3977.
[26] L. Britcher, H. Rahiala, K. Hakala, P. Mikkola, J. B.Rosenholm, *Chem. Mater.,* 2004, **16**, 5713–5720.
[27] D. E. Babushkin, N. V. Semikolenova, V. N. Panchenko, A. P.Sobolev, V. A. Zakharov, E. P. Talsi, *Macromol. Chem.Phys.,* 1997, **198**, 3845–3854.
[28] M. R. Mason, J. M. Smith, S. G. Bott, A. R. Barron, *J. Am. Chem. Soc.,* 1993, **115**, 4971–4984.
[29] C. J. Harlan, M. R. Mason, A. R. Barron, *Organometallics,* 1994, **13**, 2957–2969.
[30] R. Benn, A. Rufinska, H. Lehmkuhl, E. Janssen, C.Kruger, *Angew. Chem. Int. Ed. Engl.,* 1983, **22**, 779–780.
[31] R. Benn, E. Janssen, H. Lehmkuhl, A. Rufinska, *J. Organomet. Chem.,* 1987, **333**, 155–168.
[32] L. Bryant, C. R. Harwell, A. A. Mrse, E. F. Emery, Z. Gan, T. Caldwell, A. P. Reyes, P. Kuhns, D. W. Hoyt, L. S. Simeral, R. W. Hall, L. G. Butler, *J. Am. Chem. Soc.,* 2001, **123,** 12009–12017.
[33] F. J. Wu, L. S. Simeral, A. A. Mrse, J. L. Eilertsen, L.Negureanu, Z. Gan, F. R. Fronczek, R. W. Hall, L. G.Butler, *Inorg. Chem.,* 2007, **46**, 44–47.
[34] I. Schnell, S. P. Brown, H. Y. Low, H. Ishida, H. W.Spiess, *J. Am. Chem. Soc.,* 1998, **120,** 11784–11795.
[35] R. Anwander, C. Palm, O. Groeger, G. Engelhardt, *Organometallics*, 1998, **17**, 2027–2036.
[36] J. Li, J. A. DiVerdi, G. E. Maciel, *J. Am. Chem. Soc.*, 2006, **128**, 17093–17101.
[37] J. Trebosc, B. Hu, J. P. Amoureux, Z. Gan, *J. Magn. Reson.,* 2007, **186**, 220–227.
[38] L. Frydman, J. S. Harwood, *J. Am. Chem. Soc.,* 1995, **117**, 5367–5368.
[39] I. Hung, J. Trebosc, G. L. Hoatson, R. L. Vold, J. P. Amoureux, Z. Gan, *J. Magn. Reson.,* 2009, **201**, 81–86.
[40] X. Wang, J. Adhikari, L. J. Smith, *J. Phys. Chem. C*, 2009, **113**, 17548–17559.
[41] M. P. J. P. Amoureux, R. K. H. D. M. Grant, Encyclopedia of Nuclear Magnetic Resonance, 2002, **9** Wiley
[42] S. J. Obrey, S. G. Bott, A. R. Barron, *Organometallics*, 2001, **20**, 5119–5124.
[43] E. Mazoyer, J. Trebosc, A. Baudouin, O. Boyron, J. Pelletier, J. M. Basset, M. J. Vitorino, C. P. Nicholas, R. M. Gauvin, M. Taoufik, L. Delevoye, *Angew. Chem. Int. Ed.,* 2010, **49**, 9854–9858.
[44] Z. Boudene, T. De Bruin, H. Toulhoat, P. Raybaud, *Organometallics*, 2012, **31**, 8312–8322.
[45] K. Mackenzie, M. Smith, *Materials Series Multinuclear Solid-State NMR of Inorganic Materials*, 2002, 6, Pergamon,.
[46] R. N. Kerber, A. Kermagoret, E. Callens, P. Florian, D. Massiot, A. Lesage, C. Coperet, F. Delbecq, X. Rozanska, P. Sautet, *J. Am. Chem. Soc.*, 2012, **134**, 6767–6775.
[47] R. Benn, E. Janssen, H. Lehmkuhl, A. Rufinska, *J. Org. Chem.,* 1987, **333**, 169–180.
[48] H. S. Zijlstra and S. Harder, *Eur. J. Inorg. Chem.*, 2015, 19–43.

4.5. Oligomerization and polymerization of ethylene using supported aluminum alkylating agents.

This work was performed during a 4-weeks stay in UFRGS (Porto Alegre) thanks to a fellowship granted by the COMUE Lille-Nord de France

4.5.1. Introduction

In the petrochemical industry, one of the main goals is the synthesis of chemicals that are building blocks for higher added-value products. In this field, the oligomerization of olefins is the reaction of choice which involves the sequential addition of olefinic group to form higher homologues. Depending of the need, the number of units in the molecule can be tuned (Figure 4.5.1).

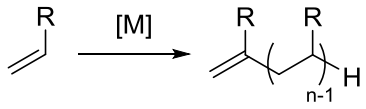

Figure 4.5.1 Oligomerization and polymerization of building blocks

This reaction can imply two olefins (n=2, dimerization reaction), three olefins (n= 3, trimerization reaction), and so on, up to polymerization n>> 20) which is the addition of high number of units. The simplest olefin available is ethylene that can form products of high interest like butene, hexene or even the polyethylene if the polymerization is occurring. A key issue here is the selectivity, as in parallel to oligomerization, double bond isomerization can occur, afford internal olefins (Figure 4.5.2).

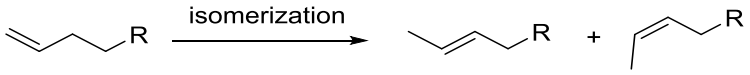

Figure 4.5.2 Isomerization of α-olefins

The formation of oligomers is achieved through catalytic processes relying on transition metals as in the SHOP process developed by Shell[1]. This reaction allows the formation of C_4 to C_{30} olefins. The C_4 to C_8 olefins are commonly used as co-monomers for production of low density polyethylene. The C_8 to C_{12} fraction has applications as plasticizers. Products of C_{12} to C_{16} can be used as starting compounds for detergents synthesis and C_{30} to C_{40} are employed as oil lubricants. In the literature, one can found an impressive number of reports on oligomerization mediated by a wide range of catalysts. Among these, systems with high selectivity toward a specific olefin can be found. Indeed, highly valuable α-olefins as 1-butene, 1-hexene or 1-octene can be obtained selectively through the dimerization[2], trimerization[3] and tetramerization,[4] respectively. Due to the increasing demand in α-olefins[5], the development of more efficient or novel systems is of high fundamental and economical interest. To perform the oligomerization or the polymerization, the catalyst (that

can be tuned to selectively form one olefin instead of another[6]) usually needs to be activated by an alkylating agent as methylaluminoxane, AlR_xCl_y or AlR_3. In order to develop molecularly-defined, supported catalysts able to perform gas phase reactions, we set forth to study of the development of supported aluminum co-catalysts and their effect on a given cobalt catalyst's performance. This takes place in the continuity of our work on immobilized aluminum alkyl species (see 4.4 Investigations on the structure and silica surface reactivity of methylaluminoxane (MAO)). We will thus explore the influence of the nature of this cocatalyst on the activity and selectivity in the ethylene oligomerization reaction.

4.5.2. Results and discussions

In the framework of a collaboration with the team of Michele De Souza (Universidade Federale de Rio Grande do Sul, Porto Alegre, Brazil), we selected a cobalt catalyst for our investigations. The de Souza team has successfully used this catalyst to form selectively C6 molecule using 1-propylene with high turnover number[7] (Scheme 4.5.1).

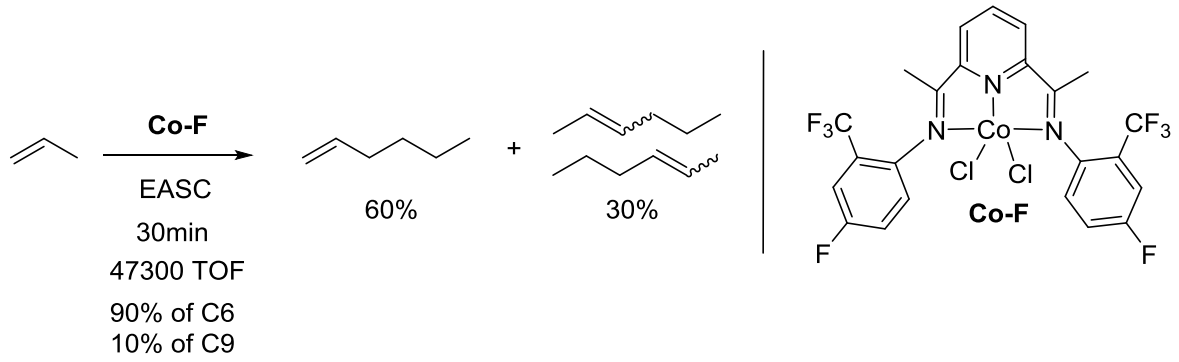

Scheme 4.5.1 Oligomerization of ethylene with Co-F

First tests with several molecular alkylaluminum species were carried out to validate the procedure (Scheme 4.5.2) before switching to the heterogeneous versions. The results are listed in Table 4.5.1. The quantification was done by GC after that the reaction mixture was cooled down in order to avoid partial evaporation of the products (the boiling point of 1-buitene is -6.25 °C). Best results are obtained by the EASC (ethylaluminum sesquichloride, $Al_2Et_3Cl_3$) (Entries 1 and 2) with activity of 1165 mmol of butene produced per mmol of cobalt catalyst per hour. The TMA is less active (Entries 3, 4, 5) but is more selective. Indeed, in the same conditions (Entries 2 et 3) the system is 4 time less active when it is activated by TMA but the selectivity in 1-butene compared to 2-butene is better (99 *vs.* 78 %, respectively). Variation of the ratio [Al]/[M] confirm the optimal ratio as described in literature[8], as where a [Al]/[M] ratio of 600 affords better results than 60 in terms of activity (Entries 3 and 4). Performing reaction at 0 °C induces an enhancement in activity in the case of EASC-based system, whereas in the case of TMA, loss of activity is observed (Entries 1 and 5). Regarding this, several phenomena could be at hand. Indeed, the catalytic systems generated in situ are on the one hand stabilized by lower temperature, but reactions should be slower under these conditions. However, this may be compensated by the higher

solubility of the olefin at lower temperature. Combination of these effects thus results in these contrasted observations between TMA- and EASC-based systems.

Thus, the setup is validated, which enables the exploration of supported co-catalysts' influence. These runs have also shown that the alkylation needs to be performed under ethylene atmosphere, as otherwise no catalytic activity develops. This shows that the thus-formed active species is unstable in the absence of olefinic substrate.

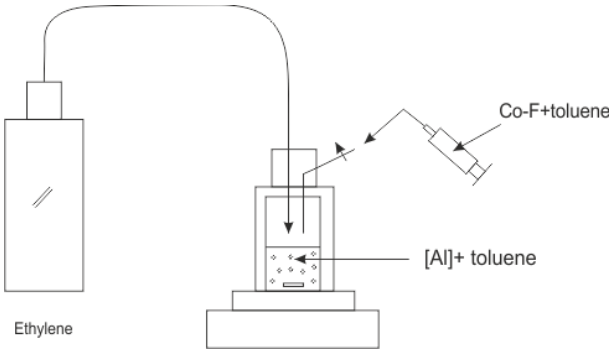

Scheme 4.5.2 Experimental setup for oligomerization of ethylene

Entry	Co-cat.	n Co-F (µmol)	Ratio Al/[M]	Temp. (°C)	Time (h)	A (mmol butene.mmol $cat^{-1}.h^{-1}$)	Select. A/B, C	A (g of polym. mmol $cat^{-1}.h^{-1}$) / g of PE
1	EASC	3	600	0	1	1164	95	-
2	EASC	3	600	20	1	403	78	-
3	TMA	3	600	20	1	164	99	-
4	TMA	3	60	20	1	39	99	-
5	TMA	3	60	0	1	16	99	-
6	$EASC_{200}$	3	600	0	1	0	0	
7	$EASC_{200}$	3	60	0	1	88	98	
8	$EASC_{200}$	3	6	0	1	19	90	
9	$EASC_{200}$	3	60	20	1	136	75	
10	$EASC_{200}$	5	60	20	1	219	68	
11	TMA_{200}	3	60	20	1	-	-	1267/3.8
12	TMA_{200}	3	60	20	0,5	-	-	1467/2.2
13	TMA_{200}	3	60	0	0,5	-	-	1334/2.0
14	TMA_{200}	1,5	120	20	0,5	-	-	1067/0.8

Table 4.5.1 Oligomerization of ethylene using Co-F with molecular and heterogeneous alkylaluminum co-catalysts

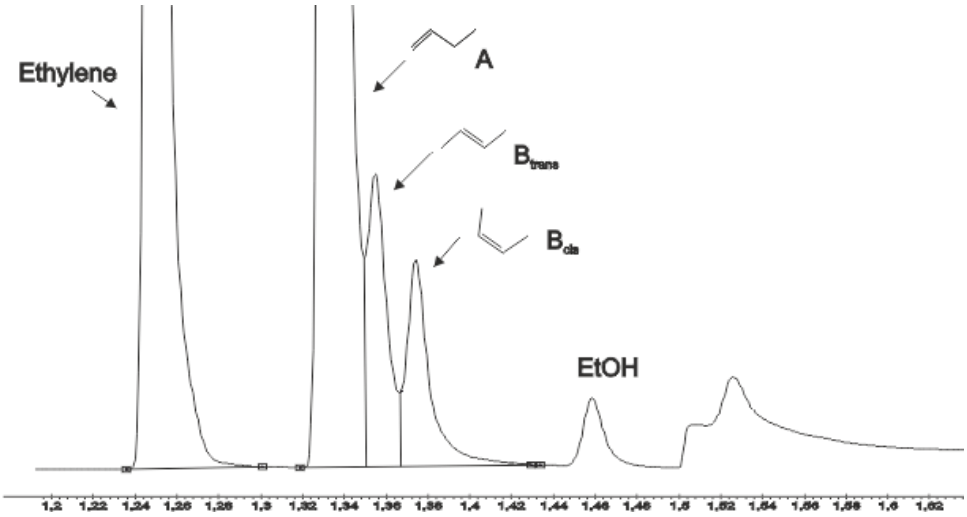

Figure 4.5.3 GC of oligomerization of ethylene with Co-F and EASC, 1h

Then, we proceeded to the experiment with the supported alkylaluminum alkyls. EASC and TMA were grafted onto a partially dehydroxylated silica (heated at 200 °C during 15h under vacuum), affording respectively **$EASC_{200}$** and **TMA_{200}**. We decided to focus on the SiO_{2-200} instead of a high dehydroxylated silica (such as SiO_{2-700} for instance) in order to produce materials with a high loading of aluminum. The silanol density on this support is of 1.48 $mmol.g^{-1}$, and we used 10 molar equivalent of alkylaluminum to prepare the supported version.

The DRIFT of the material reveals the total consumption of the non-interacting silanols (disappearance of the band at 3747 cm^{-1}), and a significant decrease in the intensity of interacting silanols' signal (Figure 4.5.4). However, some silanols in interactions are still visible (broad band at 3650 cm^{-1}). The elongations bands at 2957, 2899, 2856, 2827 cm^{-1} and the one at 2956, 2916, 2874 cm^{-1} respectively for the **TMA_{200}** and the **$EASC_{200}$** can be attributed to the vibrations of sp^3 C-H bonds confirming the grafting of aluminum alkyl species. The ^1H MAS NMR spectrum of **TMA_{200}** in Figure 4.5.5 features a shoulder at 2.9 ppm for the Si-O-H of the interacting silanols. The broad signals at 0.0 ppm -0.6 ppm can be attributed respectively to $Si\text{-}CH_3$ and $Al\text{-}CH_3$.

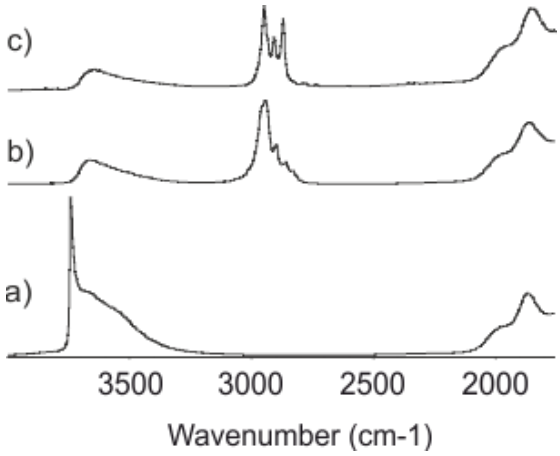

Figure 4.5.4 DRIFT of a) $SiO_{2\text{-}200}$, b) TMA_{200}, c) $EASC_{200}$

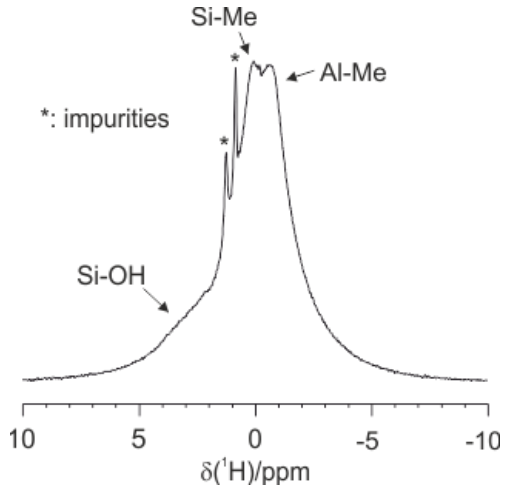

Figure 4.5.5 ^{1}H MAS NMR spectrum of **TMA_{200}**

Preliminary mixing test of the Co-F and the alkylating agent reveal interesting contrasted reactivity of TMA compared to EASC. Indeed, the reaction mixture is green when the cobalt complex is activated in solution with EASC or with the supported equivalent **$EASC_{200}$**. However, mixing the Co-F precatalyst with both TMA and **TMA_{200}** affords red and purple solutions, respectively (Figure 4.5.6). Hypothesis of different modes of alkylation is proposed involving of the participation of the non-innocent pyridine-dimine ligand[9].

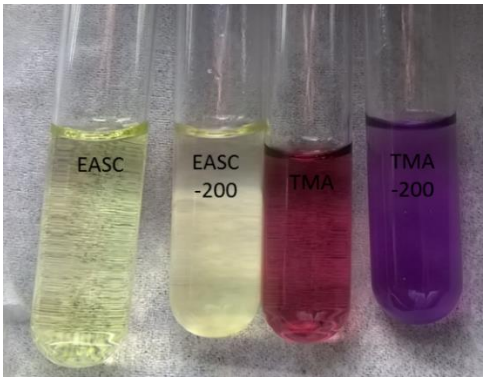

Figure 4.5.6 Mixing of Co-F with several alkylaluminum reagents

The experiments with the supported alkylaluminum reagents are listed in Table 4.5.1. The best ratio of [Al]/[M] is 60 while 600 was the best with the homogeneous version. This is interesting, as this implies that such heterogeneized systems are less costly compared to their molecular counterparts. Similar tendency was also observed when comparing olefin polymerization systems involving molecular and supported MAO cocatalysts (see above section 4.4). Thus, under optimal experimental conditions the maximum in activity is of 219 mmol of butene.mmol.cat^{-1}.h^{-1}, lower than the TON of 1164 reached using molecular EASC. Interestingly, the use of TMA_{200} affords no butene (or light olefins) but polyethylene. The activity of towards polyethylene formation is relatively good with a maximum of about 1500 kg of polyethylene per mol of Co-F per hour. The active species is quite stable, as activity is similar between 30 minutes and 1 hour (1470 and 1270 $kg_{PE}/mol_{Co\text{-}F}/h$, respectively, entries 12 and 11). Performing reaction at 0 °C resulted in no improvement in activity (Entries 12 and 13). Higher aluminum/cobalt ratio is detrimental to activity (Entry 14). This selectivity contrasts with the outcome from combination of the Co pre-catalyst and molecular TMA, which affords C_4 product, and no trace of polyethylene. This may be attributed to the activation of the catalyst that will differ with a constrained silica-supported TMA. Alternatively, it may also derive from a more efficient chain transfer from the metal to the co-catalyst (chain-shuttling), which would be faster than chain termination reactions[10]. The GPC analysis (Table 4.5.2) of the thus-produced polyethylenes show overall the formation of low molecular weight polyethylene with medium to high polydispersity, from 1.8 to 12.6. The poor control of the system can be explained by changes in the nature of active species depending on reaction conditions (decomposition over time or under higher temperature), or to the lack of proper mass transfer within this slurry-type process due the experimental setup (magnetic stirred instead of mechanical propeller, for instance). Investigations on the way the TMA_{200} activates the Co-F should be carried out in order to be able to tune the system and thus to obtain a better control. The ^{1}H NMR spectrum of the polymer produced in run 11 shows peaks at 5.0 ppm for the CH_2 protons within the terminal double bond, and at 5.89 ppm for the CH protons in this fragment. A signal at 2.1 ppm is assigned to the CH_2 in allylic position and the intense peak at 1.4 ppm corresponds to the CH_2 within the polyethylene chain (

Figure 4.5.7). Furthermore, the terminal methyl group protons resonate at 1.0 ppm. The ^{13}C NMR presented in Figure 4.5.8 features signals from terminal vinylidene fragments at 138.9 and 113.7 ppm for the sp^2 carbons, and at 33.4 ppm for the carbon in allylic position. Peaks accounting for CH_2-CH_2-CH_3 are also observed at 31.2, 22.3 and 13.6 ppm respectively for the carbons from the polymer chain. Minor signals accounting for other unsaturated fragments (^{1}H: 5.5 ppm, ^{13}C: 130.0, 120.2 ppm) are due to presence of minor isomerization products. These analysis shows that the main termination of the polymer occurred via a β-H elimination reaction.

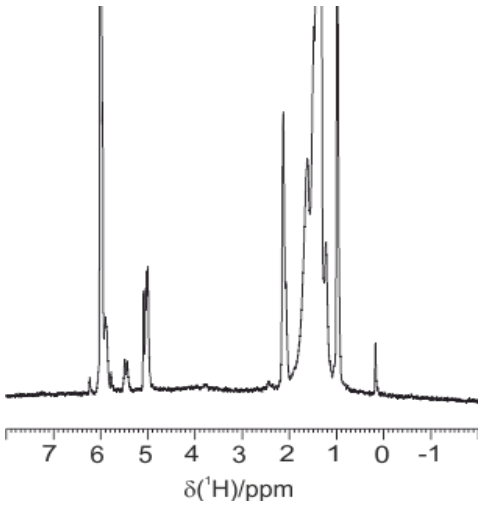

Figure 4.5.7 ^{1}H of polyethylene obtained with TMA_{200}, 400 MHz, 393K, $CD_2Cl_4D_2$

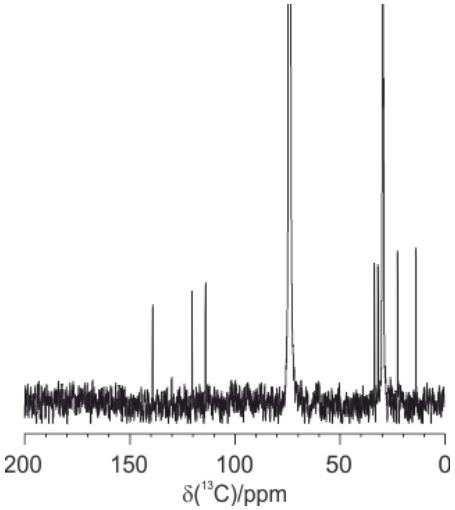

Figure 4.5.8 ^{13}C of polyethylene obtained with TMA_{200}, 107 MHz, 393K, $CD_2Cl_4D_2$

Entry	n Co-F (µmol)	Ratio Al/[M]	Temp. (°C)	Time(h)	A (g of polym. mmol $cat^{-1}.h^{-1}$) / g of PE	Mn	Mw	I (Mw/Mn)
11	3	60	20	1	1267/3.8	500	900	1.8
12	3	60	20	0,5	1467/2.2	500	1900	3.8
13	3	60	0	0,5	1334/2.0	700	8800	12.6
14	1,5	120	20	0,5	1067/0.8	500	2100	4.2

Table 4.5.2 GPC results

4.5.3. Conclusion

We have compared activity in ethylene oligomerization of systems combining a cobalt pre-catalyst supported with either molecular or supported alkyl aluminum activators. Under homogeneous conditions, good activity is obtained in the case of ethylaluminum sesquichloride(EASC), with high selectivity towards 1-butene. Trimethylaluminum (TMA) generates a less active system, though with excellent selectivity. When using the supported versions of these activators, the EASC-derived system experience demonstrates lesser activity, with overall decrease in selectivity. In the case of supported TMA, good activity towards polymerization of ethylene was achieved, in sharp contrast to the analogous molecular system. The analysis of the low-molecular polyethylene produced by the heterogeneous system reveals that mostly linear species are formed.

4.5.4. Experimental part

General Considerations: Manipulations were carried out under argon atmosphere in an M-Braun glove-box or by using Schlenk techniques. Toluene was dried by using conventional

reagents and stored in the glove-box over 3Å molecular sieves. Diffuse reflectance infrared spectra were collected with a Harrick cell on a Nicolet Avatar spectrometer fitted with a MCT detector.

Synthesis of Co-F: In a Schlenk tube, $CoCl_2(THF)_{1.5}$ (0.169 g, 0.71 mmol) is dissolved with THF (15 mL). Another Schlenk tube is filled with the 2,6-*bis*[1-(2-trifluormethyl-4-fluorophenylimine)ethylpyridine (0.363 g, 0.75 mmol) and dried for 2 hours under vacuum. Then 10 mL of THF are added and the solution is poured to the vessel containing the cobalt precursor. After 24h, the green solid is filtered, washed 3 times with THF then dried under vacuum to obtain a yield of 86%. Elemental analysis (w %): C 47.17, H 3.13, N 6.11. theoretical C 47.18, H 3.37, N 6.11

Synthesis of supported of alkylaluminum ($EASC_{200}$ or TMA_{200}): A double-Schlenk vessel was loaded with a 20 mL toluene solution of alkylaluminum (1 g, 14.8 mmol) in one compartment and with silica dehydroxylated at 200°C (1 g) with 10 mL of toluene in the other compartment. After 15h of stirring, the supernatant liquid was then separated by filtration into the other compartment, from which the solvent was gas-phase transferred by trap-to-trap distillation back into the compartment containing the modified support in order to wash away the residual molecular precursor. This operation was repeated thrice and the resulting material was then dried under secondary vacuum (10^{-6} mbar) at room temperature for 5 h.

Procedure for oligomerization/polymerization: In a glove box, a stainless reactor is filled with the alkyluminum (481 mg, 2 mmol) or the material (121 mg, 0.18 mmol) and 15 ml of toluene. Filled with 2 bar of ethylene and stirred for 10 min. Then under an atmosphere of ethylene, a solution of 15 ml of toluene and Co-F (2 mg, 0.003 mmol) is added through a syringe and the system is filled with a continuous flow of 10 bar of ethylene. After the reaction time, the reactor is cooled down at -40 °C to allow the analysis in GC. In the case of the **TMA_{200}** the polymer formed is dissolved in THF then precipitated with MeOH.

4.6. Conclusion

In conclusion, several aluminum species have been successfully grafted onto silica. The first example was with a salen ligand, in the view of developing heterogeneous systems for carbonation of epoxides. Mono- and bi-nuclear species have been prepared and immobilized on dehydroxylated silica. ^{27}Al MAS NMR allowed understanding of the surface species structure. In spite of positive catalytic results in epoxide carbonatation, both blank tests and leaching studies cast doubt on the efficiency of the supported aluminum salen systems for this transformation. In a second part, a new coordination compound has been prepared and grafted onto high dehydroxylated silica. Advanced solid- state NMR spectroscopy showed the presence of a mixture of surface species, differing in the nature of the coordinated donor ligand, namely either THF or a siloxane moiety. We also devoted part of our studies to silica-supported aluminum alkyl derivatives, an important class of co-catalysts for several processes. Thus, the structure of MAO in the solid state was investigated, most particularly

with ^{27}Al MAS NMR, revealing elements directly connected to its structure, which also applied to silica-supported MAO, a cocatalyst currently used in major industrial processes. Additionally, we also relied on silica-supported alkyl and chloroalkyl aluminum species as heterogeneous cocatalysts for olefin oligomerization mediated by a cobalt complex. Marked differences with the molecular activators was observed, resulting in a specific case in the formation of polyethylene instead of short olefins. This was ascribed to a more efficient shuttling of the growing chain, most probably induced by electronic changes resulting from immobilization of the aluminum center onto silica.

---

[1] W. Keim, *Angew. Chem. Int. Ed.,* 2013, **52**, 12492–12496.
[2] J. Hou, W-H. Sun, S. Zhang, Y. Deng, X. Lu, *Organometallics*, 2006, **25**, 236
[3] J.T. Dixon, M.J. Green, F.M. Hess, D.H. Morgan, *J. Organomet. Chem.* 2004, **689**, 3641
[4] A. Bollmann, K. Blann, J.T. Dixon, F.M. Hess, E. Killian, H. Maumela, D.S. McGuinness, D.H. Morgan, A. Neveling, S. Otto, M. Overett, A.M.Z. Slawin, P. Wasserscheid, S. Kuhlmann, *J. Am. Chem. Soc.* 2004, **126**, 14712
[5] A. Forestiere, H. Olivier-Bourbigou, L. Saussine, *Oil Gas Sc. I Technol. Rev. IFP.* 2009, **64**, 649
[6] J. Sckupinska, *Chem. Rev,* 1991, **91**, 613
[7] A.P. Rodrigues Ehlert, E. Miraglia Carvalho, D. Thiele, C. Favero, I. Vicente, K. Bernardo-Gusmao, R. Stieler, R. F. De Souza, M. Oberson De Souza, *Catal. Today.,* 2017, **296**,272-276
[8] D. Thiele, R.F. De Souza, *J. Mol. Catal. A. Chem*, 2011, **340**, 83-88
[9] G.W. Margulieux, M.J. Bezdek, Z.R. Turner, P.J. Chirik, *J. Am. Chem. Soc.* 2017, **139**, 6110−6113
[10] P. Zinck, *Polym. Int.*2016, **65**, 11-15

5. Development of new silica-supported L,X-type ligands by surface modification

5.1. Introduction

Direct immobilization of the metal center on the silica surface represents the most convenient pathway to generate well defined species. However, this approach is most often limited to early transition metals, electrophilic enough to establish a strong, covalent bond with surface oxygen centers. In the case of low bonding energy, typically with late transition metals, leaching may occur: when considering catalytic applications, this means that loss of activity from supported species may be observed. During the reaction, the catalyst would be released in the supernatant. Several examples have been described, where late transition metal siloxide species have been used for catalysis, including as grafted species[1]. However, we reasoned that, to circumvent the weak point due to the non-strong bonding of the metal to the surface, one would benefit from the use of a neighboring strong donor ligand that could form a bidentate ligand upon reaction with the silanol and complexation of the donor moiety (Scheme 5.1.1.) Moreover, this may provide access to tuned grafted species, were the nature of the chelating framework may impact not only the resilience towards leaching, but also the catalytic performances of the resulting material.

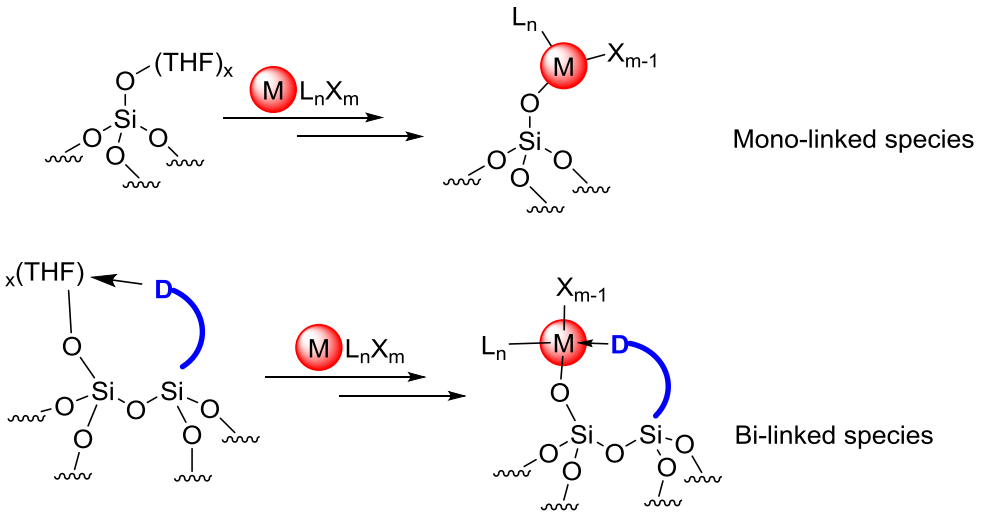

Scheme 5.1.1 Concept proposition of the generation of bi-anchored species

Thus, to tackle this problem, we propose to modify silica by introducing a donor function in the vicinity of a silanol. The strategy consists of treating the silica surface at high temperature (1000 °C), then reacting it with a functionalized carbon-based nucleophile bearing a potential donor ligand functionality. This donor would be connected to the silica surface by a strong Si-C bond (Scheme 5.1.2).

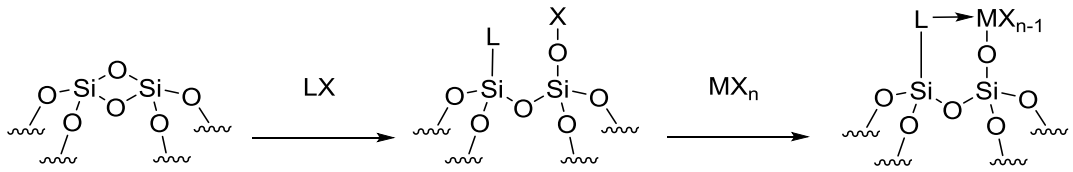

Scheme 5.1.2 Preparation of bi-anchored species

The possibility to modify the surface of silica by organolithium or Grignard reagents was demonstrated by Kim and coworkers[2] using **$SiO_{2\text{-}1000}$** as a support. Indeed, **$SiO_{2\text{-}1000}$** bears mostly siloxane bridges on its surface, with a very low quantity of residual silanols. This thermal treatment, which causes water evolution by condensing neighboring silanols, generates siloxane groups Si-O-Si. These may be part of ring of varying size, most often 6- or 8-membered. However, the use of elevated annealing temperature allows for the formation of highly strained, reactive 4-membered rings[3]. These groups have been shown to be sensitive towards nucleophilic attack by organometallic reagents[4]. In addition, Scott and coworkers described that the reaction of Mg(*n*Bu)$_2$ with silica dehydroxylated at 500 °C affords a mixture of sites resulting from protonolysis by silanol and from opening of siloxane, which shows that such strong nucleophiles may react with silica even with such rather mild pre-treatment conditions[5].We will describe here our studies devoted to the design of such systems, using carbon-based nucleophiles connected to a N-donor function, along with examples of Pd and Ir complexation and preliminary catalytic results.

5.2. Preliminary studies: nucleophilic attack on highly dehydroxylated silica by *n*-BuLi

In a first stage, we explored the reactivity of **$SiO_{2\text{-}1000}$** towards *n*-butyl lithium, in order to confirm literature results and get familiar with the topic. Thus, Aerosil silica was heated at 700 °C for 5h then at 1000 °C during 15h under vacuum (Scheme 5.2.1). Heating the support at such high temperatures removes most of the silanols from the surface, as confirmed by DRIFT spectroscopy. The Figure 5.2.1 presents the comparison between silica dehydroxylated at 700 °C and at 1000 °C. The $\upsilon_{O\text{-}H}$ elongation band for isolated silanol is strongly decreased on $SiO_{2\text{-}1000}$ indicating the high degree of dehydroxylation on the surface. However, some silanols are still present. This has been proposed to be due to their presence as “trapped” silanols inside the structure, which prevents further reaction. It may also be due to the difficulty to find two neighboring silanols to condensate into a siloxane, as the surface density is dramatically decreased[6]. From the literature, the silanol content on this support is estimated to 0.2 OH.nm^{-2} 6.

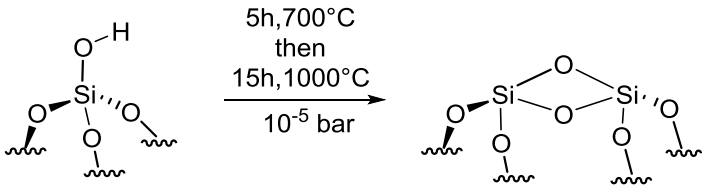

Scheme 5.2.1 Preparation of **$SiO_{2\text{-}1000}$**

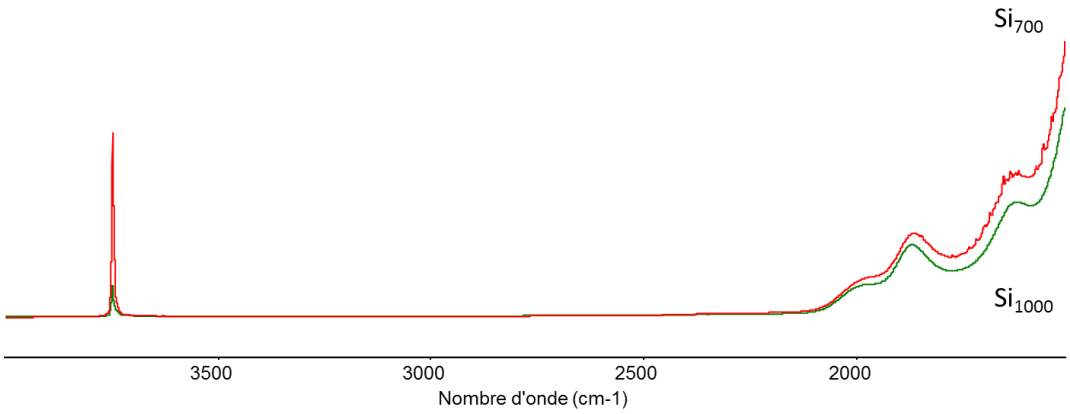

Figure 5.2.1.DRIFT spectra of $SiO_{2\text{-}1000}$(green line) and $SiO_{2\text{-}700}$ (red line)

Once the **$SiO_{2\text{-}1000}$** support was obtained, we proceeded to the reaction with an organolithium derivative (R-Li) in order to generate ≡SiR and ≡SiOLi sites.

We carried out the reaction of *n*-butyllithium with **$SiO_{2\text{-}1000}$** in diethyl ether, at -80 °C for the addition then return to the room temperature for 15 hours (Scheme 5.2.2).

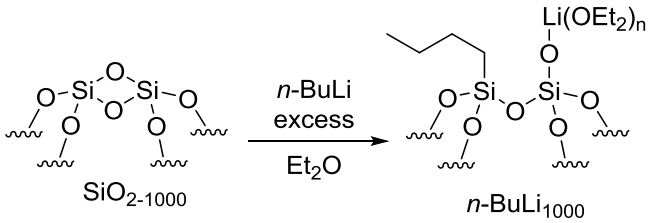

Scheme 5.2.2 Treating **$SiO_{2\text{-}1000}$** with *n*-BuLi to form **$SiO_{2\text{-}1000}$-Bu**

After several washings, the resulting material (**$SiO_{2\text{-}1000}$-Bu**) was dried under vacuum and the DRIFT spectrum was recorded for comparison with the pristine support (Figure 5.2.2).

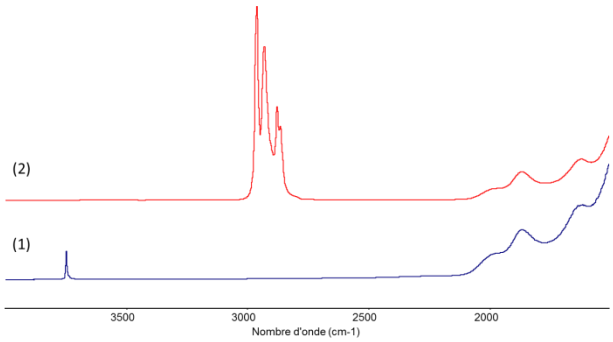

Figure 5.2.2. DRIFT spectra of **$SiO_{2\text{-}1000}$** (1) and **$SiO_{2\text{-}1000}$-Bu** (2)

The first observation is the disappearance of the $\upsilon_{O\text{-}H}$ band at 3747 cm^{-1} showing a complete reaction of *n*-BuLi with the silanols. The $\upsilon_{C\text{-}H}$ bands observed at 2960, 2930, 2877 and 2858 cm^{-1} are in line with the presence of alkyl groups on the surface. The material was analyzed by solid-state NMR. The ^{1}H MAS NMR spectrum (Figure 5.2.3) features 2 signals: The first

one at 0.83 ppm for the CH_3 protons and the other at 1.36 ppm for CH_2 groups. Noteworthy, $SiCH_2$ protons are expected around 0.6 ppm[7].

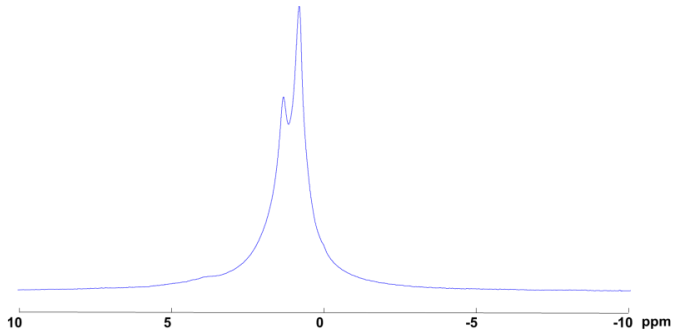

Figure 5.2.3. ^{1}H NMR spectrum of **$SiO_{2\text{-}1000}$-Bu** (800 MHz, ro=20 kHz)

However, the resolution is not enough to more precisely characterize the material. Noteworthy, no signal accounting for OCH_2 moiety (and thus, for the presence of ether) is observed. The ^{29}Si CPMAS NMR spectrum features 4 signals. In agreement with the literature[8], the signals at -107 and -96 ppm correspond to Q_4 and Q_3 sites, respectively (Q_4 site is a silicium linked by 4 oxygen from the structure of the material. Same observation for a Q_3 where 4 oxygen are bonded by the same silicium but one of them is not a Si-OSi site). The signal at -57 ppm (T_3) indicates the generation of ≡SiR site7. The presence of a signal at -16 ppm, assigned to a D_2 site (=SiR_2) indicates that the reaction proceeded further than mono-alkylation. These results are in line with the observations from the Kim group. They showed that the *n*-BuLi is too reactive for the support and can form ≡$SiBu_2$2. This confirms the validity of our experimental conditions and this material will be used as a reference for the following experiments.

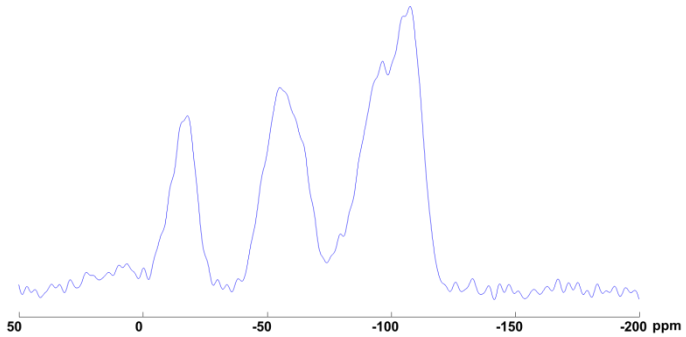

Figure 5.2.4. ^{29}Si CPMAS NMR spectrum of **$SiO_{2\text{-}1000}$-Bu** (9.4 T, ro= 6 kHz)

In order to restore the silanol function for further grafting and extract the lithium atoms, we washed the **$SiO_{2\text{-}1000}$-Bu** with aqueous hydrochloric acid (12.5 mL, 2.5 M) then washed successively by water, methanol then diethyl ether that have been removed under vacuum for 5h (Scheme 5.2.3). On the DRIFT spectrum, the intensity of C-H elongations is lower than in **$SiO_{2\text{-}1000}$-Bu**, indicating that we destroyed some of our ≡SiR sites. A broad band centered at 3500 cm^{-1} indicates the presence of Si-OH in interaction (Figure 5.2.5) as expected for a washing with an aqueous solution of HCl. Similar results were obtained using non-acidic

water treatment. Treating the material with an aqueous solution is thus a too strong treatment to keep the sites intact. Following these difficulties, and bearing in mind that grafting of late transition metal species would proceed more efficiently by halide displacement than by protonolysis, we decided to proceed with the host material in its silanolate form.

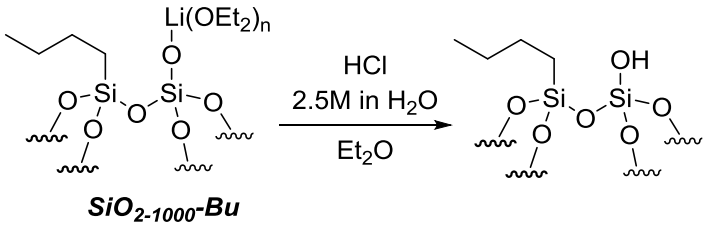

SiO$_{2\text{-}1000}$-Bu

Scheme 5.2.3 Expected reaction upon washing the **SiO$_{2\text{-}1000}$-Bu** with HCl

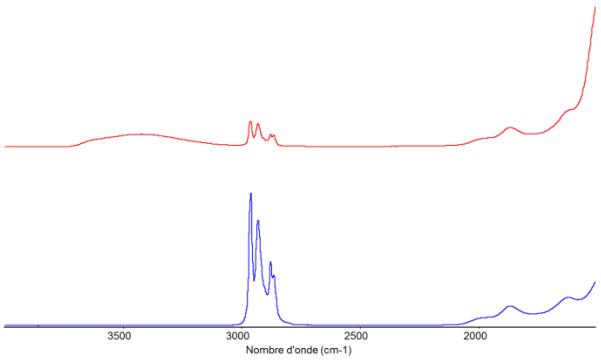

Figure 5.2.5. DRIFT of **SiO$_{2\text{-}1000}$-Bu** before (bottom) and after (top) HCl washing

5.3. Surface proligands

In order to have a functionalized silica for further efficient complexation of metal complexes, the species grafted onto the silicon center (≡SiR) must feature donor ability to enhance the stability of the metal grafting onto the silica by establishing a chelate ring. We selected N-based ligands that possess good stability and chelating ability: pyridine (Pyr), 2-methylpyridine (picoline, Pic) and dimethylbenzylamine (DMBA). Reaction of the organometallic derivatives of these compounds (obtained either by C-H deprotonation using n-BuLi or by Br/Li or Br/Mg exchange) with **SiO$_{2\text{-}1000}$** was foreseen to afford materials **SiO$_{2\text{-}1000}$-Pyr**, **SiO$_{2\text{-}1000}$-Pic**, and **SiO$_{2\text{-}1000}$-DMBA**, respectively (Scheme 5.3.1).

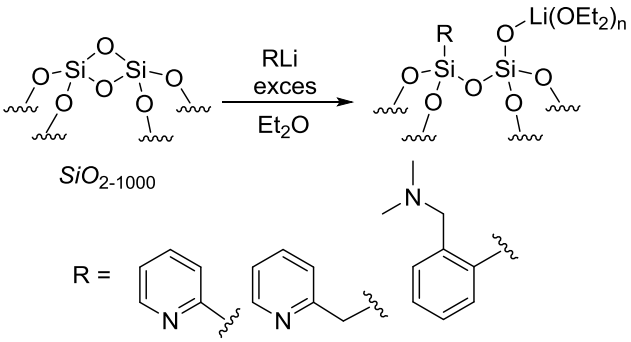

Scheme 5.3.1 Synthesis of **$SiO_{2\text{-}1000}$-Pyr**, **$SiO_{2\text{-}1000}$-Pic**, **$SiO_{2\text{-}1000}$-DMBA**

5.3.1. Using *o*-pyridyl lithium as nucleophile: **$SiO_{2\text{-}1000}$-Pyr**

The *o*-pyridyl lithium is generated in situ using the freshly distilled bromopyridine and *n*-butyllithium. The exothermicity of the reaction is controlled by adding the alkyl lithium reagent to bromopyridine, in solution with diethyl ether, dropwise at -80°C. After a few drops, the colorless solution turns to bright red, confirming the generation of the anion. This solution is then used as such on **$SiO_{2\text{-}1000}$**, after the addition the mixture returns to room temperature and is stirred for 15h.

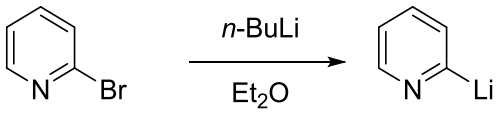

Scheme 5.3.2 Synthesis of the *o*-pyridyl lithium reagent

The DRIFT spectrum of **$SiO_{2\text{-}1000}$-Pyr** (generated with *n*-BuLi and bromopyridine) is presented in Figure 5.3.1.

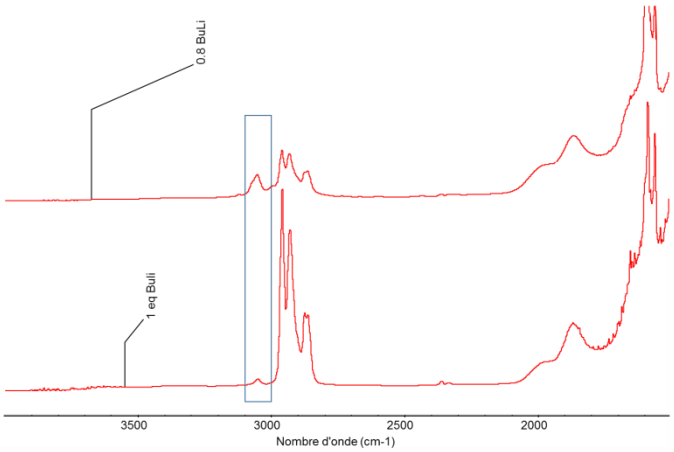

Figure 5.3.1. DRIFT spectra of **$SiO_{2\text{-}1000}$-Pyr** generated with 1 eq of *n*-BuLi (bottom) and with 0.8 eq (top)

The spectrum is comparable to that of **$SiO_{2\text{-}1000}$-Bu**. Sp^2 C-H elongation band at 3050 cm^{-1} is indicative of presence of pyridine on the surface. A decrease in *n*-BuLi equivalent (1 to 0.8) during the Pyr-Li anion procedure is beneficial to the grafting of pyridyl fragment, as shown

by the increase in the relative proportion of sp^2 C-H fragments on the DRIFT spectrum. However, *n*-BuLi is still detected on the surface. It can be explained by the presence of unreacted *n*-butyl lithium of reactant which opens the siloxane bridges. No quantification of the amount and the availability of these bridges can be performed. The washing with water (Figure 5.3.2) or ethanol (Figure 5.3.3) gave no positive results, resulting in complete degradation or no reaction, respectively.

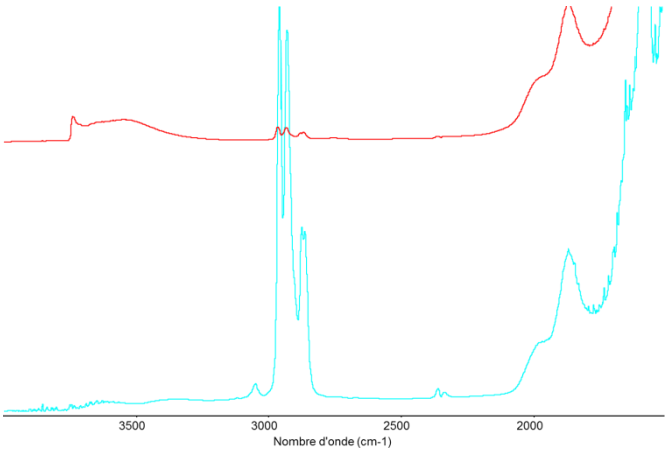

Figure 5.3.2. DRIFT spectra of **$SiO_{2\text{-}1000}$-Pyr** before (bottom) and after washing with H_2O (top)

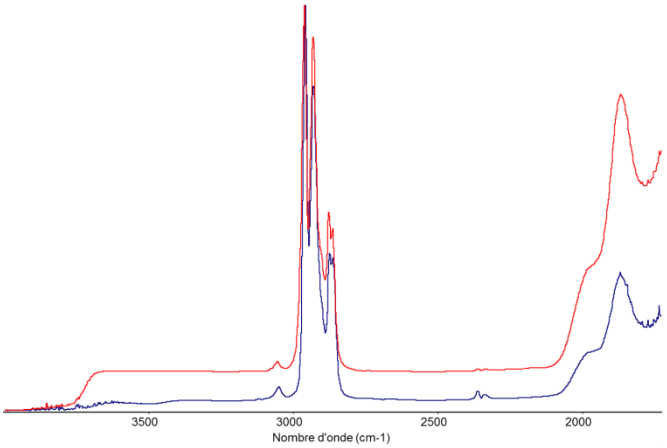

Figure 5.3.3. DRIFT spectra of **$SiO_{2\text{-}1000}$-Pyr** before (bottom) and after washing with ethanol (top)

The ^1H MAS NMR spectrum of **$SiO_{2\text{-}1000}$-Pyr** features signals at 1.33 and 0.74 ppm for CH_2 and CH_3 from *n*-BuSi fragments as observed above , along with peaks at 8.5 and 7.0 ppm due to the *o*-CH and *m*,*p*-CH of the pyridine ring, respectively.

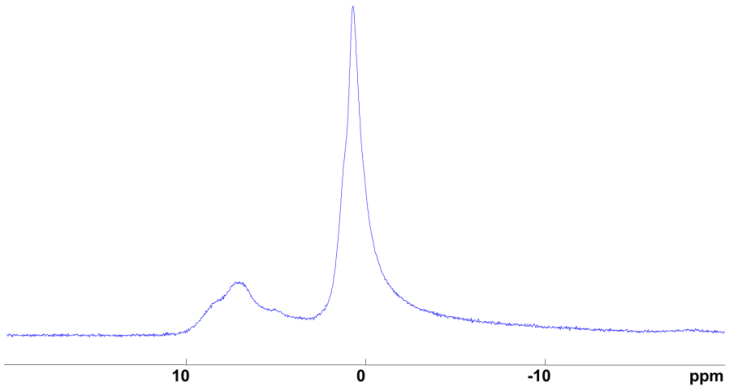

Figure 5.3.4. ^{1}H NMR spectrum of **$SiO_{2\text{-}1000}$-Pyr** (18.8 T, ro=20 kHz)

The ^{29}Si CPMAS NMR spectrum features a signal at -105 ppm for the siloxane groups (Q4), with a broad shoulder around -81 ppm, in line with the presence of ≡SiAr groups.[9] Only weak peaks around -20 to -60 ppm are observed, showing that reaction is rather selective.

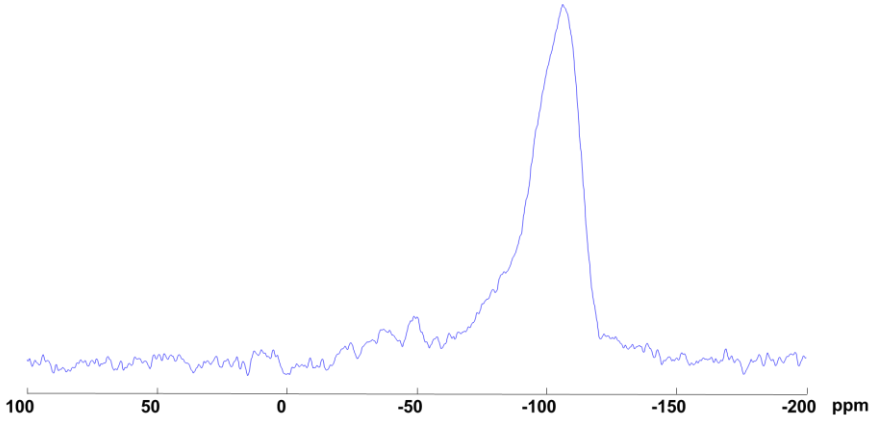

Figure 5.3.5. ^{29}Si CPMAS NMR spectrum of **$SiO_{2\text{-}1000}$-Pyr** (9.4 T, ro= 6 kHz)

Using lithium dimethylamine (LDA) instead of *n*-BuLi gave not better results, as evidenced in the Figure 5.3.6 where no T_3 are observed in ^{29}Si CPMAS NMR).

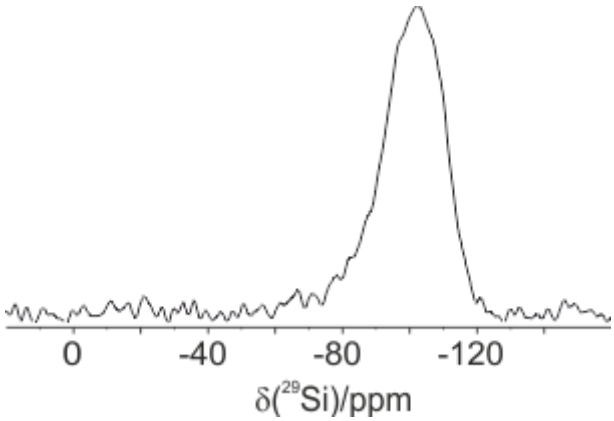

Figure 5.3.6 ^{29}Si CPMAS NMR spectrum of **$SiO_{2\text{-}1000}$-Pyr** generated by LDA instead of *n*-BuLi, 9.4 T, ro= 6 kHz

5.3.2. Using methyl(*o*-pyridyl) lithium as nucleophile: **$SiO_{2\text{-}1000}$-Pic**

The 2-methylpyridine framework is an attractive target, as it is expected to lead to larger, more flexible chelate rings, thus more prone to complex metal centers on the surface (Scheme 5.3.3). The methyl(*o*-pyridyl) lithium is as previously generated in situ using the freshly distilled picoline. The anion is generated in solution, which turns from colorless to bright orange. The analogous Grignard reagent has also been prepared by transmetallation using thus synthetized methyl(*o*-pyridyl) lithium and $MgBr_2$.

Both organo-magnesium and -lithium pathways have been probed. The organo-magneisum was obtained by adding the magnesium dibromide onto the lithiated picoline at -40°C for 30 min. Then the addition onto the silica was carried out with the same conditions described earlier. Similar results were obtained with both reactants. The DRIFT spectrum features bands at 3059, 3015, 2956, 2933 and 2867 for sp^2 and sp^3 C-H elongation. No elongation band of silanol are detected at 3747 cm^{-1}, confirming the consumption of the hydroxyl groups during the synthesis (Figure 5.3.7.).

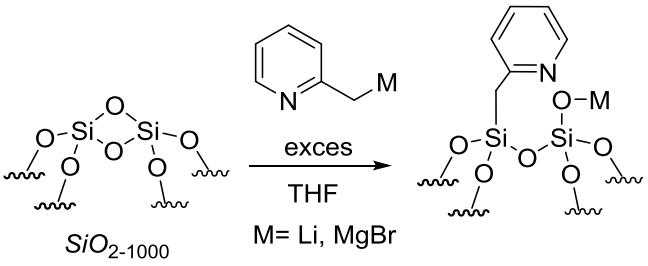

Scheme 5.3.3 Synthesis of **$SiO_{2\text{-}1000}$-Pic**

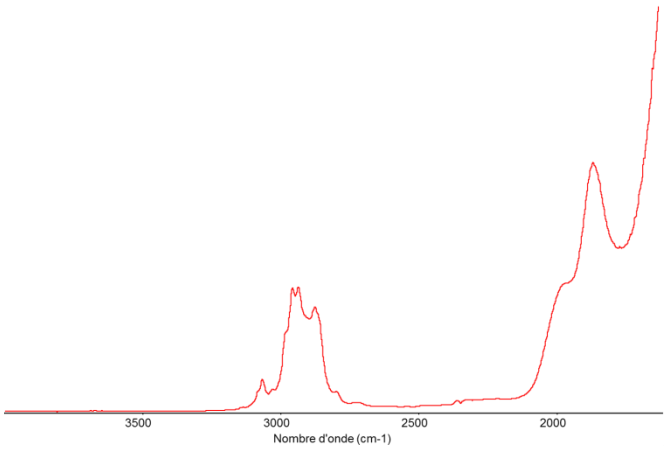

Figure 5.3.7. DRIFT spectrum of **$SiO_{2\text{-}1000}$-Pic**

The ^1H MAS NMR spectrum comprises signals from 8.7 to 6.1 ppm accounting for aromatic CH protons and several peaks in the aliphatic protons' region at 1.62, 1.10 and 0 ppm for CH_2 of the methylenic group on the picoline and butyl groups (Figure 5.3.8).

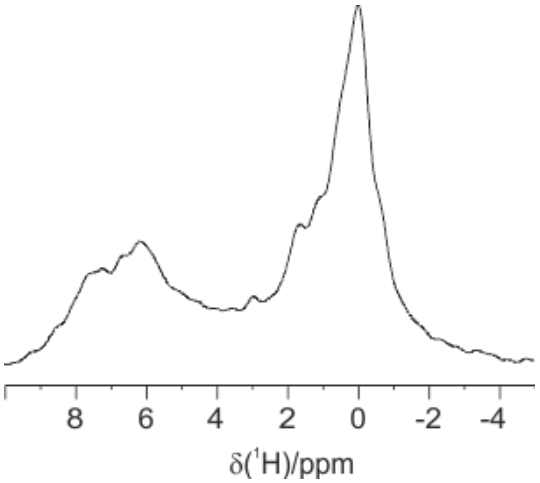

Figure 5.3.8. ^{1}H MAS NMR spectrum of **$SiO_{2\text{-}1000}$-Pic** (9.4 T, ro= 10 kHz)

The ^{29}Si CPMAS NMR spectrum features a signal for Q_4 sites at -100 ppm and a further one at -67ppm for T_3 sites that can be attributed to the ≡$SiCH_2$Pyr moieties[10] (Figure 5.3.9). The ^{13}C CPMAS NMR presents signals at 159, 148, 135, 122 and 102 ppm for the aromatic carbons from the pyridine, while a signal at 24 ppm stands for the $SiCH_2$ moiety. The relatively broad signal in the alkyl zone (from 40 to 0 ppm) confirms the presence of *n*-butyl chains within the material (Figure 5.3.10). Noteworthy, the sharp peak at 10 ppm in characteristic of $SiCH_2CH_2$ (to be compared with the *n*-butyl-substituted polyoligosilsesquioxane, where this group resonates at 11.6 ppm7).

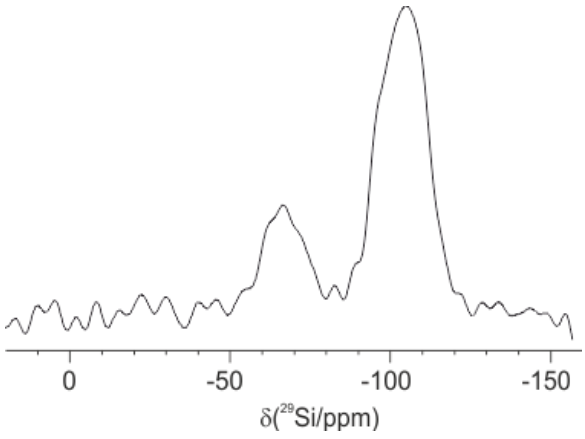

Figure 5.3.9. ^{29}Si CPMAS NMR spectrum of **$SiO_{2\text{-}1000}$-Pic** (9.4 T, ro= 6 kHz)

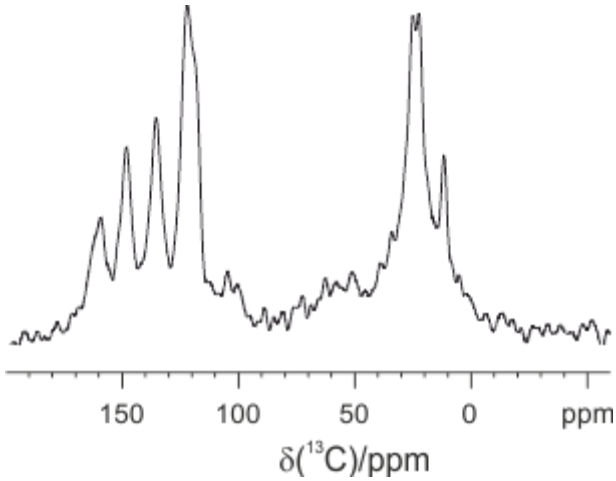

Figure 5.3.10 ^{13}C CP MAS NMR spectrum of **$SiO_{2\text{-}1000}$-Pic** (9.4 T, ro= 10 kHz)

5.3.3. Using lithiated DMBA as nucleophile: **$SiO_{2\text{-}1000}$-DMBA**

The N,N-dimethylbenzylamine has also been probed as potential tether. This type of ligand has been extensively used in organometallic chemistry, mostly by the van Koten team[11]. Alkylation procedures are clearly described and can thus be efficiently implemented.

Functionalization of $SiO_{2\text{-}1000}$ with metallated dimethylbenzylamine (DMBA) (prepared from the dimethylbenzylamine and the *n*-BuLi to obtain a stable white solid[12]) was attempted under similar reaction conditions than with the previous material (Scheme 5.3.4).

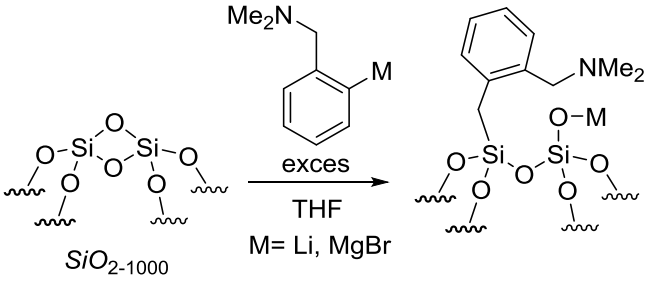

Scheme 5.3.4 Synthesis of **$SiO_{2\text{-}1000}$-DMBA**

The comparison of DRIFT spectra from **$SiO_{2\text{-}1000}$** and **$SiO_{2\text{-}1000}$-DMBA** reveals the disappearance of the elongation band of silanol at 3747 cm^{-1} confirming the consumption of hydroxyl group. In addition, bands at 3051, 2938, 2858, 2829 and 2785 cm^{-1} for sp^2 and sp^3 C-H elongation vibrations (Figure 5.3.11).

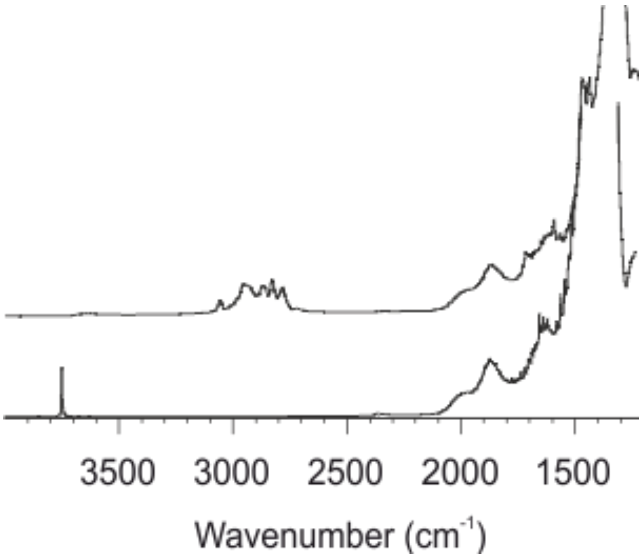

Figure 5.3.11. DRIFT spectra of **$SiO_{2\text{-}1000}$** (bottom) and **$SiO_{2\text{-}1000}$-DMBA** (top)

The ^{1}H MAS NMR spectrum, as observed with the other materials presents 2 signals from 8 to 5 ppm accounting for aromatic CH protons and several peaks in the aliphatic protons' region centered at 0.2 ppm for CH_2 of the methylenic group on the picoline and $-N(CH_3)_2$ (Figure 5.3.12).

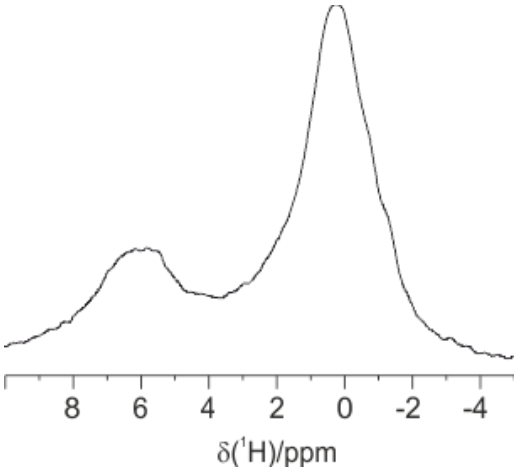

Figure 5.3.12. ^{1}H MAS NMR spectrum of **$SiO_{2\text{-}1000}$-DMBA** (top)

The ^{29}Si CPMAS NMR shows 2 signals. A weak one at -77 ppm that can be attributed to a T_3 group as expected and a larger one at -106 ppm for both Q_3 and Q_4 sites. The shift of the ≡SiR bond (R= CH_2PhNMe_2) confirms the strong influence of the nature of alkyl group onto the chemical shift in ^{29}Si NMR[13].

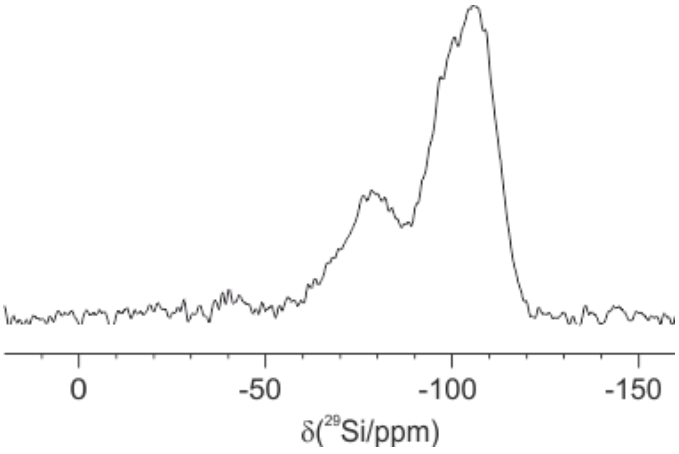

Figure 5.3.13. ^{29}Si CPMAS NMR spectrum of **$SiO_{2\text{-}1000}$-DMBA**

5.4. Pd and Ir surface complexes from **$SiO_{2\text{-}1000}$-Pic**

From our above-described investigations, silica functionalized using α-metallated 2-methylpyridine is the most appropriate support, as efficient functionalization could be achieved. We thus selected it to proceed to the second step of the project, namely complexation of late transition metals on this host material (Scheme 5.4.1).

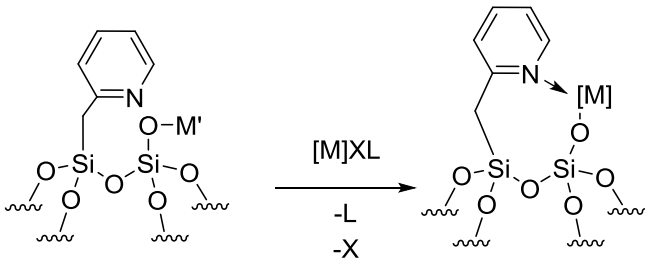

Scheme 5.4.1. Immobilization of a catalyst onto the **$SiO_{2\text{-}1000}$-Pic**

The choice of the immobilized metal centers was performed according to their relevance to catalytic processes. Furthermore, the molecular precursors were selected depending on the presence of at least one labile donor atom or a potentially vacant site (to be substituted by pyridyl moiety from **$SiO_{2\text{-}1000}$-Pic**) and a X-type ligand site (to be substituted by silanolate moiety from **$SiO_{2\text{-}1000}$-Pic**). Thus, our first attempts were performed using $[Pd(PhCN)_2Cl_2]$ and $[Ir(COD)Cl]_2$.

5.4.1. Immobilization of $[Pd(PhCN)_2Cl_2]$

This complex is commonly used in classical organometallic catalytic reactions like C-C bond coupling reaction or carboxylation[14]. The metal center is complexed by labile benzonitrile ligands that can be easily displaced during the grafting onto **$SiO_{2\text{-}1000}$**. Furthermore, these coordinated nitrile functions are convenient spectroscopic probes for IR monitoring of the course of the reaction.

After 15h, at room temperature, the reaction of $Pd(PhCN)_2Cl_2$ with **$SiO_{2\text{-}1000}$** in CH_2Cl_2 affords **$SiO_{2\text{-}1000}$-Pic-Pd** as a yellow material, which has been characterized by several techniques (Scheme 5.4.2).

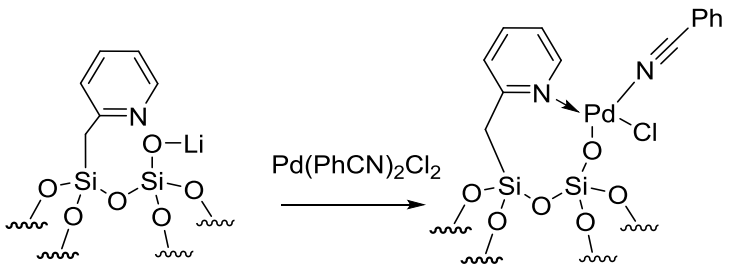

Scheme 5.4.2. Immobilization of $Pd(PhCN)_2Cl_2$ onto the **$SiO_{2\text{-}1000}$-Pic**

The DRIFT spectrum (Figure 5.4.1) features the characteristic bands (already described above) for silica-bound picoline showing that the material retains this framework (2959, 2926 and 2863 cm^{-1}). Silanols in interaction are present as indicated by the broad band centered at 3500 cm^{-1}. Furthermore, bands at 2287 and 2253 cm^{-1} are indicative of complexed benzonitrile ligands. For comparison, the molecular precursor $[Pd(PhCN)_2Cl_2]$ gives rise to 2 bands at 2286 and 2261 cm^{-1}.

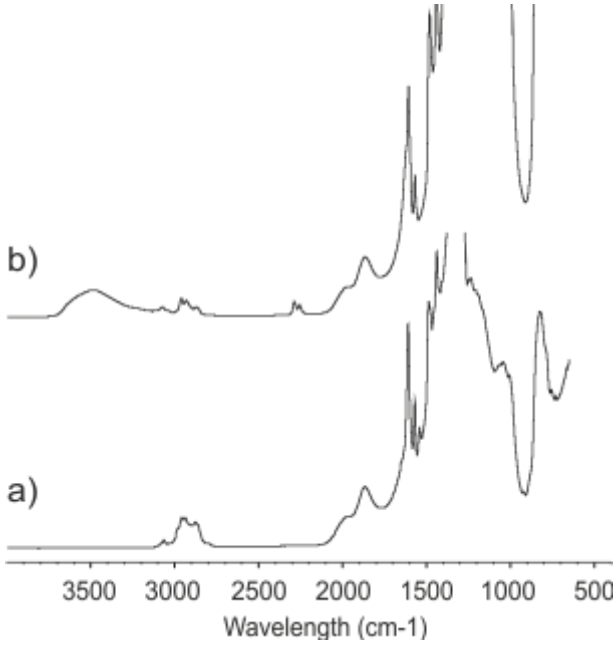

Figure 5.4.1. DRIFT spectra of a) **$SiO_{2\text{-}1000}$-Pic** and b) **$SiO_{2\text{-}1000}$-Pic-Pd**

The elemental analysis reveals a Pd loading at 0.65 $mmol.g^{-1}$. The high loading confirms the grafting of the palladium onto the surface. The ^1H MAS NMR is presented in Figure 5.4.2. Same peaks as observed with **$SiO_{2\text{-}1000}$-Pic** are present confirming the stability of the material after the grafting. The lack of resolution in both the aromatic and aliphatic zone prevents full assignment. However, one can observe an increase in the intensity of the aromatic protons

signal (at about 7 ppm), along with a new signal at 3 ppm, which may be due to a CH_2 from coordinated picoline fragment.

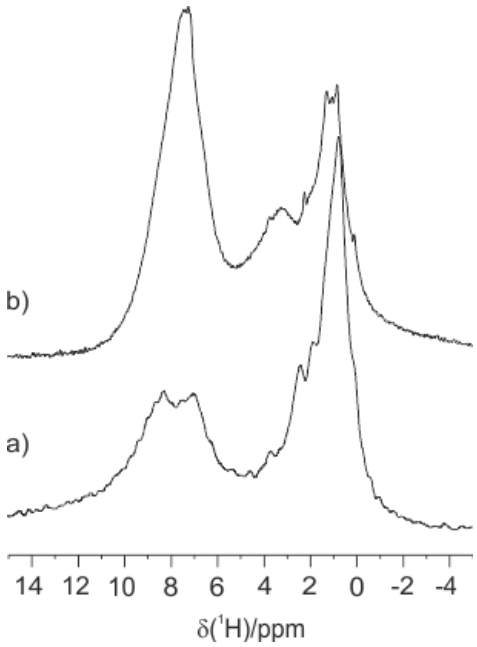

Figure 5.4.2. ^{1}H MAS NMR spectra of a) **$SiO_{2\text{-}1000}$-Pic** and b) **$SiO_{2\text{-}1000}$-Pic-Pd** (18.8 T, ro= 20 kHz)

Further investigations using a 2D ^{1}H-^{1}H DQSQ NMR experiment were carried out (Figure 5.4.3). Two correlations are observed: the site A indicates spatial proximity between protons at 7.3 ppm (*m*-CH of pyridine group) and the one at 3.2 ppm (benzylic protons). The site B features an interaction with the *m*-CH of pyridine group (7.3 ppm) with protons at 1.07 ppm, which is proposed to account for Si-nBu sites.

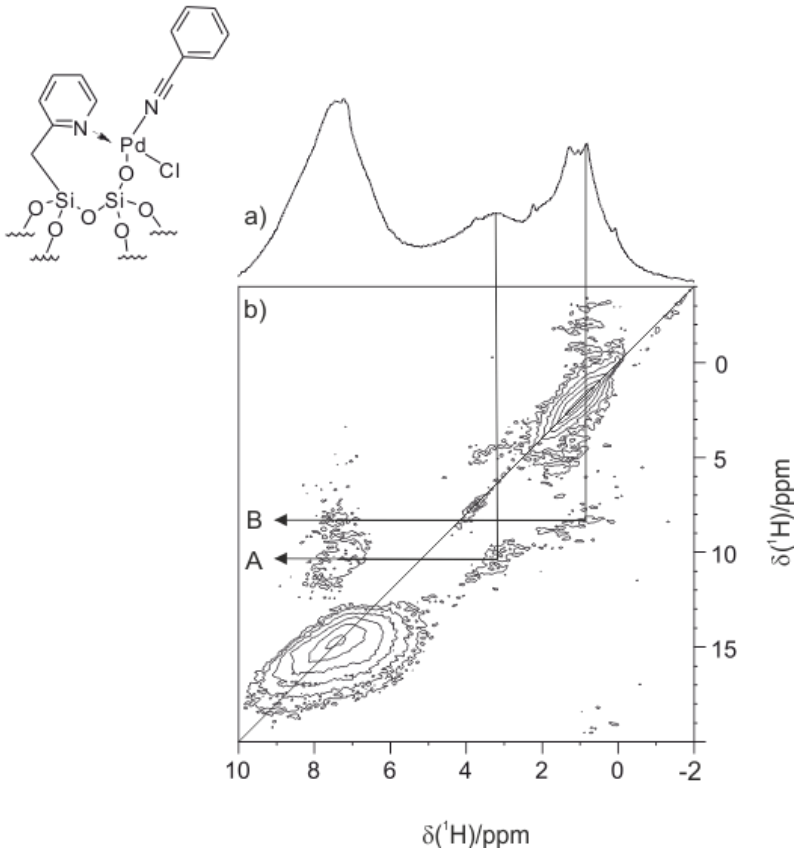

Figure 5.4.3. ^{1}H (a) and ^{1}H-^{1}H DQ-SQ (b) MAS NMR spectra of **$SiO_{2\text{-}1000}$-Pic-Pd** (18.8 T, spinning speed 20 kHz)

The ^{29}Si CPMAS of **$SiO_{2\text{-}1000}$-Pic-Pd** is compared to the starting material in Figure 5.4.4. Two signals are observed at -66 ppm and -105 for ≡$SiCH_2$Pyr and ≡SiOSi≡, respectively. It confirms that the picoline fragments within this material are retained after the grafting and the previously formed bonds are still here.

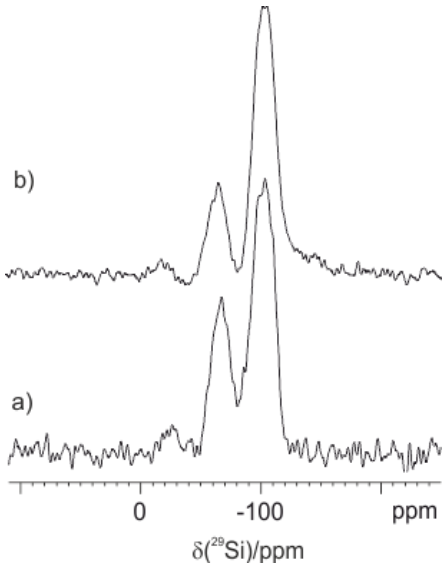

Figure 5.4.4. ^{29}Si CPMAS NMR spectra of a) **$SiO_{2\text{-}1000}$-Pic**, b) **$SiO_{2\text{-}1000}$-Pic-Pd** (9.4 T, ro= 6 kHz)

The ^{13}C CPMAS NMR spectrum is presented in Figure 5.4.5. Peaks in the 165-128 ppm region account for the aromatic carbons of picoline and phenyl group, along with that from the nitrile group (observed at 112 (CCN), 116 (CN), 129, 132, 133 (C_6H_5) ppm in liquid state NMR[15]). The signal at 25 ppm results from the CH_2 of the picoline.

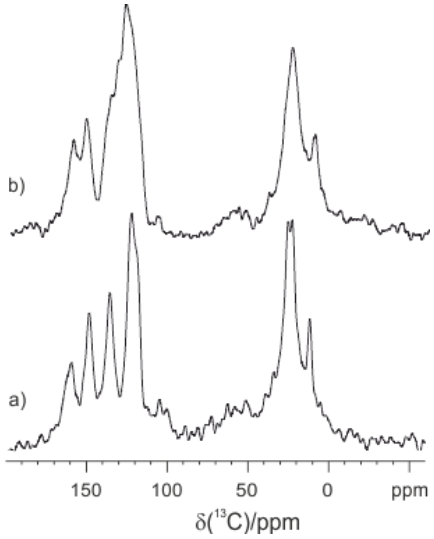

Figure 5.4.5. ^{13}C CPMAS NMR of a) **$SiO_{2\text{-}1000}$-Pic**, b) **$SiO_{2\text{-}1000}$-Pic-Pd**, 9.4 T, ro= 6 kHz, 9.4 T, ro= 10 kHz

As these characterization elements afford promising elements, future efforts will be targeted at potential catalytic applications in catalysis such as carboxylation, or olefin oligomerization. Scanning electronic microscope analysis still needs to be carried out to check if the palladium did form nanoparticles, which could explain the high metal loading.

5.4.2. Immobilization of $[Ir(COD)Cl]_2$

Despite its high cost, iridium is widely used in catalysis for several reactions such as hydrosilylation[16] or C-H activation[17]. The recycling of such catalysts thanks to our approach would be highly desirable. We thus selected the $[Ir(COD)Cl]_2$, a commercial complex, as precursor for reaction with **$SiO_{2\text{-}1000}$-Pic**.

The reaction of this complex with supported picoline in toluene affords **$SiO_{2\text{-}1000}$-Pic-Ir** as a yellow material after 15h of reaction (Scheme 5.4.3).

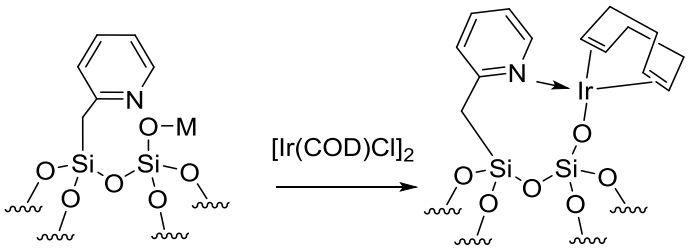

Scheme 5.4.3. Immobilization of $[Ir(COD)Cl]_2$ onto **$SiO_{2\text{-}1000}$-Pic**

The DRIFT spectra of the molecular precursor and its immobilized counterpart are shown in the Figure 5.4.6. C-H elongations are observed at 3076, 3017 cm^{-1} (sp^2 C-H) and 2960, 2934, 2887, 2875 and 2838 cm^{-1} (sp^2 C-H) assigned to the CH and CH_2 from both cyclooctadiene and picoline. C-C double bond-related vibrations are observed at 1478 and 1435 cm^{-1}. In order to check if the iridium is present on the surface with available coordination sites, we exposed our material to an atmosphere of CO (about 15 bar) to observe the coordination of one or more CO groups onto the metallic center. The DRIFT spectrum of the resulting material is shown in the Figure 5.4.6-c. Characteristic ν_{CO} bands from metal-bound carbonyl groups appeared at 2063, 2022 and 2001 cm^{-1} confirming at least the presence of iridium in the surface, with different CO coordination ability. The C=C related bands decrease in intensity, in line with displacement of COD by CO. The elemental analysis reveals a loading of 0.24 $mmol.g^{-1}$ of iridium. This loading is relatively lower that the material synthetized with the palladium and can be explained by the bulkiness of the COD ligand, and/or by a cleaner reaction.

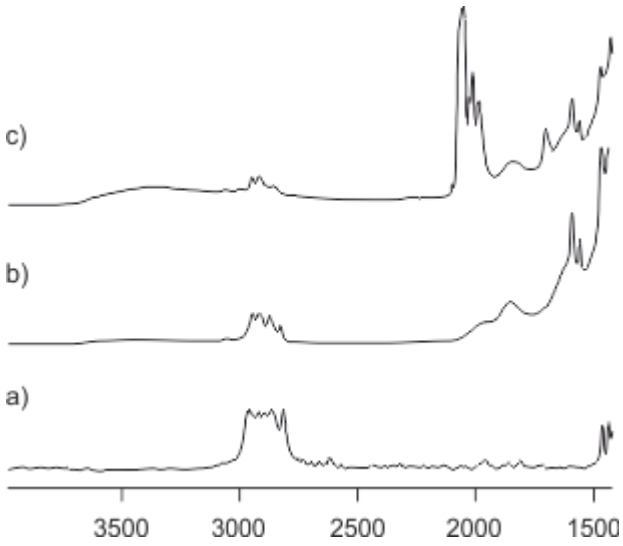

Figure 5.4.6.DRIFT spectra of a) $[Ir(COD)Cl]_2$, b) **$SiO_{2\text{-}1000}$-Pic-Ir** and c) **$SiO_{2\text{-}1000}$-Pic-Ir** after reaction with CO

The comparison of the ^1H MAS NMR spectra of **$SiO_{2\text{-}1000}$-Pic** and **$SiO_{2\text{-}1000}$-Pic-Ir** reveals the apparition of a shoulder at 3.9 ppm that can be attributed to the cyclooctadiene from the iridium species (Figure 5.4.7).

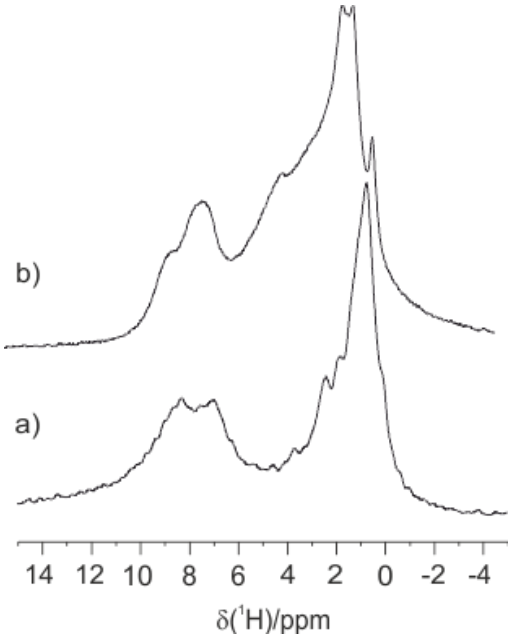

Figure 5.4.7. ^{1}H MAS NMR spectra of a) **$SiO_{2\text{-}1000}$-Pic** and b) **$SiO_{2\text{-}1000}$-Pic-Ir**

As a comparison, these protons resonate at 4.2 ppm in $[IrCODCl]_2$[18]. The ^{1}H-^{1}H DQSQ NMR spectrum reveals spatial proximities (site A) between the protons at 7.26 and the one at about 4 to 3 ppm, as observed previously with the **$SiO_{2\text{-}1000}$-Pic-Pd.** The attribution remains the same and corresponds to interaction between the aromatic protons from the pyridine and the benzylic protons (Figure 5.4.8).

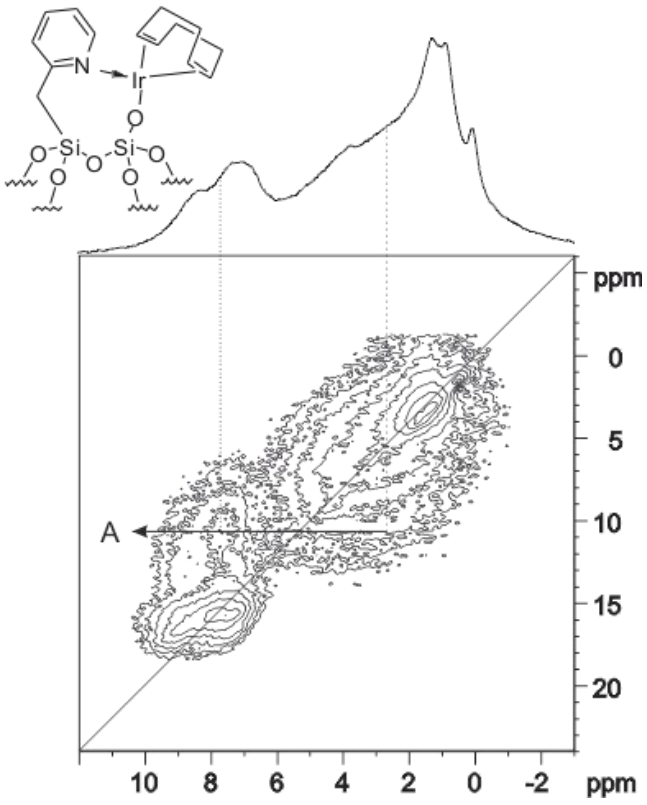

Figure 5.4.8. ^{1}H (a) and ^{1}H-^{1}H DQ-SQ (b) MAS NMR spectra of **$SiO_{2\text{-}1000}$-Ir**, 18.8 T, ro= 20 kHz)

However, the quality of the spectrum is not enough to obtain clearcut information at this stage. ^{29}Si CPMAS NMR confirmed the presence of ≡SiR species by the peak at -70.5 ppm, and a signal accounting for siloxane groups can be seen at -100.1 ppm (Figure 5.4.9).

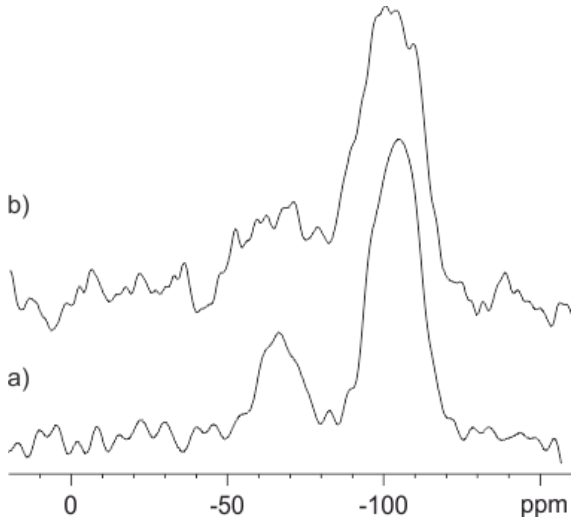

Figure 5.4.9. ^{29}Si CPMAS NMR spectra of a) **$SiO_{2\text{-}1000}$-Pic**, b) **$SiO_{2\text{-}1000}$-Pic-Ir**, 9.4 T, ro= 6 kHz

The ^{13}C CPMAS NMR spectrum features new signals compared to the **$SiO_{2\text{-}1000}$-Pic-Ir**, at about 60 ppm assigned to the olefinic carbons from bound cyclooctadiene. As a comparison, these carbons resonate at 62 ppm in the molecular precursor (Figure 5.4.10). Scanning electronic microscope analysis still needs to be carried out to check if the iridium did form nanoparticles.

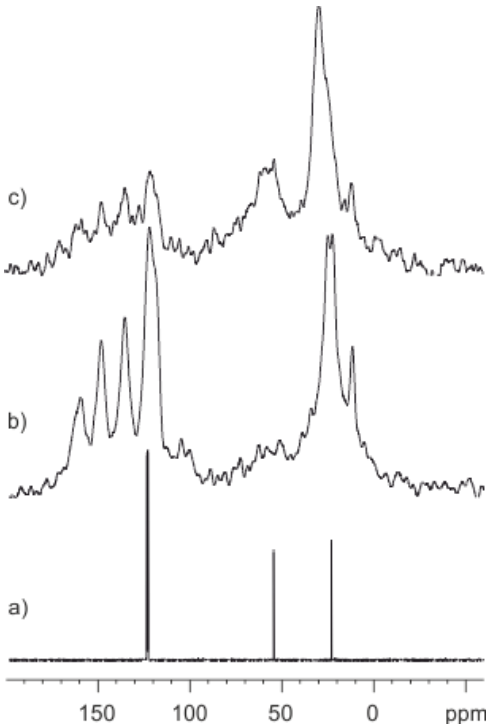

Figure 5.4.10 a) ^{13}C NMR spectrum of $[IrCl(COD)]_2$ in liquid state, b) ^{13}C CP MAS NMR spectrum of **$SiO_{2\text{-}1000}$-Pic**, c) ^{13}C CP MAS NMR spectrum of **$SiO_{2\text{-}1000}$-Pic-Ir**, (9.4 T, ro= 6 kHz and 10 kHz)

Having demonstrated the presence of iridium centers on the surface, preliminary activity test in C-H bond borylation with B_2Pin_2[19] was performed, which gave positive results (Scheme 5.4.4 and Figure 5.4.11). A glass reactor was filled with **$SiO_{2\text{-}1000}$-Pic-Ir** (50 mg, 0.012 mmol), C_6D_6 (2 mL, 23 mmol), B_2Pin_2 (127 mg, 0.5 mmol), which represents a loading of Ir of 2.5%. The reaction mixture was heated at 110 °C for 15 h. The supernatant was then analyzed by ^1H NMR, showing a 12 % (and thus, accounting for about 42 TON). As a comparison, $[Ir(COD)Cl]_2$ affords a TON of 7000 in similar conditions, which shows that we are clearly very far from having developed an efficient system[20]. No recycling was attempted at this stage.

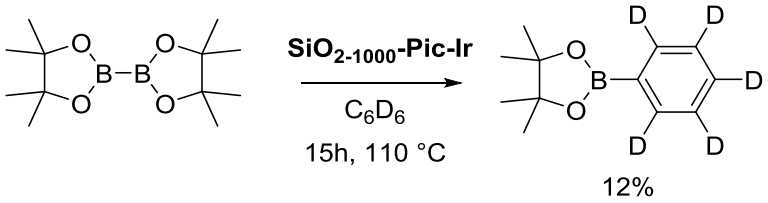

Scheme 5.4.4. Reaction of B_2Pin_2 with C_6D_6 catalyzed by **$SiO_{2\text{-}1000}$-Pic-Ir**

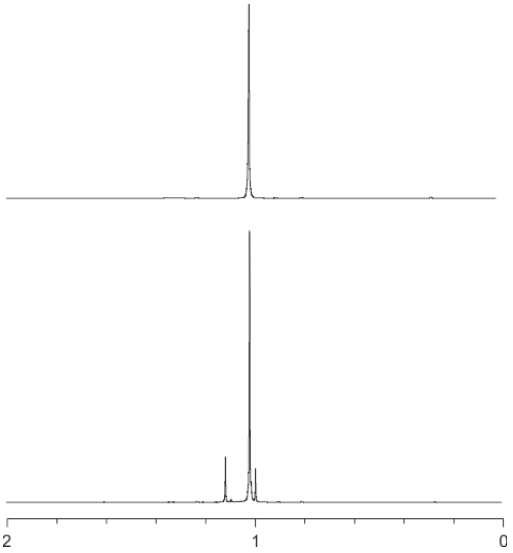

Figure 5.4.11. ^1H NMR spectra of the reaction of B_2Pin_2 with C_6D_6 catalyzed by **$SiO_{2\text{-}1000}$-Pic-Ir** before (top) and after (bottom) catalysis

5.5. Conclusion

In this section of the manuscript, we have described our efforts to prepare silica-supported bidentate ligands, where one *N*-based donor ligand would be introduced in the direct vicinity of a siloxyde (or silanol) group. This would provide a bidentate framework, able to form a stable N,O-chelate upon coordination of an organometallic framework. To reach this goal,

we proposed to react *N*-functionalized carbon-based nucleophiles with silica treated at very high temperature (1000 °C), which generates strained siloxane sites that would be highly reactive towards these alkylating agents. In a first instance, we have probed the surface chemistry of *n*-butyl lithium, as described in the literature. This proved to afford functionalized materials, though with low selectivity towards monoalkylation. The approach was extended to three other precursors for grafted *N*-ligands, namely *ortho*-lithiated pyridine, α-lithiated picoline and *ortho*-lithiated *N,N*-dimethylbenzylamine. The thus-obtained materials were analyzed by infrared and multinuclear MAS NMR, showing incorporation of the desired function on the silica surface. Among these examples, lithiated picoline afforded the most satisfactory results. This host material was then reacted with two organometallic complexes, namely $[Pd(PhCN)_2Cl_2]$ and $[Ir(COD)Cl]_2$. The resulting hybrid materials were characterized by combination of elemental analysis, infrared and MAS NMR spectroscopies, showing that coordination occurred, though definitive evidence of formation of the foreseen complexes is still out of reach. Further investigations, for instance using EXAFS spectroscopy, would help in assessing the metal coordination sphere in these two examples. Preliminary catalytic studies involving the supported iridium species were performed, showing very low activity in C-H borylation. Future studies should focus on refining the synthetic process of the supported proligands, on the structural characterization of the above-described complexes, and on extension of this chemistry to other metal derivatives, for instance with nickel species able to perform olefin oligomerisation, where N-O chelate proved be efficient ligand frameworks.

5.6. Experimental section

General Considerations: Manipulations were carried out under argon atmosphere in an M-Braun glove-box or by using Schlenk techniques. THF, Et_2O and pentane were dried by using conventional reagents and stored in the glove-box over 3Å molecular sieves. Liquid-state NMR spectroscopic analyses were run with a Bruker Avance 300 spectrometer. Solid-state MAS NMR spectra were recorded on a Bruker Avance 400 spectrometer (^{1}H: 400.12 MHz, ^{13}C: 100.63 MHz, ^{27}Al: 104.26 MHz) and on a Bruker Avance 800 spectrometer (^{1}H: 800.13 MHz, ^{27}Al: 208.49 MHz). For ^{1}H experiments, the spinning frequency was 20 kHz, the recycle delay was 10s and 32 scans were collected with a 90° pulse excitation of 3.5 µs. The two-dimensional homonuclear experiment (DQ-MAS) was obtained at a spinning frequency of 20 kHz by using excitation and reconversion pulse blocks of two rotor periods each (200 µs). The 90° pulse length was 2.25 µs, the recycle delay was 10 s, and 16 scans were collected for each slice (350 in total). The ^{13}C CPMAS spectra at 9.4 T were acquired at a spinning frequency of 10 kHz, a delay time of 5 s, 12288 scans. The ^{29}Si CPMAS spectra at 9.4 T were acquired at a spinning frequency of 6 kHz, a delay time of 3 s, 9000 scans. The excitation pulse was set at 4.4 µs. The Chemical shifts were given in ppm with respect to adamantane as external reference for ^{1}H NMR, glycine for ^{13}C NMR, and TMS for ^{29}Si NMR. Diffuse reflectance infrared spectra were collected with a Harrick cell on a Nicolet Avatar

spectrometer fitted with a MCT detector. Elemental analyses were conducted at London Metropolitan University (CHN) and at LASIR, University of Lille (Ir, Pd).

Synthesis of $SiO_{2\text{-}1000}$: A quartz tube is filled with 1.5 g of Aerosil 380 silica and heated under vacuum (10^{-5} mbar) at 700 °C for 15h then 5h at 1000 °C. The nearly full dehydroxylation of the surface is checked by DRIFT analysis where only few isolated silanols are observed (3747 cm^{-1}).

Synthesis of SiO_2-Pyr: A double-Schlenk vessel was loaded with a 15 mL diethyl ether solution of bromopyridine (316 mg, 2 mmol) in one compartment and with silica dehydroxylated at 1000°C (1 g) with 10 mL of Et_2O in the other compartment. A commercial solution of *n*-BuLi (1M, 2 mL) is added to the solution of bromopyridine cooled at -80 °C and immediately forms a bright red solution. After 4h hours of stirring at room temperature, the solution is poured to the other compartment. After 15h of stirring, the supernatant liquid was then separated by filtration into the other compartment, from which the solvent was gas-phase transferred by trap-to-trap distillation back into the compartment containing the modified support in order to wash away the residual molecular precursor. This operation was repeated thrice and the resulting material **SiO_2-Pyr** was then dried under secondary vacuum (10^{-6} mbar) at 80 °C for 5 h.

Synthesis of SiO_2-Pic: A double-Schlenk vessel was loaded with a 15 mL THF solution of 2-methylpyridne (300 mg, 3.2 mmol) in one compartment and with silica dehydroxylated at 1000°C (1 g) with 10 mL of THF in the other compartment. A commercial solution of *n*-BuLi (1M, 3 mL) is added to the solution of 2-methylpyridine cooled at -40 °C and immediately forms a bright orange solution. After 4h hours of stirring at room temperature, the solution is poured to the other compartment. After 15h of stirring, the supernatant liquid was then separated by filtration into the other compartment, from which the solvent was gas-phase transferred by trap-to-trap distillation back into the compartment containing the modified support in order to wash away the residual molecular precursor. This operation was repeated thrice and the resulting material **SiO_2-Pic** was then dried under secondary vacuum (10^{-6} mbar) at 80 °C for 5 h.

Synthesis of SiO_2-DMBA: A double-Schlenk vessel was loaded with a 15 mL THF solution of dimethylbenzylamine (330 mg, 2 mmol) in one compartment and with silica dehydroxylated at 1000°C (1 g) with 10 mL of THF in the other compartment. The solution is poured to the other compartment at -40 °C. After 15h of stirring, the supernatant liquid was then separated by filtration into the other compartment, from which the solvent was gas-phase transferred by trap-to-trap distillation back into the compartment containing the modified support in order to wash away the residual molecular precursor. This operation was repeated thrice and the resulting material **SiO_2-DMBA** was then dried under secondary vacuum (10^{-6} mbar) at 80 °C for 5 h.

Synthesis of $SiO_{2\text{-}1000}$-Pic-Pd: A double-Schlenk vessel was loaded with a 10 mL CH_2Cl_2 solution of $PdCl_2(PhCN)_2$ (153 mg, 0.4 mmol) in one compartment and with **SiO_2-Pic** (200 mg) with 10 mL of CH_2Cl_2 in the other compartment. The solution is poured to the other compartment at room temperature. After 15h of stirring, the supernatant liquid was then separated by filtration into the other compartment, from which the solvent was gas-phase transferred by trap-to-trap distillation back into the compartment containing the modified support in order to wash away the residual molecular precursor. This operation was repeated thrice and the resulting light brown material **SiO_2-Pic-Pd** was then dried under secondary vacuum (10^{-6} mbar) at 80 °C for 5 h.

Synthesis of $SiO_{2\text{-}1000}$-Pic-Ir: A double-Schlenk vessel was loaded with a 10 mL toluene solution of $[IrCODCl]_2$ (134 mg, 0.2 mmol) in one compartment and with **SiO_2-Pic** (100 mg) with 10 mL of CH_2Cl_2 in the other compartment. The solution is poured to the other compartment at room temperature. After 15h of stirring, the supernatant liquid was then separated by filtration into the other compartment, from which the solvent was gas-phase transferred by trap-to-trap distillation back into the compartment containing the modified support in order to wash away the residual molecular precursor. This operation was repeated thrice and the resulting yellow material **SiO_2-Pic-Pd** was then dried under secondary vacuum (10^{-6} mbar) at 80 °C for 5 h.

Borylation of C_6D_6 : A glass reactor is filled with **$SiO_{2\text{-}1000}$-Pic-Ir** (50 mg, 0.0012 mmol, 5% Ir), C_6D_6 (2 mL, 1 eq, 0.025 mmol), B_2Pin_2 (127 mg, 2 eq, 0.5 mmol). Quantified in ^1H NMR

---

[1] a) B. Marciniec, K. Szubert, M.J. Potrzebowski, I. Kownacki and K. Łeszczak, *Angew. Chem.* Int. Ed, 2008, **47**, 541-544. b) B. Marciniec, S. Rogalski, M.J. Potrzebowski and C. Pietraszuk, *ChemCatChem.*,2011, **3**, 904-910

[2] J.E. Lim, C.B. Shim, J.M. Kim, B.Y. Lee and J.E. Yie, *Angew. Chem. Int. Ed.,* 2004, **43**, 3839-3842

[3] B. A. Morrow, I. A. Cody, *J. Phys. Chem.* 1976, **80**, 1995

[4] a) H. Ahn, T. J. Marks, *J. Am. Chem. Soc.* 2002, **124**, 7103-7110; b) C. P. Nicholas, H. Ahn, T. J. Marks, *J. Am. Chem. Soc.* 2003, **125**, 4325-4331

[5] S.L. Scott, M.-Y. Lee, *Chem. Eur. J.* 2011, **17**, 4632-4639

[6] L. T. Zhuravlev, *Langmuir*, 1987, **3**, 316–318.

[7] C. Bolln, A. Tsuchida, H. Frey, R. Mülhaupt, *Chem. Mater.* 1997, **9***,* 1475-1479

[8] F. Uhlig, D. Dortmund, *Inorg. Chem.,* 2000, **46**, 208–222.

[9] F.J. Feher and T.A. Budzichowski, *J. Organomet. Chem.*, 1989, **373**, 153-163

[10] T. Vancompernolle, A. Valente, T. Chenal, P. Zinck, I. Del Rosal, L. Maron, M. Taoufik, S. Harder, R.M. Gauvin, *Organometallics,* 2017, 10.1021/acs.organomet.7b00538 or see section 3.2

[11] G. Van Koten, *J. Organomet. Chem.*, 2013, **730**,156-164

[12] L.E. Manzer, *J. Am. Chem. Soc.* 1978, **20**, 8073

[13] D.A. Loy, B.M. Baugher, C.R. Baugher, D.A. Schneider and K. Rahmimian, *Chem. Mater.* 2000, **12**, 3624-3632

[14] a) M. Beller, W. Mägerlein, A. F. Indolese, C. Fischer, *Synthesis*, 2001, **27**, 1098-1110. b) K. Kumar, A. Zapf, D. Michalik, A. Tillack, T. Heinrich, H. Bottcher, M. Arlt, M. Beller, *Org. Lett.,* 2004, **6**, 7-10. 28. c) L. Ashfield; C. F. J. Barnard, *Org. Process Res. Dev.,* 2007, **11**, 39-43

[15] E. Szłyk, M. Barwiołek, *Thermochim. Acta*, 2009, **495**, 85–89

[16] J. Jeong, S. Park, S. Chang, *Chem. Sci.,* 2016, **7**, 5362-5370

[17] T. Ishiyama, J. Takagi,K. Ishida, N. Miyaura, N.R. Anastasi, J.F. Hartwig, *J. Am. Chem. Soc.,* 2002, **3**, 124, 390–391

[18] S. Sakaguchi, T. Mizuta, Y. Ishii, *Org. Lett,* 2006, **8**, 2461

[19] T. Tagata, M. Nishida, *Adv. Synth. Catal.* 2004, **346**, 1655-1660

[20] L.P. Press, A.J. Kosanovich, B.J. McCulloch, O.V. Ozerov, *J. Am. Chem. Soc.* 2016, **138**, 9487-9497

6. Conclusion

Within the framework of this thesis, we have studied the surface organometallic chemistry of rare-earth metals and of aluminum onto silica. Our goal was to perform precise synthesis of grafted materials, aiming at the generation of well-defined species amenable to the building of structure-activity relationships. Beyond mastering of the reaction conditions (including suitable molecular precursors and conveniently prepared inorganic supports), this relies on extensive use of spectroscopic techniques to fully understand the grafting chemistry and the structure of the supported species. One of the most powerful techniques in this context is solid state NMR. We have thus explored several silica-supported systems with relevance to catalysis, relying when possible on advanced solid state NMR, and occasionally on DFT calculations.

We have thus described the synthesis of several rare-earth metal-based materials that have been employed for reaction of polymerization of polar and non-polar monomers as well as in fine chemistry reactions such as alkyne dimerization. In the case of the grafting of a trisbenzyl derivative, we have demonstrated that the grafting reaction proceeds via distinct pathways involving the La-C bond, namely protonolysis by silanol, or insertion into Si-O-Si groups on the surface, as confirmed by DFT calculations. The resulting material catalyzes efficiently a range of reactions typical for rare-earth metals. Perspectives to this work are the extension of this chemistry to the $[Ln(CH_2Ph)_3(THF)_n]$ family, which would demonstrate the effect of the nature of the rare-earth metal (ionic radius, Lewis acidity) onto the catalysis properties. In a related effort, we prepared well-defined silica-grafted rare-earth amide species and used these in terminal alkyne dimerization, focusing not only on conversion rate but also on selectivity, which was different from that of analogous molecular species. Most particularly, the exacerbated electrophilicity of the grafted metal center strongly influences selectivity. Furthermore, specific investigations on the scandium derivatives were carried out using ^{45}Sc NMR. The modification within the metal coordination sphere were shown to impact on the NMR parameters. This opens options for the use of this spectroscopic tool for future studies on molecular and supported scandium species, though in the case of grafted metal centers, distribution effects and low quantity of NMR active are severe problems, for which solutions must be sought to conveniently model those and increase signal-to-noise ratio, respectively.

In a further stage, several aluminum species have been grafted onto silica for the development of heterogeneous (co)catalysts and for the advances on understanding of aluminum surface chemistry. The first example featured a salen ligand, in the view of developing heterogeneous systems for carbonation of epoxides. Mono- and bi-nuclear species have been prepared and immobilized on dehydroxylated silica. ^{27}Al MAS NMR allowed understanding of the surface species structure. In spite of positive catalytic results in epoxide carbonatation, both blank tests and leaching studies cast doubt on the efficiency of

the supported aluminum salen systems for this transformation. In a second stage, a new coordination compound has been prepared and grafted onto high dehydroxylated silica. Advanced solid- state NMR spectroscopy showed the presence of a mixture of surface species, differing in the nature of the coordinated donor ligand, namely either THF or a siloxane moiety. Finally, we also devoted part of our studies to silica-supported aluminum alkyl derivatives, an important class of co-catalysts for several processes. Thus, the structure of MAO in the solid state was investigated, most particularly with ^{27}Al MAS NMR, revealing elements directly connected to its structure, which also applied to silica-supported MAO, a cocatalyst currently used in major industrial processes. Additionally, we also relied on silica-supported alkyl and chloroalkyl aluminum species as heterogeneous cocatalysts for olefin oligomerization mediated by a cobalt complex. Marked differences with the molecular activators was observed, resulting in a specific case in the formation of polyethylene instead of short olefins. This was ascribed to a more efficient shuttling of the growing chain, most probably induced by electronic changes resulting from immobilization of the aluminum center onto silica.

In the last section of the manuscript, we have described our efforts to prepare silica-supported bidentate ligands, where one *N*-based donor ligand would be introduced in the direct vicinity of a siloxyde (or silanol) group, providing *in fine* a bidentate framework, able to form a stable N,O-chelate upon coordination of an organometallic framework. To reach this goal, we proposed to react *N*-functionalized carbon-based nucleophiles with silica treated at very high temperature (1000 °C), which generates strained siloxane sites that would be highly reactive towards these alkylating agents. The approach was probed with three precursors for grafted *N*-ligands, namely *ortho*-lithiated pyridine, α-lithiated picoline and *ortho*-lithiated *N,N*-dimethylbenzylamine, which were grafted onto silica. Lithiated picoline afforded the most satisfactory results. This host material was then reacted with two organometallic complexes, namely $[Pd(PhCN)_2Cl_2]$ and $[Ir(COD)Cl]_2$. The resulting hybrid materials were characterized by combination of elemental analysis, infrared and MAS NMR spectroscopies, showing that coordination occurred, though definitive evidence of formation of the foreseen complexes is still out of reach. Further investigations, for instance using EXAFS spectroscopy, would help in assessing the metal coordination sphere in these two examples. Preliminary catalytic studies involving the supported iridium species were performed, showing very low activity in C-H borylation. Future studies should focus on refining the synthetic process of the supported proligands, on the structural characterization of the above-described complexes, and on extension of this chemistry to other metal derivatives, for instance with nickel species able to perform olefin oligomerisation, where N-O chelate proved be efficient ligand frameworks.

Thus, thanks to fundamental organometallic chemistry studies involving the control of the site available on the silica and the tuning of experimental conditions (solvent, reactant,

time), we generated highly efficient lanthanum benzyl material for polymerization and fine chemistry and we made the full characterization of its behavior during the grafting thanks to specific solid state nmr sequences. We also have developed a whole family of rare earth material active for the dimerization of terminal alkynes with investigations about the selectivity toward head-to-head dimer and head-to-tail dimer but also toward the trimer formation. Based on these results we investigated the modification of the coordination sphere of a scandium catalyst before and after the grafting using the ^{45}Sc NMR as main characterization. We pursued the application of SOMC with aluminum based catalyst that were applied for the carbonatation of epoxides with again a full study of the aluminum center immobilized onto the silica. Thanks to a fruitful collaboration with our colleagues of Lyon1, we participate to the structure elucidation and its effect on the catalysis of MAO silica-grafted materials.

As we developed a solid background in alkylaluminum immobilized on the surface, we developed a project with the Brazilian team of Michèle de Souza whose the aluminum based material is employed as a effective cocatalyst for oligomerization and polymerization depending of the nature of the alkyl on the aluminum center.

During the final stage of the present thesis, some preliminary test were performed with the modification of the silica by a pyridine derivative and then the grafting of metallic center in order to generate two type of linkage which could allow to solve issues with non oxophilic metals that tends to leach during catalytic transformations. An iridium and palladium catalysts were successfully immobilized via this method and promising results were obtained.

Summary

The generation of heterogeneous catalysts featuring well-defined active centers is of high importance, considering the expected benefits in terms of efficiency and of understanding. We used the surface organometallic chemistry approach to address this issue, focusing on the grafting of rare-earth metals and aluminum derivatives onto silica, and relying mostly on advanced, high-field solid state NMR for detailed characterization at the molecular level, with an emphasis on quadrupolar nuclei.

Thus, the grafting of lanthanum benzyl and rare-earth metal silylamide precursors onto silica was studied, along with applications in several catalytic processes related to polymerization and fine chemistry. The impact from the immobilization is mostly found in selectivity, as supported species behave differently from the molecular counterparts. Furthermore, several aluminum species (salen derivatives, along with alkyl and chloroalkyl complexes) were immobilized onto silica, affording catalysts and cocatalysts for the carbonatation of epoxides and for the polymerization and oligomerization of olefins. There again, strong influence of the grafting was observed on the products resulting from catalysis, for instance shifting from short chain olefins to polyethylene upon use of grafted cocatalysts for oligomerization. Finally, a novel methodology for the introduction of chelating bidentate monoanionic fragments onto silica was introduced and implemented for palladium and iridium species' immobilization. Preliminary catalytic applications were encouraging.

Résumé

La préparation de catalyseurs hétérogènes comportant des sites actifs bien définis est de première importance, du fait des bénéfices attendus en termes d'efficacité et de compréhension. Dans cette optique, nous avons utilisé une approche de chimie organométallique de surface pour le développement de catalyseurs supportés à base de terres rares et d'aluminium, en nous fondant sur la RMN du solide avancée à haut champ pour la caractérisation au niveau moléculaire, notamment appliquée aux noyaux quadripolaires.

Ainsi, le greffage sur silice de dérivés benzyle de lanthane et amidures de terres rares a été étudié, ainsi que leur application dans différentes réactions catalytiques en polymérisation et chimie fine. L'impact de l'immobilisation est principalement visible sur la sélectivité de ces transformations, les espèces supportées se comportant différemment de leurs homologues moléculaires. De plus, plusieurs composés à base d'aluminium (dérivés salen, alkyls et chloro-alkyles) ont été immobilisés sur silice, générant ainsi des catalyseurs et cocatalyseurs pour la carbonatation d'époxides et pour la polymérisation et l'oligomérisation des alcènes. Là encore, une forte influence du greffage a été observée, dans la nature des produits issus de la catalyse, avec par exemple le passage d'oléfines à chaîne courte à du polyéthylène suite à l'utilisation de cocatalyseur greffé en oligomérisation. Enfin, une nouvelle méthodologie pour l'introduction de fragments chélatants bidentates monoanioniques sur la silice a été présentée et appliquée à l'immobilisation de complexes de palladium et d'iridium. Les résultats catalytiques préliminaires sont encourageants.